

**The development and  
evaluation of antibacterial  
polymer-phyllsilicate  
composite systems for the  
treatment of infected wounds**

**Ashley Ryan Hamilton**

MPharm (Hons) MFRPSI MRPharmS

Thesis submitted in partial fulfilment of the  
requirements of Liverpool John Moores University for  
the degree of Doctor of Philosophy

November 2017

# Contents

Contents .....	I
Acknowledgements.....	VII
List of abbreviations.....	VIII
Publications and disseminations from this research project.....	X
Abstract.....	XIII
<b>1. Introduction.....</b>	<b>1</b>
1.1. A brief history of clay minerals in health.....	1
1.2. The physicochemical properties of clay minerals.....	4
1.2.1. Structure and chemistry of clay mineral layers.....	4
1.2.2. Layer arrangement and particle formation.....	9
1.2.3. Behaviour in dispersion.....	13
1.2.4. Interaction with charged molecules.....	17
1.3. Modifying clay minerals.....	19
1.3.1. Acid activation.....	20
1.3.2. Modification with organic compounds.....	20
1.3.3. Modification with inorganic cations.....	22
1.3.4. Modification with inorganic anions.....	23
1.4. A clinical need for improved antimicrobial stewardship.....	24
1.5. Aim and objectives of this research project.....	29
1.6. References.....	32

<b>2. Interaction between phyllosilicates and tetracycline antibacterial agents . .</b>	<b>41</b>
2.1. Introduction . . . . .	41
2.2. Materials and methods. . . . .	47
2.2.1. Materials. . . . .	47
2.2.2. Adsorption of tetracycline and doxycycline. . . . .	47
2.2.2.1. Effect of dispersion pH. . . . .	47
2.2.2.2. Kinetics of tetracycline and doxycycline adsorption. . . . .	48
2.2.2.3. Adsorption isotherms for tetracycline and doxycycline. . . . .	48
2.2.3. Mechanism of clay-tetracycline and clay-doxycycline interactions. . . . .	49
2.2.4. Antibacterial activity assessment. . . . .	50
2.3. Results and discussion. . . . .	52
2.3.1. Effects of dispersion pH on adsorption. . . . .	52
2.3.2. Adsorption kinetics. . . . .	56
2.3.3. Adsorption isotherms. . . . .	62
2.3.4. X-ray diffraction analyses. . . . .	72
2.3.5. FTIR analyses. . . . .	80
2.3.6. Antibacterial activity. . . . .	86
2.4. Conclusions. . . . .	94
2.5. References. . . . .	96

<b>3. Interaction between phyllosilicates and ciprofloxacin</b> .....	<b>104</b>
3.1. Introduction .....	104
3.2. Materials and methods .....	108
3.2.1. Materials .....	108
3.2.2. Adsorption of ciprofloxacin .....	108
3.2.2.1. Effect of dispersion pH .....	108
3.2.2.2. Adsorption kinetics and isotherms .....	109
3.2.3. Mechanism of clay-ciprofloxacin interactions .....	109
3.2.4. Antibacterial activity assessment .....	109
3.3. Results and discussion .....	110
3.3.1. Effects of dispersion pH on ciprofloxacin adsorption .....	110
3.3.2. Adsorption kinetics .....	113
3.3.3. Adsorption isotherms .....	116
3.3.4. XRD analysis .....	119
3.3.5. FTIR analysis .....	123
3.3.6. Antibacterial properties .....	125
3.4. Conclusions .....	128
3.5. References .....	130
<b>4. Development and evaluation of candidate wound dressing materials</b> .....	<b>134</b>
4.1. Introduction .....	134
4.1.1. An overview of wounds, wound healing, and the role of infection .....	135



4.1.2.	An overview of wound care products. ....	140
4.1.3.	Polymer-phyllsilicate composites as potential materials for wound care. ....	144
4.1.4.	Development and evaluation of novel polymer- phyllsilicate composites for wound care applications. ...	147
4.2.	Materials and methods. ....	149
4.2.1.	Materials. ....	149
4.2.2.	Formulation of candidate composites. ....	149
4.2.2.1.	Pre-formulation studies. ....	149
4.2.2.2.	Development of candidate films. ....	150
4.2.2.3.	Formulation of ciprofloxacin-containing composite films. ....	150
4.2.2.4.	Development of candidate foams. ....	151
4.2.2.5.	Formulation of ciprofloxacin-containing composite foams. ....	152
4.2.3.	Qualitative analysis of composite materials. ....	153
4.2.4.	Optical properties of film formulations. ....	154
4.2.5.	Semi-quantitative analysis of the mechanical strength of foam materials. ....	154
4.2.6.	FTIR analysis of films and foam formulations. ....	155
4.2.7.	XRD analysis of films and foam formulations. ....	155
4.2.8.	Thermal analysis of films and foam formulations. ....	156
4.2.9.	Water vapour permeability of film and foam formulations	156

4.2.10. Behaviour of film and foam formulations in a synthetic wound environment. ....	157
4.2.10.1. Swelling behaviour of formulations on the synthetic wound surface. ....	158
4.2.10.2. Adherence of formulations to the wound surface. ....	159
4.2.11. Ciprofloxacin-release profiles from film and foam formulations. ....	159
4.2.12. Antimicrobial properties of film and foam formulations. . .	161
4.2.13. Cytotoxicity (keratinocyte cell viability) studies of film and foam formulations. ....	161
4.2.14. Statistical analysis. ....	163
4.3. Results and discussion. ....	164
4.3.1. Evaluation and selection of an ideal film formulation. ....	164
4.3.1.1. Qualitative analysis of pre-formulation film materials. ....	164
4.3.1.2. Qualitative evaluation of ciprofloxacin-containing films. ....	171
4.3.1.3. Optical properties of film formulations. ....	173
4.3.2. Evaluation and selection of an ideal foam formulation. ....	178
4.3.2.1. Qualitative analysis of pre-formulation foam materials. ....	178

4.3.2.2.	Qualitative evaluation of ciprofloxacin-containing foam materials.....	183
4.3.2.3.	Semi-quantitative analysis of the mechanical strength of foam materials.....	185
4.3.3.	FTIR analysis of films and foam formulations.....	188
4.3.4.	XRD analysis of film and foam composites.....	195
4.3.5.	Thermal analysis of film and foam formulations.....	199
4.3.6.	Water vapour permeability of film and foam formulations	207
4.3.7.	Swelling behaviour of formulations on the wound surface	212
4.3.8.	Adherence of formulations to the wound surface.....	218
4.3.9.	Drug-release profiles.....	222
4.3.10.	Antimicrobial properties.....	227
4.3.11.	Keratinocyte cell viability.....	231
4.4.	Conclusions.....	235
4.5.	References.....	237
<b>5.</b>	<b>Concluding remarks &amp; future directions.....</b>	<b>247</b>
5.1.	References.....	254
<b>Appendix I – Posters presented at conferences.....</b>		<b>257</b>

## Acknowledgements

I would like to thank my supervisory team, Dr Elsie Gaskell, Dr Matthew Roberts, and Dr Gillian Hutcheon, for all their support and input throughout this research project. I would especially like to thank Elsie for all her wisdom, encouragement and patience over the past 5-years. Thank you for keeping me sane.

Thank you to all the staff within the school of pharmacy and biomolecular sciences for support with equipment and techniques. Particular thanks are extended to Dr Nicola Dempster, Philip Salmon, Campbell Woods, and Dr Andrew Evans.

My sincerest gratitude is given to Jane Doyle and David Shaw from BYK Additives for their insight and extensive knowledge around phyllosilicates and letting me make my own batch of Laponite®. Thank you to Maurice for letting me utilise your network of colleagues, this was invaluable for applying isotherm models to this research.

I would also like to say thank you to my fellow *Room2.09* postgraduate students Nitesh, Alessandro, Francesco, Massimo, Adel, and Nashwa for all your moral support during my time at LJMU.

Finally, I could not have gotten through this process without the support of my family. I would especially like to thank Neil Mawby for all his support over the past year and making sure I have the time and freedom to sit down and write!

## List of abbreviations

Å	Ångström (1 Å= 0.1 nm)
AAC	Acetic acid
Alg	Alginate
ATR	Attenuated Total Reflection
BNF	British National Formulary
BSA	Bovine serum albumin
CAN	Acetonitrile
CEC	Cation exchange capacity
CFU	Colony Forming Unit
CIP	Ciprofloxacin
CM	Clay mineral
DC	Doxycycline
DH	Department of Health
DMEM	Dulbecco's Modified Eagle Medium
DNA	Deoxyribonucleic acid
EDTA	Ethylene-diamine-tetraacetic acid
FTIR	Fourier-transform Infrared Spectroscopy
GLY	Glycerol
HaCaT	Keratinocyte cell line
HPLC	High Performance Liquid Chromatography
HVAlg	High viscosity alginate
KN	Kaolin
LRD	Laponite® RD
LVAIg	Low viscosity alginate
LXL21	Laponite® XL21
MDR-TB	Mutli-drug-resistant Tuberculosis
mEq	Milli equivalents
MMTK10	Montmorillonite K-10
MRSA	Methicillin resistant <i>Staphylococcus aureus</i>

MTT	3-(4,5-dimethylthiazol-2-yl)-2,5-diphenyl tetrazolium bromide
MVAIg	Medium viscosity alginate
NaCl	Sodium Chloride
NCTC	National Collection of Type Cultures
NHS	National Health Service
NICE	National Institute of Health and Care Excellence
PBS	Phosphate buffered saline
PVA	Polyvinyl alcohol
rMMT	Refined Montmorillonite
rpm	Revolutions per minute
RPS	Royal Pharmaceutical Society
SD	Standard deviation
SEM	Scanning electron microscopy
SSA	Specific Surface Area
SSSI	Skin and Skin-structure infections
SSTI	Skin and Soft tissue Infections
SWF	Synthetic wound fluid
TC	Tetracycline
TEM	Transmission electron microscopy
TGA	Thermogravimetric analysis
UV-Vis	Ultraviolet- Visible spectrophotometry
WHO	World Health Organisation
WVTR	Water vapour transmission rate
XRD	X-Ray diffraction

# Publications and disseminations from this research project

## **Original research papers**

Hamilton, R., Hutcheon, G.A., Roberts, M., Gaskell, E.E. (2014) Formulation and antibacterial properties of clay-ciprofloxacin composites. *Applied Clay Science* 87:129-135

## **Review articles**

Gaskell, E.E., Hamilton, R. (2014) Antimicrobial clay-based materials for wound care. *Future Medicinal Chemistry*, 6(6):641-655

## **Oral presentations**

Hamilton, R. (2014) Development and evaluation of antibacterial polymer-phyllosilicate composite systems for the treatment of infected wounds, Presented at the 51st Annual Meeting of the Clay Minerals Society, Texas A&M University, College Station, Texas, USA, 20<sup>th</sup> May 2014.

Hamilton, R., Roberts, M., Hutcheon, G., Gaskell, E.E. (2013) An investigation of ciprofloxacin adsorption onto clays for optimal drug release, Presented at the LJMU Faculty of Science Research Seminar, Liverpool John Moores University, UK, 12th June 2013.

## **Poster presentations**

Hamilton, R., Roberts, M., Hutcheon, G.A., Gaskell, E.E. (2014) The development of novel antimicrobial polymer-clay composite systems, Presented at the 51st Annual Meeting of the Clay Minerals Society, Texas A&M University, College Station, Texas, USA, 20<sup>th</sup> May 2014.

Hamilton, R., Bonenfant, O., Roberts, M., Hutcheon, G., Gaskell, E.E. (2012) The antimicrobial properties of montmorillonite and Laponite<sup>®</sup> composites containing tetracycline and ciprofloxacin, Presented at PharmSci 2012, Nottingham, UK, 13th September 2012.

Hamilton, R., Bonenfant, O., Roberts, M., Hutcheon, G., Gaskell, E.E. (2012) The antimicrobial properties of clay composites containing tetracycline and ciprofloxacin, Presented at the 6th Mid-European Clay Conference, Průhonice, Czech Republic, 4th-9th September 2012.

Gaskell, E.E., Hamilton, R., Hutcheon, G., Roberts, M. (2012) Antibacterial properties of Cu- and Zn-exchanged Laponites<sup>®</sup>, Presented at the 6th Mid-European Clay Conference, Průhonice, Czech Republic, 4th-9th September 2012.

Hamilton, R., Roberts, M., Hutcheon, G., Gaskell, E.E. (2012) An investigation of ciprofloxacin adsorption onto clays for optimal drug release, Presented at the Salford Postgraduate Annual Research Conference, Salford University, UK, 30th-31st May 2012.



Hamilton, R., Roberts, M., Hutcheon, G., Gaskell, E.E. (2012) An investigation of ciprofloxacin adsorption onto clays for optimal drug release, Presented at the LJMU Faculty of Science Research Seminar, Liverpool John Moores University, UK, 9th May 2012.

Hamilton, R., Roberts, M., Hutcheon, G., Gaskell, E.E. (2012) Utilising montmorillonite K-10 and Laponite® for delivery of ciprofloxacin. Presented at the UK & Ireland Controlled Release Society, Aston University, UK, 2nd May 2012.

## Abstract

Clays and clay minerals (phyllosilicates) have been used for millennia to treat a range of human maladies, such as infected wounds and diseases of the skin. The unique chemistry of phyllosilicates allows them to support the wound environment and encourage healing. Their physicochemical properties can also be utilised to develop modified drug-release formulations and also enables their incorporation into polymer matrices for the development of advanced wound care materials. By developing novel antibacterial phyllosilicate-polymer composite materials it should be possible to support wound healing, whilst simultaneously treating infections locally to avoid systemic adverse effects and prevent the development of antimicrobial resistance.

In this research project the clay minerals kaolin (KN), refined montmorillonite (rMMT), montmorillonite K10 (MMTK10), Laponite® RD (LRD), and Laponite® XL21 (LXL21) were investigated for their differing structure and physicochemical properties. Their ability to adsorb and desorb the antibacterial agents tetracycline (TC), doxycycline (DC) and ciprofloxacin (CIP) was determined through a series of adsorption kinetics and isotherm studies. LRD and LXL21 were shown to have the highest drug-carrying capacity and were also able to relinquish this drug-load to inhibit the proliferation of key wound pathogens; *Staphylococcus epidermidis*, *Propionibacterium acnes*, and *Pseudomonas aeruginosa*. XRD and FTIR analyses demonstrated that these drug molecules could be adsorbed into the interlayer space and edge groups of the Laponite® particles.

LXL21-CIP composites were successfully incorporated into alginate polymer matrices through interaction of the exposed edge-groups on LXL21 and the hydroxyl groups of the alginate to produce novel nanocomposite film and foam materials. Selection of candidate materials was initially undertaken qualitatively with the support of a tissue viability nurse at the Royal Liverpool and Broadgreen University Hospitals NHS Trust. Important properties for wound-dressings such as adsorptive capacity, water vapour transmission rate, and keratinocyte compatibility were measured quantitatively and compared to materials already used for wound care in the UK. Both the film and foam materials were shown to have properties that would be beneficial for wound healing and were also able to release CIP in a controlled manner with notable activity against *S. epidermidis*, *P. acnes*, and *P. aeruginosa*.

The nanocomposite film formulation developed in this research project showed promise for future clinical applications and future work should be undertaken to further optimise their manufacture and fully characterise their ability to support the healing of infected wounds. Although the nanocomposite foams require further research, the work presented in this thesis suggests they could also be promising materials for wound care applications.

# Chapter 1

## Introduction

### 1.1. A brief history of clay minerals in health

Clays have been used for health purposes throughout ancient and modern history in many forms and applications (Gaskell and Hamilton, 2014). Of note, and possibly the oldest application, is their use in the treatment of skin conditions and wounds.

There is tentative evidence that *Homo neanderthalensis*, and later *Homo erectus*, utilised earths for the treatment of wounds and the management of skin irritations (Carretero, 2002; Dawson and Oreffo, 2013). It has been postulated that these early humans learned this behaviour from other primates who are still observed applying muds and clays to their skin. In modern science it is well noted that many animals ingest clays for numerous perceived health benefits (Newton, 1991; Slamova et al., 2011; Williams and Haydel, 2010). This *geophagy* was also practiced widely amongst human populations across the globe and even though its popularity has diminished within modern healthcare it still remains a traditional therapy within various cultures (Kikouama and Balde, 2010; Vermeer and Ferrell, 1985).

Some of the most ancient uses of clay are believed to have taken place in Mesopotamia over 4000 years ago (Carretero, 2002; Gomes and Silva, 2007; Rytwo, 2008). During the spread of mankind across the globe the practice of using clays, muds, and earths in the treatment of skin conditions and wounds continued. The Ancient

Egyptians are well known for their interest in complex therapies and it should come as no surprise that they developed medicaments and cosmetics from clays and muds (Rytwo, 2008). The *Papyrus Ebers* details a wide range of uses for clays within Egyptian healthcare and it has also been documented that Nubian Earth was utilised as an anti-inflammatory (Bryan, 1930; Carretero, 2002; Gomes and Silva, 2007).

Ancient Greek and Roman civilisations, credited for their scientific and medical intuition, also found uses for clays in healthcare (Bunnell et al., 2007; Gomes et al., 2013). Whilst clays and muds could possibly have been considered a panacea it is known that specific applications were developed for the management of wounds. Of note are the works of the Greek physician Galen, who in the second century, developed *terra sigillata*; red earth found on the island of Lemnos, which was shaped and stamped with the imprint of the Goddess Diana (Dannenfeldt, 2012). The use of *terra sigillata* spread across Europe and was still popular during the sixteenth century. This resulted in many countries sourcing clays from local deposits and developing their own versions of the *terra sigillata* and the respective seals, which continued into the early seventeenth century (Dannenfeldt, 2012).

The 1618 edition of the *Pharmacopoeia Londinensis* contained monographs on earths from Lemnos and Malta, alongside the later *terra Silesiaca* [sic]. In the eighteenth century there were around thirty of these sealed earths available across Europe but their popularity was minimal compared to the original terrae. Paracelsus and paracelsian physicians became eager to understand how treatments and medicines worked through experimentation, observation, and understanding – something that

misaligned to the traditional uses of *terra sigillata* and *terra Silesiaca* (Dannenfeldt, 2012).

During the Renaissance periods the culture of spas and bath houses blossomed and their popularity continued well into the nineteenth and twentieth centuries (Gibson, 1954; Jackson, 1990; Palmer, 1990; van Tubergen and van der Linden, 2002). As well as offering visitors the opportunity to bathe in “natural” and “mineral” waters the bath houses also offered therapies utilising muds and sediments (Palmer, 1990; van Tubergen and van der Linden, 2002). In Britain the popularity of the baths and spas declined in the first quarter of the twentieth century until the industry finally collapsed when the National Health Service excluded spa therapy as a treatment option (van Tubergen and van der Linden, 2002). Pelotherapy, which is the application of matured muds and clays to the skin (Carretero and Lagaly, 2007; Carretero, 2002; Gomes et al., 2013; Tateo and Summa, 2007; Tateo et al., 2009; Viseras et al., 2007), developed as a discipline during the twentieth century but has been viewed mainly as a cosmetic investment rather than a clinical intervention. Regardless of this, the demand for health spas and their respective therapies has increased over the past twenty-five years and it has developed into a successful industry once more. One study into the use of mud packs in rheumatoid arthritis (Sukenik et al., 1990) produced inconclusive results and more robust trials are needed before the value of such therapies are truly determined.

Regardless of this lack of evidence clays continue to be utilised in the formulation of modern medicines and are detailed within early pharmacopoeia and pharmaceutical

codexes (Pharmaceutical Society of Great Britain, 1911, 1907), where they are still listed for modern use. *Calamine lotion*, containing bentonite (British Pharmacopoeia Commission, 2017a), and *Kaolin Poultice* (British Pharmacopoeia Commission, 2017b) for example, still remain within the current British Pharmacopoeia but for the most part clays are used as excipients within oral formulations as swelling agents, disintegrating agents, and lubricants (Carretero, 2002; Carretero and Pozo, 2009; Rodrigues et al., 2013; Viseras et al., 2010).

Academic research of clays and clay-minerals has grown in recent years and a small number of teams are looking at the antimicrobial and healing properties of clays, with others investigating the possible application of clays and clay minerals for wound care. Knowledge of the physicochemical properties of clay-minerals is vital for understanding their potential application in the management of infected wounds and skin and skin-structure infections.

## **1.2. The physicochemical properties of clay minerals**

### *1.2.1. Structure and chemistry of clay mineral layers*

Phyllosilicates are layered materials with a unique structure and chemistry. Each individual layer is formed of characteristic sheets that can be categorised into two distinct types: tetrahedral silicon oxide sheets and octahedral metal hydroxide sheets (Bergaya and Lagaly, 2013; Brigatti et al., 2013).

The tetrahedral sheet is generally made of silicon oxide arranged in a tetrahedral formation (figure 1.1 A). The tetrahedra arrange themselves by joining at the corners

to share basal oxygen atoms with their neighbouring tetrahedra. When six of these tetrahedra come together they form a distinct hexagonal-ring pattern. These rings can be seen throughout the continuous silicon oxide sheet, as represented in figure 1.1 B (Brigatti et al., 2013). The second type of sheet within the phyllosilicate layers is the metal hydroxide octahedral sheet. The individual units of this sheet comprise a multivalent metal ion in coordination with six hydroxyl groups, in octahedral formation (figure 1.1 C). This central metal ion is commonly  $Mg^{2+}$ ,  $Fe^{2+}$ ,  $Fe^{3+}$  or  $Al^{3+}$ . The individual units align alongside each other and undergo edge oxygen sharing to form a tight, continuous, octahedral sheet as depicted in figure 1.1 D (Brigatti et al., 2013).

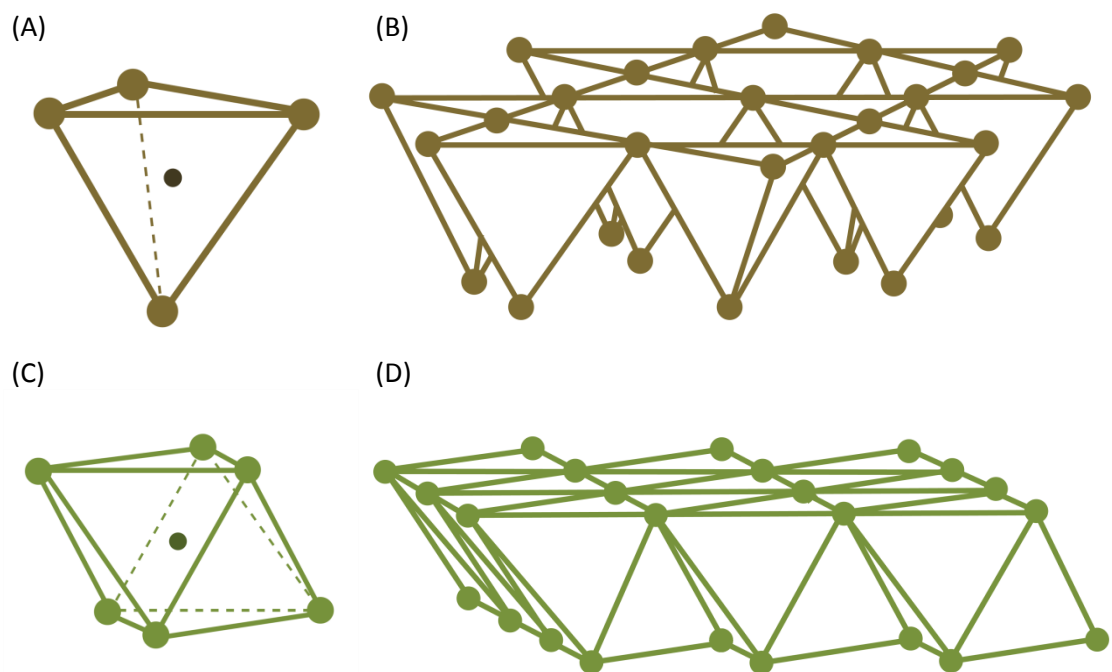


**Figure 1.1.** Diagrams representing the atomic arrangements within phyllosilicates, rather than the individual bonds present. Individual silicon oxide tetrahedra (A) arrange via corner-sharing in ring-like arrangements to form a continuous tetrahedral sheet (B). The individual metal hydroxide octahedra (C) align through edge-sharing to form a continuous octahedral sheet (D).



The valence of the cations within the octahedral sheet plays a very important role in its chemistry and structure; dictating whether the sheet is classified as trioctahedral or dioctahedral. If the valence is equivalent to II (e.g.  $\text{Mg}^{2+}$  or  $\text{Fe}^{2+}$ ) then the sheet will assume a trioctahedral formation, whereby every position in the sheet is occupied by a complete octahedron with central cation. However, if the valency of the cations within the sheet is equivalent to III (e.g.  $\text{Fe}^{3+}$  or  $\text{Al}^{3+}$ ) then the overall sheet will become dioctahedral. For every two fully occupied octahedra within a dioctahedral sheet, one position will not have a central cation (Swartzen-Allen and Matijevic, 1974). This does not affect the overall structure of the sheet, when considering the arrangement of oxygen atoms, but has a profound effect on the overall charge of the sheet, and thus the phyllosilicate layer.

In order for the phyllosilicate layers to be formed these two sheets need to join together and they do so through a condensation reaction and thus further oxygen sharing. The apical oxygen atoms of the tetrahedra are thusly shared with the corresponding points on the octahedral sheet, so that the basal oxygen atoms become the outward facing surface (Bergaya and Lagaly, 2013). If any of the oxygen atoms within the octahedral sheet are not shared with the tetrahedral sheet they can present themselves as hydroxyl groups instead. Positions where this is likely to occur are in the centre of the tetrahedral ditrigonal ring structure, at the edges of the sheet, and where the octahedral sheet only binds to one tetrahedral sheet.

If a layer consists of only one tetrahedral sheet bound to one octahedral sheet this phyllosilicate structure is known as a 1:1 layer (figure 1.2 A). However, it is possible for

two tetrahedral sheets to sandwich an octahedral sheet, which is referred to as a 2:1 layer (figure 1.2 B) (Konta, 1995). These layers often form disc-like shapes and their size can also be highly variable. For example, the synthetic clay mineral Laponite® is classified as a nano-material as the diameter of the layers is around 20-30 nm (Avery and Ramsay, 1986; Daniel et al., 2008; Pálková et al., 2010). This is in contrast to the natural clay minerals kaolin and montmorillonite, which can have a layer-diameter greater than 200 nm (Aochi and Farmer, 2011; Paineau et al., 2011b; Poli et al., 2008).

The differences between the chemistry of 1:1 and 2:1 layers is particularly interesting and can have a profound effect on the overall behaviour of the clay mineral that they form. When considering the structure of the individual sheets and layers, the most important property the chemistry affects is the charge of the layer.

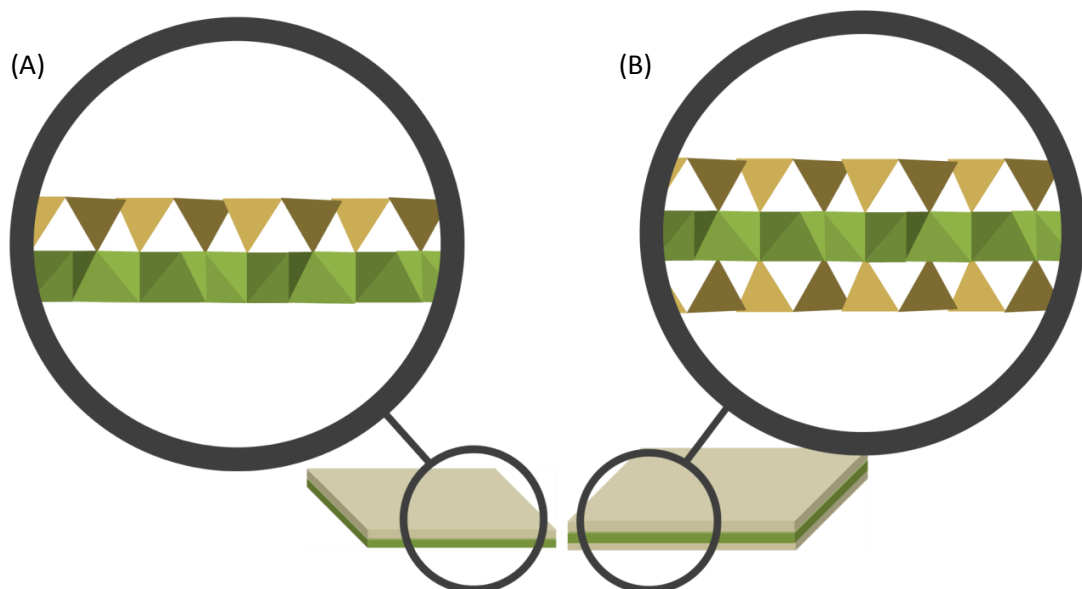


**Figure 1.2.** Artistic representation of a 1:1 clay mineral particle (A) and a 2:1 clay mineral particle (B). The magnifications show how the tetrahedral sheets (brown triangles) and octahedral sheets (green continuous layer) condense to form the phyllosilicate layers.

The process of isomorphic substitution can take place in both the tetrahedral and octahedral sheets, causing a charge deficiency across the phyllosilicate layer (Swartzen-Allen and Matijevic, 1974). Within the tetrahedral sheet the  $\text{Si}^{4+}$  atoms are able to be substituted for cations of lower charge. This process is more common within the octahedral sheet where  $\text{Fe}^{3+}$  or  $\text{Al}^{3+}$  cations may be substituted for cations of lower valence, such as  $\text{Fe}^{2+}$  or  $\text{Mg}^{2+}$ . These substitutions lead to what is described as a charge deficiency across the phyllosilicate layer, which manifests as a negative charge on the faces of the layers (Aochi and Farmer, 2011; Czímerová et al., 2006; Madejova, 2003). The 1:1 clays are generally neutral in nature, or have a very minimal surface charge. The 2:1 clays on the other hand may exhibit high degrees of surface charge. This is not the only mechanism by which a negative charge can be formed; missing cations from trioctahedral sheets can also lead to an increased negative charge at the layer surface (Brigatti et al., 2013).

The edges of clay-mineral particles are characterised by exposed hydroxyl groups from the metal-hydroxide sheet, but also the formation of SiOH groups where the silicate sheet discontinues (Czímerová et al., 2006; Daniel et al., 2008; Swartzen-Allen and Matijevic, 1974). These edge groups are important as their charge is pH dependant, with their pKa determined by the wider clay-mineral structure. For example, the edge groups on Laponite<sup>®</sup> are generally positively charged below pH 9 (Daniel et al., 2008) and become increasingly negatively charged above this pH. It is this mix of negatively charged surfaces and positively charged edges that give phyllosilicate materials their unique surface and colloidal properties (section 1.2.3).

Not all phyllosilicate layers form into disc-like shapes or form particles. One example of such minerals is palygorskite, which is termed a modulated clay mineral. Instead of forming disc-like structures, these modulated clay minerals, display regular inversions of the phyllosilicate layer, which leads to the development of ribbon-like structures (Lopez-Galindo et al., 2007; C Viseras et al., 2007; White and Hem, 1983). These modulated phyllosilicates are sometimes referred to as fibrous clay minerals (Tateo and Summa, 2007). Halloysite is another phyllosilicate that does not form disk-like structures but forms tubular structures with a lumen in the nanometre scale (Aguzzi et al., 2007; Konta, 1995). These nanotubes have received much attention in recent years for a number of applications including drug delivery.

### *1.2.2. Layer arrangement and particle formation*

Clay mineral layers do not remain in isolation in dry powder (as described here) or when in aqueous dispersion (see section 1.2.3), but instead form associations with each other.

The 1:1 layers form direct associations with each other through hydrogen bonding between the tetrahedral sheet of one layer and the octahedral sheet of an adjacent layer (Miranda-Trevino and Coles, 2003). This strong association results in very small gallery heights, which is also termed the interlayer space (figure 1.3 A). Measurements of the interlayer space of 1:1 clay minerals, such as kaolin, have shown the gallery height to be as small as 7Å (Konta, 1995).

In contrast to this, the 2:1 phyllosilicate layers have a tendency to repel each other due to the negative charge of both layer surfaces. To overcome this repulsion inorganic cations (e.g.  $\text{Na}^+$  and  $\text{Ca}^{2+}$ ) present in the interlayer space counterbalance the negative charge (figure 1.3 B) (Konta, 1995; Madejova, 2003). The abundance of these cations is determined by the charge distribution across the layer surfaces and the contents of the phyllosilicate layers. Isomorphic substitution within the tetrahedral and octahedral sheets is able to alter the species of the cations present within the interlayer space (Brigatti et al., 2013). Counterbalancing cations present within the interlayer space of 2:1 clay minerals allow the phyllosilicate layers to form stacks, and therefore particles. They increase the size of the interlayer space, which has been reported as  $10\text{\AA}$  (Konta, 1995). It is also important to note that these interlayer cations may be either hydrated or dehydrated, dependant on the clay mineral, its surrounding environment, and the nature of the cations themselves. Cations with a hydrated shell, such as  $\text{Na}^+$  and  $\text{Ca}^+$ , can take up more space and have been shown to increase the interlayer space between phyllosilicate layers to  $15\text{\AA}$  (Konta, 1995).

These interlayer, counterbalancing, cations play an important role in clay mineral properties, having an effect on their swelling capacity and electrochemistry. It is also possible for these endogenous cations to be exchanged for exogenous inorganic and organic cations. This is known as the cation exchange capacity (CEC) of clay minerals and is quantified as milliequivalents per unit mass of clay mineral (generally  $\text{mEq}/100\text{g}$ ).

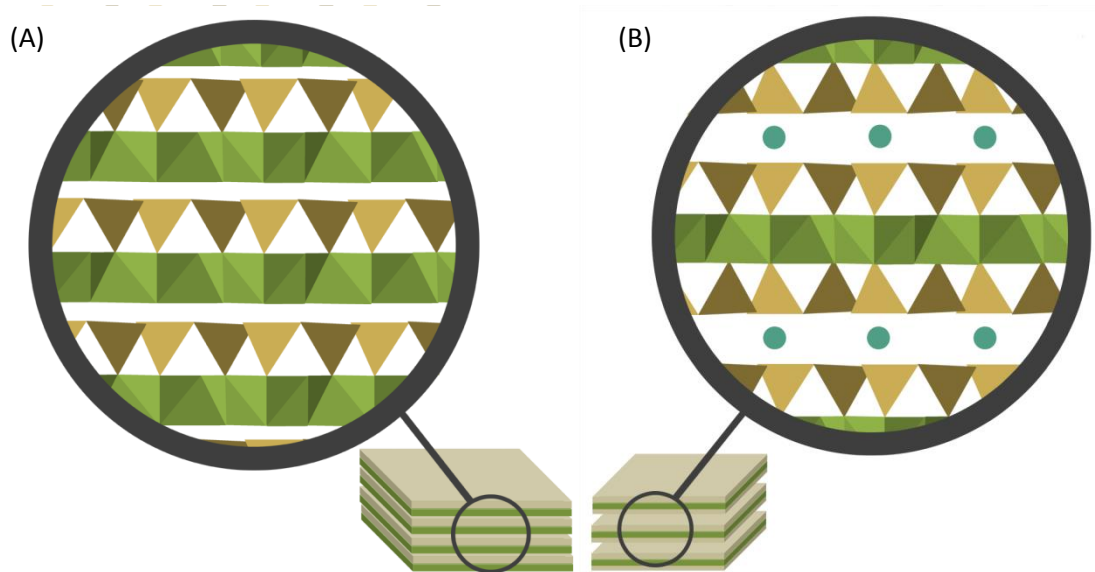


**Figure 1.3.** Artistic representation of the layer arrangement within a 1:1 clay mineral particle (A) and a 2:1 clay mineral particle (B). The magnifications demonstrate the differences in interlayer space between these clay mineral species, with the teal circles representing the counterbalancing cations within the 2:1 clay mineral interlayer space.

One species of 2:1 clay mineral that has a slightly different interlayer chemistry are the chlorites. Instead of having individual inorganic cations to balance the negative surface charge of the phyllosilicate layer, the chlorites have a single octahedral metal hydroxide sheet within the interlayer space, which counterbalances the phyllosilicate layer charge (Konta, 1995). The metal within this hydroxide sheet is generally magnesium. Because of this unique structure chlorites are sometimes defined as 2:1:1 clay minerals.

It is also possible to obtain clay minerals that contain a mixture of phyllosilicate layers, which are termed interstratified clay minerals, and are common in nature (Drits, 2003). These interstratified minerals may contain mixtures of just 2:1 layers, or may contain

mixtures of 1:1 and 2:1 layers. One example is the 1-1 montmorillonite-kaolinite interstratified clay mineral, which contains equal proportions of montmorillonite (2:1) layers and kaolinite (1:1) layers (Plancon, 2001). As can be expected, differing proportions of each clay mineral are possible and their distribution throughout the mineral may not be uniform – all of which can affect the properties of an interstratified clay (Drits, 2003).

As figure 1.4 shows, phyllosilicate particles (of both 1:1 and 2:1 clay minerals) are able to associate with other phyllosilicate particles to form aggregates. Dependant on the arrangement of these particles it is possible for small interparticulate spaces to be formed. More particles may interact with these aggregates and, in turn, aggregates can associate with each other to form an assembly of aggregates resulting in visible particles that can be seen with the naked eye.

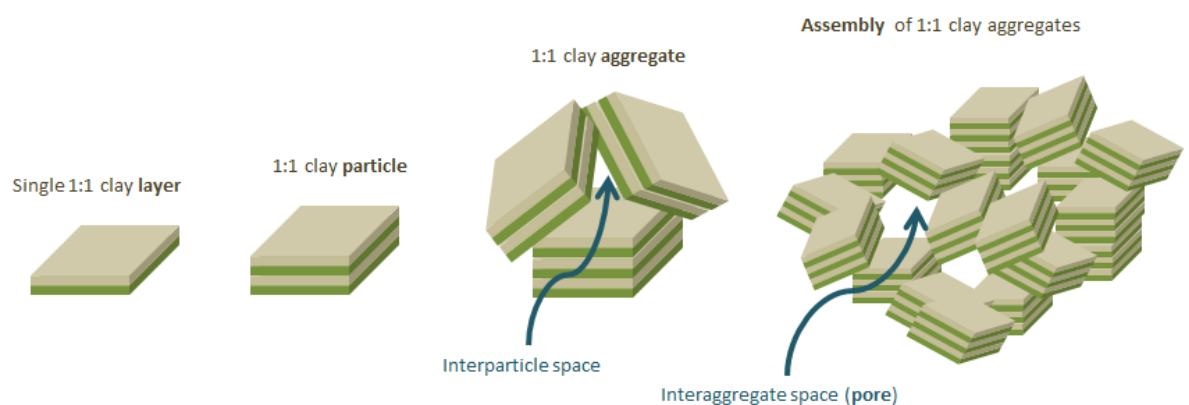


**Figure 1.4.** Artistic representation of how individual phyllosilicate layers come together to form particles, which further associate to form aggregates and then assemblies.

Larger gaps can occur between these associated aggregates to form interaggregate spaces, which are more commonly known as pores. It is possible to break up these assemblies into smaller aggregates through milling and sieving; a process regularly used by clay scientists to obtain particle sizes smaller than 2  $\mu\text{m}$  for further characterisation.

The phyllosilicate sheet and layer structures are crystalline in nature, and this often leads to them being termed as microcrystalline minerals. This crystallinity and the relative regularity of layer stacking within a particle, leads to indicative peaks on an X-ray diffractogram (XRD). However, as shown in figure 1.4, the subsequent association of these particles into aggregates is often random, leading to an overall irregular structure. Whilst peaks present on XRD diffractograms can be used to determine layer type and interlayer spacing, these peaks are not representative of a fully crystalline material, and indeed produce diffractograms reminiscent of amorphous materials.

### *1.2.3. Behaviour in dispersion*

The behaviour of clay minerals in aqueous environments has intrigued scientists for generations and has been the main drawing point for their use across history. Regardless of their structure, all clay minerals are considered hydrophilic.

The 1:1 clay minerals, due to the way their layers interact, do not swell readily and therefore do not disperse fully. For this reason their surface area is restricted to the outside of the particles. This lack of dispersion also means that 1:1 clay mineral particles will quickly sediment out of dilute dispersions without continuous agitation.



Fibrous and modulated clay minerals swell but not in the same way as the layered 2:1 particles because of a reduced reliance on the interlayer cations. In aqueous dispersions the fibrous clays interact with each other and form tangles to create a complex matrix with interspersed water. This behaviour allows the modulated clay minerals to swell to some extent and also create viscous gels. In general, it is the layered 2:1 clay minerals that have received the greatest interest from research teams, and it is also these clays that demonstrate the most interesting, and complex, chemistry in aqueous environments.

Swelling is often initiated through the direct interaction of the clay mineral surface and water molecules and also the interaction between the counterbalancing cations and water molecules (Hensen and Smit, 2002; Paineau et al., 2011a). Due to the nature of the charge distribution across the phyllosilicate layer the adsorption of water onto the surface of the clay is highly regular and many of the free-flowing, liquid, properties of water are diminished. The interlayer cations also form a hydration shell around themselves, thus increasing their overall diameter and the size of the space between the phyllosilicate layers. Once this initial process has been completed additional water molecules are recruited to the clay mineral surfaces and into the interlayer space, but in a less ordered fashion. Indeed, the regularity imposed on the water molecules, by the phyllosilicate layers and the counterbalance cations, diminishes the further away the water molecules are from these components. These two very different processes have led to the swelling of 2:1 clay minerals being described as proceeding with two different phases. The first is the crystalline swelling phase, relating to the ordered recruitment of water molecules, and the second as osmotic swelling, which relates to

the less restrictive recruitment of water molecules by the clay mineral (Hensen and Smit, 2002).

Swelling of 2:1 clay minerals exposes their internal surfaces and has a great effect on the overall surface area of the clay minerals. Expansion of the clay mineral interlayer space allows for the high aspect ratio of the phyllosilicate layers to be fully appreciated and minerals such as montmorillonite can display a surface area in the region of 500-700 m<sup>2</sup>/g (Chen et al., 1999; Kahr and Madsen, 1995).

The crystal and osmotic swelling phases are also important determinants of the electrochemical environment at the clay mineral surface in dispersion. The negatively charged surface of the phyllosilicate layer allows for the attraction of positive ions towards the surface, including counterbalancing cations and protons (H<sup>+</sup>) from the aqueous environment. This concentration of cations at the surface of the clay mineral is often referred to as the stern layer. This is accompanied by a decreasing cation concentration gradient as the distance from the phyllosilicate surface increases. This phenomenon is often described as the diffuse double layer theory.

However, the concentration of cations at the clay mineral surface does not make it impervious to the effects of protons. If the pH of the dispersion is decreased so that it is highly acidic (pH < 2) the protons can actually attack the phyllosilicate structure. The H<sup>+</sup> ions are able to infiltrate the octahedral sheet and hydrolyse the metal-oxide bonds present, thus causing dissolution of the metal cations from the octahedral sheet into the surrounding environment (Pentrák et al., 2012; Tyagi et al., 2006). Progressive

dissolution of the octahedral layer can result in an amorphous silica sheet as the remaining product (Pentrák et al., 2012).

The negatively charged surfaces, the positively charged edges, the diffuse double layer, interlayer friction and van der Waals forces all play important roles in how clay minerals behave in aqueous dispersions. As the dispersion becomes more dilute the osmotic swelling of the clay mineral layers continues until the layers are so far apart (greater than 4 nm) they dissociate from each other, a process often called exfoliation.

Initially, swelling clays can form gels as the interactions between the layers are still strong enough for a weak structure to be created. This can be achieved through face-to-edge, face-to-face and edge-to-edge interactions between the clay mineral layers. It can also be achieved through a balance between the attractive effects of van der Waals forces and the repulsive effects of the diffuse double layer (Paineau et al., 2011a). Face-to-edge interactions have been recognised as the most likely interactions in place when clay minerals form gel-like dispersions at neutral pH. A large network of face-to-edge interactions can form a 3D matrix which is referred to in the literature as the house of cards formation (Mongondry et al., 2005; Paineau et al., 2011a). These gels are often stable for long periods. An interesting, and attractive, property of gels formed from 2:1 clays is they often show non-Newtonian flow properties; so that when shaken the kinetic energy provided is great enough for the structure of the gel to break down and form a free flowing dispersion. Once energy is removed (shaking is stopped) the phyllosilicate layers will re-associate and the gel will be reformed as a product of time (Carretero and Pozo, 2009; Lopez-Galindo et al., 2007).

As the dispersion becomes even more dilute the repulsive forces between the phyllosilicate layers (driven by the diffuse double layer) prevent the layers from interacting with each other and instead of forming a gel they form a disperse *sol* (Carretero and Pozo, 2009). When phyllosilicate layers exfoliate and disperse in this manner they remain in a colloidal dispersion due to thermodynamic balance (Lagaly and Ziesmer, 2003).

#### *1.2.4. Interaction with charged molecules*

The presence of permanent and variable charges across the phyllosilicate makes for interesting interactions with charged molecules when in dispersion. One of the most commonly reported processes involves the interlayer cations and their exchange with other cations. For example, a montmorillonite with  $\text{Na}^+$  as its interlayer cation may exchange these sodium cations for other inorganic cations such as  $\text{Ca}^{2+}$ ,  $\text{Mg}^{2+}$ ,  $\text{Cu}^{2+}$ ,  $\text{Zn}^{2+}$ ,  $\text{Ag}^+$ , etc. (Swartzen-Allen and Matijevic, 1974; Top and Ülkü, 2004). However, the cation exchange process is not only limited to inorganic cations but may also occur if organic cations are present within the dispersion (Swartzen-Allen and Matijevic, 1974).

Small organic molecules (including drug molecules) that bear a positive charge are able to interact well with the clay mineral surfaces and displace the interlayer cations (Chang et al., 2009). It is well documented that clay minerals within soils are able to adsorb antibacterial agents from the environment (Figueroa-Diva et al., 2010; Figueroa et al., 2004; Kulshrestha et al., 2004). A number of research teams have also reported the interaction between clay minerals and amino acids, how this may facilitate their

functionality and reactivity (Greenland et al., 1965), and may even have contributed to the creation of life on Earth (Brack, 2013).

When cations and cationic molecules interact with the clay mineral surfaces they can cause the stern layer to become compressed towards the clay mineral surface. This causes the depth of the stern layer, and thus the size of the diffuse double layer, to reduce in size. Increased adsorption of cations will eventually lead to the repulsive forces produced by the diffuse double layer being smaller than the attractive forces brought around by van der Waals forces and inter-layer friction. Once this occurs the clay mineral layers attract each other, associate with each other and coagulate within the dispersion (Lagaly and Ziesmer, 2003; Swartzen-Allen and Matijevic, 1974). This phenomenon is often called the flocculation-point and refers to the cation concentration required to cause the clay mineral to overcome thermodynamic stability and flocculate out of dispersion. Cations of higher charge have more profound effects upon the diffuse double layer and this can be related directly to valance. For example, much more  $\text{Na}^+$  than  $\text{Ca}^{2+}$  is needed to flocculate a clay mineral, whereas less  $\text{Al}^{3+}$  than  $\text{Ca}^{2+}$  is needed to flocculate a clay mineral (Lagaly and Dekany, 2013; Swartzen-Allen and Matijevic, 1974).

Anionic components also play an important role within clay mineral dispersions, which are able to adsorb onto the edges of clay mineral layers. Adsorption of anions onto these side groups can result in an overall negative charge across the clay mineral layer, thus leading to an increasingly stabilised colloidal dispersion (Lagaly and Ziesmer, 2003; Swartzen-Allen and Matijevic, 1974). Anions are also able to interact with the

interlayer counterbalancing cations and these contribute to the diffuse double layer (Swartzen-Allen and Matijevic, 1974).

It is not just small organic molecules that are able to interact with the clay mineral surfaces, as charged groups belonging to larger constructs may also interact with the clay mineral surface. For example, clay minerals are able to adsorb proteins onto their surfaces (Cai et al., 2006; Cengiz et al., 2012; Greenland et al., 1965), and may themselves become adsorbed onto the surface of bacterial cells where they may immobilise and inhibit bacterial growth, or indeed enhance the growth of the cells to which they are adsorbed (Rong et al., 2008; Williams et al., 2011; Zhao et al., 2012; Zhou et al., 2010). As well as cellular proteins clay minerals are able to adsorb free moving proteins from dispersions including toxins, enzymes, and waste materials (Carretero, 2002; Deng et al., 2010; Sandri et al., 2016).

### **1.3. Modifying clay minerals**

Section 1.2 discussed how clay mineral layers behave in dispersion, what natural phenomena change the structure, chemistry, and colloidal behaviour of the clay mineral layers, and also what other components within the dispersion can interact with the clay mineral layers. With knowledge of how these natural phenomena can affect clay minerals it is possible to purposefully make modifications to clay minerals for a wide number of applications.

### *1.3.1. Acid activation*

In section 1.2.3 it was noted that high concentrations of  $H^+$  within dispersion can have detrimental effects on the phyllosilicate layers through dissolution of the octahedral sheet. The resultant material is, in general, an amorphous silica sheet (Madejova, 2003) but these sheets also display considerable and complex distribution of Brønsted acid sites (Komadel, 2003). A number of industrial uses have been found for these acid activated clays, including use as catalysts and catalyst supports (Komadel, 2003; Pentrák et al., 2012; Tyagi et al., 2006).

The interest in using acidified phyllosilicates as catalysts caused chemists to develop methods to control the acid activation process. There are a number of reported methods for acid activating clay minerals, and the most frequent mineral chosen is montmorillonite (Zhao et al., 2013). During this process the clay particles do not fully swell and therefore the dissolution of the particle occurs from the outside surfaces inwards. This causes swelling and distortion of the edges of the layers, which can inhibit further swelling of the clay mineral particles. A number of acid activated montmorillonites have been developed for various industrial applications, with the “Montmorillonite K-*n*” series (where *n* is 10, 20, 30 or 40) of materials being one of the most commonly used (Zhao et al., 2013).

### *1.3.2. Modification with organic compounds*

Due to their chemistry clay minerals are highly hydrophilic, allowing them to wet easily and form stable dispersions and suspensions without the need of additives. However,

this makes the interaction between clay mineral particles and lipophilic molecules difficult.

In recent years much research has been published focusing on modifying clay minerals to ensure they become lipophilic. The most common method for achieving this is exploiting the natural cationic exchange properties of clay minerals by replacing the endogenous counterbalancing cations with cationic alkylammonium molecules. The ammonium component of these molecules adsorbs onto to the phyllosilicate surface, presenting the alkyl chain outwards from the clay mineral surface. These materials have thusly been referred to as organoclays. The lipophilic layer on the organoclay is able to interact better with organic solvents, and can also enhance the adsorptive capacity for other organic molecules including drugs (da Silva et al., 2013; Lee and Kim, 2002; Murray, 2000; Önal and Sarıkaya, 2008).

Aside from this, interactions between clay minerals and organic molecules are well documented across the literature. The adsorption of cationic dyes onto the clay mineral surface has been investigated for a number of years and has been a key method to determine the true specific surface area (SSA) of clay minerals when in dispersion. Methylene blue, for example, is able to freely interact with clay mineral surfaces and a number of experimental methods have utilised this process to determine the CEC, SSA and charge of many clay minerals (Chen et al., 1999; Hajjaji and El Arfaoui, 2009; Poli et al., 2008; Yukselen and Kaya, 2008).



Not long after the interaction between clay minerals and dyes had been investigated, a small number of researchers became interested in the interaction between clay minerals and common antimicrobial compounds. This interest was originally borne from wanting to understand how more complex organic molecules interact with phyllosilicate surfaces, and also determine the true fate of antimicrobials within soils (McGinity and Lach, 1976; Sassman and Lee, 2005; White and Hem, 1983).

### *1.3.3. Modification with inorganic cations*

The process of inorganic cationic exchange has been tailored for a number of applications. This process happens naturally between the counterbalancing cations at the phyllosilicate surface and those in the surrounding dispersion. Research teams have manipulated this process by using high concentrations of inorganic cations within the dispersion to drive adsorption of the desired elements onto the clay mineral surface (Swartzen-Allen and Matijevic, 1974; Top and Ülkü, 2004) .

These metal-exchanged clays have been formulated to contain a wide number of different elements such as calcium, magnesium, iron, copper, zinc, and silver. Each element interacts with the clay mineral surface in a different way and these differences have been attributed to the atomic charge and radius. Valence of the cations has shown to be one of the most important variables that effects adsorption onto the mineral surface (Bhattacharyya and Sen Gupta, 2006; Bonferoni et al., 2007; Browne et al., 1980; Girase et al., 2011; Malachová et al., 2011; Özdemir et al., 2010; Tong et al., 2005; Zhou et al., 2004).

Copper- and silver-exchanged clay minerals have received additional interest for their use as antimicrobial agents (Girase et al., 2011; Hu and Xia, 2006; Malachová et al., 2011; Tong et al., 2005). Much of the antimicrobial killing power of these composites has been attributed to the presence, and release, of the exchanged metal ions. Silver has been used in the treatment of skin and skin structure infections for many years and is incorporated into a number of wound-care products used in current clinical practice (Aziz et al., 2012; Bergin and Wraight, 2006; RPS and BMJ, 2017). Copper has also received much interest within healthcare research as a possible antimicrobial material that could help keep hospitals cleaner and safer (Gorman and Humphreys, 2012). However, recently published evidence also suggests that the clay mineral itself plays a large role in the antimicrobial properties of these metal-exchanged clay mineral composites. It has been shown that the clay mineral is able to adsorb onto the cell surface, immobilising the bacterial cell and thus increasing the contact time of the metal ions on its surface (Haydel et al., 2008; Williams et al., 2011)

#### *1.3.4. Modification with inorganic anions*

Much of the research laid out above describes the interaction between clay mineral surfaces and various cations. However, the positively charged groups at the edge of phyllosilicate layers are also key targets for modification. These positive edges are thought to be key players in the formation of gels and contribute to the coagulation and flocculation of clay mineral dispersions. Thus, changing these edges to be negatively charged will alter their colloidal properties (Swartzen-Allen and Matijevic, 1974).

Sodium phosphate, for example, will dissociate in solution and this allows for the phosphate ion to interact with the edges of the phyllosilicate layers. This interaction is very different to those that occur at the phyllosilicate surface and is known as a ligand-exchange process whereby the hydroxyls from the exposed silanol and metal-hydroxide groups are replaced with phosphate (Lagaly and Ziesmer, 2003). This creates a permanent negative charge on the edges, which increases the repulsive tendencies in edge-to-face interactions and thus increases the colloidal stability of more concentrated clay dispersions. For example, Laponite® RD will form gels at around 3% w/v yet Laponite® RDS (*sol* grade) can easily achieve concentrations of 10% w/v due to the effects of the pyrophosphate groups at its edges (BYK Additives & Instruments, 2013; Rockwood Additives, 2012).

#### **1.4. A clinical need for improved antimicrobial stewardship**

Since the dawn of the 20<sup>th</sup> Century medical and surgical practices have been enhanced and made safer through the use of antibacterial agents. Originating with penicillin a variety of molecules are now available for a wide range of indications. However, even upon receiving his Nobel Prize in Medicine for isolating penicillin, Alexander Fleming, warned about the development of protective mechanisms and the future of resistant organisms (Fleming, 1945; Fraise, 2006).

Regardless of this, healthcare practitioners are still being accused to this day of poor prescribing practises when it comes to antibacterial agents (Anon, 2015; Lawrence, 2014; Torjesen, 2014). In order to overcome the resistance of organisms against  $\beta$ -lactam antibacterials (e.g. penicillins and cephalosporins) a number of  $\beta$ -lactamase

inhibitors have been developed, such as tazobactam, which are commonly co-formulated with penicillins, such as piperacillin (Tazocin®, piperacillin-tazobactam) (Fast and Sutton, 2013; Liscio et al., 2015; Pfizer Ltd, 2013). However, bacterial cells are able to deploy a number of tactics to build resistance to antibacterial agents, such as efflux proteins and protective enzymes. Alongside this, acquired resistance can occur through the genetic mutations that occur with each generation or through the sharing of genetic material between bacterial strains, and even species (Davies, 2013; Jones, 1999).

Over the course of the 20<sup>th</sup> Century the pharmaceutical industry and academic scientists developed a number of key classes of antibacterial agents. Some are based upon the central  $\beta$ -lactam structure found in penicillin, such as the cephalosporins and carbapenems. Others are based on completely different structures such as the tetracyclines, the quinolones, the macrolides and the aminoglycosides. A number of potent antibacterial agents have much more complex structures and are often manufactured using biological means, vancomycin is a key example of this (Patrick, 2005).

Even this wide-ranging arsenal of antimicrobial molecules has not been able to overcome the problems caused by bacterial resistance. Widespread resistance is now seen across the penicillin class of antibacterials, and increasing concern is being voiced about organisms that are also resistant to vancomycin, macrolides and carbapenems (Davies, 2013; World Health Organization, 2014, 2012). Healthcare professionals are becoming increasingly aware of the need to treat infections correctly as a failure to do

so can result in the pathogen becoming resistant not only to the drug being used, but possibly to other antibacterial agents (Costelloe et al., 2010; Public Health England, 2015; RCP HAIWP, 2011). For example, it is now well known that failure to destroy certain bacterial strains with erythromycin may also induce resistance to clindamycin (Nathwani et al., 2008; Stevens, 2009).

Since the turn of the 21<sup>st</sup> Century the emphasis on managing antibacterial resistance has become more prominent and much focus has been paid to multiple-drug-resistant, and highly virulent, strains such as methicillin resistant *Staphylococcus aureus* (MRSA), *Clostridium difficile* (often referred to as *C diff*), and multiple-drug-resistant *Mycobacterium tuberculosis* (MDR-TB) (World Health Organization, 2014, 2012). Hospitals in the UK, and indeed worldwide, have deployed a number of stewardship programmes to prevent the development and spread of resistant bacterial strains. Infection control procedures such as rigorous hand washing, alcohol gels, and isolation rooms are now embedded in everyday practice, and enforced by specialist clinicians. In addition to this, medical microbiologists and specialist pharmacists work together to develop antimicrobial prescribing guidelines specific to each hospital (Davies, 2013). By utilising knowledge of microbiology, pharmacology, infection aetiology, and local resistance trends these guidelines are designed to inform prescribing decisions for a wide range of infections giving restricted prescribing options based on disease severity and patient demographics. All of these efforts combine into what is commonly termed 'antimicrobial stewardship' (Davies, 2013; Public Health England, 2015).

However, is it only a matter of time before bacteria overcome these defence programmes and develop resistance against the second- and third-line choice of antimicrobial agents. Indeed, we are already seeing this happen. In response to this the Department of Health's (DH, part of UK Government) Chief Medical Officer published a hard-hitting report into antimicrobial prescribing and resistance, and set out a number of suggestions and challenges for the future (Davies, 2013). Around the same time, the World Health Organisation (WHO) published its vision for the future of antimicrobial stewardship (World Health Organization, 2012), setting out the six overarching policy statements shown in figure 1.5.

2011 World Health Day six point policy brief:

1. Commit to a comprehensive, financed national plan with accountability and civil society engagement.
2. Strengthen surveillance and laboratory capacity.
3. Ensure uninterrupted access to essential medicines of assured quality.
4. Regulate and promote rational use of medicines including in animal husbandry, and ensure proper patient care.
5. Enhance infection prevention and control.
6. Foster innovations and research and development for new tools.

**Figure 1.5.** The six overarching policy statements developed by the WHO in 2011 aiming to tackle global antimicrobial drug-resistance (World Health Organization, 2012).

Policy statement six concerns the discovery and development of novel antimicrobial molecules, which are vital for overcoming resistance to currently available molecules. However, it is realised that there are very few novel antibacterial molecules in the

current research pipelines and it was therefore emphasised that researchers and clinicians should also focus on new technologies for delivering, targeting and utilising the drugs we already have. This sentiment has also been echoed by the Royal Pharmaceutical Society's Pharmaceutical Science Expert Advisory Panel, which wanted to see both new technologies and molecules being developed and such developments being incentivised by Government (Royal Pharmaceutical Society, 2014).

In relation to this, there are a number of infections that benefit from topical and systemic treatment options, including certain eye and respiratory infections. However, problems in achieving efficient drug delivery have hampered the application of locally targeted medicines for wound and skin and skin structure infections. For this reason, within the UK, very few topical antibacterial formulations are available for use in the NHS (National Health Service) due to lack of evidence on effectiveness and patient outcomes (Healy and Freedman, 2006; Scottish Intercollegiate Guidelines Network, 2010; Siddiqui and Bernstein, 2010).

Metronidazole and fusidic acid are available, and often used, but only for strict indications. Metronidazole gel is utilised in the treatment of malodorous fungating wounds where the causative organism is believed to be an anaerobe (Galderma, 2013). Fusidic acid cream is only utilised for mild skin infections caused by aerobic bacteria, such as *Staphylococcus aureus* induced folliculitis (Leo Laboratories Ltd, 2013). However, should clinical assessment judge these infections as anything other than mild it is often necessary to prescribe a systemic antibacterial agent. This is done to treat the infection and prevent what is considered a superficial infection developing into a

deep-seated, and potentially fatal, sepsis. This comes at not only a financial price but also a clinical price for the patient who may experience a number of adverse effects. Systemic treatment with antimicrobials has also been linked to the development of infections by *Clostridium difficile* and other resistant bacteria (Cheer et al., 2009; Healy and Freedman, 2006; Kluytmans and Struelens, 2009).

### **1.5. Aim and objectives of this research project**

It is clear that the development of new formulations for the treatment of infected wounds should be a priority for pharmaceutical science research. However, as highlighted by the Royal Pharmaceutical Society's report *New Medicines, Better Medicines, Better use of medicines* the pharmaceutical industry currently has few incentives to develop drugs and formulations for such conditions (Royal Pharmaceutical Society, 2014).

Clay minerals have been used in the treatment of wounds for hundreds of years and their unique chemistry may be utilised in other ways. The complex chemistry of clay minerals may enable their use as novel drug-carriers, novel excipients, and as material modifiers (Aguzzi et al., 2007; Gomes and Silva, 2007; Lopez-Galindo et al., 2007; Viseras et al., 2010). It is exciting that these characteristics could also be used to benefit the wound healing process, including the adsorption of wound exudates and waste (Dannenfeldt, 2012; Dawson and Oreffo, 2013; Williams et al., 2011). The interaction between clay minerals and organic materials such as drugs and polymers has been reported across the literature with increasing focus on utilising these phyllosilicate-based materials for drug-delivery (Rodrigues et al., 2013). Unfortunately,



many of those who have considered using clay minerals for drug-delivery purposes have had little clinical input, and therefore little potential clinical impact.

The aim of this project was to develop and evaluate novel antibacterial polymer- phyllosilicate composite systems for the treatment of infected wounds. The specific objectives to address this aim were:

1. To understand and model the interaction between clay minerals and carefully selected antibacterial drugs.
2. To determine the best conditions and parameters for the development of clay-drug composites.
3. To develop candidate antibacterial wound dressing materials utilising phyllosilicate materials as a key component.
4. To evaluate the physical and chemical properties of these candidate materials and determine their clinical potential for the management of infected wounds.
5. To determine the antimicrobial properties of the clay-drug composites and the candidate materials.

To ensure scientific and clinical rigour within this project a collaboration was developed between academics at the School of Pharmacy and Biomolecular Sciences at Liverpool John Moores University (Liverpool, UK), clay mineral scientists at BYK Additives Ltd. (Widnes, UK; formerly Rockwood Additives Ltd.), and the nurse-led tissue viability team at the Royal Liverpool and Broadgreen University Hospitals NHS Foundation Trust (Liverpool, UK).

The research presented within this thesis aims to lay the foundations of further research into the development of novel phyllosilicate-containing antimicrobial wound dressings. In essence, this work acts as a pathfinder project that builds on current knowledge, develops new knowledge, and shows the potential application of polymer-phyllosilicate composite systems within wound care. Chapter 2 investigates the interaction between selected clay minerals and tetracycline antibacterial agents; establishing what influences the interaction between these compounds and determining their antibacterial effects. Chapter 3 applies the knowledge developed in chapter 2 to a different antibacterial agent; ciprofloxacin. Finally, Chapter 4 utilises the clay-ciprofloxacin composites established in chapter 3 in the development and evaluation of candidate materials for the treatment of infected wounds.

## 1.6. References

- Aguzzi, C., Cerezo, P., Viseras, C., Caramella, C., 2007. Use of clays as drug delivery systems: Possibilities and limitations. *Appl. Clay Sci.* 36, 22–36. doi:10.1016/j.clay.2006.06.015
- Anon, 2015. GPs continue to prescribe outdated antibiotics for gonorrhoea. *Pharm. J.* 294.
- Aochi, Y.O., Farmer, W.J., 2011. Effects of surface charge and particle morphology on the sorption/desorption behavior of water on clay minerals. *Colloids Surfaces A Physicochem. Eng. Asp.* 374, 22–32. doi:10.1016/j.colsurfa.2010.10.039
- Avery, R.G., Ramsay, J.D.F., 1986. Colloidal Properties of Synthetic Hectorite Clay Dispersions II . Light and Small Angle Neutron Scattering. *J. Colloid Interface Sci.* 109, 448–454.
- Aziz, Z., Abu, S.F., Chong, N.J., 2012. A systematic review of silver-containing dressings and topical silver agents (used with dressings) for burn wounds. *Burns* 38, 307–18. doi:10.1016/j.burns.2011.09.020
- Bergaya, F., Lagaly, G., 2013. General introduction: Clays, clay minerals, and clay science, in: Bergaya, F., Lagaly, G. (Eds.), *Handbook of Clay Science Part A: Fundamentals*. Elsevier, Oxford, UK, pp. 1–19.
- Bergin, S., Wraight, P., 2006. Silver based wound dressings and topical agents for treating diabetic foot ulcers. *Cochrane Database Syst Rev.* Issue 1.
- Bhattacharyya, K.G., Sen Gupta, S., 2006. Pb(II) uptake by kaolinite and montmorillonite in aqueous medium: Influence of acid activation of the clays. *Colloids Surfaces A Physicochem. Eng. Asp.* 277, 191–200. doi:10.1016/j.colsurfa.2005.11.060
- Bonferoni, M., Cerri, G., Degennaro, M., Juliano, C., Caramella, C., 2007. Zn<sup>2+</sup>-exchanged clinoptilolite-rich rock as active carrier for antibiotics in anti-acne topical therapy. In-vitro characterization and preliminary formulation studies. *Appl. Clay Sci.* 36, 95–102. doi:10.1016/j.clay.2006.04.014
- Brack, A., 2013. Clay Minerals and the Origin of Life, in: Bergaya, F., Lagaly, G. (Eds.), *Handbook of Clay Science Part A: Fundamentals*. Elsevier, Oxford, UK, pp. 507–522.
- Brigatti, M.F., Galan, E., Theng, B.K.G., 2013. Structure and mineralogy of clay minerals, in: Bergaya, F., Lagaly, G. (Eds.), *Handbook of Clay Science Part A: Fundamentals*. Elsevier, Oxford, UK, pp. 21–81.
- British Pharmacopoeia Commission, 2017a. Calamine Lotion, in: *British Pharmacopoeia (Volume III)*. London.

- British Pharmacopoeia Commission, 2017b. Kaolin Poulitice, in: British Pharmacopoeia (Volume III).
- Browne, J.E., Feldkamp, J.R., White, J.L., Hem, S.L., 1980. Characterization and adsorptive properties of pharmaceutical grade clays. *J. Pharm. Sci.* 69, 816–23.
- Bryan, C.P., 1930. *The Papyrus Ebers*. The Garden City Press Ltd., Letchworth, UK (1930).
- Bunnell, J.E., Finkelman, R.B., Centeno, J.A., Selinus, O., 2007. Medical Geology: a globally emerging discipline. *Geol. Acta* 5, 273–281.
- BYK Additives & Instruments, 2013. Laponite RDS.
- Cai, P., Huang, Q.-Y., Zhang, X.-W., 2006. Interactions of DNA with clay minerals and soil colloidal particles and protection against degradation by DNase. *Environ. Sci. Technol.* 40, 2971–6.
- Carretero, M.I., 2002. Clay minerals and their beneficial effects upon human health. A review. *Appl. Clay Sci.* 21, 155–163. doi:10.1016/S0169-1317(01)00085-0
- Carretero, M.I., Lagaly, G., 2007. Clays and health: An introduction. *Appl. Clay Sci.* 36, 1–3. doi:10.1016/j.clay.2006.09.001
- Carretero, M.I., Pozo, M., 2009. Clay and non-clay minerals in the pharmaceutical industry Part I. Excipients and medical applications. *Appl. Clay Sci.* 46, 73–80. doi:10.1016/j.clay.2009.07.017
- Cengiz, S., Çavaş, L., Yurdakoç, K., 2012. Bentonite and sepiolite as supporting media: Immobilization of catalase. *Appl. Clay Sci.* 65–66, 114–120. doi:10.1016/j.clay.2012.06.004
- Chang, P.-H., Li, Z., Yu, T.-L., Munkhbayer, S., Kuo, T.-H., Hung, Y.-C., Jean, J.-S., Lin, K.-H., 2009. Sorptive removal of tetracycline from water by palygorskite. *J. Hazard. Mater.* 165, 148–55. doi:10.1016/j.jhazmat.2008.09.113
- Cheer, K., Shearman, C., Jude, E.B., 2009. Managing complications of the diabetic foot. *Bmj* 339, b4905–b4905. doi:10.1136/bmj.b4905
- Chen, G., Pan, J., Han, B., Yan, H., 1999. Adsorption of Methylene Blue on Montmorillonite. *J. Dispers. Sci. Technol.* 20, 1179–1187.
- Costelloe, C., Metcalfe, C., Lovering, A., Mant, D., Hay, a. D., 2010. Effect of antibiotic prescribing in primary care on antimicrobial resistance in individual patients: systematic review and meta-analysis. *Bmj* 340, c2096–c2096. doi:10.1136/bmj.c2096
- Czímerová, A., Bujdák, J., Dohrmann, R., 2006. Traditional and novel methods for estimating the layer charge of smectites. *Appl. Clay Sci.* 34, 2–13. doi:10.1016/j.clay.2006.02.008

- da Silva, M.L.G., Fortes, A.C., Oliveira, M.E.R., Freitas, R.M., Silva Filho, E.C., La Roca Soares, M.F., Soares-Sobrinho, J.L., Silva Leite, C.M., 2013. Palygorskite organophilic for dermopharmaceutical application. *J. Therm. Anal. Calorim.*
- Daniel, L.M., Frost, R.L., Zhu, H.Y., 2008. Edge-modification of laponite with dimethyl-octylmethoxysilane. *J. Colloid Interface Sci.* 321, 302–9. doi:10.1016/j.jcis.2008.01.032
- Dannenfeldt, K.H., 2012. The introduction of a new sixteenth-century drug: terra Silesiaca. *Med. Hist.* 28, 174–188. doi:10.1017/S0025727300035717
- Davies, S.C., 2013. Annual Report of the Chief Medical Officer, Volume Two, 2011, Infections and the rise of antimicrobial resistance. Department of Health, London.
- Dawson, J.I., Oreffo, R.O.C., 2013. Clay: new opportunities for tissue regeneration and biomaterial design. *Adv. Mater.* 25, 4069–86. doi:10.1002/adma.201301034
- Deng, Y., Velázquez, A.L.B., Billes, F., Dixon, J.B., 2010. Bonding mechanisms between aflatoxin B1 and smectite. *Appl. Clay Sci.* 50, 92–98. doi:10.1016/j.clay.2010.07.008
- Drits, V.A., 2003. Structural and chemical heterogeneity of layer silicates and clay minerals. *Clay Miner.* 38, 403–432. doi:10.1180/0009855033840106
- Fast, W., Sutton, L.D., 2013. Metallo- $\beta$ -lactamase: Inhibitors and reporter substrates. *Biochim. Biophys. Acta - Proteins Proteomics* 1834, 1648–1659. doi:10.1016/j.bbapap.2013.04.024
- Figuroa-Diva, R. a, Vasudevan, D., MacKay, A. a, 2010. Trends in soil sorption coefficients within common antimicrobial families. *Chemosphere* 79, 786–93. doi:10.1016/j.chemosphere.2010.03.017
- Figuroa, R. a, Leonard, A., MacKay, A. a, 2004. Modeling tetracycline antibiotic sorption to clays. *Environ. Sci. Technol.* 38, 476–83.
- Fleming, A., 1945. Penicillin. Nobel Lect.
- Fraise, A.P., 2006. Tigecycline: the answer to beta-lactam and fluoroquinolone resistance? *J. Infect.* 53, 293–300. doi:10.1016/j.jinf.2006.05.014
- Galderma, 2013. Metrogel [WWW Document]. *Electron. Med. Compend.* URL <http://www.medicines.org.uk/emc/medicine/696> (accessed 7.20.15).
- Gaskell, E.E., Hamilton, A.R., 2014. Antimicrobial clay-based materials for wound care. *Future Med. Chem.* 6, 641.
- Gibson, E.H., 1954. Baths and washhouses in the English public health agitation, 1839–48. *J. Hist. Med. Allied Sci.* 9, 391–406.
- Girase, B., Depan, D., Shah, J.S., Xu, W., Misra, R.D.K., 2011. Silver–clay nanohybrid

- structure for effective and diffusion-controlled antimicrobial activity. *Mater. Sci. Eng. C* 31, 1759–1766. doi:10.1016/j.msec.2011.08.007
- Gomes, C., Carretero, M.I., Pozo, M., Maraver, F., Cantista, P., Armijo, F., Legido, J.L., Teixeira, F., Rautureau, M., Delgado, R., 2013. Peloids and pelotherapy: Historical evolution, classification and glossary. *Appl. Clay Sci.* 75–76, 28–38. doi:10.1016/j.clay.2013.02.008
- Gomes, C., Silva, J., 2007. Minerals and clay minerals in medical geology. *Appl. Clay Sci.* 36, 4–21. doi:10.1016/j.clay.2006.08.006
- Gorman, J., Humphreys, H., 2012. Application of copper to prevent and control infection. Where are we now? *J. Hosp. Infect.* 81, 217–223. doi:10.1016/j.jhin.2012.05.009
- Greenland, D.J., Laby, R.H., Quirk, J.P., 1965. Adsorption of Amino-Acids and Peptides by Montmorillonite and Illite. Part 1. -Cation Exchange and Proton Transfer. *Trans. Faraday Soc.* 61, 2013–2023.
- Hajjaji, M., El Arfaoui, H., 2009. Adsorption of methylene blue and zinc ions on raw and acid-activated bentonite from Morocco. *Appl. Clay Sci.* 46, 418–421. doi:10.1016/j.clay.2009.09.010
- Haydel, S.E., Remenih, C.M., Williams, L.B., 2008. Broad-spectrum in vitro antibacterial activities of clay minerals against antibiotic-susceptible and antibiotic-resistant bacterial pathogens. *J. Antimicrob. Chemother.* 61, 353–61. doi:10.1093/jac/dkm468
- Healy, B., Freedman, A., 2006. Infections. *BMJ* 332, 838–841.
- Hensen, E.J.M., Smit, B., 2002. Why Clays Swell. *J. Phys. Chem. B* 106, 12664–12667. doi:10.1021/jp0264883
- Hu, C.H., Xia, M.S., 2006. Adsorption and antibacterial effect of copper-exchanged montmorillonite on *Escherichia coli* K88. *Appl. Clay Sci.* 31, 180–184. doi:10.1016/j.clay.2005.10.010
- Jackson, R., 1990. Waters and spas in the classical world. *Med. Hist. Suppl.* 10, 1–13.
- Jones, R.D., 1999. Bacterial resistance and topical antimicrobial wash products. *Am. J. Infect. Control* 27, 351–63.
- Kahr, G., Madsen, F.T., 1995. Determination of the cation exchange capacity and the surface area of bentonite, illite and kaolinite by methylene blue adsorption. *Appl. Clay Sci.* 9, 327–336. doi:10.1016/0169-1317(94)00028-O
- Kikouama, O.J.R., Balde, L., 2010. From edible clay to a clay-containing formulation for optimization of oral delivery of some trace elements: a review. *Int. J. Food Sci. Nutr.* 61, 803–822. doi:10.3109/09637486.2010.486759

- Kluytmans, J., Struelens, M., 2009. Meticillin resistant *Staphylococcus aureus* in the hospital. *BMJ* 338, b364–b364. doi:10.1136/bmj.b364
- Komadell, P., 2003. Chemically modified smectites. *Clay Miner.* 38, 127–138. doi:10.1180/0009855033810083
- Konta, J., 1995. Clay and man: clay raw materials in the service of man. *Appl. Clay Sci.* 10, 275–335. doi:10.1016/0169-1317(95)00029-4
- Kulshrestha, P., Giese, R.F., Aga, D.S., 2004. Investigating the molecular interactions of oxytetracycline in clay and organic matter: insights on factors affecting its mobility in soil. *Environ. Sci. Technol.* 38, 4097–105.
- Lagaly, G., Dekany, I., 2013. Colloid Clay Science, in: Bergaya, F., Lagaly, G. (Eds.), *Handbook of Clay Science Part A: Fundamentals*. Elsevier, Oxford, UK, pp. 243–345.
- Lagaly, G., Ziesmer, S., 2003. Colloid chemistry of clay minerals: the coagulation of montmorillonite dispersions. *Adv. Colloid Interface Sci.* 100–102, 105–128. doi:10.1016/S0001-8686(02)00064-7
- Lawrence, J., 2014. Prescribing advice fails to halt rise in antibiotics for coughs and colds. *Pharm. J.* 293.
- Lee, S.Y., Kim, S.J., 2002. Delamination behavior of silicate layers by adsorption of cationic surfactants. *J. Colloid Interface Sci.* 248, 231–8. doi:10.1006/jcis.2002.8222
- Leo Laboratories Ltd, 2013. Fucidin Cream [WWW Document]. *Electron. Med. Compend.* URL <http://www.medicines.org.uk/emc/medicine/2374> (accessed 7.20.15).
- Liscio, J.L., Mahoney, M. V., Hirsch, E.B., 2015. Ceftolozane/tazobactam and ceftazidime/avibactam: two novel  $\beta$ -lactam/ $\beta$ -lactamase inhibitor combination agents for the treatment of resistant Gram-negative bacterial infections. *Int. J. Antimicrob. Agents* 1–6. doi:10.1016/j.ijantimicag.2015.05.003
- Lopez-Galindo, A., Viseras, C., Cerezo, P., 2007. Compositional, technical and safety specifications of clays to be used as pharmaceutical and cosmetic products. *Appl. Clay Sci.* 36, 51–63. doi:10.1016/j.clay.2006.06.016
- Madejova, J., 2003. FTIR techniques in clay mineral studies. *Vib. Spectrosc.* 31, 1–10.
- Malachová, K., Praus, P., Rybková, Z., Kozák, O., 2011. Antibacterial and antifungal activities of silver, copper and zinc montmorillonites. *Appl. Clay Sci.* 53, 642–645. doi:10.1016/j.clay.2011.05.016
- McGinity, J.W., Lach, J.L., 1976. Adsorption of Various Pharmaceuticals to Montmorillonite. *J. Pharm. Sci.* 65, 896–902.

- Miranda-Trevino, J.C., Coles, C.A., 2003. Kaolinite properties, structure and influence of metal retention on pH. *Appl. Clay Sci.* 23, 133–139. doi:10.1016/S0169-1317(03)00095-4
- Mongondry, P., Tassin, J.F., Nicolai, T., 2005. Revised state diagram of Laponite dispersions. *J. Colloid Interface Sci.* 283, 397–405. doi:10.1016/j.jcis.2004.09.043
- Murray, H.H., 2000. Traditional and new applications for kaolin, smectite, and palygorskite: a general overview. *Appl. Clay Sci.* 17, 207–221. doi:10.1016/S0169-1317(00)00016-8
- Nathwani, D., Morgan, M., Masterton, R.G., Dryden, M., Cookson, B.D., French, G., Lewis, D., 2008. Guidelines for UK practice for the diagnosis and management of methicillin-resistant *Staphylococcus aureus* (MRSA) infections presenting in the community. *J. Antimicrob. Chemother.* 61, 976–994. doi:10.1093/jac/dkn096
- Newton, P., 1991. The use of medicinal plants by primates: A missing link? *Trends Ecol. Evol.* 6, 297–299. doi:10.1016/0169-5347(91)90009-M
- Önal, M., Sarıkaya, Y., 2008. The effect of organic cation content on the interlayer spacing, surface area and porosity of methyltributylammonium-smectite. *Colloids Surfaces A Physicochem. Eng. Asp.* 317, 323–327. doi:10.1016/j.colsurfa.2007.10.029
- Özdemir, G., Limoncu, M.H., Yapar, S., 2010. The antibacterial effect of heavy metal and cetylpridinium-exchanged montmorillonites. *Appl. Clay Sci.* 48, 319–323. doi:10.1016/j.clay.2010.01.001
- Paineau, E., Bihannic, I., Baravian, C., Philippe, A.-M., Davidson, P., Levitz, P., Funari, S.S., Rochas, C., Michot, L.J., 2011a. Aqueous suspensions of natural swelling clay minerals. 1. Structure and electrostatic interactions. *Langmuir* 27, 5562–73. doi:10.1021/la2001255
- Paineau, E., Michot, L.J., Bihannic, I., Baravian, C., 2011b. Aqueous suspensions of natural swelling clay minerals. 2. Rheological characterization. *Langmuir* 27, 7806–19. doi:10.1021/la2001267
- Pálková, H., Madejová, J., Zimowska, M., Bielańska, E., Olejniczak, Z., Lityńska-Dobrzyńska, L., Serwicka, E.M., 2010. Laponite-derived porous clay heterostructures: I. Synthesis and physicochemical characterization. *Microporous Mesoporous Mater.* 127, 228–236. doi:10.1016/j.micromeso.2009.07.019
- Palmer, R., 1990. “In this our lightye and learned tyme”: Italian baths in the era of the Renaissance. *Med. Hist. Suppl.* 10, 14–22.
- Patrick, G.L., 2005. Antibacterial Agents, in: *An Introduction to Medicinal Chemistry*. Oxford University Press, Gosport, UK, pp. 379–439.
- Pentrák, M., Czímerová, A., Madejová, J., Komadel, P., 2012. Changes in layer charge of



clay minerals upon acid treatment as obtained from their interactions with methylene blue. *Appl. Clay Sci.* 55, 100–107. doi:10.1016/j.clay.2011.10.012

Pfizer Ltd, 2013. Tazocin 4 g / 0.5 g powder for solution for infusion [WWW Document]. *Electron. Med. Compend.* URL <http://www.medicines.org.uk/emc/medicine/28280> (accessed 7.20.15).

Pharmaceutical Society of Great Britain, 1911. Massa Kaolini B.P.C., in: *British Pharmaceutical Codex*. Pharmaceutical Press, London, UK, p. 1272.

Pharmaceutical Society of Great Britain, 1907. Mass Kaolini, in: *British Pharmaceutical Codex*. Pharmaceutical Press, London, UK, p. 568.

Plancon, A., 2001. Order-disorder in clay mineral structures. *Clay Miner.* 36, 1–14.

Poli, A.L., Batista, T., Schmitt, C.C., Gessner, F., Neumann, M.G., 2008. Effect of sonication on the particle size of montmorillonite clays. *J. Colloid Interface Sci.* 325, 386–90. doi:10.1016/j.jcis.2008.06.016

Public Health England, 2015. Start Smart - Then Focus Antimicrobial Stewardship Toolkit for English Hospitals. London.

RCP HAIWP, 2011. RCP insight: Effective antibiotic prescribing – Top Ten Tips.

Rockwood Additives, 2012. Laponite RD [WWW Document]. *Prod. Bull.* URL [http://www.rockwoodadditives.com/product\\_bulletins\\_eu/PB\\_Laponite\\_RD.pdf](http://www.rockwoodadditives.com/product_bulletins_eu/PB_Laponite_RD.pdf)

Rodrigues, L.A.D.S., Figueiras, A., Veiga, F., de Freitas, R.M., Nunes, L.C.C., da Silva Filho, E.C., da Silva Leite, C.M., 2013. The systems containing clays and clay minerals from modified drug release: a review. *Colloids Surf. B. Biointerfaces* 103, 642–51. doi:10.1016/j.colsurfb.2012.10.068

Rong, X., Huang, Q., He, X., Chen, H., Cai, P., Liang, W., 2008. Interaction of *Pseudomonas putida* with kaolinite and montmorillonite: a combination study by equilibrium adsorption, ITC, SEM and FTIR. *Colloids Surf. B. Biointerfaces* 64, 49–55. doi:10.1016/j.colsurfb.2008.01.008

Royal Pharmaceutical Society, 2014. *New Medicines, Better Medicines, Better use of Medicines - A Guide to the Science Underpinning Pharmaceutical Practice*. London.

RPS and BMJ, 2017. Appendix 5: Wounds management products and elasticated garments, in: Khanderia, S. (Ed.), *British National Formulary (Online Edition)*. Pharmaceutical Press and BMJ Group, London, UK.

Rytwo, G., 2008. Clay Minerals as an Ancient Nanotechnology : Historical Uses of Clay Organic Interactions , and Future Possible Perspectives. *Macla* 9, 15–17.

Sandri, G., Bonferoni, M.C., Rossi, S., Ferrari, F., Aguzzi, C., Viseras, C., Caramella, C., 2016. Clay minerals for tissue regeneration, repair, and engineering, *Wound Healing Biomaterials*. Elsevier Ltd. doi:10.1016/B978-1-78242-456-7.00019-2

- Sassman, S. a, Lee, L.S., 2005. Sorption of three tetracyclines by several soils: assessing the role of pH and cation exchange. *Environ. Sci. Technol.* 39, 7452–9.
- Scottish Intercollegiate Guidelines Network, 2010. Management of chronic venous leg ulcers. (SIGN Guideline No 120).
- Siddiqui, A.R., Bernstein, J.M., 2010. Chronic wound infection: facts and controversies. *Clin. Dermatol.* 28, 519–26. doi:10.1016/j.clindermatol.2010.03.009
- Slamova, R., Trckova, M., Vondruskova, H., Zraly, Z., Pavlik, I., 2011. Clay minerals in animal nutrition. *Appl. Clay Sci.* 51, 395–398. doi:10.1016/j.clay.2011.01.005
- Stevens, D.L., 2009. Treatments for skin and soft-tissue and surgical site infections due to MDR Gram-positive bacteria. *J. Infect.* 59 Suppl 1, S32-9. doi:10.1016/S0163-4453(09)60006-2
- Sukenik, S., Buskila, D., Neumann, L., Kleiner-Baumgarten, A., Zimlichman, S., Horowitz, J., 1990. Sulphur bath and mud pack treatment for rheumatoid arthritis at the Dead Sea area. *Ann. Rheum. Dis.* 49, 99–102.
- Swartzen-Allen, S.L., Matijevic, E., 1974. Surface and colloid chemistry of clays. *Chem. Rev.* 74, 385–400. doi:10.1021/cr60289a004
- Tateo, F., Ravaglioli, A., Andreoli, C., Bonina, F., Coiro, V., Degetto, S., Giaretta, A., Menconi Orsini, A., Puglia, C., Summa, V., 2009. The in-vitro percutaneous migration of chemical elements from a thermal mud for healing use. *Appl. Clay Sci.* 44, 83–94. doi:10.1016/j.clay.2009.02.004
- Tateo, F., Summa, V., 2007. Element mobility in clays for healing use. *Appl. Clay Sci.* 36, 64–76. doi:10.1016/j.clay.2006.05.011
- Tong, G., Yulong, M., Peng, G., Zirong, X., 2005. Antibacterial effects of the Cu(II)-exchanged montmorillonite on *Escherichia coli* K88 and *Salmonella choleraesuis*. *Vet. Microbiol.* 105, 113–22. doi:10.1016/j.vetmic.2004.11.003
- Top, A., Ülkü, S., 2004. Silver, zinc, and copper exchange in a Na-clinoptilolite and resulting effect on antibacterial activity. *Appl. Clay Sci.* 27, 13–19. doi:10.1016/j.clay.2003.12.002
- Torjesen, I., 2014. Prescribing of antibiotics increases by 6% in four years. *Pharm. J.* 293.
- Tyagi, B., Chudasama, C.D., Jasra, R.V., 2006. Determination of structural modification in acid activated montmorillonite clay by FT-IR spectroscopy. *Spectrochim. Acta. A. Mol. Biomol. Spectrosc.* 64, 273–8. doi:10.1016/j.saa.2005.07.018
- van Tubergen, A., van der Linden, S., 2002. A brief history of spa therapy. *Ann. Rheum. Dis.* 61, 273–276.
- Vermeer, D.E., Ferrell, R.E., 1985. Nigerian Geophagical Clay: A Traditional Antidiarrheal Pharmaceutical. *Science (80- )*. 227, 634–636.

- Viseras, C., Aguzzi, C., Cerezo, P., Lopezgalindo, A., 2007. Uses of clay minerals in semisolid health care and therapeutic products. *Appl. Clay Sci.* 36, 37–50. doi:10.1016/j.clay.2006.07.006
- Viseras, C., Cerezo, P., Sanchez, R., Salcedo, I., Aguzzi, C., 2010. Current challenges in clay minerals for drug delivery. *Appl. Clay Sci.* 48, 291–295. doi:10.1016/j.clay.2010.01.007
- White, J.L., Hem, S.L., 1983. Pharmaceutical Aspects of Clay-Organic Interactions. *Ind. Eng. Chem. Prod. Res. Dev.* 22, 665–671.
- Williams, L.B., Haydel, S.E., 2010. Evaluation of the medicinal use of clay minerals as antibacterial agents. *Int. Geol. Rev.* 52, 745–770. doi:10.1080/00206811003679737
- Williams, L.B., Metge, D.W., Eberl, D.D., Harvey, R.W., Turner, A.G., Prapaipong, P., Poret-Peterson, A.T., 2011. What makes a natural clay antibacterial? *Environ. Sci. Technol.* 45, 3768–73. doi:10.1021/es1040688
- World Health Organization, 2014. Antimicrobial Resistance: Global report on surveillance 2014. France.
- World Health Organization, 2012. The evolving threat of antimicrobial resistance: Options for action. World Health Organization, Switzerland.
- Yukselen, Y., Kaya, A., 2008. Suitability of the methylene blue test for surface area, cation exchange capacity and swell potential determination of clayey soils. *Eng. Geol.* 102, 38–45. doi:10.1016/j.enggeo.2008.07.002
- Zhao, H., Zhou, C.H., Wu, L.M., Lou, J.Y., Li, N., Yang, H.M., Tong, D.S., Yu, W.H., 2013. Catalytic dehydration of glycerol to acrolein over sulfuric acid-activated montmorillonite catalysts. *Appl. Clay Sci.* 74, 154–162. doi:10.1016/j.clay.2012.09.011
- Zhao, W., Liu, X., Huang, Q., Walker, S.L., Cai, P., 2012. Interactions of pathogens *Escherichia coli* and *Streptococcus suis* with clay minerals. *Appl. Clay Sci.* 69, 37–42. doi:10.1016/j.clay.2012.07.003
- Zhou, Y., Chen, H., Yao, J., He, M., Si, Y., Feng, L., Wang, F., Wang, G., Choi, M.M.F., 2010. Influence of clay minerals on the *Bacillus halophilus* Y38 activity under anaerobic condition. *Appl. Clay Sci.* 50, 533–537. doi:10.1016/j.clay.2010.10.008
- Zhou, Y., Xia, M., Ye, Y., Hu, C., 2004. Antimicrobial ability of Cu<sup>2+</sup> -montmorillonite. *Appl. Clay Sci.* 27, 215–218. doi:10.1016/j.clay.2004.06.002

## Chapter 2

# Interaction between phyllosilicates and tetracycline antibacterial agents

### 2.1. Introduction

The tetracycline class of antibacterial agents is one of the oldest classes after the penicillins, with chlortetracycline being isolated as a natural compound in the late 1940s (Griffin et al., 2010; Varanda et al., 2006). Since this, and the realisation that chlortetracycline activity could be modified and enhanced, a number of tetracycline molecules have been developed and launched to the market including tetracycline, doxycycline, oxytetracycline and minocycline (RPS and BMJ, 2017). Whilst no official additions have been made to this class for a number of years it cannot be denied that tigecycline, founding member of the glycylcycline class of antibacterial compounds designed to overcome resistance against tetracyclines (Fraise, 2006; Grolman, 2007), is a further modification of the tetracycline structure.

The chemistry of tetracycline antibacterial agents is highly complex and they can undergo a number of reactions in aqueous solution. As shown in figure 2.1 agents within this class have a number of groups which are able to undergo protonation or deprotonation. The  $pK_a$  values of doxycycline and tetracycline are very similar, due to their similar structure. Minocycline has an additional  $pK_a$  value due to a second



The central ring structure allows for the formation of partially conjugated systems and the delocalisation of electrons across various parts of the molecule (Sarmah et al., 2006). Upon deprotonation the resultant negative charge is not fixed to one sole atom or group, but can be spread across a number of conjugated atoms and groups (Leeson et al., 1963). On one side of the molecule (presented at the top of the molecules in figure 2.1) there are a large number of hydroxyl and oxygen groups, which generate a negative charge on this region of the molecule. This negative charge is able to attract and coordinate with inorganic cations such as calcium, iron, and magnesium ions in solution (Jin et al., 2007; Parolo et al., 2010). In turn, this can significantly alter the clinical efficacy of these drugs (Griffin et al., 2010).

The tetracycline antibacterial molecules inhibit the development, growth and division of bacterial cells through interaction with the 30S subunit of the bacterial ribosome, thus causing inhibition and cessation of protein manufacture (Grassi, 1993; Griffin et al., 2010). Tetracyclines show activity against both Gram-negative and Gram-positive bacteria (Grassi, 1993) but are much more active against Gram-positive bacteria. Their chemistry makes them particularly soluble in acidic environments, meaning they still maintain their bioavailability when taken orally, and are able to achieve good penetration and effective concentrations across many tissues (Grassi, 1993). Their wide distribution throughout body tissues, and their broad spectrum antibacterial activity, makes these agents useful in the treatment of skin and skin structure infections (Dawson and Dellavalle, 2013; Perkins and Heard, 1999; Sandwell and West Birmingham Hospitals NHS Trust, 2011; Seaton, 2009; Smith, 2004; Stevens, 2009; The Royal Liverpool and Broadgreen University Hospitals NHS Trust, 2012; Unal, 2009a). In

addition to active antibacterial treatment, doxycycline is commonly used for malaria prophylaxis (Giovagnoli et al., 2010). More recently, the activity of the tetracyclines has also been investigated as a possible treatment option for arthritic disease (Greenwald, 2011; Griffin et al., 2010), chronic airway disease (Griffin et al., 2010; Joks and Durkin, 2011; Raza et al., 2006), and even Alzheimer's dementia (Costa et al., 2011; Griffin et al., 2010).

As mentioned in section 1.4, mismanagement of antibacterial agents has led to the development of resistant bacteria and problematic infections. The tetracycline class of drugs has been increasingly afflicted by such resistance (Griffin et al., 2010; Varanda et al., 2006) thus the development of new, topical, delivery systems for the treatment of wound, skin and skin structure infections could avoid resistance developing within microbiota located in other parts of the body. The development of a topical delivery system for tetracyclines should also reduce the precautions and side effects that need to be considered when prescribing these agents. For example, patients would no longer need to avoid ingesting milk or other polyvalent metallic cation containing products (RPS and BMJ, 2017). It would also be possible to reduce the overall dose required to treat wound, skin and skin structure infections by using topical formulations, and thus systemic absorption would also be reduced. In turn, this will reduce the incidence of general adverse effects such as nausea and vomiting, and more specific adverse effects such as hepatic impairment and antibiotic-associated-diarrhoea from organisms like *Clostridium difficile* (RPS and BMJ, 2017; Tsankov et al., 2003).

The interactions between tetracycline and clay minerals have previously been investigated by a number of researchers in the second half of the twentieth century. However, much of this research focused only on the qualitative and quantitative analysis of such interactions (Aguzzi et al., 2005; Figueroa et al., 2004; Li et al., 2010; Pils and Laird, 2007; Porubcan et al., 1978) and the results used to speculate the fate of tetracyclines in soil (Pils and Laird, 2007; Sarmah et al., 2006; Sassman and Lee, 2005). More recently this has spurred research teams to determine the applicability of clay minerals as adsorbent materials for antibacterial agents in hospital and veterinary effluent (Chang et al., 2009a, 2009c).

An increasing body of research (Rodrigues et al., 2013; Viseras et al., 2010) is being published on the subject of using clay-minerals to deliver a wide-range of drugs such as donepezil (Park et al., 2008), chlorhexidine (Samlíková et al., 2017), ciprofloxacin (Hamilton et al., 2014), clindamycin (Porubcan et al., 1978), gentamicin (Rapacz-kmita et al., 2017), hydralazine (Sánchez-Martín et al., 1988), ibuprofen (Tan et al., 2014), itraconazole (Jung et al., 2008), and ofloxacin (Wang et al., 2014), amongst others. However, very little research has looked at utilising phyllosilicate materials as drug-carriers for tetracycline molecules with the aim of developing novel drug-delivery materials (Parolo et al., 2010).

In this chapter the interaction between tetracycline and doxycycline with a range of clay minerals will be investigated. The natural clays kaolin, montmorillonite, and the latter's acid activated counterpart, montmorillonite K-10, alongside two synthetic clay minerals Laponite® RD and Laponite® XL21, were selected for this work. A more



detailed overview of the structure and chemistry of these clay minerals is given in section 1.2. Tetracycline and doxycycline have similar structures (figure 2.1) and acid dissociation constants. Investigating the adsorption of these drugs onto clay minerals will allow the effects of the clay mineral structure and the dispersion environment to be characterised. The adsorption kinetics and isotherms are reported here, alongside analysis of the interactions between tetracycline and doxycycline and the phyllosilicates.

## 2.2. Materials and methods

### 2.2.1. Materials

Kaolin (KN) [empirical formula:  $\text{Al}_2\text{Si}_2\text{O}_8 \cdot \text{H}_2\text{O}$  (PubChem, 2016)], washed and sieved, was obtained from Fisher (UK); and refined montmorillonite (rMMT) [empirical formula:  $\text{Al}_{3.2}\text{Mg}_{0.8}\text{Si}_8\text{O}_{20}(\text{OH})_4 \cdot \text{Na}_{0.8}$  (BYK Additives & Instruments, 2013)], was donated by (BYK Additives & Instruments Ltd., Widnes, UK). An acid activated montmorillonite, montmorillonite K-10 (MMTK10) [empirical formula:  $\text{Al}_2\text{Si}_4\text{O}_{10}(\text{OH})_2 \cdot n\text{H}_2\text{O}$  (California Earth Minerals Inc., 2008)] was obtained from Acros (UK). Two synthetic hectorite-like clays, Laponite<sup>®</sup> RD (LRD) and Laponite<sup>®</sup> XL21 (LXL21) [empirical formula for Laponite<sup>®</sup>:  $(\text{Si}_8\text{Mg}_{5.5}\text{Li}_{0.3}\text{O}_{20}(\text{OH})_4)^{-0.7} \cdot \text{Na}_{+0.7}$  (BYK Additives & Instruments, 2014)], were donated by BYK Additives & Instruments Ltd. (Widnes, UK).

Tetracycline hydrochloride (TC) (>98% by HPLC) was obtained from Sigma Aldrich (UK) and doxycycline monohydrate (DC) (>98% by HPLC) was received from Medicis Pharmaceutical (UK).

### 2.2.2. Adsorption of tetracycline and doxycycline

#### 2.2.2.1. Effect of dispersion pH

To determine the effect of dispersion pH on drug binding 250 mg of clay mineral was dispersed in 15 mL deionised water for 2 hours at 7000 rpm. To these dispersions 10 mL of a 2.5 mg/mL solution of TC or DC was added and the pH adjusted to between 1.0 and 12.0 with dilute HCl and NaOH. After 24 hours mixing, aliquots of the dispersions were centrifuged (EBA20, Hettich Zentrifugen) at 3000 rpm for 10 minutes to separate the clay from the supernatant. Each experiment was undertaken in triplicate. The

concentration of drug remaining in supernatant was determined by UV-Visible spectrophotometry (Genesys 10UV, Thermo Scientific) scanning wavelengths between 200 – 400 nm and measured in triplicate.

#### *2.2.2.2. Kinetics of tetracycline and doxycycline adsorption*

Adsorption kinetics were undertaken using dispersions of 500 mg KN, 10 mg rMMT, 100 mg MMTK10, 10 mg LRD, or 10 mg LXL21 in 90 mL deionised water. After a period of 2 hours the clay dispersions was adjusted to pH 2.0, pH 5.0 for TC and pH 5.5 for DC, and pH 11.0. Drug was dissolved in deionised water and solutions adjusted to the appropriate pH. The drug solution (2 mg in 10 mL) was added to the clay-mineral dispersion and 1 mL samples taken at regular time intervals between 0 and 60 minutes, then less regularly until 48 hours. The samples were filtered through 0.2 µm filters (Minisart, UK) and analysed by UV-Vis spectrophotometry to determine the amount of drug remaining in the supernatant. Due to the nano-size of LRD and LXL21 particles these samples were forced to flocculate with an equal volume of 10 % w/v NaCl solution immediately before filtration. The amount of TC and DC adsorbed over time was tested against the first, pseudo-first, second, and pseudo-second orders of kinetics to determine which model the adsorption fitted best. Each test was repeated in triplicate.

#### *2.2.2.3. Adsorption isotherms for tetracycline and doxycycline*

Adsorption isotherms were obtained by dispersing 250 mg clay in 15 mL deionised water for 2 hours. Varying concentrations of drug solution were added to the dispersions and a final experiment volume of 25 mL ensured. These experiments were

undertaken in triplicate at pH 2.0 and pH 11.0 for both TC and DC, and at pH 5.0 for TC and pH 5.5 for DC, to further determine the effect of pH on adsorption. Adsorption onto KN was allowed to take place over a 24 hour period, whilst adsorption onto the other clays was over a 4-hour period; allowing equilibrium to be reached as confirmed by the kinetics studies. Samples were filtered through 0.2  $\mu\text{m}$  filters (Minisart, UK) and analysed with UV-Vis spectrophotometry to determine the amount of TC and DC remaining in the supernatant. Samples containing LRD and LXL21 were flocculated with an equal volume of 10 % w/v NaCl solution immediately before filtration. The amount of TC and DC adsorbed onto the clay minerals was tested against the Freundlich, Langmuir, and Temkin isotherm models to determine which model of adsorption fitted best.

Solid clay-drug composites from the pH-effect and adsorption isotherm experiments were collected by centrifugation and freeze-drying (Heto FD 2.5, at  $-50^{\circ}\text{C}$ ) for further analysis.

### *2.2.3. Mechanism of clay-tetracycline and clay-doxycycline interactions*

To determine whether TC and DC were adsorbed onto the surfaces or the interlayer space of the clay minerals X-Ray diffractometry (XRD) was employed. Samples were randomly orientated on aluminium discs and scanned between 3 and 20 deg  $2\theta$  using a Rigaku miniflex with a  $\text{CuK}\alpha 1$  radiation source. Each sample was scanned five times and the individual scans combined to reduce noise and clarify diffractions. The interlayer spacing of each sample was calculated from the  $d_{001}$  peak using the internal Rigaku miniflex analysis software.

The interaction of specific functional groups of the TC and DC molecules with the clay mineral surfaces were identified using infrared spectroscopy. Fourier-Transform Infrared (FT-IR) analysis was undertaken on a Perkin Elmer Spectrum BX FT-IR spectrometer with GladiATR attachment. Thirty-two scans were run between 4000 – 400  $\text{cm}^{-1}$  with an interval of 1.0  $\text{cm}^{-1}$  and a resolution of 2.0. Spectra for the antibiotics at varying pH were used to confirm adsorption shift(s) as a result of charge variation.

#### 2.2.4. Antibacterial activity assessment

In order to test the antibacterial efficacy of the clay-drug composites zone of inhibition experiments were undertaken against *Staphylococcus epidermidis* (NCTC 13360), *Propionibacterium acnes* (NCTC 737), and *Pseudomonas aeruginosa* (NCTC 12903). Liquid cultures of the bacteria were grown at 37 °C to a turbidity equal to a McFarland 0.5, which equates to a culture density of approximately  $1.5 \times 10^8$  colony forming units (CFU) per millilitre (McFarland, 1907). *S. epidermidis* and *P. aeruginosa* were grown in aerobic conditions in nutrient broth (Oxoid), whereas *P. acnes* was grown anaerobically in brain-heart broth (Oxoid).

Serial 1 in 10 dilutions of the McFarland 0.5 culture were performed and 200  $\mu\text{L}$  of each resultant culture was spread onto pre-poured nutrient agar (Oxoid) plates. After growing at 37 °C for 24 hours, for *S. epidermidis* and *P. aeruginosa*, and 48 hours for *P. acnes* the individual colonies were counted on the plates that did not exhibit confluent growth. These colony counts were used to back-calculate the CFU/mL in the starting McFarland 0.5 culture. For *P. acnes* brain-heart infusion agar was used and the plates were incubated under anaerobic conditions at 37 °C for 48 hours.

To undertake the zone of inhibition tests 1 mL of a 1 in 10 dilution of the McFarland 0.5 culture was used to inoculate 19 mL of molten agar (appropriate to each bacterial strain, as indicated above). The inoculated agar was then poured into 80 mm diameter agar plates and allowed to set in a fridge for one hour. Wells 5 mm in diameter were made in the agar using a sterilised cork-borer.

To demonstrate the efficacy of the unmodified drug 50  $\mu\text{L}$  of TC and DC solutions were placed into each well, at concentrations ranging between 5  $\mu\text{g}/\text{mL}$  and 250  $\mu\text{g}/\text{mL}$ . Dispersions of the unmodified clays at 40  $\text{mg}/\text{mL}$  were tested in the same way. Based on the drug load within the clay-drug composites, 40  $\text{mg}/\text{mL}$  dispersions of selected clay-drug composites were formed and 50  $\mu\text{L}$  of these injected into the wells. The plates were incubated under the appropriate conditions and the zones of inhibition measured with digital callipers. Each sample was tested three times and each zone of inhibition was measured five times.

## 2.3. Results and discussion

### 2.3.1. Effects of dispersion pH on adsorption

The pH of the dispersion was shown to have a profound effect on the adsorption of TC and DC onto the selected clay minerals, with the most obvious changes in adsorption behaviour occurring at extremes of pH. The pattern of TC adsorption (data not shown) onto each clay mineral over the pH spectrum were very similar to those observed for DC (figure 2.2), likely a result of their similar structures and locations of protonation.

Both of these molecules have similar  $pK_a$  values, indicating that the charge on the TC and DC molecule plays an important role on the adsorption onto the clay minerals. However, this does not fully explain the changes in TC and DC adsorption observed at extremes of pH.

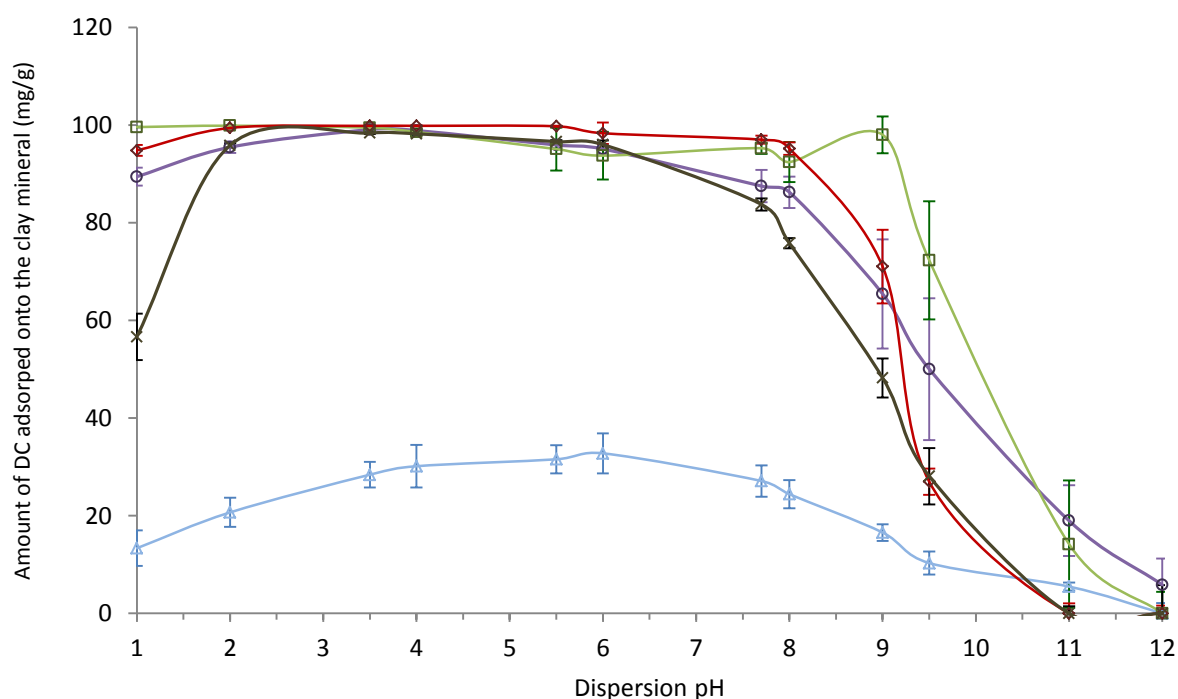


**Figure 2.2.** Average (mean  $\pm$ SD,  $n=3$ ) adsorption of doxycycline onto KN (blue triangles), MMTK10 (purple circles), rMMT (green squares), LRD (red diamonds), and LXL21 (black crosses) under the influence of varying dispersion pH.

At a pH of 2 or less both TC and DC are in their mono-positive forms which would favour adsorption onto the negatively charged clay mineral surface. However, at these pH values a reduction in TC and DC adsorbance was observed across all clays, except rMMT, and there are a number of possible reasons for this. As described in section 1.3.1, clay minerals are known to degrade in acidic solutions, causing a reduction in cation exchange capacity (CEC) and altering the structure of the clay mineral. This effect is likely the cause of the decrease in TC and DC adsorption onto LRD and LXL21, whose physical properties were visually observed to change as the pH was reduced below 2. The dispersion of LXL21 and LRD was no longer clear but became opalescent and more viscous; a likely effect of metal ion dissolution and remaining amorphous silica. A slight decrease in absorbance of TC and DC was also observed on MMTK10 but this cannot easily be explained by the effects of protons on the clay mineral structure, as this clay mineral has already been through a much more rigorous acidification process (Zhao et al., 2013). The increased concentration of protons in the dispersion may well be competing with TC and DC cations for exchange sites on the clay surface. It is likely that the increase in proton concentration reduced drug adsorbance by condensation of the Stern layer, followed by flocculation (Segad et al., 2010; Swartzen-Allen and Matijevic, 1974), and thus limited access to the interlayer space of the 2:1 clay minerals.

When the dispersion pH is between  $pK_{a2}$  and  $pK_{a3}$  for TC and DC the dimethyl amino group still retains its positive charge, with the negative charges being located across the A ring and the high density ketone-hydroxyl system on the molecules (figure 2.1) (Parolo et al., 2010). The close proximity of these negative charges to the dimethyl



amino group will make repulsion from the clay mineral surface more likely and thus reduce the amount of drug adsorption. As the pH of the dispersion is increased above the  $pK_{a3}$  the dimethyl amino group deprotonates, resulting in a di-negative species with no positive charge (Browne et al., 1980; Chang et al., 2009b). It should also be noted that as the pH of the dispersion increases the charge on the edge of the clay mineral layers changes from positive to negative, potentially causing further repulsion of negatively charged drug particles (Lagaly and Ziesmer, 2003; Swartzen-Allen and Matijevic, 1974). The greatly reduced adsorption of TC and DC at pH 11, and no adsorption at all for all clays at pH 12, except for MMTK10, shows that a positive charge on a drug molecule is required for significant adsorption to occur onto these clay minerals. Indeed, the same phenomenon was reported by Porubcan et al. (1978) who used XRD to demonstrate diminished adsorbance at pH 11. However, the data reported here show MMTK10 has a higher proportion of acid sites on its surface and these sites may have retained a positive charge that allowed some drug adsorption to occur.

From these data it is clear that a pH between 3.0 and 7.0 is ideal for adsorption of TC and DC onto clay minerals, which was also reported by Porubcan et al. (1978) and a number of other research groups (Figuerola et al., 2004; Parolo et al., 2013, 2010, 2008). Indeed, when the pH favours increasing proportions of zwitterionic molecules (pH 5.0 for TC and 5.5 for DC) this may favour further adsorption onto the clay mineral surface as indicated by the increased adsorption onto KN at this pH. However, this phenomenon was not as clearly demonstrated for the other clay minerals tested. More

data are presented throughout this chapter to further investigate the effects of dispersion pH on TC and DC adsorption.

The type of clay mineral used and the pH of the adsorption environment were shown to affect the amount of drug adsorbed. KN adsorbed the least drug compared to all the other clay minerals tested. In dispersion the KN layers are not able to dissociate from each other and therefore the total surface area available for adsorption is low, resulting in low adsorption capacity (Miranda-Trevino and Coles, 2003). This is compounded by the fact KN has a minimal CEC. Cation exchange has been proposed as the main mechanism of TC adsorption onto clay minerals (Figueroa et al., 2004; Li et al., 2010; Parolo et al., 2013) and this is discussed further throughout this chapter. Based on the theory of surface area and CEC it is unsurprising that rMMT, LXL21, and LRD adsorbed much more drug compared to KN. The differences in adsorption behaviour between 1:1 and 2:1 clay minerals has been discussed in chapter 1 and these differences become evident when the trends in figure 2.2 are compared. Essentially, the platelets of these clay minerals are able to dissociate in a water dispersion allowing the drug to adsorb onto the internal surfaces of the clay mineral particles. These data demonstrate that clay mineral CEC and specific surface area (SSA) values are also important factors in the adsorption of drug molecules (Aguzzi et al., 2005). Whilst the data presented in this section do not easily discriminate between the adsorption capacity of the 2:1 clay minerals used, the data presented in subsequent sections 2.3.2 and 2.3.3 elucidate these differences.

### 2.3.2. Adsorption kinetics

The pH of the dispersion media played a crucial role in the rate of TC and DC (figure 2.3) adsorption onto the clay minerals. Basic dispersions with a pH of 11 were shown to be least favourable for TC and DC adsorption, appearing to have a shallow adsorption profile thus indicating slower rate of adsorption. It should also be noted that the quantity of TC and DC adsorbed was also greatly reduced at pH 11 compared to pH 2 and pH 5.0 for TC or pH 5.5 for DC, the reasons for which are described in detail above. At pH 11 there was greater variation in the amount of TC and DC adsorbed (standard deviations represented by error bars in figure 2.3), compared to at pH 2 or pH 5.0 for TC and pH 5.5 for DC. This is likely a result of the clay mineral surfaces and edges being negatively charged; repelling the negative charges that would be present on these tetracycline molecules. NaOH was used to adjust the pH to 11 and as described by Zhao et al. (2012) the positively charged  $\text{Na}^+$  ions were likely competing with TC and DC for the clay-mineral surfaces, reducing the likelihood of these drugs adsorbing onto the clay-minerals and introducing greater variability to these results. Adjusting the dispersion pH to 2 or at a level that favours the zwitterionic state of TC (pH 5.0) and DC (pH 5.5) were shown to hasten and favour drug adsorption onto the clay minerals as observed through the gradient and amplitude of the rate of adsorption graphs given in figure 2.3.

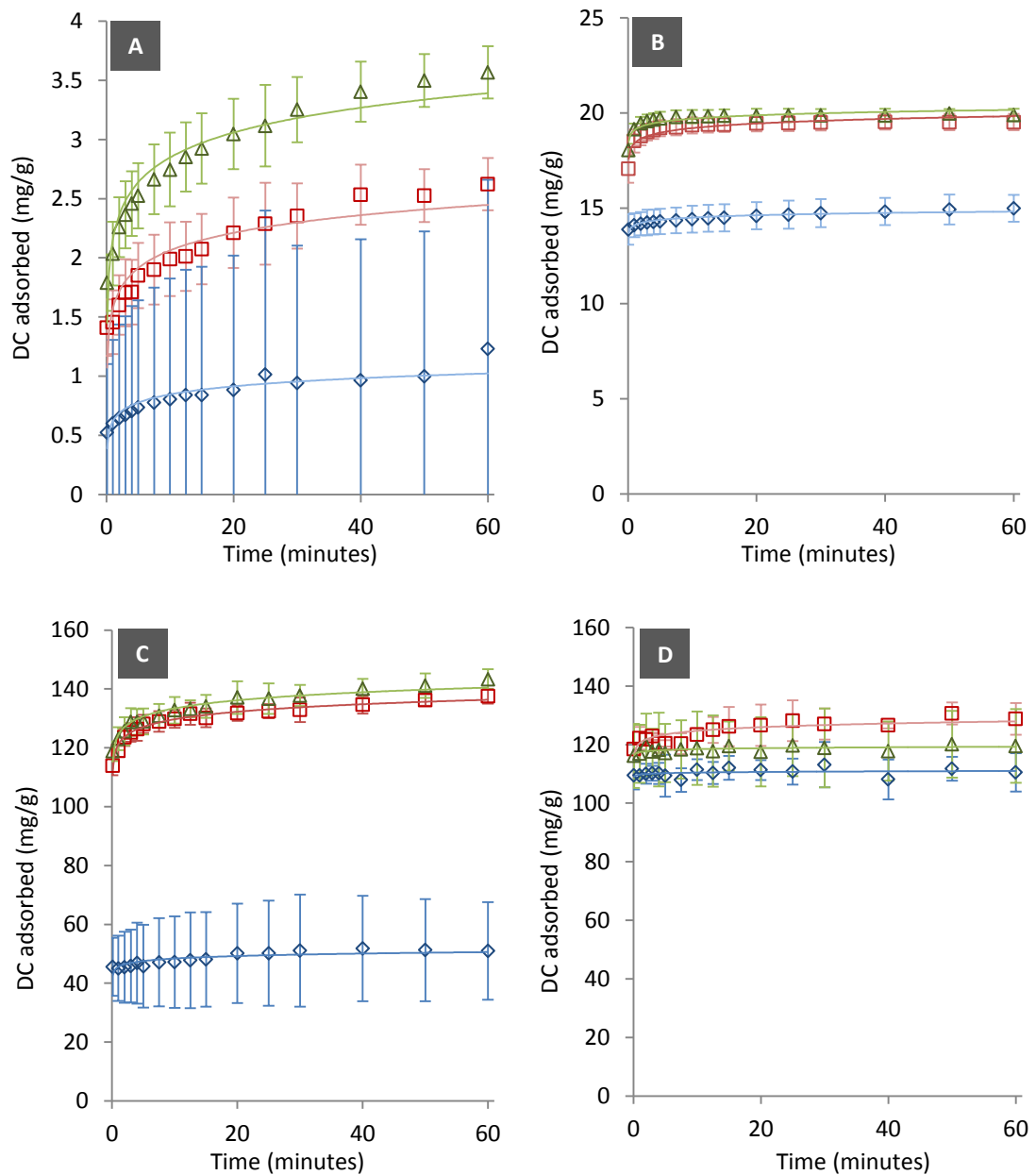


**Figure 2.3.** Rate of drug adsorption (mean  $\pm$ SD,  $n=3$ ) depicted by amount of DC adsorbed onto (A) KN, (B) MMTK10, (C) rMMT, and (D) LXL21 at pH 2 (red squares), pH 5.5 (green triangles), and pH 11 (blue diamonds) at defined time points.

However, to further investigate and characterise the effect of drug, clay mineral, and dispersion pH on the kinetics of drug adsorption the data were applied to first-order (equation 2.1), second-order (equation 2.2), pseudo first-order (equation 2.3) and pseudo second-order (equation 2.4) adsorption kinetic models (Kammerer et al., 2011; Tien and Ramarao, 2014).

Equation 2.1

$$\frac{\Delta(q_e - q_t)}{\Delta t} = -k(q_e - q_t)$$

Equation 2.2

$$\frac{\Delta(q_e - q_t)}{\Delta t} = -k(q_e - q_t)^2$$

Where  $q_e$  (mg/g) is the amount of drug adsorbed at equilibrium and  $q_t$  (mg/g) is the amount of drug adsorbed at time  $t$  (seconds) with a rate constant of  $k$  ( $s^{-1}$ ).

Equation 2.3

$$\ln(q_e - q_t) = \beta - kt$$

Equation 2.3 is the linearised form of the pseudo first-order model where  $q_e$  (mg/g) is the amount of drug adsorbed at equilibrium and  $q_t$  (mg/g) is the amount of drug adsorbed at time  $t$  (s).  $\beta$  and  $k$  (the rate constant,  $s^{-1}$ ) can be found by plotting  $\ln(q_e - q_t)$  against  $t$ , whereby  $\beta$  is the intercept and  $k$  is the slope.

Equation 2.4

$$\frac{t}{q_t} = \frac{1}{kq_e^2} + \frac{1}{q_e} \times t$$

Equation 2.4 is the linearised form of the pseudo second-order model where  $q_e$  (mg/g) is the amount of drug adsorbed at equilibrium and  $q_t$  (mg/g) is the amount of drug adsorbed at time  $t$  (h). By plotting  $t/q_t$  versus  $t$  the rate constant  $k$  (g/mg·h) can be obtained from the slope and  $q_e$  from the intercept.  $kq_e^2$  is the initial rate of adsorption (mg/g·h) and is found mathematically once  $k$  and  $q_e$  are derived.

When experimental data were plotted against the linearised pseudo first (equation 2.3) and pseudo second order (equation 2.4) kinetic models the data fitted better to the pseudo second order (figure 2.4 and table 2.1), which suggests that the adsorption of TC and DC involves two adsorption sites on the clay mineral surface (Kammerer et al., 2011).

By utilising the pseudo second order model it was possible to determine the initial rate of TC and DC adsorption, derive rate constants, and also estimate the amount of drug that can be adsorbed onto the clay mineral at equilibrium (table 2.1). As observed from the experimental data (figure 2.3) the structure of the clay mineral and the pH of the dispersion environment played an important role in the adsorption rate and amount of TC and DC.

The initial rate of adsorption differed greatly depending on the structure of the clay mineral used. The adsorption rate onto MMTK10 (3262 – 25000 mg/g·h) was one to two orders of magnitude faster than that of KN (4.01 – 110.86 mg/g·h). The clay minerals that were able to fully swell showed adsorption rates that were a further one to two orders of magnitude faster than that calculated for MMTK10. LXL21 and LRD demonstrated an ability to adsorb TC and DC at much faster rates than rMMT. In dispersion, LRD and LXL21 layers will almost completely dissociate from each other at the concentrations used in these studies, resulting in a much greater available surface area for interaction with TC and DC (Neumann and Sansom, 1971). It can therefore be assumed that there is less competition for available adsorption sites allowing a much faster initial rate of adsorption.

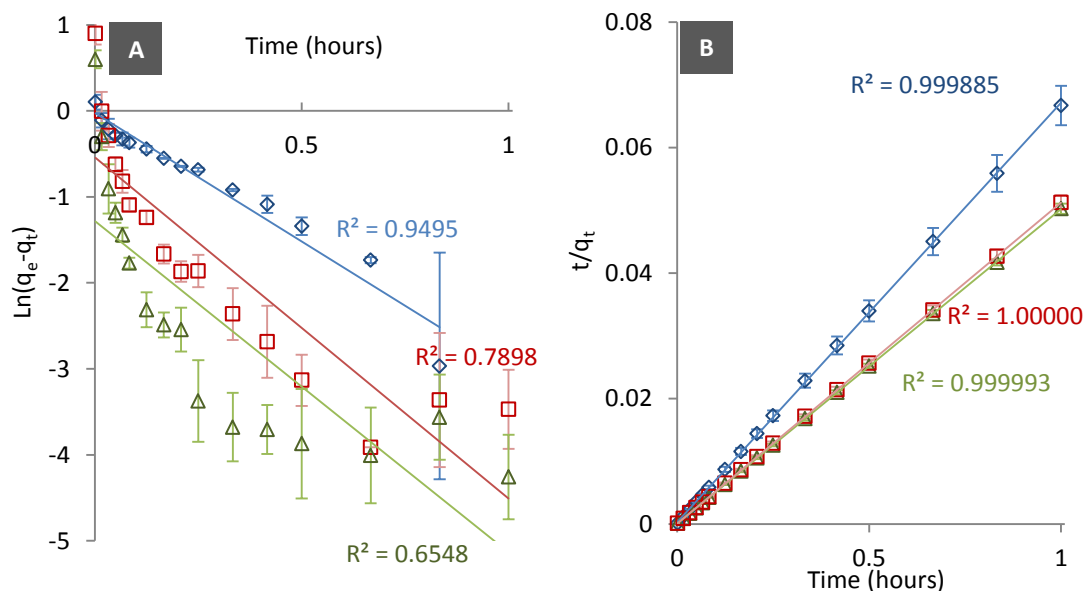


**Figure 2.4.** Pseudo first-order kinetics (A) and pseudo second-order kinetics (B) for the adsorption of DC onto rMMT at pH 2 (red squares), pH 5.5 (green triangles), and pH 11 (blue diamonds) at defined time points (mean  $\pm$ SD, n=3).

Data for TC and DC adsorption onto KN, MMTK10, rMMT, LXL21 indicate that an acidic environment is more favourable for the adsorption of these two drugs, which was also reported by a number of other teams that solely investigated the adsorption of TC onto clay minerals (Chang et al., 2009a; Parolo et al., 2013, 2010). Parolo et al. (2013 and 2010) suggested that the presence of positive charges on the TC and DC molecules allows them to interact readily with the negatively charged clay mineral surface. As the pH increases the TC and DC molecules become increasingly negatively charged (Parolo et al., 2008) which can lead to repulsion from the clay mineral surface. At pH 11 the TC and DC molecules are predominantly negatively charged and the edge charges on the clay mineral particles will likely have transitioned from positive to negative. This results in a system wherein the individual components repel each other and this explains the drop in rate of adsorption observed at this pH (Parolo et al., 2008). This trend did not translate to LRD and this might be for a number of reasons. The chemistry of LRD allows it to adjust dispersions to around pH 9, whereas LXL21 buffers to a more neutral pH. This may result in a more positive charge remaining at edge sites at pH 11, which would allow adsorption onto the clay mineral edges. The aspect ratio of Laponite® layers is around 1:20 (20 nm diameter, 1 nm thick) so a significant proportion of LRD surface area is composed of edge sites. As the electrolyte concentration is increased by addition of NaOH it is possible that LRD layers re-associated, using the sodium ions as interlayer cations (Perkins et al., 1974). This would contribute to a reduction in the availability of clay mineral surface for interaction, resulting in the edge sites being the predominant site for interaction. Whilst the re-association of layers was likely to occur with other clay minerals, including LXL21, the extent of drug adsorption was adversely effected by the edge sites bearing a repulsive negative charge.



**Table 2.1.** Goodness of fit ( $R^2$ ) of selected kinetic orders for the adsorption of TC and DC onto selected clay minerals at defined pH. Where  $k$  is the rate constant,  $q_e$  is the estimated amount of drug adsorbed.

Clay Mineral	Drug	pH	Pseudo 1 <sup>st</sup> Order	Pseudo 2 <sup>nd</sup> Order			
			( $R^2$ )	( $R^2$ )	Initial rate (mg/g h)	$k$ (g/mg h)	$q_e$ (mg/g)
KN	TC	2	0.9432	0.9975	110.86	10.56	3.24
		5	0.9672	0.9905	40.145	6.25	2.54
		11	0.1853	0.9156	62.112	412.87	0.39
	DC	2	0.7762	0.9949	65.36	9.43	2.63
		5.5	0.6423	0.9957	97.09	7.55	3.59
		11	0.9021	0.9672	4.01	27.54	0.38
MMTK10	TC	2	0.9203	0.9999	3,714	6.52	23.88
		5	0.7860	0.9999	3,262	6.33	22.71
		11	0.6624	0.9982	228.04	20.50	3.35
	DC	2	0.8346	1.0000	14,300	37.39	19.55
		5.5	0.6946	0.9999	25,000	62.93	19.93
		11	0.9724	0.9998	3,333	14.90	14.96
rMMT	TC	2	0.9393	0.9999	37,593	1.51	157.82
		5	0.7263	0.9999	45,871	2.97	124.36
		11	0.0344	0.9987	12,150	16.10	27.47
	DC	2	0.7898	0.9997	20,000	1.07	136.99
		5.5	0.6548	0.9996	14,285	0.70	142.86
		11	0.9495	0.9996	5,000	2.21	47.62
LRD	TC	2	0.5097	0.9999	105,263	3.99	162.48
		5	0.1938	0.9999	62,893	3.95	126.19
		11	0.0715	0.9999	208,333	12.08	131.31
	DC	2	0.7394	0.9999	100,000	4.87	143.27
		5.5	0.7791	0.9998	20,000	0.93	147.06
		11	0.3898	0.9998	29,000	1.54	137.60
LXL21	TC	2	0.2121	0.9998	78,125	6.05	113.67
		5	0.5563	0.9999	69,444	6.03	107.34
		11	0.0915	0.9998	90,909	5.97	123.397
	DC	2	0.4827	0.9997	25,000	1.42	132.80
		5.5	0.1466	0.9999	100,000	7.08	118.86
		11	0.1589	0.9997	44,200	39.29	110.42

### 2.3.3. Adsorption isotherms

Adsorption isotherms are mathematical models that have been utilised for many years to describe various adsorption phenomenon of compounds from gaseous or aqueous environments onto solid and porous surfaces. The Langmuir model assumes that a single layer of molecules will adsorb onto a surface, consisting of identical adsorption sites, to form a monolayer without any interactions between adsorbate molecules

(figure 2.5 A). In contrast, the Freundlich model is not limited to the formation of a monolayer and also accounts for adsorption surfaces of heterogeneous adsorption sites, whereby adsorption occurs at the sites allowing for greatest adsorption intensity first (Figure 2.5 B). The Temkin isotherm is specifically designed to derive the energy of adsorption, which is expressed as heat of adsorption, by accounting for direct interactions between the adsorbate and the adsorbent surface (Figure 2.5 C) (Foo and Hameed, 2014; Kammerer et al., 2011). Although originally developed to describe the adsorption of gaseous compounds onto solid surfaces (Foo and Hameed, 2014), these models have been widely applied to disperse aqueous systems; notably the adsorption of organic molecules onto clay mineral surfaces (Chang et al., 2016; Kammerer et al., 2011; Li et al., 2011; Zhao et al., 2012).

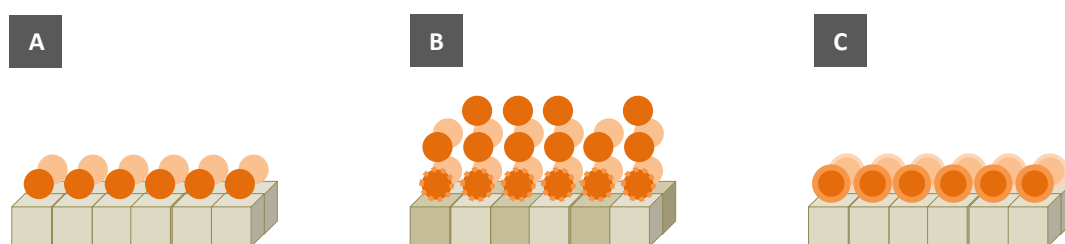


**Figure 2.5.** Artistic representation of the (A) Langmuir, (B) Freundlich, and (C) Temkin adsorption models. The brown squares represent sites of adsorption on a surface (different shades represent heterogeneous adsorption sites). The orange circles represent the adsorbate, whereby the dashed outer ring represents indirect interaction and the solid outer ring represents direct interaction with the surface.

Utilising these differing adsorption models allows the interaction between TC and DC and the clay mineral surfaces to be described in more detail with regards to the impact of clay mineral chemistry and dispersion pH on adsorption capacity, TC and DC

arrangement at the clay mineral surface, and adsorption energies. By measuring the drug concentration remaining within the supernatant and the calculated mass of drug adsorbed per gram of clay mineral it was possible to plot adsorption isotherms for each of the interactions tested at each pH. Examining this process over a range of DC and TC concentrations allowed for more accurate evaluation of the drug adsorption capacity of these clay minerals.

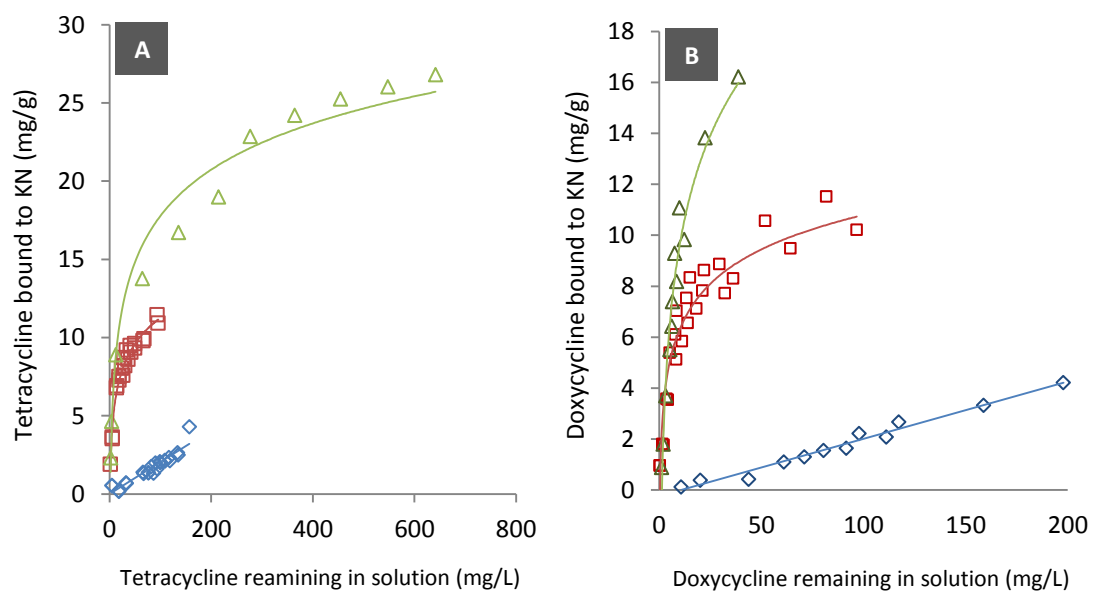


**Figure 2.6.** Adsorption isotherms (n=3) for the adsorption of (A) TC and (B) DC onto KN at pH 2 (red squares), pH 5.0 for TC and pH 5.5 for DC (green triangles), and pH 11 (blue diamonds).

Figure 2.6 gives the experimental data and adsorption isotherms obtained for the adsorption of TC and DC onto KN, whereas figure 2.7 gives adsorption isotherms for TC onto MMTK10. The compiled results for the adsorption of TC and DC onto each clay mineral at each defined pH are given in table 2.2

The experimental data were plotted against linearised versions of the Langmuir (equation 2.5), Freundlich (equation 2.6) and Temkin (equation 2.7) adsorption models (Kammerer et al., 2011).

Equation 2.5

$$\frac{1}{q_e} = \frac{1}{K_L C_e} + \frac{1}{Qm_L}$$

Linearised Langmuir equation where  $q_e$  is the calculated amount of drug adsorbed per gram of clay mineral,  $C_e$  is the measured concentration of drug remaining in supernatant (mg/L) at equilibrium,  $Qm_L$  is the monolayer capacity (mg/g), and  $K_L$  is the Langmuir constant(L/g). The values for  $Qm_L$  and  $K_L$  can be derived from the intercept and gradient when plotting the inverse of  $q_e$  against the inverse of  $C_e$ .

Equation 2.6

$$\log q_e = \log K_F + b_F \log C_e$$

Linearised Freundlich equation where  $q_e$  is the calculated amount of drug adsorbed per gram of clay mineral (mg/g),  $C_e$  is the measured concentration of drug remaining in supernatant (mg/L) at equilibrium,  $K_F$  is the Freundlich constant (L/g) and a representation of adsorption capacity, and  $b_F$  is a representation of the adsorption

intensity (no units). Values for  $K_F$  and  $b_F$  are found from the slope and intercept from the plot of  $\log q_e$  against  $\log C_e$ .

Equation 2.7

$$q_e = B \ln A + B \ln C_e$$

Linearised Temkin equation where  $q_e$  is the calculated amount of drug adsorbed per gram of clay mineral (mg/g),  $C_e$  is the measured concentration of drug remaining in supernatant (mg/L),  $A$  is the isotherm constant (L/mg), and  $B$  is the heat of adsorption (J/mol).  $A$  and  $B$  are derived from plotting  $q_e$  against  $\ln C_e$ . The isotherm energy constant  $b_T$  (no units) can be determined through equation 2.8.

Equation 2.8

$$B = \frac{R T}{b_T}$$

Where  $R$  is the gas constant and  $T$  is the temperature of the system.

Experimental data were plotted against the linearised isotherm models so that the fit to each adsorption model could be determined for each experiment at each of the dispersion pH tested. Examples of these plots are given in figures 2.7 B, C, and D for the adsorption of TC onto MMTK10 (figure 2.7 A) at pH 5. Equations of the line were used to directly and indirectly determine certain behaviours expressed during the adsorption process (Kammerer et al., 2011). The Langmuir model was used to estimate

the amount of drug required to form a monolayer at the clay mineral surface (mg/g), the Freundlich model was used to estimate the intensity of the adsorption process ( $b_F$ , dimensionless value), while the Temkin model was used to estimate the heat of adsorption ( $B$ , J/mol) (Kammerer et al., 2011). Table 2.2 gives the fit of each experiment to each of the adsorption models tested, alongside the derived adsorption behaviours.

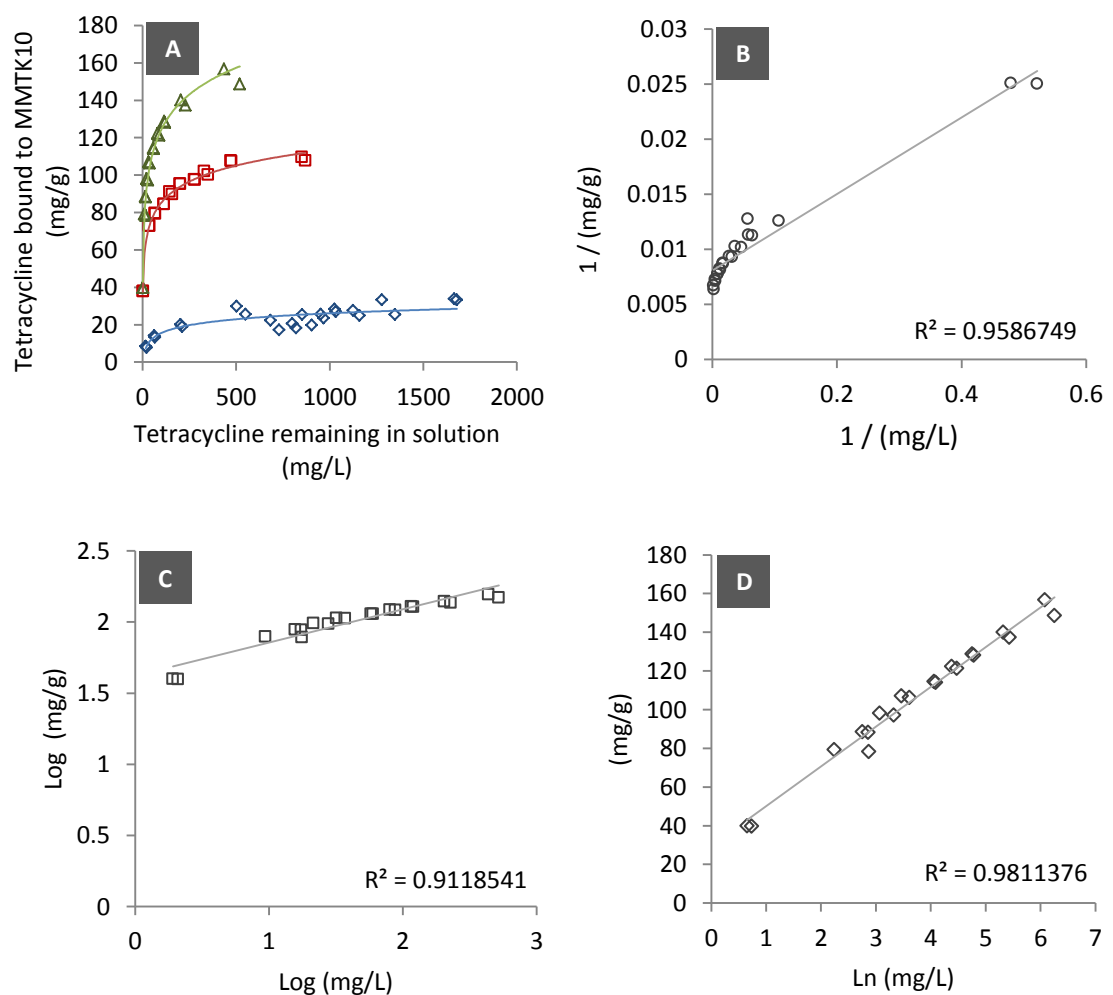


**Figure 2.7.** (A) Adsorption isotherms for the adsorption of TC onto MMTK10 at pH 2 (red squares), pH 5 (green triangles), and pH 11 (blue diamonds). The adsorption measurements at pH 5 were plotted against the (B) Langmuir model, (C) Freundlich model, and (D) Temkin model.

**Table 2.2.** Correlation of fit between experimental adsorption data to the Langmuir, Freundlich, and Temkin adsorption isotherm models. Where  $S_m$  is the monolayer coverage,  $b_F$  is a dimensionless value for adsorbance intensity, and  $B$  is the heat of adsorption.

Clay Mineral	Drug	pH	Langmuir ( $R^2$ )	Freundlich ( $R^2$ )	Temkin ( $R^2$ )	$S_m$ (mg/g)	$b_F$	$B$ (J/mol)
KN	TC	2	0.9811	0.9272	0.8472	10.82	1.93	2.27
		5	0.9719	0.9328	0.9283	25.80	3.10	4.50
		11	0.9811	0.9529	0.9158	3.84	150.45	1.13
	DC	2	0.9128	0.9129	0.9181	7.18	1.80	1.95
		5.5	0.9690	0.8424	0.8246	23.51	1.86	2.87
		11	0.9514	0.7422	0.6403	2.73	187.71	1.22
MMTK10	TC	2	0.9443	0.9712	0.9915	94.15	35.62	12.34
		5	0.9587	0.9119	0.9811	123.72	42.01	20.57
		11	0.8839	0.8251	0.7228	25.18	4.21	4.59
	DC	2	0.9557	0.9065	0.9528	94.94	39.69	12.42
		5.5	0.9958	0.9472	0.9523	106.36	19.93	18.36
		11	0.9093	0.9678	0.9715	13.03	7.14	11.51
rMMT	TC	2	0.8170	0.9288	0.9016	171.51	79.20	45.84
		5	0.9648	0.9931	0.8623	130.22	16.96	37.41
		11	0.6642	0.6015	0.5011	17.31	7.81	2.51
	DC	2	0.9856	0.9626	0.9918	266.82	59.99	61.06
		5.5	0.9768	0.9214	0.8308	158.65	12.65	33.95
		11	0.9516	0.8516	0.6518	31.46	1.63	6.55
LRD	TC	2	0.9899	0.9890	0.9057	266.04	6.79	39.10
		5	0.6374	0.7138	0.5370	74.33	1.49	84.87
		11	0.9883	0.9894	0.8939	158.19	7.45	30.43
	DC	2	0.9816	0.9751	0.9205	189.27	11.27	39.51
		5.5	0.9897	0.9859	0.9079	308.45	1.60	72.08
		11	0.9338	0.9190	0.7445	109.04	1.50	25.97
LXL21	TC	2	0.9947	0.9960	0.8947	227.35	2.27	30.22
		5	0.9977	0.9940	0.8893	238.12	1.60	36.83
		11	0.9951	0.9941	0.9048	78.55	2.00	56.93
	DC	2	0.9784	0.9706	0.8037	215.84	2.79	31.90
		5.5	0.9943	0.9947	0.8457	290.46	1.40	39.26
		11	0.9540	0.9747	0.8513	110.34	1.01	36.72

The adsorption of TC and DC onto KN was shown to more closely follow the Langmuir model than the Freundlich or Temkin models. This indicates that the adsorption of these drug molecules onto the surface of KN was a saturable process and a monolayer was formed at the surface of the KN particles (Kammerer et al., 2011). As predicted from the pH variability studies (section 2.3.1), and also reported by Figueroa, et al. (2004), the adsorption of TC and DC was more pronounced when the dispersion pH favoured zwitterionic drug molecules and this was reflected in the monolayer saturation ( $S_m$ , mg/g) values obtained at these pH compared to at pH 2 or 11. The estimated intensity of adsorption ( $b_F$ ) was found to be far greater at pH 11 compared to the lower pH tested. This change in adsorption intensity was not observed for the adsorption of TC and DC onto the other clay minerals tested and was therefore concluded to be the result of the structure of KN and its behaviour at pH 11. Whereas the diffuse double layer and the edge charges change dramatically over the full pH range tested, these changes are not likely to occur in 1:1 clays minerals such as KN. In turn this could have allowed the negatively charged TC and DC molecules to interact with the edges of the KN particles more intensely than the faces of the KN layers.

Results for the adsorption of TC and DC onto MMTK10 followed similar patterns to those seen in the initial pH investigations and the study of adsorption kinetics. More drug was adsorbed onto the MMTK10 at pH that favoured the zwitterionic form of the drug molecules and this in turn resulted in a more concentrated monolayer being formed at the clay mineral surface (Figueroa et al., 2004; Porubcan et al., 1978). This indicates that inducing the zwitterionic form of TC and DC allows the drug molecules to become more tightly packed at the clay mineral surface. The adsorption of TC and DC



at pH 2, when the molecules are predominantly positively charged, allowed for good adsorption and a concentrated monolayer but interaction between both components was less intense than at pH 5 or 5.5. The interaction between the drug molecules and MMTK10 was found to be least intense at pH 11, which is reflected in the small amounts of drug adsorbed and the less densely packed monolayer estimated through the Langmuir model.

The adsorption of TC and DC onto rMMT presented a number of differences when compared to the acid activated counterpart, MMTK10. All of the values derived from experimentation indicate that the adsorption of the drug molecules onto rMMT is more intense at pH 2 compared to higher pH. In turn, this resulted in a large adsorption of drug and a more densely packed monolayer being estimated through the Langmuir model. The structure and chemistry of rMMT gives it a high surface charge and a large CEC when compared to the other clay minerals used in this study. The high negative charge surfaces will interact more readily with positively charged molecules, explaining the very large adsorption of drug at pH 2. These data also suggest the adsorption of TC and DC onto rMMT is predominantly via cation exchange as a positively charged molecule will be needed to displace the counterbalancing cations from the clay mineral surface (Chang et al., 2009c).

The same pattern in adsorption behaviour was not observed for LRD and LXL21. When the adsorption process was undertaken at pH 5.0 for TC and pH 5.5 for DC more drug was adsorbed onto the clay mineral surface and the Langmuir model predicted a higher concentration of drug within the monolayer. As for the other clay minerals, a

dispersion pH of 11 was least favourable for adsorption. Undertaking the adsorption at pH 2 was not as favourable as for that favouring zwitterionic charge. The layers of LXL21 and LRD are more labile in acidic media than rMMT (Thompson and Butterworth, 1992), breaking down easily to release structural cations and affecting surface charge and CEC. This in turn can reduce the adsorption capacity of the increasingly amorphous clay mineral and explains the reduction in drug adsorption observed. However, at pH 2 the intensity of interaction was determined to be larger than at pH 5.0 or pH 5.5. Modification of the LXL21 and LRD layer structure not only reduces the charge distribution across the layer but can intensify the acid sites present and it may be possible that these sites interact more strongly with the drug molecules. It may also be possible that any residual CEC resulted in the strong interactions that were also observed for the adsorption of TC and DC onto rMMT. The intensity of adsorption was much lower at pH 5 or pH 5.5 and was generally equivalent or lower than the intensity derived for adsorption at pH 11 suggesting that cation exchange is not the only process by which TC and DC interact with LRD and LXL21 and secondary interactions may also play a role (Aguzzi et al., 2005; Parolo et al., 2008). Minimal differences in how well the data fitted the Langmuir or Freundlich model were observed, so little distinction between the models could be made. There are similarities between the Langmuir and Freundlich adsorption models whereby the initial stage of adsorption involving low concentrations of adsorbate, depicted by a straight line of increasing surface adsorption, is the same for both models. The Langmuir model diverges from the Freundlich model when it considers the formation of a monolayer at the sorbent surface (Kammerer et al., 2011; Langmuir, 1918). This also supports why no plateau of monolayer formation was observed on the LRD and LXL21 adsorption isotherms

plotted. Therefore, it may be possible that no distinct monolayer of TC or DC formed at the surface of LXL21 or LRD and that drug adsorption under certain circumstances is able to continue far beyond the expected monolayer formation value.

The heat of adsorption ( $B$ , J/mol) calculated using the Temkin model was low for all of the composites examined, indicating that the interaction between DC and TC and the clay minerals was by physisorption, such as van der Waals forces, rather than by chemisorption, such as covalent bonding, (Itodo and Itodo, 2010; Puttamat and Pavarajarn, 2016). The effect of the clay mineral surface charge was observed here as the heat of adsorption, and therefore the strength of the physisorption, for DC and TC onto KN were generally lower compared to the other clay minerals. These weak interactions are necessary, however, to allow the drug molecules to desorb from the clay mineral surfaces and impose their effects on bacterial cells (see section 2.3.6)

#### *2.3.4. X-ray diffraction analyses*

The use of X-ray in the elucidation of clay mineral structure is common across the literature and is a well-established method for determining the size of the interlayer space. A number of other authors have utilised powder XRD to measure structural and chemical changes in clay minerals as a result of a wide range of chemical processes, including the adsorption of organic molecules (Li et al., 2010; Rives et al., 2014; Xuan et al., 2013).

The X-ray diffractograms for the naturally occurring KN and rMMT (figure 2.8 A) show many similarities but also a number of key differences. The similarities are borne

through the similar molecular contents and arrangements of the phyllosilicate sheets and layers. Some differences in the diffraction can be attributed to the extra silicate sheet in rMMT. One of the most important differences between these two clay minerals' diffractograms is the position and shape of the  $d_{001}$  peak, located at 9.0 deg  $2\theta$  for KN and 7.4 deg  $2\theta$  for rMMT, which is a result of the diffraction caused by the inner surfaces of the interlayer space. This  $d_{001}$  diffraction can be used to determine the distance between clay mineral layers, utilising Bragg's Law (equation 2.9), and is a useful measure of whether the guest molecules have been integrated into the interlayer space of the clay mineral (Datta, 2013; Joshi et al., 2010; Vaiana et al., 2011; Zhao et al., 2013).

Equation 2.9

$$n\lambda = 2d \sin \theta$$

Where  $\lambda$  is the wavelength of the X-Ray beam (0.154 nm),  $\theta$  is the Bragg's scattering angle, and  $d$  is the spacing (nm, convertible to Å) between the clay mineral sheets.

The irregularity of clay mineral layer arrangement within aggregates (section 1.2.2) and imperfections across the structure of the clay mineral layers (section 1.2.1) means that diffractograms for these materials do not strictly obey Bragg's Law (Drits, 2003). It is known that clay mineral layers do not always align perfectly and may contain imperfections such as overlapping and bending, which can all affect the regularity of the  $d_{001}$  diffraction (Villar et al., 2012). The width and asymmetry of the  $d_{001}$  diffraction is greater in rMMT because the layers are not held together in as tight and regular

fashion as in KN but are associated by various interlayer cations, which can lead to changes in the interlayer spacing (Kaufhold and Dohrmann, 2009). Regardless of these limitations XRD analysis is still widely used to determine the location of organic molecules adsorbed onto clay minerals (Chang et al., 2009b; Li et al., 2010; Park et al., 2008; Parolo et al., 2008; Rives et al., 2014; Sánchez-Martín et al., 1988; Xuan et al., 2013).

The diffractogram of MMTK10 (figure 2.8 A) is presented alongside that of rMMT to demonstrate the differences between these, originally similar, clay minerals. The overall unremarkable diffractogram for MMTK10 is similar to that recorded by Kaygusuz and Erim (2013) and could be a result of the dissolution of ions from the metal hydroxide sheet (Kaygusuz and Erim, 2013; Nunes et al., 2007; Tong et al., 2013). It is possible that the diffractions at 26.5, 35.0, and 46.0 deg  $2\theta$  are caused by silicate sheets, as these are present in the same position across KN, rMMT, and MMTK10. The diffractograms for LRD and LXL21 have been presented separately (figure 2.8 B) to clearly demonstrate the difference in X-ray diffractions caused by these synthetic clay minerals in comparison to the natural and processed clay minerals. Diffractions for LRD and LXL21 are located at the same positions and are representative of the very similar structure and chemical content of these two species (BYK Additives & Instruments, 2014). Whilst chemically synthesising clay minerals such as LRD and LXL21 leads to a material free from impurities (Neumann and Sansom, 1971), which is very attractive for pharmaceutical purposes, the diffractograms are indicative of a much more amorphous material compared to KN and rMMT. On a molecular level the structure of LRD and LXL21 is likely to be more regular and crystalline than for KN and rMMT.

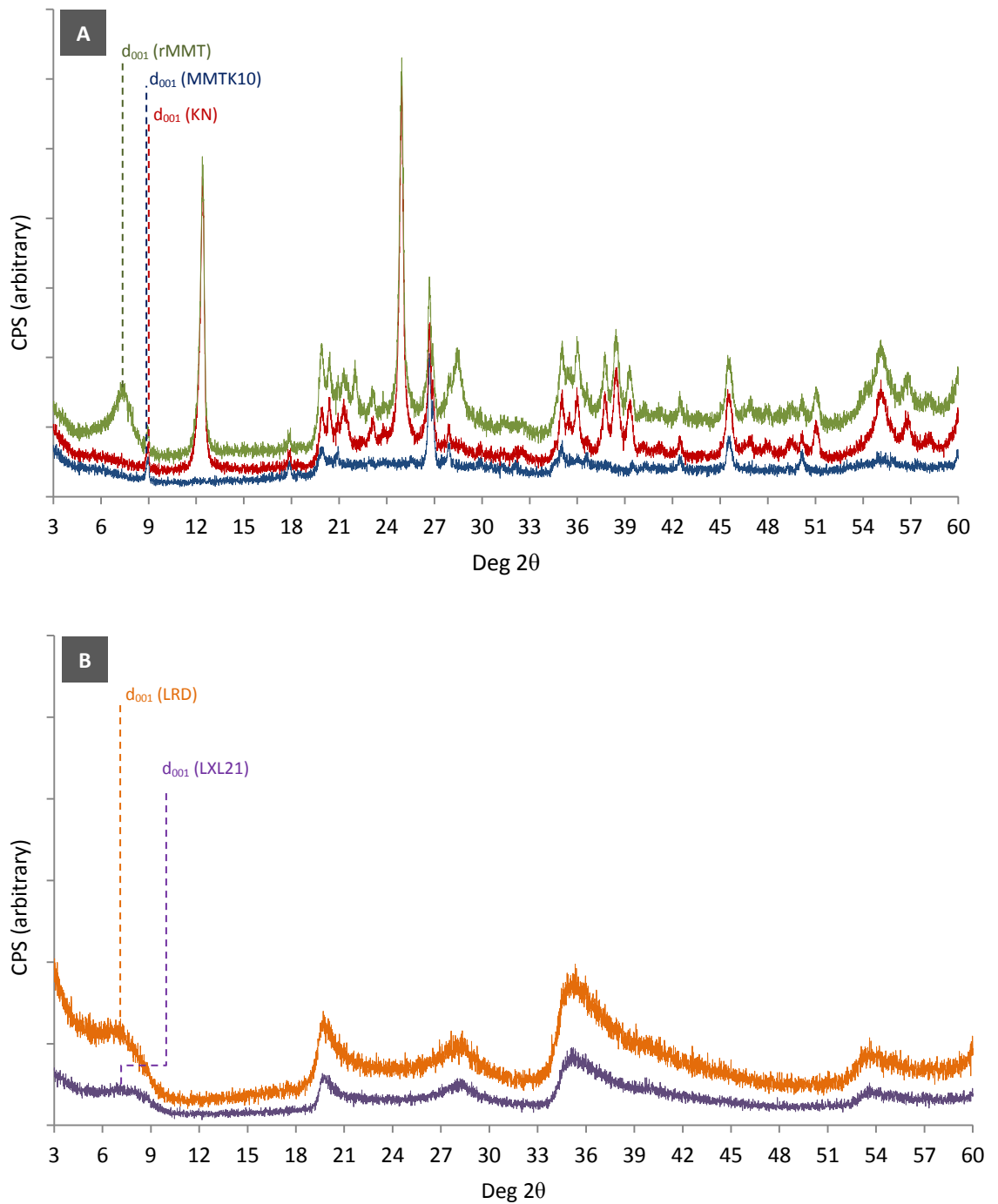


**Figure 2.8.** X-ray diffractograms of kaolin (red), refined montmorillonite (green), and montmorillonite K-10 (blue) are shown in A. X-ray diffractograms of Laponite® RD (orange) and Laponite® XL21 (purple) are shown in B.

However, the layer diameter of LRD and LXL21 is much smaller than that of rMMT and KN leading to an irregular structure on the macro scale, as layers form particles and aggregates (Avery and Ramsay, 1986; Lagaly and Ziesmer, 2003). In turn, this leads to wide asymmetric  $d_{001}$  peaks (Janeba et al., 1998) potentially making determination of the location of adsorbed TC and DC more difficult.

The diffractograms for TC and DC are presented in figure 2.9 and represent a typical XRD pattern for crystalline materials. The diffractions in these two patterns are much more clearly defined and symmetric in comparison to the clay mineral diffractograms. The high-regularity of the molecular arrangement is also demonstrated through the intensity of the peaks, which is far greater than those obtained for any of the clay minerals. Whilst the molecular structures of TC and DC are very similar the way they interact and arrange in crystal lattices is different and this leads to the differences in diffraction patterns obtained.

The layers of KN are held tightly and closely together by hydrogen bonds, which makes them hard to separate (Miranda-Trevino and Coles, 2003). The adsorption of TC and DC onto KN resulted in no significant change in the shape or position of the  $d_{001}$  peak (figure 2.10 A) indicating that neither of these drugs adsorbed into the interlayer space, which remained 7.15 Å in distance in all composites tested. TC and DC were more likely to be adsorbed onto the outer surfaces of the KN particles (Miranda-Trevino and Coles, 2003), supporting the overall reasoning for the low adsorption capacity of KN observed above.

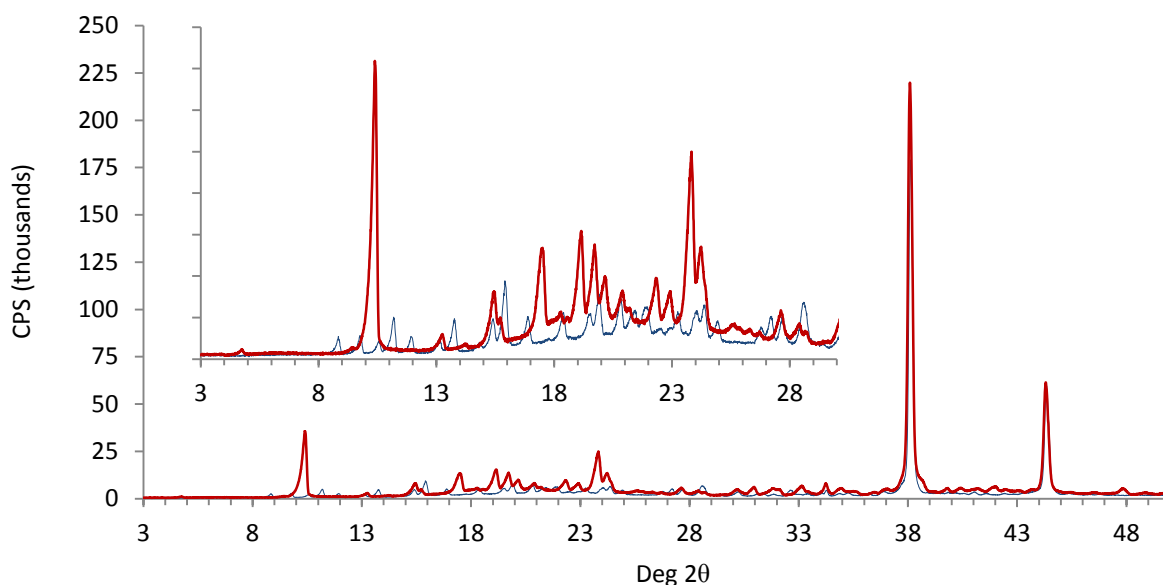


**Figure 2.9.** X-ray diffractograms of unmodified tetracycline (blue) and doxycycline (red). Inlay is expanded region of 3-30 deg  $2\theta$ .

The  $d_{001}$  diffraction in MMTK10 also remained at the same position as the amount of drug adsorbed increased (figure 2.10 B). This indicates that the structural changes brought about by acid activation also inhibit the infiltration of TC and DC into any remaining interlayer space. However, this poorly defined  $d_{001}$  peak becomes less defined and all but absent in the diffractograms obtained for the highest drug loading possible for MMTK10. One explanation for this is adsorption onto the outer surface of the MMTK10 particles prevented the formation of normal clay mineral aggregates and thus the normal pseudo-crystalline structure that creates the  $d_{001}$  diffraction was lost (Janeba et al., 1998).

Significant changes in the shape and position of the  $d_{001}$  diffraction were observed as TC and DC were increasingly adsorbed onto rMMT (figure 2.10 C), LRD (figure 2.10 D),



and LXL21 (data not shown as very similar to LRD). For all three of these clay minerals the adsorption of TC and DC caused the  $d_{001}$  diffraction to shift to the left, representing an increase in the size of the interlayer space (Chang et al., 2009b; Parolo et al., 2008). The increase in interlayer space was shown to be limited for rMMT as the size of the interlayer space was shown increase to, but remain at, 16.44 Å even as the DC loading increased from 73.71 to 102.95 mg/g. However, as the drug loading onto LRD and LXL21 increased further so did the size of the interlayer space. For example, as the TC loading onto LRD increased from 8.31 mg/g to 83.14 mg/g then to 154.47 mg/g the interlayer space was found to be 12.7 Å, 13.97 Å, and 18.06 Å respectively. The width and asymmetry of the LRD and LXL21  $d_{001}$  diffraction also increased, suggesting that large amounts of drug present within the interlayer space is able to push the clay mineral layers apart and exfoliate the particle structure (Chang et al., 2009b). The ability of Laponite® to continue expanding its interlayer space to the point of exfoliation is also seen in water, where it almost completely exfoliates to form a colloidal dispersion (Mongondry et al., 2005; Phuoc et al., 2009).

No shift in the  $d_{001}$  diffraction peak was observed for any of the controls and standards investigated. No peak shift was observed for any of the clay minerals after they had been dispersed in water and dried in the same way as the composite materials, indicating that no additional water molecules were recruited by the counterbalancing cations that could account for the observed interlayer space increase. Physical mixes of the clay mineral and drug powders provided diffractograms containing peaks for both the clay minerals and the drug powders alone, but showed no significant peak shifts and the  $d_{001}$  diffraction remained intact. This confirms that adsorption of drug

molecules onto clay mineral layers is facilitated by dispersion in water. These data confirm that swelling clays are able to adsorb drug molecules into their interlayer space, which allows the 2:1 swelling clay minerals to adsorb greater amounts of drug molecules than the non-swelling 1:1 clay minerals.

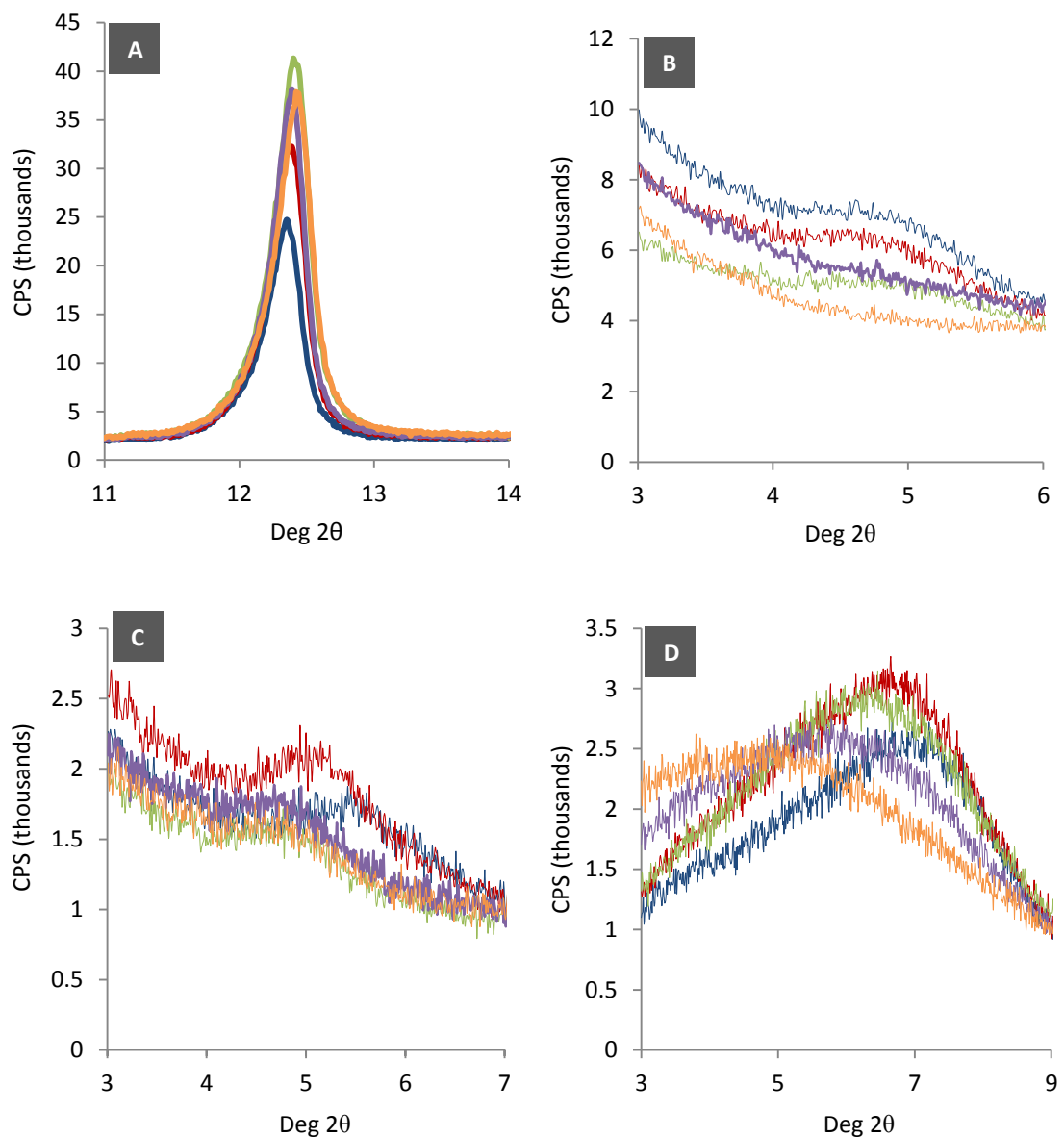


**Figure 2.10.** X-ray diffractions for doxycycline adsorbed onto (A) kaolin, (B) montmorillonite K-10, (C) rMMT, and (D) LRD. Colours of the lines represent different concentrations of DC loading (orange > purple > green > red > blue)

There was a notable lack of TC or DC diffraction peaks in the composite samples and the whole diffractogram was comparable to that of the unmodified clay minerals, with the exception of diffraction peak shifts caused by interlayer space expansion. This indicates that the TC and DC molecules were adsorbed onto the clay mineral surfaces in an amorphous arrangement (Ito et al., 2001) and that the surfaces or pores of the clay minerals did not act as foci for crystallisation of the drug.

### 2.3.5. FTIR analyses

FTIR is a useful technique for identifying functional groups within a compound or mixture and is often used to support the elucidation of drug molecule structures. Molecules, such as TC and DC have individual and characteristic spectra with the majority of absorbance modes being present within the fingerprint region (1500 to 500  $\text{cm}^{-1}$ ). Clay minerals also have a number of characteristic modes within this region (figure 2.11). The most prominent absorbance around 1000  $\text{cm}^{-1}$  is from the Si-O stretch within the tetrahedral sheets. Absorbences lower down the spectra result from M-OH bonds within the octahedral sheets; notably Al-OH at 912  $\text{cm}^{-1}$  in KN, 924  $\text{cm}^{-1}$  in rMMT, and 897  $\text{cm}^{-1}$  in LXL21 (as a shoulder on the Si-O adsorption); Fe-OH at 802  $\text{cm}^{-1}$  and 685  $\text{cm}^{-1}$  in rMMT; and Mg-OH at 607  $\text{cm}^{-1}$  in KN, 603  $\text{cm}^{-1}$  in rMMT, and 653  $\text{cm}^{-1}$  in LXL21 (Madejova, 2003; Tyagi et al., 2006).

There are clear differences in the fingerprint regions between KN and the other clay minerals and this is due to the differing structure, content, and bonding within the 1:1 and 2:1 layer sheets, and potentially the differing interactions between the clay

mineral layers (Madejova, 2003). The spectra for rMMT and MMTK10 are presented together (figure 2.11 B) to demonstrate how the acid activation process can affect the structure of these clay minerals. The loss or reduction of shoulder absorbances at  $924\text{ cm}^{-1}$  and  $802\text{ cm}^{-1}$  are due to dissolution of Al and Fe from the clay mineral sheets in acid environments. A slight shift in the Si-O absorbance is also observed after the acid-activation process, which is a result of the differing electric and bonding environment within the increasingly amorphous silicate sheet (Tyagi et al., 2006).

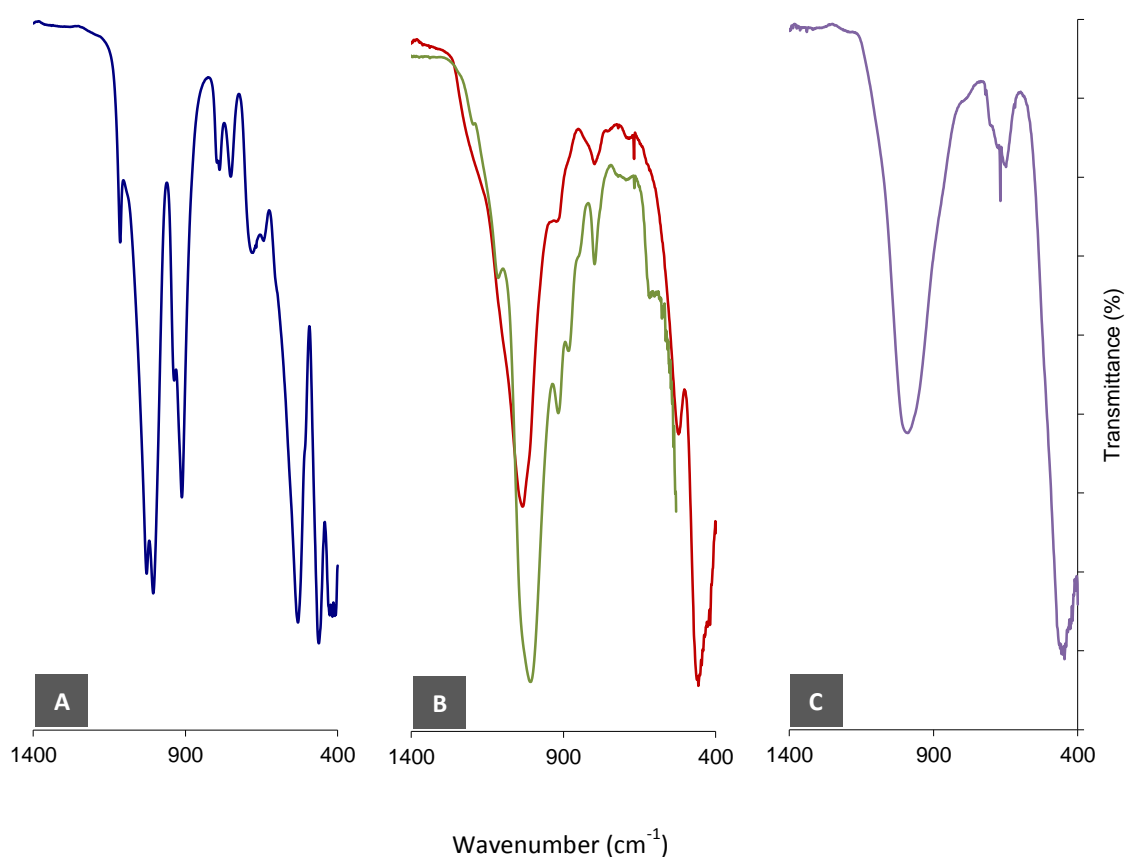


**Figure 2.11.** Extracts from the FTIR spectra of (A) KN, (B) MMTK10 (red line) and rMMT (green line), and (C) LXL21 (LRD showed no distinguishable differences). These spectra extracts show the fingerprint region of characteristic clay mineral IR absorbance bands.

As the amount of drug adsorbed onto a clay mineral increases the amplitude of the absorbances also increases (figure 2.12, see insert). The presence of this fingerprint region in the spectra of the composites is useful for proving the presence of drug within the composite materials, but can also be used to determine the nature of the interaction between drugs and clay minerals (Madejova, 2003; Porubcan et al., 1978). To balance the increase of drug within the composite material, the characteristic Si-O band reduced in intensity. This is unlikely to be due to a change in clay mineral structure as no deformations were observed. Instead this is simply a result of the changing ratio of drug:clay within the composite materials.

The TC O-H/N-H stretching mode, which generally appears around  $3350\text{ cm}^{-1}$  is masked by the broad O-H band at  $3500\text{ cm}^{-1}$  (Chang et al., 2009c), which decreased in amplitude as the amount of drug present within the composites increased. This absorbance band is characteristic in clay mineral samples and is generated by water molecules (Madejova, 2003). Much of the water within the clay mineral structure, especially within the 2:1 swelling minerals, is associated with the counterbalancing cations. Thus, a reduction in intensity of this band may indicate a loss of hydratable counterbalancing cations and support the conclusion that cation exchange is the proposed method of DC and TC adsorption onto the clay mineral surface (Madejova, 2003; Rapacz-kmita et al., 2017).

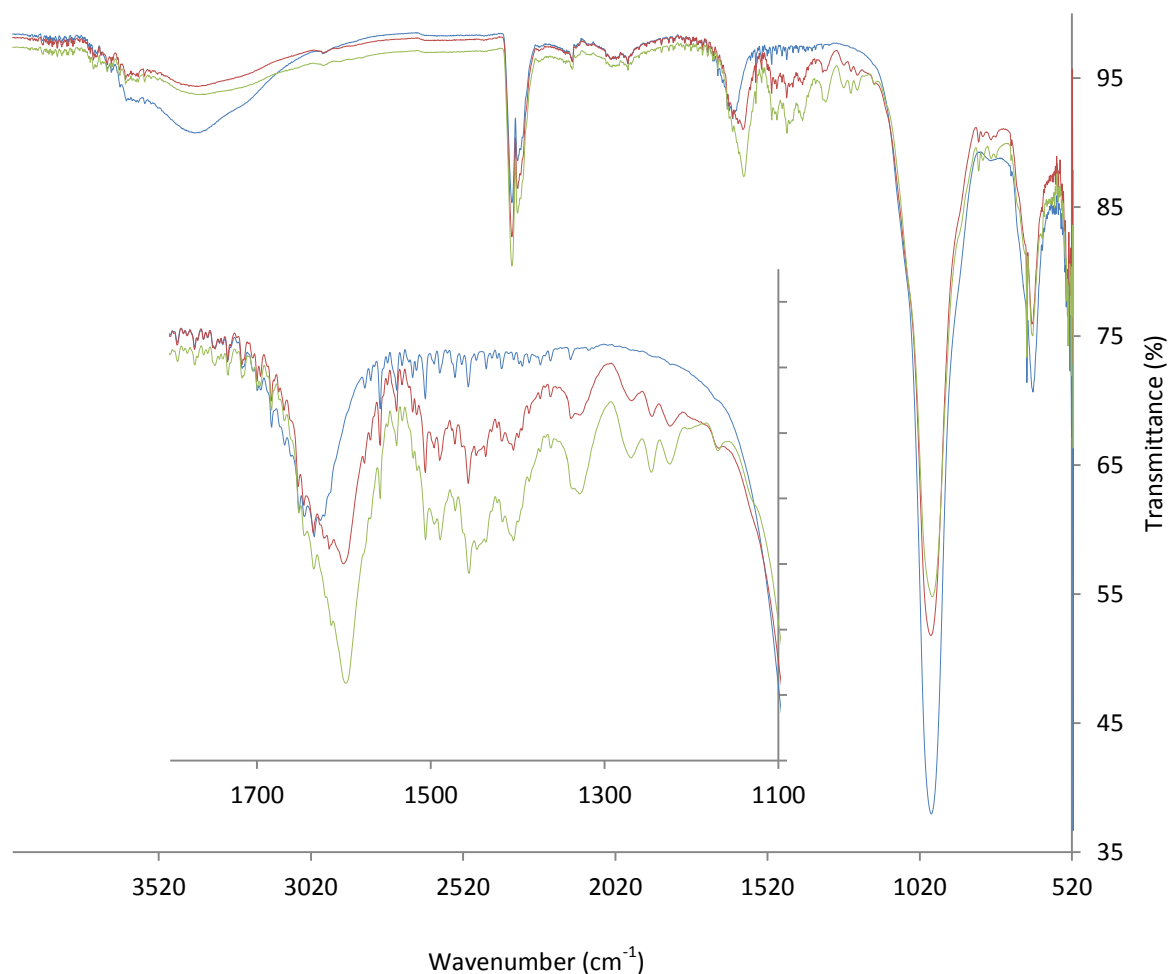


**Figure 2.12.** FTIR spectra of increasing amounts of DC adsorbed onto LRD. The lowest DC adsorption (blue line) and highest adsorption (green line) are presented alongside a DC-LRD composite whose DC loading is around the monolayer formation point (red line).

The interaction between DC and TC onto the clay mineral surfaces was also observed via shifting of key absorbances in the spectra. The absorbance at 1250 cm<sup>-1</sup> is a characteristic C-N stretching mode whose position is shown to shift as the pH favours differing charges on the tertiary amine group of TC and DC (de Sousa et al., 2008; Parolo et al., 2010; Zhao et al., 2012). As shown in figure 2.13 this absorbance was shown to shift from 1250 cm<sup>-1</sup> to 1245 cm<sup>-1</sup> when TC was absorbed onto rMMT,

indicating an interaction between this positively charged group and the clay mineral surface; most likely the negatively charged faces. Similar shifts were seen for TC and DC onto all the clay minerals tested (data not shown) except at pH 11, where so little drug was adsorbed it was very difficult to interpret the spectra. Indeed, it is expected that the tertiary amine group on TC deprotonates above pH 9.6 ( $pK_{a3}$ ; pH 9.1 for DC) so a shift in absorbance may be less easily observed. The absorbance at  $1508\text{ cm}^{-1}$  was assigned to the amide II band, with a secondary peak at  $1513\text{ cm}^{-1}$  generally assigned to N-H stretch at the amide II group (Caminati et al., 2002; Chang et al., 2009a; Li et al., 2010; Parolo et al., 2008; Zhao et al., 2012). Figure 2.13 also demonstrates the  $1508\text{ cm}^{-1}$  absorbance did not change position when in a clay-drug composite, whilst the accompanying adsorption at  $1513\text{ cm}^{-1}$  did not appear in the spectra for the clay-TC and-DC composites. This could be due to the relative intensities of the absorbance reducing the resolution of the peaks, which would suggest there is no interaction between the clay-mineral surface and the amide groups. However, the shifting or disappearance of the  $1513\text{ cm}^{-1}$  absorbance, resulting in a single absorbance at  $1508\text{ cm}^{-1}$  could indicate some interaction between this group and the clay mineral surface. The amide group and O3 complex holds a negative charge above  $pK_{a1}$  (Parolo et al., 2008) and it would be plausible to suggest any interaction with this group would be with the positively charged edges of the clay mineral, providing the pH of the clay dispersion does not favour a negative charge at these edge sites (see section 1.2.3). Further evidence for an interaction with the amide groups is presented in figure 2.13, which shows the amide C=O absorbance at  $1655\text{ cm}^{-1}$  (Li et al., 2010; Zhao et al., 2012) shifting to  $1650\text{ cm}^{-1}$ .

These spectra demonstrate that FTIR can be used to detect the presence of drug molecules within clay-drug composites. Indeed, with further work this analytical technique could be quantitative and support the data determined mathematically through adsorption isotherms.

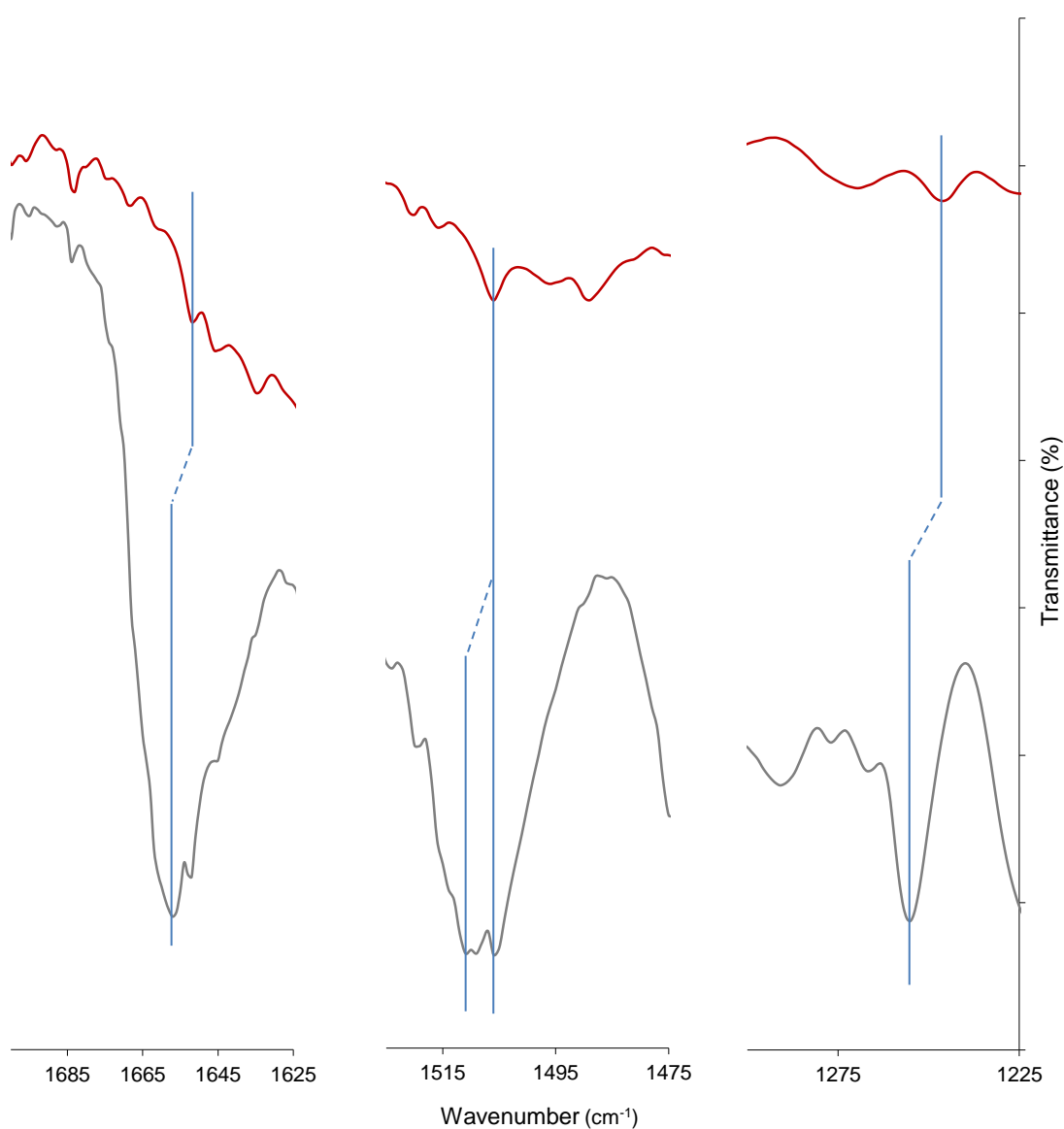


**Figure 2.13.** FTIR spectra for TC at pH 5 (grey line) and rMMT-TC composite formed at pH 5 (red line).

Absorbances are paired via the blue lines, with dotted junctions indicating shifts.



The FTIR spectra presented here also demonstrated the structural differences between the clay minerals and the effects of an acidic environment on their chemical composition. More interestingly, by identifying characteristic peaks within the fingerprint region of DC and TC spectra, it was possible to determine that the dimethyl amino group was able to interact with the clay mineral face sites, whilst the amide group was able to interact with the edge sites. Interaction between TC and DC and the face sites could potentially be via a cation exchange process, as the absorbance for water molecules within the composites reduced significantly and may be a result of hydratable cations being displaced by drug molecules.

#### *2.3.6. Antibacterial activity*

Clay minerals on their own exhibited no zone of inhibition and therefore no discernible antibacterial activity (figure 2.14 A). This is in contrast to other studies that showed varying inhibitory effects of clay minerals on the growth of bacterial cells (Mpuchane et al., 2010; Otto and Haydel, 2013; Williams et al., 2011, 2008; Williams and Haydel, 2010). Williams, and colleagues, determined that it is likely that the exchangeable ions play a leading role in the antibacterial properties of some clay minerals (Williams et al., 2011). However, it is likely that contact with bacterial cells is required for clay minerals to impose their antibacterial effects (Williams and Haydel, 2010). The methods utilised in these experiments separated the bacterial cells from the clay minerals to determine whether the drug molecules desorbed from the composites and whether they remained active. Deionised water was used to disperse the un-modified clay minerals so it is unlikely for any interlayer cations to be displaced from the clay minerals into the growth medium. Alongside this, the cations held within the interlayer space of the

clay minerals tested were predominantly  $\text{Na}^+$ , which has no inherent antibacterial activity unlike other metallic cations such as silver, copper and zinc (Magaña et al., 2008; Malachová et al., 2011).

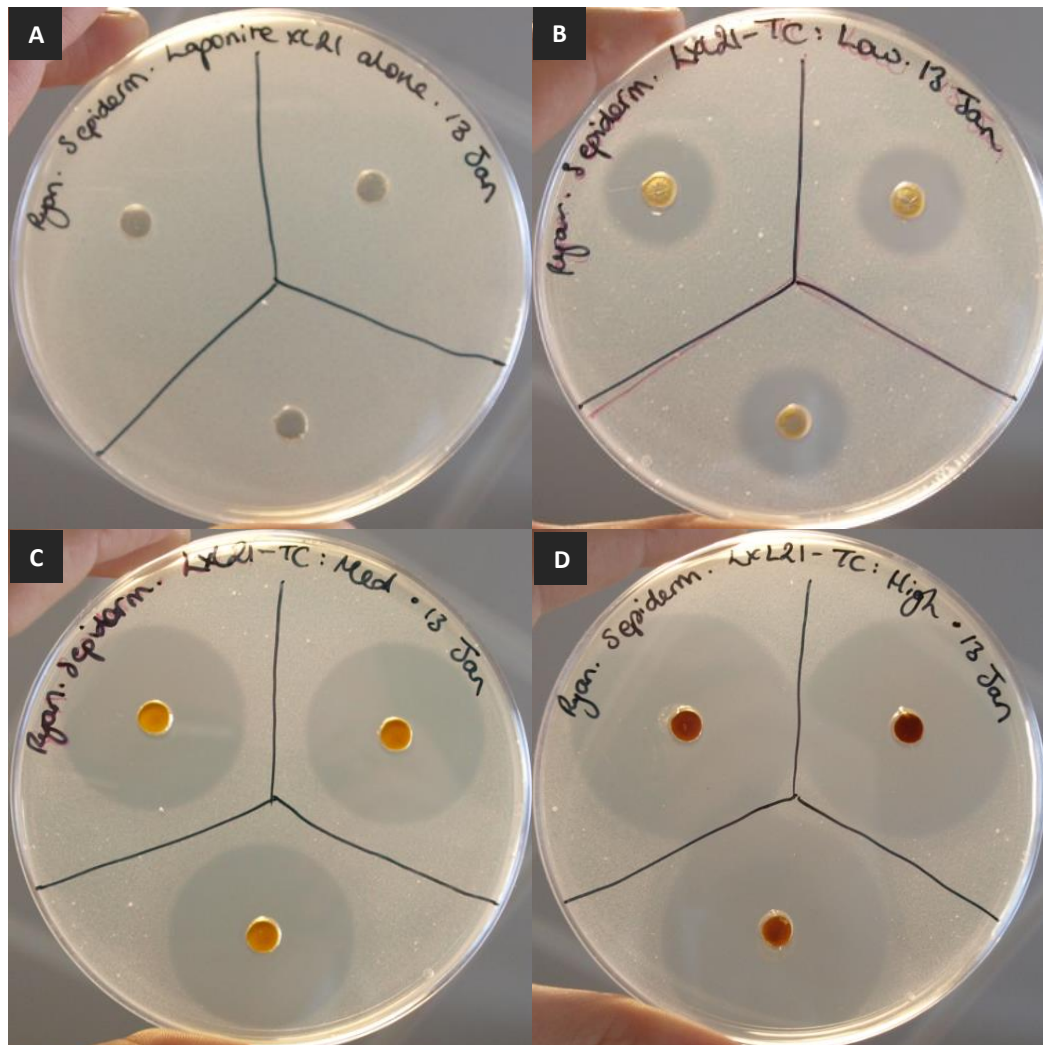


**Figure 2.14.** Examples of *S. epidermidis* cultures in nutrient agar tested via the well-diffusion method against 2 mg LXL21 (A), and composites of LXL-TC containing (B) 10.21 mg/g, (C) 79.19 mg/g, and (D) 124.15 mg/g of TC.

It is equally likely that any zones of inhibition observed from the clay-drug composites were caused by diffusion of TC and DC from the composites and into the growth medium. As the concentration of the standard solutions of TC and DC increased so did the zone of inhibition, proving that this method could discriminate between clay-drug composites that released TC and DC on rehydration and those that did not. By plotting the zone of inhibition (mm) against the  $\text{Log}_{10}$  of drug concentration (mg/mL) standard curves with high correlation ( $r^2 > 0.955$ ) were obtained, showing that this methodology could reliably detect increasing amounts of TC and DC release through increasing zone diameters.

As the concentration of drug increased within each clay-drug composite the zone of inhibition also increased in diameter (figure 2.14 B-D), proving that there were increasing concentrations of drug within the materials as determined in section 2.3.3 and this awarded greater antibacterial powers to the composites. Moreover, these data prove that the antibacterial effect of the drug molecules is maintained during the formation and storage of the clay-drug composites making them important and interesting materials for future research and further development.

TC and DC were shown to have antibacterial effects against all the bacterial strains but were more effective against the Gram-positive strains due to their mode of action (figure 2.15). It is important to note the reduced efficacy of TC and DC against *P. aeruginosa* compared to *P. acnes* and *S. epidermidis*. *Pseudomonas spp.* are Gram-negative bacteria which have less permeable cell membranes, which can reduce the penetration of many antibacterial agents.

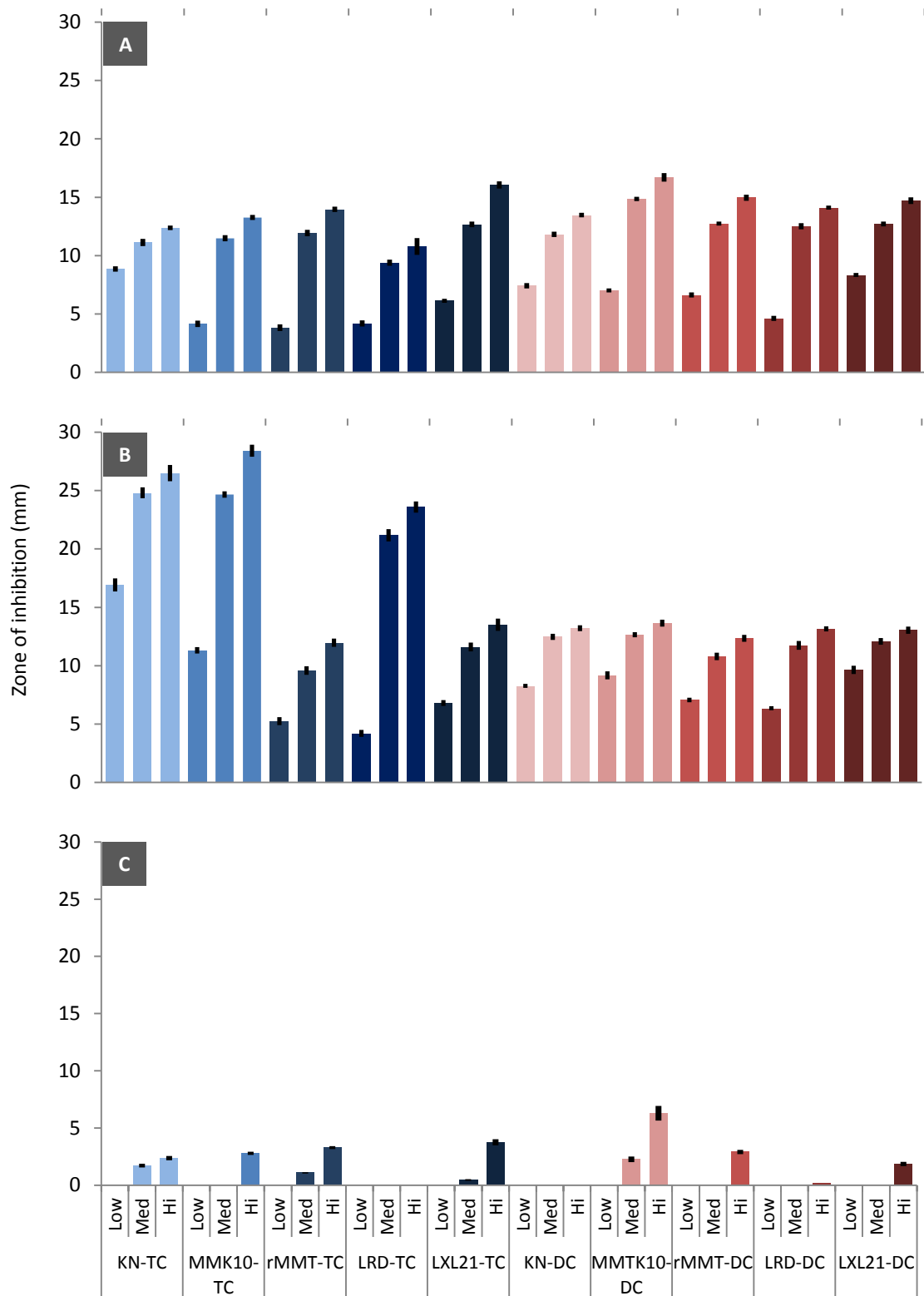


**Figure 2.15.** Zones of inhibition (mean  $\pm$ SD, n=3) formed by clay-TC and clay-DC composites, of varying drug loading, against *S. epidermidis* (A), *P. acnes* (B), and *P. aeruginosa* (C).

Alongside this *P. aeruginosa* is able to produce a number of efflux proteins which are placed within the cell membranes to pump out a wide range of antibacterial drugs including the tetracycline class. In addition to this innate resistance *P. aeruginosa* is able to acquire and develop further resistance even during a course of anti-pseudomonal treatment (Chatterjee et al., 2016; Kobayashi et al., 2009; Lister et al., 2009; Potron et al., 2015).

Whilst the majority of skin and skin structure infections (SSSIs) are caused by Gram-positive organisms such as *S. epidermidis*, *S. aureus*, *P. acnes*, and *Streptococcus* species, the prevalence of *P. aeruginosa* causing and complicating infections and diseases, including SSSIs, is increasingly being reported (Dryden, 2009). Many Gram-negative bacteria, including *P. aeruginosa*, have now been identified as a risk to human health in the same way as *MRSA* and *Clostridium difficile* (Dryden, 2009; World Health Organization, 2012). There is much scope for improving activity of these clay-drug composites against *P. aeruginosa* and it is possible that another antibacterial agent with better activity against Gram-negative bacteria, such as a fluoroquinolone (Unal, 2009b), could overcome the problem and this will be investigated in chapter 3.

Across the clay-drug composites tested the difference in diameter of the zone-of-inhibition was much greater between the low and medium loaded materials, compared to the difference in diameter induced between the medium and highly loaded composites (figure 2.15). However, this perceived reduction in efficacy is not actually directly related to the potency of the materials formed. As the diameter of the zone of inhibition increases the area of effect increases more than is initially

perceived. Thus, small increases in the diameter of a larger circle in fact account for a larger increase in area of effect than changes in diameter of a smaller circle would.

The diameters for the zones of inhibition were converted into areas of effect (excluding the central-well) to give a true expression of the efficacy. By using the McFarland 0.5 measurements it was possible to calculate the number of bacterial cells per square millimetre of agar, which could be further used to determine the average number of cells affected (table 2.3). The calculated efficacy of preventing bacterial-cell growth increased by a smaller proportion when the drug-load increased from medium to high than it did when the drug-load increased from low to medium. This complements the trends observed in the zone of inhibition measurements, suggesting that diffusion through increasing volumes of agar was not solely responsible for this phenomenon. This assumption is further supported when the chemistry of each clay mineral is considered.

Composites formed from KN were shown to create zones of inhibition that were comparable to those formed by other composites, which is interesting as KN-TC and KN-DC composites contained much less drug than many of the other composites tested. This suggests that the KN-TC and KN-DC composites are able to release their drug load more freely. KN is a 1:1 clay-mineral with minimal surface charge (Kahr and Madsen, 1995) and may therefore hold onto TC and DC molecules less strongly than the highly charged 2:1 clay minerals (rMMT and Laponites®) used in this study (see section 1.2).

The composites with low drug binding had not formed a monolayer and therefore the drugs were interacting directly with the surface of the clay minerals through strong interactions. As the drug loading increased to 'medium' and 'high' a monolayer had likely formed and additional drug would have adsorbed through secondary weaker interactions. However, these secondary interactions did not result in the drug molecules being able to dissociate more easily away from the clay mineral surface.

**Table 2.3.** Calculated mean average number of bacterial cells that were prevented from growing by drug molecules which had diffused from clay-TC and clay-DC composites of different drug load.

Composite	Drug Load (mg/g)	Average number of bacterial cells inhibited ( $\times 10^5$ )		
		<i>S. epidermidis</i>	<i>P. acnes</i>	<i>P. aeruginosa</i>
KN-TC	4.75	1.88	2.01	-
	14.97	2.75	4.00	2.53
	29.92	3.29	4.51	3.82
MMTK10-TC	10.30	0.58	1.00	-
	98.19	2.90	3.95	-
	148.69	3.71	5.13	4.77
rMMT-TC	10.01	0.24	1.25	-
	111.15	1.42	3.24	1.45
	158.06	1.86	4.71	5.99
LRD-TC	9.82	0.59	0.21	-
	129.71	2.07	2.99	-
	199.75	2.61	3.65	-
LXL21-TC	10.21	0.48	1.86	-
	79.19	1.58	4.47	0.54
	124.15	2.38	5.80	7.24
KN-DC	3.71	0.65	2.55	-
	9.83	1.40	5.06	-
	16.23	1.75	5.58	-
MMTK10-DC	9.97	0.59	3.02	-
	114.81	2.07	5.18	3.64
	146.77	2.55	5.90	15.65
rMMT-DC	9.71	0.54	1.98	-
	92.88	1.59	3.96	-
	133.70	2.10	4.97	5.05
LRD-DC	7.00	0.31	1.67	-
	112.72	1.54	4.56	0.37
	175.36	1.90	5.55	4.81
LXL21-DC	5.92	0.78	3.27	-
	82.96	1.58	4.78	-
	132.33	2.04	5.46	2.79

One limitation of the method used to test the antibacterial activities of these composites is they are time-limited in a number of ways, which could have affected the zones of inhibition obtained. Firstly, the drug needs to dissociate from the composite and diffuse through the surrounding agar, whilst bacterial cells proliferate. The zone of inhibition is formed at a boundary where the antibacterial concentration in the agar is strong enough to prevent bacterial growth, and those areas where it is not. Such bacteriostatic and bactericidal concentrations take time to develop, during which time the bacterial cells outside of the effective concentration continue to grow and replicate. Any bacterial colonies that are able to replicate to sufficient densities to be visible before TC and DC reach effective concentrations will still be visible after cell-death. Therefore, drug may continue to diffuse through the agar but the true extent of drug release cannot be measured.

Secondly, the drug molecules can only desorb from the composite when it is hydrated. These bacteriological studies were carried out at body temperature, which facilitated gradual evaporation of water from the composite dispersions to such an extent that these were dry at 24-hours incubation time. This could also mask the true extent of drug release from these composite materials especially if modified release properties are present, as has been reported by a number of other teams (Park et al., 2008; Rodrigues et al., 2013).

Regardless of these limitations the results are important as they show the clay-drug composites formed are able to relinquish their drug load and have a significant antibacterial effect, especially as the drug-load increases.



## 2.4. Conclusions

In this series of experiments TC and DC were successfully adsorbed onto KN, MMTK10, rMMT, LRD and LXL21 under various conditions. It was found that the adsorption of TC and DC onto the clay minerals was rapid and followed pseudo-second order kinetics. Adsorption isotherms fitted the Langmuir model, indicating that these drug molecules could form a monolayer on the clay mineral surfaces. The data also indicates that once this monolayer is formed at the clay mineral surface, further adsorption takes place via weaker secondary interactions between the adsorbed drug molecules. The pH of the dispersions was shown to be the most important parameter for optimising TC and DC adsorption onto the clay mineral surfaces. A pH that favoured the formation of the zwitterionic state was shown to allow for the greatest amount of TC and DC to be adsorbed onto the clay minerals. Not only this, but this pH (5.0 for TC and 5.5 for DC) was unlikely to affect the structure of the clay minerals.

Through XRD and FTIR it was determined that these drug molecules adsorbed into the interlayer space of swelling 2:1 clay minerals (rMMT, LRD, and LXL21) but probably only adsorbed onto the outer surfaces of KN. It is likely that positively charged amino groups within these drug molecules allowed for direct interaction with the negatively charged clay-mineral surfaces. It is also possible that negatively charged amide groups on the drug molecules could adsorb onto the positively charged edge-sites of the clay mineral layers. Indeed, a dispersion pH that favoured negatively charged drug molecules resulted in almost negligible drug adsorption – likely a result of clay-mineral edge-sites becoming negatively charged creating an overwhelming repulsion between the clay-mineral layers and the drug molecules.

The clay-drug composites formed were shown to be active against three strains of bacteria that are commonly implicated in skin and skin structure infections; *S. epidermidis*, *P. acnes* and *P. aeruginosa*. However, very little activity was seen against *P. aeruginosa* and this is likely due to the mode of action of TC and DC and the biological structure of these species of bacteria. Increasing drug-load within the composites resulted in greater antibacterial effect. The chemistry of the clay-minerals was also shown to influence desorption of drug molecules from the composites. Under the conditions tested, KN, which has weak surface forces, was shown to relinquish its drug load much more easily than highly charged clays such as LRD and LXL21.

These results are promising and will inform further experiments into the adsorption of drugs onto clay mineral surfaces and their onward use within wound dressing materials. It is unknown whether these findings are specific to TC and DC or whether they can be applied to other drug molecules. Therefore, chapter 3 will set out to determine whether these findings can be applied to another antibacterial agent with differing chemistry and better activity against *P. aeruginosa*.

## 2.5. References

- Aguzzi, C., Viseras, C., Cerezo, P., Rossi, S., Ferrari, F., López-Galindo, A., Caramella, C., 2005. Influence of dispersion conditions of two pharmaceutical grade clays on their interaction with some tetracyclines. *Appl. Clay Sci.* 30, 79–86. doi:10.1016/j.clay.2005.03.007
- Avery, R.G., Ramsay, J.D.F., 1986. Colloidal Properties of Synthetic Hectorite Clay Dispersions II . Light and Small Angle Neutron Scattering. *J. Colloid Interface Sci.* 109, 448–454.
- Browne, J.E., Feldkamp, J.R., White, J.L., Hem, S.L., 1980. Acid-base equilibria of tetracycline in sodium montmorillonite suspensions. *J. Pharm. Sci.* 69, 811–5.
- BYK Additives & Instruments, 2014. Laponite: performance additives.
- BYK Additives & Instruments, 2013. Optigel – Rheological Additives for Aqueous Phases in Cosmetics and Personal Care.
- California Earth Minerals Inc., 2008. Material Safety Data Sheet Material Safety Data Sheet. doi:10.1017/CBO9781107415324.004
- Caminati, G., Focardi, C., Gabrielli, G., Gambinossi, F., Mecheri, B., Nocentini, M., Puggelli, M., 2002. Spectroscopic investigation of tetracycline interaction with phospholipid Langmuir–Blodgett films. *Mater. Sci. Eng. C* 22, 301–305. doi:10.1016/S0928-4931(02)00217-5
- Center for Drug Evaluation and Research, 2005. Application Numer 21-821.
- Chang, P.-H., Jean, J.-S., Jiang, W.-T., Li, Z., 2009a. Mechanism of tetracycline sorption on rectorite. *Colloids Surfaces A Physicochem. Eng. Asp.* 339, 94–99. doi:10.1016/j.colsurfa.2009.02.002
- Chang, P.-H., Li, Z., Jiang, W.-T., Jean, J.-S., 2009b. Adsorption and intercalation of tetracycline by swelling clay minerals. *Appl. Clay Sci.* 46, 27–36. doi:10.1016/j.clay.2009.07.002
- Chang, P.-H., Li, Z., Yu, T.-L., Munkhbayer, S., Kuo, T.-H., Hung, Y.-C., Jean, J.-S., Lin, K.-H., 2009c. Sorptive removal of tetracycline from water by palygorskite. *J. Hazard. Mater.* 165, 148–55. doi:10.1016/j.jhazmat.2008.09.113
- Chang, P.H., Jiang, W.T., Li, Z., Kuo, C.Y., Wu, Q., Jean, J.S., Lv, G., 2016. Interaction of ciprofloxacin and probe compounds with palygorskite PFI-1. *J. Hazard. Mater.* 303, 55–63. doi:10.1016/j.jhazmat.2015.10.012
- Chatterjee, M., Anju, C.P., Biswas, L., Anil Kumar, V., Gopi Mohan, C., Biswas, R., 2016. Antibiotic resistance in *Pseudomonas aeruginosa* and alternative therapeutic options. *Int. J. Med. Microbiol.* 306, 48–58. doi:10.1016/j.ijmm.2015.11.004
- Costa, R., Speretta, E., Saraiva, M.J., Crowther, D.C., Cardoso, I., 2011. Testing the Therapeutic Potential of Doxycycline in a *Drosophila melanogaster* model of

- Alzheimer's Disease. *Alzheimer's Dement.* 7, S458.  
doi:10.1016/j.jalz.2011.05.1325
- Datta, S.M., 2013. Clay–polymer nanocomposites as a novel drug carrier: Synthesis, characterization and controlled release study of Propranolol Hydrochloride. *Appl. Clay Sci.* 80–81, 85–92. doi:10.1016/j.clay.2013.06.009
- Dawson, A.L., Dellavalle, R.P., 2013. Acne vulgaris. *BMJ* 346, f2634.  
doi:10.1136/bmj.f2634
- de Sousa, F.B., Oliveira, M.F., Lula, I.S., Sansiviero, M.T.C., Cortés, M.E., Sinisterra, R.D., 2008. Study of inclusion compound in solution involving tetracycline and  $\beta$ -cyclodextrin by FTIR-ATR. *Vib. Spectrosc.* 46, 57–62.  
doi:10.1016/j.vibspec.2007.10.002
- Drits, V.A., 2003. Structural and chemical heterogeneity of layer silicates and clay minerals. *Clay Miner.* 38, 403–432. doi:10.1180/0009855033840106
- Dryden, M.S., 2009. Skin and soft tissue infection: microbiology and epidemiology. *Int. J. Antimicrob. Agents* 34 Suppl 1, S2-7. doi:10.1016/S0924-8579(09)70541-2
- Figueroa, R. a, Leonard, A., MacKay, A. a, 2004. Modeling tetracycline antibiotic sorption to clays. *Environ. Sci. Technol.* 38, 476–83.
- Foo, K.Y., Hameed, B.H., 2014. Insights into the modeling of adsorption isotherm systems. *Pet. Coal* 56, 552–561. doi:10.1016/j.cej.2009.09.013
- Fraise, A.P., 2006. Tigecycline: the answer to beta-lactam and fluoroquinolone resistance? *J. Infect.* 53, 293–300. doi:10.1016/j.jinf.2006.05.014
- Giovagnoli, S., Tsai, T., DeLuca, P.P., 2010. Formulation and release behavior of doxycycline-alginate hydrogel microparticles embedded into pluronic F127 thermogels as a potential new vehicle for doxycycline intradermal sustained delivery. *AAPS PharmSciTech* 11, 212–20. doi:10.1208/s12249-009-9361-8
- Grassi, G.G., 1993. Tetracyclines — extending the atypical spectrum. *Int. J. Antimicrob. Agents* 3, S31–S46. doi:10.1016/0924-8579(93)90033-2
- Greenwald, R. a, 2011. The road forward: the scientific basis for tetracycline treatment of arthritic disorders. *Pharmacol. Res.* 64, 610–3. doi:10.1016/j.phrs.2011.06.010
- Griffin, M.O., Fricovsky, E., Ceballos, G., Villarreal, F., 2010. Tetracyclines : a pleiotropic family of compounds with promising therapeutic properties . Review of the literature. *AM J Physiol Cell Physiol* 299, C539–C548.  
doi:10.1152/ajpcell.00047.2010.
- Grolman, D.C., 2007. Therapeutic applications of tigecycline in the management of complicated skin and skin structure infections. *Int. J. Infect. Dis.* 11 Suppl 1, S7-15.  
doi:10.1016/S1201-9712(07)60002-2
- Hamilton, A.R., Hutcheon, G.A., Roberts, M., Gaskell, E.E., 2014. Formulation and antibacterial profiles of clay – ciprofloxacin composites. *Appl. Clay Sci.* 87, 129–

135. doi:10.1016/j.clay.2013.10.020

- Ito, T., Sugafuji, T., Maruyama, M., 2001. Skin Penetration by Indomethacin is Enhanced by Use of an Indomethacin / Smectite Complex. *J. Supramol. Chem.* 1 217–219.
- Itodo, A.U., Itodo, H.U., 2010. Sorption energies estimation using Dubinin-Radushkevich and temkin adsorption isotherms. *Life Sci. J.* 7, 68–76.
- Janeba, D., Capkova, P., Weiss, Z., Schenk, H., 1998. Characterization of intercalated smectites using xrd profile analysis in the low-angle region. *Clays Clay Miner.* 46, 63–68.
- Jin, L., Amaya-mazo, X., Apel, M.E., Sankisa, S.S., Johnson, E., Zbyszynska, M.A., Han, A., 2007. Ca<sup>2+</sup> and Mg<sup>2+</sup> bind tetracycline with distinct stoichiometries and linked deprotonation. *Biophys. Chem.* 128, 185–196. doi:10.1016/j.bpc.2007.04.005
- Joks, R., Durkin, H.G., 2011. Non-antibiotic properties of tetracyclines as anti-allergy and asthma drugs. *Pharmacol. Res.* 64, 602–9. doi:10.1016/j.phrs.2011.04.001
- Joshi, G. V, Kevadiya, B.D., Bajaj, H.C., 2010. Controlled release formulation of ranitidine-containing montmorillonite and Eudragit E-100. *Drug Dev. Ind. Pharm.* 36, 1046–53. doi:10.3109/03639041003642073
- Jung, H., Kim, H.-M., Choy, Y. Bin, Hwang, S.-J., Choy, J.-H., 2008. Itraconazole–Laponite: Kinetics and mechanism of drug release. *Appl. Clay Sci.* 40, 99–107. doi:10.1016/j.clay.2007.09.002
- Kahr, G., Madsen, F.T., 1995. Determination of the cation exchange capacity and the surface area of bentonite, illite and kaolinite by methylene blue adsorption. *Appl. Clay Sci.* 9, 327–336. doi:10.1016/0169-1317(94)00028-0
- Kammerer, J., Carle, R., Kammerer, D.R., 2011. Adsorption and Ion Exchange: Basic Principles and Their Application in Food Processing. *J. Agric. Food Chem.* 59, 22–42. doi:10.1021/jf1032203
- Kaufhold, S., Dohrmann, R., 2009. Stability of bentonites in salt solutions | sodium chloride. *Appl. Clay Sci.* 45, 171–177. doi:10.1016/j.clay.2009.04.011
- Kaygusuz, H., Erim, F.B., 2013. Alginate/BSA/montmorillonite composites with enhanced protein entrapment and controlled release efficiency. *React. Funct. Polym.* 73, 1420–1425. doi:10.1016/j.reactfunctpolym.2013.07.014
- Kobayashi, H., Kobayashi, O., Kawai, S., 2009. Pathogenesis and clinical manifestations of chronic colonization by *Pseudomonas aeruginosa* and its biofilms in the airway tract. *J. Infect. Chemother.* 15, 125–142. doi:10.1007/s10156-008-0691-3
- Lagaly, G., Ziesmer, S., 2003. Colloid chemistry of clay minerals: the coagulation of montmorillonite dispersions. *Adv. Colloid Interface Sci.* 100–102, 105–128. doi:10.1016/S0001-8686(02)00064-7
- Langmuir, I., 1918. The adsorption of gases on plane surfaces of glass, mica and

- platinum. *J. Am. Chem. Soc.* 345, 1361–1403.
- Leeson, L.J., Krueger, J.E., Nash, R.A., 1963. Concerning the structural assignment of the second and third acidity constants of the tetracycline antibiotics. *Tetrahedron Lett.* 18, 1155–1160.
- Li, Z., Chang, P.-H., Jean, J.-S., Jiang, W.-T., Wang, C.-J., 2010. Interaction between tetracycline and smectite in aqueous solution. *J. Colloid Interface Sci.* 341, 311–9. doi:10.1016/j.jcis.2009.09.054
- Li, Z., Chang, P.-H., Jiang, W.-T., Jean, J.-S., Hong, H., 2011. Mechanism of methylene blue removal from water by swelling clays. *Chem. Eng. J.* 168, 1193–1200. doi:10.1016/j.cej.2011.02.009
- Lister, P.D., Wolter, D.J., Hanson, N.D., 2009. Antibacterial-resistant *Pseudomonas aeruginosa*: Clinical impact and complex regulation of chromosomally encoded resistance mechanisms. *Clin. Microbiol. Rev.* 22, 582–610. doi:10.1128/CMR.00040-09
- Madejova, J., 2003. FTIR techniques in clay mineral studies. *Vib. Spectrosc.* 31, 1–10.
- Magaña, S.M., Quintana, P., Aguilar, D.H., Toledo, J. a., Ángeles-Chávez, C., Cortés, M. a., León, L., Freile-Pelegrín, Y., López, T., Sánchez, R.M.T., 2008. Antibacterial activity of montmorillonites modified with silver. *J. Mol. Catal. A Chem.* 281, 192–199. doi:10.1016/j.molcata.2007.10.024
- Malachová, K., Praus, P., Rybková, Z., Kozák, O., 2011. Antibacterial and antifungal activities of silver, copper and zinc montmorillonites. *Appl. Clay Sci.* 53, 642–645. doi:10.1016/j.clay.2011.05.016
- McFarland, J., 1907. The nephelometer: An instrument for estimating the number of bacteria in suspensions used for calculating the opsonic index and for vaccines. *J. Am. Med. Assoc.* XLIX, 1176–1178.
- Miranda-Trevino, J.C., Coles, C. a., 2003. Kaolinite properties, structure and influence of metal retention on pH. *Appl. Clay Sci.* 23, 133–139. doi:10.1016/S0169-1317(03)00095-4
- Mongondry, P., Tassin, J.F., Nicolai, T., 2005. Revised state diagram of Laponite dispersions. *J. Colloid Interface Sci.* 283, 397–405. doi:10.1016/j.jcis.2004.09.043
- Mpuchane, S.F., Ekosse, G.-I.E., Gashe, B.A., Morobe, I., Coetzee, S.H., 2010. Microbiological characterisation of southern African medicinal and cosmetic clays. *Int. J. Environ. Health Res.* 20, 27–41. doi:10.1080/09603120903254025
- Neumann, B.S., Sansom, K.G., 1971. The rheological properties of dispersions of Laponite, a synthetic hectorite-like clay, in electrolyte solutions. *Clay Miner.* 9, 231–243.
- Nunes, C.D., Vaz, P.D., Fernandes, A.C., Ferreira, P., Romão, C.C., Calhorda, M.J., 2007. Loading and delivery of sertraline using inorganic micro and mesoporous

- materials. *Eur. J. Pharm. Biopharm.* 66, 357–365. doi:10.1016/j.ejpb.2006.11.023
- Otto, C.C., Haydel, S.E., 2013. Exchangeable ions are responsible for the in vitro antibacterial properties of natural clay mixtures. *PLoS One* 8, e64068. doi:10.1371/journal.pone.0064068
- Park, J.K., Choy, Y. Bin, Oh, J.-M., Kim, J.Y., Hwang, S.-J., Choy, J.-H., 2008. Controlled release of donepezil intercalated in smectite clays. *Int. J. Pharm.* 359, 198–204. doi:10.1016/j.ijpharm.2008.04.012
- Parolo, M.E., Avena, M.J., Pettinari, G., Zajonkovsky, I., Valles, J.M., Baschini, M.T., 2010. Antimicrobial properties of tetracycline and minocycline-montmorillonites. *Appl. Clay Sci.* 49, 194–199. doi:10.1016/j.clay.2010.05.005
- Parolo, M.E., Avena, M.J., Savini, M.C., Baschini, M.T., Nicotra, V., 2013. Adsorption and circular dichroism of tetracycline on sodium and calcium-montmorillonites. *Colloids Surfaces A Physicochem. Eng. Asp.* 417, 57–64. doi:10.1016/j.colsurfa.2012.10.060
- Parolo, M.E., Savini, M.C., Vallés, J.M., Baschini, M.T., Avena, M.J., 2008. Tetracycline adsorption on montmorillonite: pH and ionic strength effects. *Appl. Clay Sci.* 40, 179–186. doi:10.1016/j.clay.2007.08.003
- Perkins, N.C., Heard, C.M., 1999. In vitro dermal and transdermal delivery of doxycycline from ethanol/migliol 840 vehicles. *Int. J. Pharm.* 190, 155–64.
- Perkins, R., Brace, R., Matijevic, E., 1974. Colloid and Surface Properties of Clay Suspensions I. Laponite CP. *J. Colloid Interface Sci.* 48, 417–426.
- Phuoc, T.X., Howard, B.H., Chyu, M.K., 2009. Synthesis and rheological properties of cation-exchanged Laponite suspensions. *Colloids Surfaces A Physicochem. Eng. Asp.* 351, 71–77. doi:10.1016/j.colsurfa.2009.09.039
- Pils, J.R. V, Laird, D.A., 2007. Sorption of Tetracycline and Chlortetracycline on K- and Ca-Saturated Soil Clays, Humic Substances, and Clay-Humic Complexes. *Environ. Sci. Technol.* 41, 1928–1933.
- Porubcan, L.S., Serna, C.J., White, J.L., Hem, S.L., 1978. Mechanism of Adsorption of Clindamycin and Tetracycline by Montmorillonite. *J. Pharm. Sci.* 67, 1081–1087.
- Potron, A., Poirel, L., Nordmann, P., 2015. Emerging broad-spectrum resistance in *Pseudomonas aeruginosa* and *Acinetobacter baumannii*: Mechanisms and epidemiology. *Int. J. Antimicrob. Agents* 45, 568–585. doi:10.1016/j.ijantimicag.2015.03.001
- PubChem, 2016. Kaolin - Compound Summary for CID 56841936 [WWW Document]. PubChem open Chem. database. URL <https://pubchem.ncbi.nlm.nih.gov/compound/kaolin#section=Top> (accessed 9.3.16).
- Puttamat, S., Pavarajarn, V., 2016. Adsorption study for removal of Mn(II) ion in

- aqueous solution by hydrated ferric(III) oxides. *Int. J. Chem. Eng. Appl.* 7, 239–243. doi:10.18178/ijcea.2016.7.4.581
- Qiang, Z., Adams, C., 2004. Potentiometric determination of acid dissociation constants (pKa) for human and veterinary antibiotics. *Water Res.* 38, 2874–90. doi:10.1016/j.watres.2004.03.017
- Rapacz-kmita, A., Bu, M.M., Stodolak-zych, E., Miko, M., Dudek, P., Trybus, M., 2017. Characterisation , in vitro release study , and antibacterial activity of montmorillonite-gentamicin complex material. *Mater. Sci. Eng. C* 70, 471–478. doi:10.1016/j.msec.2016.09.031
- Raza, M., Ballering, J.G., Hayden, J.M., Robbins, R. a, Hoyt, J.C., 2006. Doxycycline decreases monocyte chemoattractant protein-1 in human lung epithelial cells. *Exp. Lung Res.* 32, 15–26. doi:10.1080/01902140600691399
- Rives, V., del Arco, M., Martín, C., 2014. Intercalation of drugs in layered double hydroxides and their controlled release: A review. *Appl. Clay Sci.* 88–89, 239–269. doi:10.1016/j.clay.2013.12.002
- Rodrigues, L.A.D.S., Figueiras, A., Veiga, F., de Freitas, R.M., Nunes, L.C.C., da Silva Filho, E.C., da Silva Leite, C.M., 2013. The systems containing clays and clay minerals from modified drug release: a review. *Colloids Surf. B. Biointerfaces* 103, 642–51. doi:10.1016/j.colsurfb.2012.10.068
- RPS and BMJ, 2017. Tetracyclines, in: Baxter, K. (Ed.), *British National Formulary (Online Edition)*. RPS and BMJ, London, p. Section 5.1.3.
- Samlíková, M., Hole, S., Hundáková, M., Pazdziora, E., Valá, M., 2017. Preparation of antibacterial chlorhexidine / vermiculite and release study. *Int. J. Miner. Process.* 159, 1–6. doi:10.1016/j.minpro.2016.12.002
- Sánchez-Martín, M.J., Sánchez-Camazano, M., Sayalero, M.L., Dominguez-Gil, A., 1988. Physicochemical study of the interaction of montmorillonite with hydralazine hydrochloride, a cardiovascular drug. *Appl. Clay Sci.* 3, 53–61. doi:10.1016/0169-1317(88)90005-1
- Sandwell and West Birmingham Hospitals NHS Trust, 2011. *Antimicrobial Prescribing Formulary*. Birmingham City Hospital, Birmingham (UK), [Internal Document].
- Sarmah, A.K., Meyer, M.T., Boxall, A.B. a, 2006. A global perspective on the use, sales, exposure pathways, occurrence, fate and effects of veterinary antibiotics (VAs) in the environment. *Chemosphere* 65, 725–59. doi:10.1016/j.chemosphere.2006.03.026
- Sassman, S. a, Lee, L.S., 2005. Sorption of three tetracyclines by several soils: assessing the role of pH and cation exchange. *Environ. Sci. Technol.* 39, 7452–9.
- Seaton, R.A., 2009. Skin and soft tissue infection focus on meticillin-resistant S aureus. *Clin. Pharm.* 1, 23–28.



- Segad, M., Jönsson, B., Akesson, T., Cabane, B., 2010. Ca/Na montmorillonite: structure, forces and swelling properties. *Langmuir* 26, 5782–90. doi:10.1021/la9036293
- Smith, C., 2004. Dermatological pharmacology: systemic agents. *Medicine (Baltimore)*. 32, 18–20. doi:10.1383/medc.32.12.18.55397
- Stevens, D.L., 2009. Treatments for skin and soft-tissue and surgical site infections due to MDR Gram-positive bacteria. *J. Infect.* 59 Suppl 1, S32-9. doi:10.1016/S0163-4453(09)60006-2
- Swartzen-Allen, S.L., Matijevic, E., 1974. Surface and colloid chemistry of clays. *Chem. Rev.* 74, 385–400. doi:10.1021/cr60289a004
- Tan, D., Yuan, P., Annabi-bergaya, F., Liu, D., Wang, L., Liu, H., He, H., 2014. Loading and in vitro release of ibuprofen in tubular halloysite. *Appl. Clay Sci.* 96, 50–55. doi:10.1016/j.clay.2014.01.018
- The Royal Liverpool and Broadgreen University Hospitals NHS Trust, 2012. Skin and Soft Tissue Infections Prescribing Guidance. Royal Liverpool University Hospital, Liverpool (UK), [Internal Document].
- Thompson, D.W., Butterworth, J.T., 1992. The Nature of Laponite and Its Aqueous Dispersions. *J. Colloid Interface Sci.* 151, 236–243.
- Tien, C., Ramarao, B. V., 2014. Further examination of the relationship between the Langmuir kinetics and the Lagergren and the second-order rate models of batch adsorption. *Sep. Purif. Technol.* 136, 303–308. doi:10.1016/j.seppur.2014.08.013
- Tong, D.S., Xia, X., Luo, X.P., Wu, L.M., Lin, C.X., Yu, W.H., Zhou, C.H., Zhong, Z.K., 2013. Catalytic hydrolysis of cellulose to reducing sugar over acid-activated montmorillonite catalysts. *Appl. Clay Sci.* 74, 147–153. doi:10.1016/j.clay.2012.09.002
- Tsankov, N., Broshtilova, V., Kazandjieva, J., 2003. Tetracyclines in dermatology. *Clin. Dermatol.* 21, 33–39. doi:10.1016/S0738-081X(02)00324-3
- Tyagi, B., Chudasama, C.D., Jasra, R. V, 2006. Determination of structural modification in acid activated montmorillonite clay by FT-IR spectroscopy. *Spectrochim. Acta. A. Mol. Biomol. Spectrosc.* 64, 273–8. doi:10.1016/j.saa.2005.07.018
- Unal, S., 2009a. Treatment options for skin and soft tissue infections: “oldies but goldies”. *Int. J. Antimicrob. Agents* 34 Suppl 1, S20-3. doi:10.1016/S0924-8579(09)70545-X
- Unal, S., 2009b. Treatment options for skin and soft tissue infections: “oldies but goldies”. *Int. J. Antimicrob. Agents* 34 Suppl 1, S20-3. doi:10.1016/S0924-8579(09)70545-X
- Vaiana, C.A., Leonard, M.K., Drummy, L.F., Singh, K.M., Bubulya, A., Vaia, R.A., Naik, R.R., Kadakia, M.P., 2011. Epidermal Growth Factor: Layered Silicate Nanocomposites for Tissue Regeneration. *Biomacromolecules* 12, 3139–3146.

- Varanda, F., de Melo, M.J.P., Caco, A.I., Dohrn, R., Makrydaki, F.A., Voutas, E., Tassios, D., Marrucho, I.M., 2006. Solubility of Antibiotics in Different Solvents . 1 . Hydrochloride Forms of Tetracycline, Moxifloxacin, and Ciprofloxacin. *Ind. Eng. Chem. Res.* 45, 6368–6374.
- Villar, M.V., Gómez-Espina, R., Gutiérrez-Nebot, L., 2012. Basal spacings of smectite in compacted bentonite. *Appl. Clay Sci.* 65–66, 95–105.  
doi:10.1016/j.clay.2012.05.010
- Viseras, C., Cerezo, P., Sanchez, R., Salcedo, I., Aguzzi, C., 2010. Current challenges in clay minerals for drug delivery. *Appl. Clay Sci.* 48, 291–295.  
doi:10.1016/j.clay.2010.01.007
- Wang, Q., Zhang, J., Zheng, Y., Wang, A., 2014. Adsorption and release of ofloxacin from acid- and heat-treated halloysite. *Colloids Surf. B. Biointerfaces* 113, 51–8.  
doi:10.1016/j.colsurfb.2013.08.036
- Williams, L.B., Haydel, S.E., 2010. Evaluation of the medicinal use of clay minerals as antibacterial agents. *Int. Geol. Rev.* 52, 745–770.  
doi:10.1080/00206811003679737
- Williams, L.B., Haydel, S.E., Giese, R.F., Eberl, D.D., 2008. Chemical and mineralogical characteristics of French green clays used for healing. *Clays Clay Miner.* 56, 437–452. doi:10.1346/CCMN.2008.0560405.CHEMICAL
- Williams, L.B., Metge, D.W., Eberl, D.D., Harvey, R.W., Turner, A.G., Prapaipong, P., Poret-Peterson, A.T., 2011. What makes a natural clay antibacterial? *Environ. Sci. Technol.* 45, 3768–73. doi:10.1021/es1040688
- World Health Organization, 2012. The evolving threat of antimicrobial resistance: Options for action. WHO, Geneva, Switzerland.
- Xuan, Y., Jiang, G., Li, Y., Wang, J., Geng, H., 2013. Inhibiting effect of dopamine adsorption and polymerization on hydrated swelling of montmorillonite. *Colloids Surfaces A Physicochem. Eng. Asp.* 422, 50–60.  
doi:10.1016/j.colsurfa.2013.01.038
- Zhao, H., Zhou, C.H., Wu, L.M., Lou, J.Y., Li, N., Yang, H.M., Tong, D.S., Yu, W.H., 2013. Catalytic dehydration of glycerol to acrolein over sulfuric acid-activated montmorillonite catalysts. *Appl. Clay Sci.* 74, 154–162.  
doi:10.1016/j.clay.2012.09.011
- Zhao, Y., Gu, X., Gao, S., Geng, J., Wang, X., 2012. Adsorption of tetracycline (TC) onto montmorillonite: Cations and humic acid effects. *Geoderma* 183–184, 12–18.  
doi:10.1016/j.geoderma.2012.03.004

## Chapter 3

### Interaction between phyllosilicates and ciprofloxacin

#### 3.1. Introduction

Chapter 2 demonstrated that clay minerals adsorb tetracycline antibacterial agents onto their surfaces and subsequently release these molecules into their surrounding environment for activity against a range of bacterial strains commonly implicated in skin and skin structure infections. However, the poor activity of tetracycline (TC) and doxycycline (DC) against Gram-negative bacteria, such as *Pseudomonas aeruginosa*, is limited by their mode of action (Chatterjee et al., 2016; Lister et al., 2009) therefore other agents such as antipseudomonal penicillins or quinolones may be more clinically appropriate (Unal, 2009).

Ciprofloxacin (CIP) is an antibacterial agent in the quinolone class and is commonly used in UK healthcare for a range of infections, including skin and skin structure infections (Healy and Freedman, 2006; Sandwell and West Birmingham Hospitals NHS Trust, 2011; The Royal Liverpool and Broadgreen University Hospitals NHS Trust, 2012). CIP exhibits broad spectrum activity having greatest effect against Gram-negative bacteria, including *P. aeruginosa*, and some activity against Gram-positive species (Eboka and Okeri, 2005; Phillips et al., 1990; Vance-Bryan et al., 1990; Wispelwey, 2005). Pharmacologically, it is a concentration-dependant agent with a significant post-antibiotic effect (Athamna et al., 2004) that induces bacterial cell death through inhibition of DNA-gyrase and topoisomerase-IV (Mackenzie and Gould, 1993; Vance-

Bryan et al., 1990). CIP also has an attractive pharmacokinetic profile allowing it to distribute throughout the body and achieving adequate concentrations within peripheral tissues (such as the dermis and epidermis) when given orally and parenterally (Vance-Bryan et al., 1990). However, CIP, like other fluoroquinolones, has significant drawbacks when used systemically. In addition to adverse drug reactions such as Achilles tendonitis and QT prolongation (Prabhakar and Krahn, 2004; Vance-Bryan et al., 1990), the quinolone class of antibacterials have a close association with the development of secondary *Clostridium difficile* superinfections (Dingle et al., 2017). Therefore, delivering CIP topically for skin and skin structure infections could overcome these risks as systemic concentrations will be much lower than in current practice.

CIP has two dissociation constants of 6.1 ( $pK_{a1}$ ) and 8.7 ( $pK_{a2}$ ). In acidic environments CIP exists predominantly as a cation with dissociation of hydrogen from the carboxylic acid group increasing above pH 4 to form zwitterionic species (figure 3.1) that dominate between pH 6.1 and 8.7. Maximum zwitterionic species exists around pH 7.2 (isoelectric point,  $pI$ ), above which the proportion of zwitterionic species decreases as a second hydrogen dissociates from the heterocyclic amine group to form an anionic species, which completely dominates above pH 10 (Vasudevan et al., 2009; Wang et al., 2011).

A number of teams have reported the interaction between CIP and a range of clay-minerals, determining the mechanism of these interactions and how the properties of the dispersion can affect the nature of the interaction (Wang et al., 2011, 2010; Wu et

al., 2010). Whilst this portfolio of work is much smaller than that for tetracyclines (see section 2.1), Wang and colleagues have undertaken considerable research investigating the mechanism of CIP adsorption onto clay-mineral particles and proposed a molecular arrangement within the interlayer space (Wang et al., 2011, 2010).

The findings presented in this chapter, published early 2014 (Hamilton et al., 2014), is the only known study investigating CIP-clay composites as antibacterial materials for the treatment of infections. The differing structure and chemistry of CIP, compared to the tetracyclines, makes it an interesting drug to investigate and determine whether the findings and theories regarding drug adsorption developed in chapter 2 are transferable to other molecules. Its broader spectrum of activity also makes CIP an important drug to investigate to determine whether it can be used in the formulation of phyllosilicate-polymer wound-care products. For this reason, the clay-CIP composites formed were tested against the same common skin and skin structure pathogens *Staphylococcus epidermidis*, *Propionibacterium acnes*, and *Pseudomonas aeruginosa*.

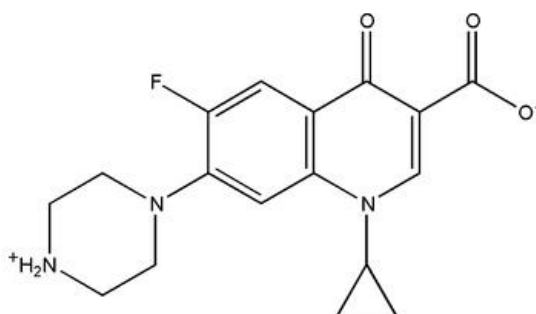


**Figure 3.1.** Chemical structure of ciprofloxacin in its zwitterionic form (drawn with Chemdraw Chem3D, Perkin Elmer)

The chemical and structural properties of clay-minerals was shown to play a significant role in TC and DC adsorption, so three were chosen for studying the adsorption of CIP based on their chemical and physical properties; kaolin (KN) as a 1:1 clay mineral with minimal surface area, low surface charge, and low CEC; Laponite® RD (LRD) as a 2:1 clay mineral with large surface area, moderate surface charge, large CEC, and attractive dispersion properties; and montmorillonite K-10 (MMTK10), which is an acid-activated 2:1 montmorillonite clay mineral, with moderate surface area, high surface charge, moderate CEC, and reduced dispersion potential (see chapters 1 and 2 for more information).

## 3.2. Materials and methods

### 3.2.1. Materials

Kaolin (KN), Laponite RD (LRD) and montmorillonite K-10 (MMTK10) were sourced as described in section 2.2.1. Ciprofloxacin (>98% by HPLC), hereafter CIP, was obtained from Sigma Aldrich UK.

### 3.2.2. Adsorption of ciprofloxacin

#### 3.2.2.1. Effect of dispersion pH

One gram of clay mineral was dispersed in 80 mL of deionised water for 2 h at 7000 rpm. After this initial dispersion period the pH was adjusted to between 1 and 12 using dilute NaOH or HCl. A 12.5 mg/mL CIP solution was made by dissolving CIP in dilute HCl to produce the more soluble hydrochloride form, which was then adjusted to the relevant pH and left to stand for 30 minutes to ensure solubility (Roca Jalil et al., 2015; Varanda et al., 2006). The CIP solution was then added to the clay mineral dispersion of corresponding pH. After confirming the pH of the dispersion the adsorption was continued for 24 h and each experiment was undertaken in triplicate.

Aliquots of the dispersions were centrifuged and the amount of CIP remaining in supernatant determined with UV-Visible spectrophotometry (Genesys 10V, Thermo Scientific), scanning between 200-400 nm. Standard curves ( $R^2 \Rightarrow 0.998$ ) of UV-vis absorption against CIP concentration were obtained at different pH to account for  $\lambda_{max}$  shifts occurring at different pH (275 nm and 315 nm at pH 1 to 4, 275 nm and 320 nm at pH 5 to 8.7, then 270 nm and 320 nm at pH 9 to 12). Measurements were performed in triplicate.

#### *3.2.2.2. Adsorption kinetics and isotherms*

Methods from sections 2.2.2.2 and 2.2.2.3 were modified for studying CIP adsorption kinetics and adsorption isotherms. For adsorption kinetics the concentration of clay mineral used was 500 mg/100 mL KN, 100 mg/100 mL MMTK10, or 10 mg/100 mL LRD with 2 mg/100 mL of CIP. For adsorption isotherms the concentration of each clay mineral used was 250 mg/25 mL with a range of CIP concentrations between 0.5 and 10.0 mg/mL. All dispersions were adjusted to pH 7.2 before and after adding CIP, and were repeated in triplicate.

#### *3.2.3. Mechanism of clay-ciprofloxacin interactions*

X-ray diffractograms were obtained on a Rigaku miniflex (CuK $\alpha$ 1 radiation source) and FTIR spectra were obtained on a Perkin Elmer Spectrum BX FT-IR spectrometer (GladiATR attachment). The specifics of these analytical methods used are given in section 2.2.3.

#### *3.2.4. Antibacterial activity assessment*

Zone of inhibition testing was undertaken in triplicate as per section 2.2.4. The concentration range of CIP standards was 5  $\mu$ g/mL to 250  $\mu$ g/mL, which were slightly acidified with HCl to enable dissolution. Blank wells containing acidified water were assessed to ensure the HCl was not contributing to the antibacterial effects of the CIP standard solutions.



### 3.3. Results and discussion

#### 3.3.1. Effects of dispersion pH on ciprofloxacin adsorption

For all three clay minerals tested the dispersion pH played an important role in determining drug adsorption onto the clay mineral surface (figure 3.2). A dispersion pH of 7.2 was shown to allow the greatest amount of CIP adsorption onto the surface of all three clay minerals tested and corroborates published literature that showed maximum adsorption occurs when CIP is in the zwitterionic form (Gu and Karthikeyan, 2005; Wang et al., 2010; Wu et al., 2010). These findings also support the theory developed in chapter 2 that inducing a zwitterionic state in a drug molecule may enhance its interaction with a clay mineral surface.

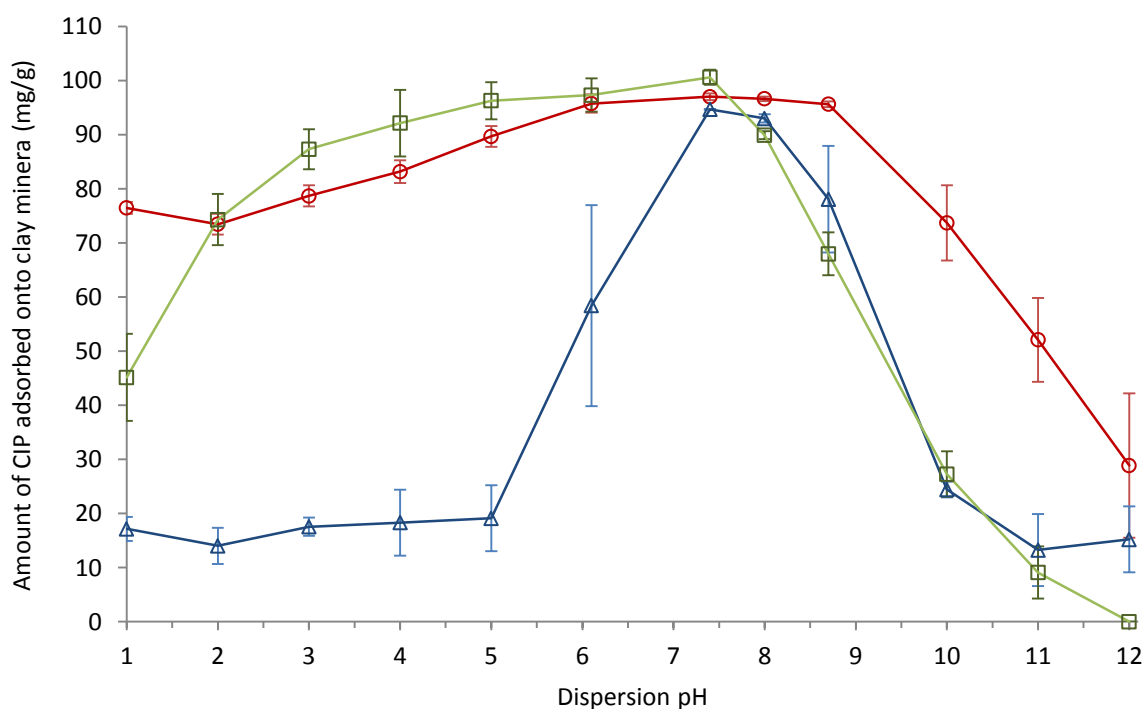


**Figure 3.2.** The effects of dispersion pH on the adsorption (mean  $\pm$ SD, n=3) of ciprofloxacin onto KN (blue triangles), MMTK10 (red circles), and LRD (green squares).

In chapter 2 the improved affinity for TC and DC in the zwitterionic form was postulated to be due to the attraction of the positive group and the repulsion of the negative groups from the clay mineral surface, leading to a more favourable arrangement of drug molecules at the clay mineral surface. In CIP these charged groups are positioned at opposite ends of the molecule (figure 3.1), unlike in TC and DC (figure 2.1), which may have significant impact on its arrangement at the clay mineral surface. It may be possible for CIP to take on an almost vertical arrangement at the clay mineral surface (Carrasquillo et al., 2008; Rivera et al., 2016), minimising the surface area of the clay mineral occupied by the adsorbed molecules, thus allowing more molecules to be adsorbed per unit of available clay mineral surface area.

When the dispersion pH is below 6.1 CIP will increasingly be in its mono-cationic form, which still allows for interactions with the negatively charged clay mineral surfaces (Wang et al., 2010). However, as the dispersion became more acidic the amount of CIP adsorbed decreased. Whilst the positive charge is favourable for interactions with the clay mineral surface, the lack of negative charge at the apical end of the molecule may result in a less than ideal arrangement of CIP at the clay mineral surface. The highly acidic environment may also have caused significant changes to the clay mineral structure through dissolution of the metallic tetrahedral sheet (Komadel, 2003; Madejova, 2003) resulting in a reduced affinity between the remaining silica mass and the CIP molecules in dispersion.

As the dispersion pH increased above 8.7 the adsorption of CIP onto all the clay minerals used was also greatly reduced. CIP will be in the mono-anionic form at high

pH and these data show this is not favourable for interaction with clay minerals. It is possible that anionic CIP molecules interact with the positive groups exposed at the edge of the clay mineral particles (Wang et al., 2010). However, as the pH of the dispersion increased beyond pH 9 the edge groups on the clay mineral layers deprotonate to become negatively charged (Lagaly and Ziesmer, 2003; Thomas et al., 1999) and are likely to repel any negatively charged CIP molecules. Yet at pH 11 and 12 the adsorption of CIP onto MMTK10 and KN was not insignificant. The mono-negative CIP molecules should be repelled from the negatively charged clay layers so the adsorption detected in these experiments may be due to alternative interactions such as van der Waals forces (Carrasquillo et al., 2008) and hydrogen bonding (Wang et al., 2010).

Differences in CIP adsorption patterns were observed between KN and MMTK10. The low adsorption onto KN can be anticipated by its small surface area, low charge, and small CEC (Kahr and Madsen, 1995) but, surprisingly, the difference in the amount of CIP adsorbed at pH 7.2 was not significantly different between the three clay minerals used. Given the chemistry of KN, MMTK10, and LRD it would be expected that KN would adsorb a smaller amount of CIP whereas LRD would adsorb the most (Kahr and Madsen, 1995; Thompson and Butterworth, 1992). The similar amounts of adsorption observed at the isoelectric point could indicate that equilibrium was reached in the MMTK10 and LRD experiments and the methodology used would not distinguish adsorption capacity (Parfitt and Rochester, 1983; Wang et al., 2010). These data could also indicate that CIP adsorption at pH 7.2 also involves secondary adsorption pathways other than CEC and direct surface interactions, allowing significantly more

adsorption onto KN (Carrasquillo et al., 2008; Wang et al., 2010; Wu et al., 2010). Studies designed to specifically investigate the kinetics and isotherms of adsorption were undertaken to better understand the adsorption of CIP onto clay minerals at pH 7.2.

### 3.3.2. Adsorption kinetics

The majority of CIP adsorption onto KN, MMTK10 and LRD took place within the first ten minutes (figure 3.3). The adsorption of CIP onto all three clay minerals was shown to fit the pseudo-second order model (table 3.1).

Even though KN adsorbed CIP at the lowest rate the system reached equilibrium after 1 hour, after which no change in the concentration of CIP remaining in the supernatant was detected (figure 3.3 A). The amount of CIP adsorbed onto each clay mineral was calculated by UV-Vis spectrophotometry of the supernatant and compared to the estimated amount adsorbed ( $q_e$ , see table 3.1). The percentage difference between these values was small for each clay mineral tested, supporting the conclusion that the adsorption followed pseudo-second order kinetics.

As for the adsorption kinetics of TC and DC onto clay minerals, large differences in CIP adsorption were observed as a result of the clay mineral chemistry, structure, and properties (see chapter 2). As expected, KN had the slowest initial rate of adsorption and the lowest amount of drug adsorption over the time tested. Both of which can be explained by its negligible charge and small surface area (Miranda-Trevino and Coles, 2003).

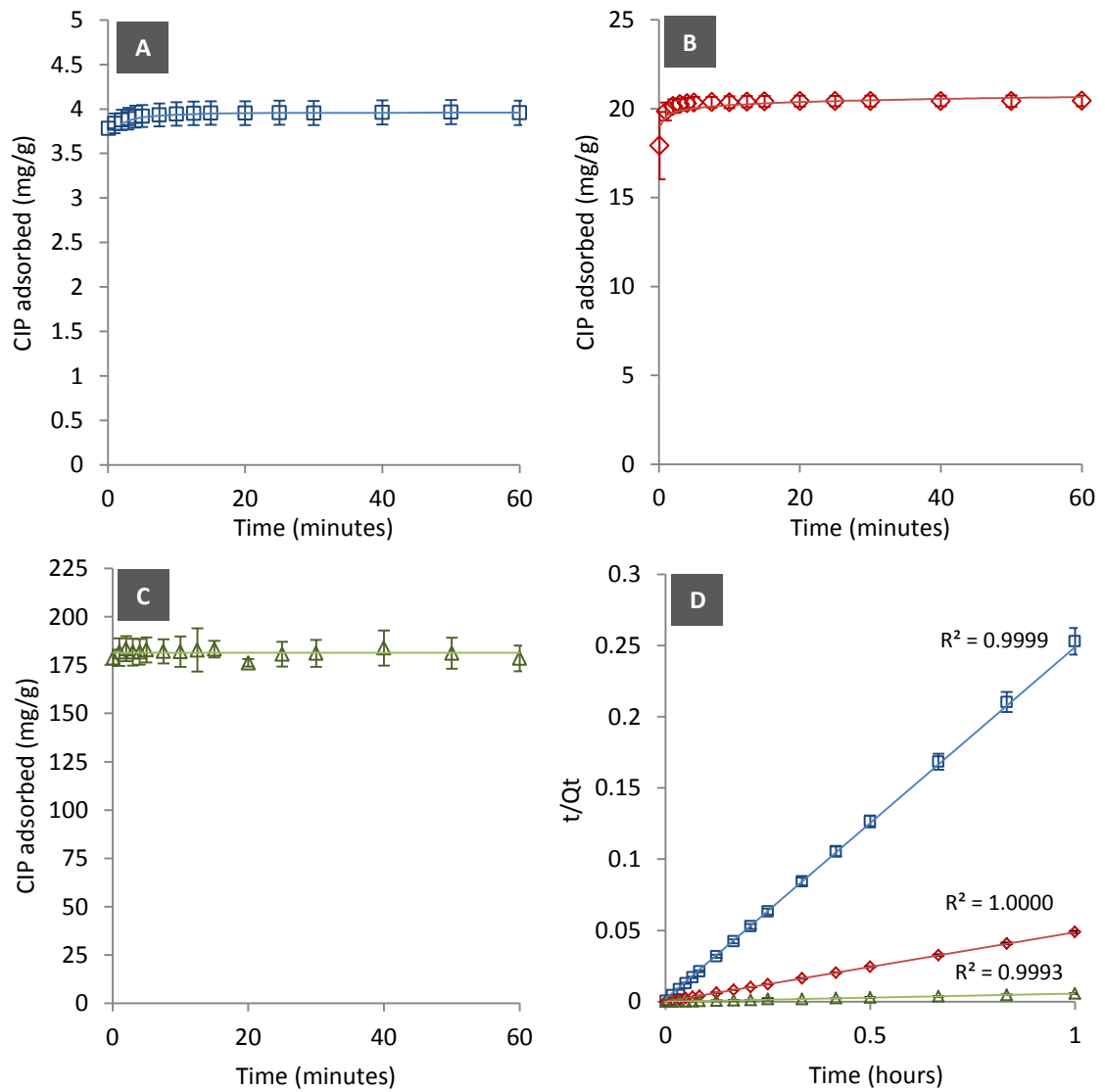


**Figure 3.3.** Amount of CIP adsorbed (mean  $\pm$ SD, n=3) onto (A) KN, (B) MMTK10 and (C) LRD at pH 7.2 at defined time-points. Figure D gives pseudo-second order adsorption kinetics (mean  $\pm$ SD, n=3) and goodness of fit ( $R^2$ ) for CIP onto KN (blue squares), MMTK10 (red diamonds) and LRD (green triangle).

**Table 3.1.** Goodness of fit ( $R^2$ ) of pseudo-first and pseudo-second order kinetic models for the adsorption of CIP onto the selected clay minerals at pH 7.2. Where K is the rate constant,  $q_e$  is the estimated amount of drug adsorbed, and %diff  $q_e$  is the difference between the estimated CIP adsorbed and that measured.

Clay Mineral	Pseudo 1 <sup>st</sup> Order	Pseudo 2 <sup>nd</sup> Order				
	( $R^2$ )	( $R^2$ )	Initial rate (mg/g h)	K (g/mg h)	$q_e$ (mg/g)	%diff $q_e$
KN	0.4097	0.9999	523.56	31.92	4.05	1.92
MMTK10	0.4969	0.9999	8333.33	19.66	20.59	0.78
LRD	0.0765	0.9982	$\infty$	$\infty$	175.44	1.84

LRD adsorbed CIP at a much faster rate than MMTK10, and was able to adsorb more onto its very large surface area. All the clay minerals were dispersed in water before the adsorption experiments were undertaken, which would have allowed the LRD layers to separate from each other, greatly increasing the surfaces available for CIP adsorption (Mongondry et al., 2005). MMTK10 is not able to swell or exfoliate to the same extent as LRD because the acid activation process can lock the layers of montmorillonite together through the formation of amorphous silica (Madejova, 2003). The effects of this dispersion process can be seen by comparing the initial rates of CIP adsorption onto MMTK10 and LRD. Due to the extremely rapid adsorption onto LRD the rate was immeasurable ( $\infty$  mg/g h, see table 3.1).

When Wang et al. (2011) compared the adsorption of CIP onto three different clay minerals they found that montmorillonite had the fastest initial adsorption rate compared to rectorite and illite. As montmorillonite is a swelling clay this supports the conclusion that clay mineral swelling and exfoliation allows for rapid adsorption of CIP (Wang et al., 2011). The initial rate of adsorption of CIP onto all three clay minerals used in these experiments (KN, MMTK10, and LRD) was much greater than that for the

adsorption of TC and DC (table 2.1). This finding has also been reported by other research teams (Wang et al., 2011; Wu et al., 2010) who also found the estimated  $q_e$  was much higher for CIP than for TC.

### 3.3.3. Adsorption isotherms

The CIP adsorption isotherms for each clay mineral were related to their structure and chemistry. For example, KN has the smallest surface area and charge, so little CIP was needed to form a monolayer on its surface (figure 3.4 A). Due to their increased CEC and SSA much more CIP could be adsorbed onto MMTK10 and LRD (Miranda-Trevino and Coles, 2003).

Monolayer coverage was directly observable for KN and MMT10, but not for LRD which appeared to continue adsorbing CIP (figure 3.4 C). Therefore, more CIP would need to be added to the system to directly detect monolayer formation. However, due to the acidity of concentrated CIP solutions it was impossible to add such high quantities of CIP without causing dissolution of metal ions from the LRD structure, or causing subsequent precipitation of CIP when the concentrated dispersions were adjusted to pH 7.2.

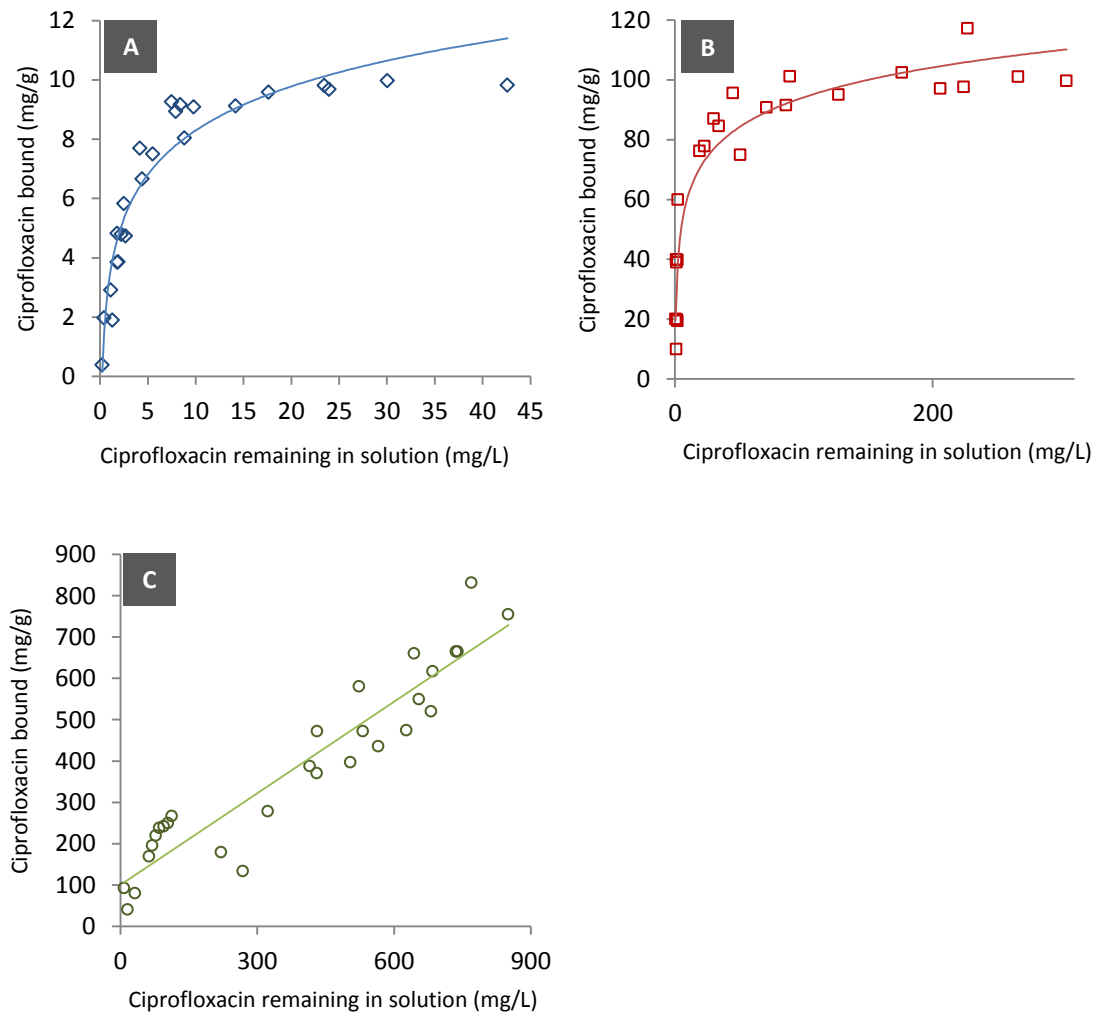


**Figure 3.4.** Adsorption isotherms ( $n=3$ ) for the adsorption of CIP onto (A) KN, (B) MMTK10, and (C) LRD at pH 7.2.

The adsorption isotherms for KN and MMTK10 were typical Langmuir isotherms, whereas the isotherm for LRD resembled that of a Freundlich isotherm (Parfitt and Rochester, 1983). This was proven mathematically when the adsorption isotherms for KN and MMTK10 showed better fit to the Langmuir model and LRD showed better fit to the Freundlich model (table 3.2). These results may be due to a monolayer not being achieved or detected by the LRD experiments. The first section of a Langmuir-like adsorption isotherm (i.e. the initial steep incline) generally fits the Freundlich



model, so it could be possible that the isotherm obtained for the adsorption of CIP onto LRD was actually the initial, Freundlich-like, section of a Langmuir-like adsorption isotherm (Parfitt and Rochester, 1983). However, as the Freundlich isotherm describes reversible multilayer adsorption (Chen, 2015) it is likely that these results prove LRD can adsorb many layers of CIP.

**Table 3.2.** Correlation of fit between experimental adsorption data to the Langmuir, Freundlich, and Tempkin adsorption isotherm models. Where  $S_m$  is the monolayer coverage,  $b_F$  is a dimensionless value for adsorption intensity, and  $B$  is the energy of adsorption.

Clay Mineral	Langmuir Model		Freundlich Model		Tempkin Model	
	Fit ( $R^2$ )	$Q_m$ (mg/g)	Fit ( $R^2$ )	$b_F$	Fit ( $R^2$ )	$B$ (J/mol)
KN	0.942	39.84	0.690	0.393	0.841	2.09
MMTK10	0.959	123.47	0.845	0.260	0.882	14.52
LRD	0.834	714.29	0.989	1.005	0.818	390.81

Significantly less CIP was required to form a monolayer on KN compared to MMTK10, which was significantly less than that for LRD. KN has a very small SSA and CEC giving it less capacity to adsorb CIP, compared to LRD, which has a vastly greater SSA and CEC. Literature correlates with these findings and suggest that although SSA is an important property to consider, CEC may have a greater role to play in determining adsorption capacity (Wang et al., 2010).

The intensity of adsorption ( $b_F$ ) was greatest for CIP adsorbing onto LRD than for the other two clays, which may be explained by the large surface charge that LRD particles carry (Pálková et al., 2010). However, this does not hold true for the adsorption of CIP onto MMTK10 as the intensity of adsorption was lower than calculated for KN. Adsorption intensity has been shown to change over the pH range (section 2.3.3) and it

may be possible that pH 7.2 does not allow for intense interactions between CIP and MMTK10. Another explanation may be that the CIP molecules do not interact well with the areas that have undergone acid-activation and the Brønsted-acid sites present do not favour CIP adsorption (Komadel, 2003).

Whilst the isotherm data does not fit the Tempkin model as well as the Langmuir or Freundlich models (table 3.2) it is still possible to derive assumptions about the heat of adsorption ( $B$ , J/mol) within these adsorption processes. Overall, the heat of adsorption indicates that CIP adsorbs onto the clay minerals via physisorption rather than chemisorption (Itodo and Itodo, 2010; Puttamat and Pavarajarn, 2016). The higher heat of adsorption of CIP onto LRD indicates greater surface coverage and may also suggest there is greater CIP-CIP interaction taking place than in the other systems (Dada et al., 2012). This is further supported by the work of Wu et al (2010), who reported that cation exchange is not the only mechanism of CIP adsorption onto clay minerals and other forms of interaction can contribute.

#### *3.3.4. XRD analysis*

The interlayer spacing for the clay minerals alone, physical blends of the clay minerals with CIP, and selected clay mineral-CIP composites was determined through the  $d_{001}$  value as previously described (see section 2.3.4).

As expected, the interlayer space of KN was found to be smaller than the MMTK10 and LRD due to its 1:1 structure and tight junctions between its layers (Miranda-Trevino and Coles, 2003). Non-significant changes in the  $d_{001}$  value were observed

when CIP was adsorbed onto KN and it can be assumed that no change in the size of the interlayer space occurred (table 3.3). It is therefore likely that the CIP adsorbed onto the external surfaces of KN only (Miranda-Trevino and Coles, 2003). This supports the data obtained from the adsorption studies above, whereby the low amount of CIP adsorption was attributed to a small surface area.

Interestingly, the  $d_{001}$  peak for MMTK10 was observed to shift to the left, indicating an increase in the interlayer space (figure 3.5) (Chang et al., 2009; Parolo et al., 2008). No difference in the size of the interlayer space was observed between the pure MMTK10 sample and the physical blend of MMTK10 and CIP. However, increases in the interlayer space were seen as the amount of CIP adsorbed increased (table 3.3).

**Table 3.3.** Interlayer spacing measured by pXRD for the clay minerals alone, physical blends with CIP, and selected clay-CIP composites of increasing drug-loading.

Clay mineral	Sample	CIP Concentration (mg/g)	Interlayer Space (Å)
KN	Control (non-modified)	-	7.19
	Physical blend	50.00	7.19
	KN-CIP (low concentration)	4.79	7.15
	KN-CIP (mid concentration)	27.54	7.15
	KN-CIP (high concentration)	81.53	7.16
MMTK10	Control (non-modified)	-	9.94
	Physical blend	100.00	9.95
	MMTK10-CIP (low concentration)	49.76	14.00
	MMTK10-CIP (mid concentration)	90.70	17.28
	MMTK10-CIP (high concentration)	117.02	16.75
LRD	Control (non-modified)	-	13.57
	Physical blend	100.00	13.67
	LRD-CIP (low concentration)	15.85	12.71
	LRD-CIP (mid concentration)	104.31	13.84
	LRD-CIP (high concentration)	128.09	13.48

A slight decrease in the  $d_{001}$  value was observed for the sample with the highest drug loading but this may not necessarily be due to a reduction in the size of the interlayer space. As seen in figure 3.5 the  $d_{001}$  peak for the sample with the highest drug load was not uniform in shape and was broad in nature. The non-uniformity of the peak indicates a loss in regularity of the distance between the clay mineral layers and peak broadening is an indication of exfoliation (Chang et al., 2009; Kaufhold and Dohrmann, 2009; Lee and Kim, 2002).

Theoretically, the exfoliation of MMTK10 and other acid activated clays is difficult. As the acidic medium induces the dissolution of the octahedral sheet, to form amorphous silica networks, the edges of these particles can become conjoined making it unlikely for them to swell and exfoliate (Komadel, 2003; Zhao et al., 2013). However, it cannot be denied that a change in the  $d_{001}$  peak was observed for the adsorption of CIP onto MMTK10. This shift may have been caused by an increasing distance between particles of MMTK10 and not the individual layers. It would be necessary to utilise additional imaging methods that can resolve the individual clay layers and the interlayer spacing, such as transmission electron microscopy (TEM) (Lee and Kim, 2002).

A change in interlayer space was not observed for the adsorption of CIP onto LRD. It was expected that swelling clay minerals, such as LRD, would demonstrate expansion of the interlayer space through the adsorption of organic molecules, a small decrease in interlayer space was actually observed when a small amount of CIP had been adsorbed onto the LRD.

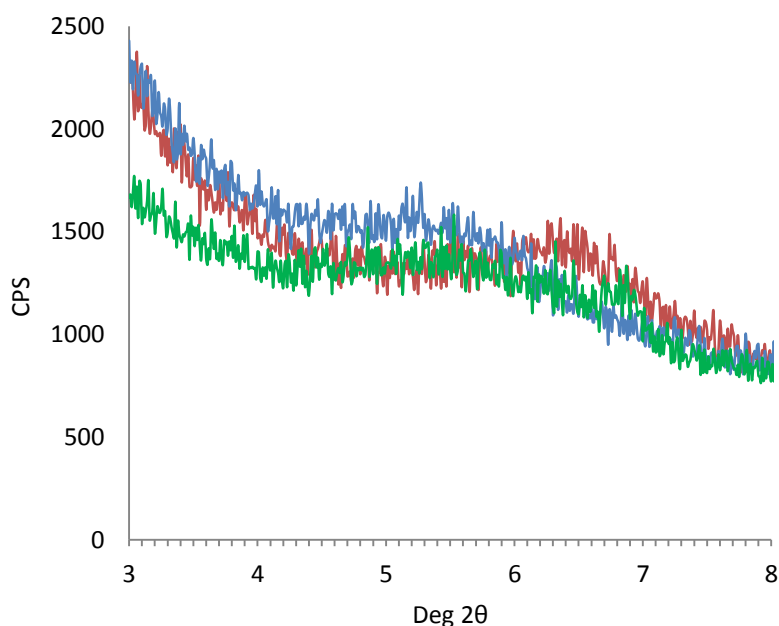


**Figure 3.5.** X-ray diffractions for CIP adsorbed onto MMTK10. Colours of the lines represent different CIP concentrations of 49.76 mg/g (red), 90.70 mg/g (blue), and 117.02 mg/g (green).

In solution LRD almost fully disperses into its individual layers and may be flocculated by the adsorption of inorganic and organic cations (Ramsay, 1986). The adsorption of CIP onto the surface of LRD may have been enough to cause a degree of flocculation, and thus shrinkage of the interlayer space. However, the  $d_{001}$  value increased back to its original value upon further adsorption of CIP. This may have been caused by the CIP molecules forcing the LRD layers apart, or may indicate the initial decrease in interlayer spacing was an artefact of the XRD analysis process. Moreover, the initial interlayer spacing was quite large and the peak was not well defined on the LRD or LRD-CIP blend samples. This could indicate that the interlayer spacing was not regular to start with, and due to its colloidal, dispersive, behaviour it is unlikely to display a regular interlayer space like montmorillonite and other smectites do. It is likely that CIP will bind to the exposed surfaces of the individual LRD layers and have no discernible

effect on the relative distances between the LRD layers, and thus no detectable change on the XRD traces.

### 3.3.5. FTIR analysis

Infrared adsorption for the clays and CIP enabled interpretation of the interaction between CIP and the clay mineral surfaces. The spectra for the unmodified clays showed the characteristic Si-O stretching band at 900-1100  $\text{cm}^{-1}$  along with metallic-group (M-OH) absorbance between 600-900  $\text{cm}^{-1}$  (Madejova, 2003). Clear differences in the shape and wavenumber of the Si-O absorption were seen between the three clay minerals, with MMTK10 having the greatest difference. Muting of the metal hydroxide peaks around 800  $\text{cm}^{-1}$  is a clear demonstration of the metal dissolution effects of acid activation on the clay mineral structure (Tyagi et al., 2006). No changes in the absorbance peaks from the clay minerals were seen in the composite samples proving that the adsorption process did not result in further dissolution of metal ions from the clay mineral sheets.

The fingerprint region of CIP was clearly defined for the drug alone, and when present within physical mixtures and composites. The absorbance peak for the positively charged amino group was identified at 1373  $\text{cm}^{-1}$  in the physical blend of CIP and MMTK10, but this shifted to 1384  $\text{cm}^{-1}$  when adsorbed onto the surface of MMTK10 (figure 3.6) This shift indicates an interaction between the positively charged amino group on the CIP molecule, and the negatively charged clay mineral surface (Trivedi and Vasudevan, 2007; Wang et al., 2011; Wu et al., 2010).

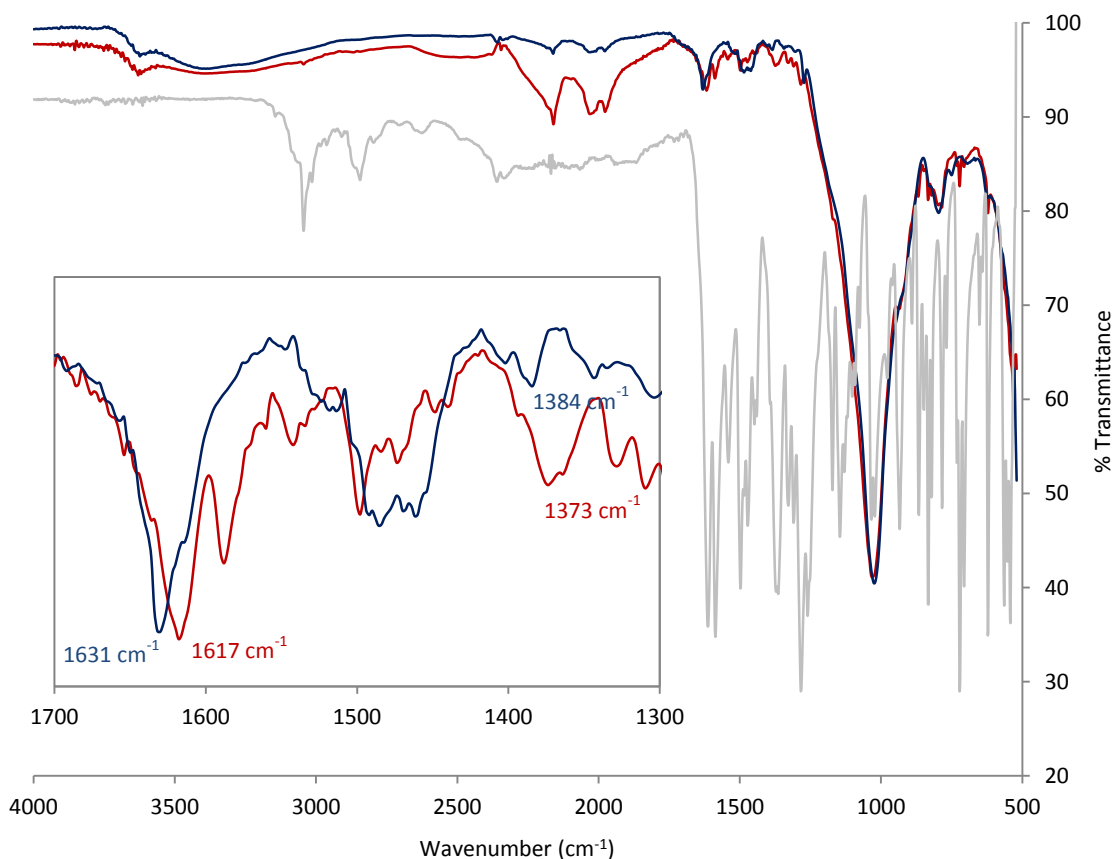


**Figure 3.6.** FTIR spectra CIP (grey line), a physical blend of MMTK10 and CIP (red line) and a MMTK10-CIP composite (blue line).

A shift of the absorbance from  $1617\text{ cm}^{-1}$  in the physical blend to  $1631\text{ cm}^{-1}$  in the composite represents an electron withdrawing effect from the ketone group adjacent to the carboxyl group (Wu et al., 2010). Other studies utilising FTIR to examine the interaction between CIP and clay minerals suggest that this negatively charged region can interact with the edge-sites of clay minerals (Wang et al., 2010), interact directly with the clay mineral surface (Chang et al., 2016), or the interlayer cations (Rivera et al., 2016). The shift in absorbance representing electron withdrawal from the ketone group suggests that such an interaction could also be taking place here.

Therefore, it is likely that CIP remained as a zwitterion during the adsorption process and it is possible that both the positive and negatively charged regions are interacting with the clay minerals.

### 3.3.6. Antibacterial properties

The clay-minerals on their own did not produce any zones of inhibition whereas solutions of CIP did create zones of inhibition. As the concentration of the CIP solution increased so did the zone of inhibition, proving that any zones of inhibition created by the clay-CIP composites was due to desorption and diffusion of CIP from the composites. As expected, due to its mode of action (Vance-Bryan et al., 1990; Wispelwey, 2005), CIP was active against all three strains of bacteria including *P. aeruginosa*. The zone of inhibition increased in size as the CIP concentration in the composite increased (figure 3.7), confirming that increasing amounts of CIP could be released from these composite materials as the drug-loading was increased.

Important differences can be seen across the concentrations of drug-loading within the composites. As the concentration of CIP in the composites increased from 'low' to 'medium' the change in zone of inhibition size was very large. However, the change in zone size between the composites marked as 'medium' and 'high' drug-loading was not as impressive. Within the composites marked as 'low' the CIP had not formed a monolayer and was therefore interacting more strongly with the clay-mineral surface, resulting in little desorption of CIP and therefore small zones of inhibition. In the composites marked as 'medium' and 'high' CIP had formed a monolayer at the clay-mineral surface and any additional absorbed CIP was likely interacting via weaker



forces, not related to cation-exchange processes (Parfitt and Rochester, 1983; Wu et al., 2010; Yan et al., 2012), and could be more easily desorbed from the composites.

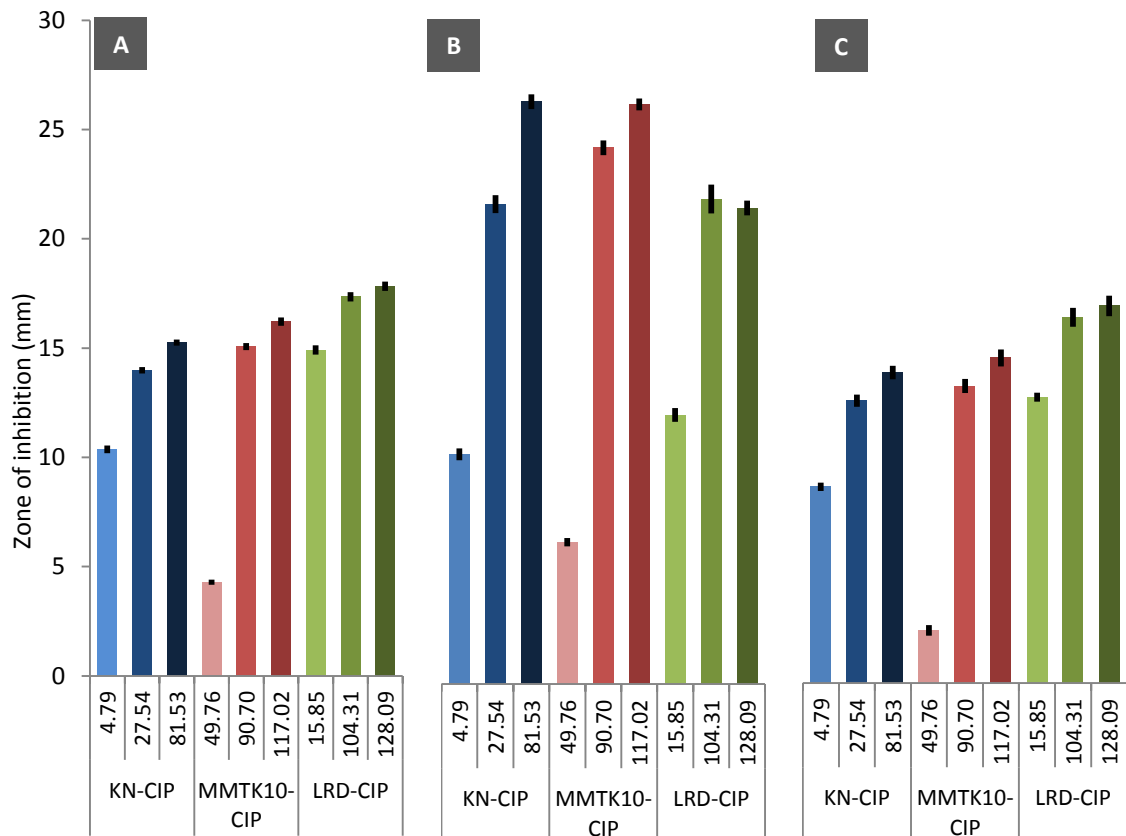


**Figure 3.7.** Zones of inhibition (mean  $\pm$ SD, n=3) formed by clay-CIP composites, of various drug-loading (mg/g), against *S. epidermidis* (A), *P. acnes* (B), and *P. aeruginosa* (C).

KN-CIP composites with 'low' drug loading created much larger zones of inhibition than MMTK10-CIP composites with 'low' CIP loading. This shows that KN holds onto CIP less strongly than MMTK10, probably due to its lower surface charge (Kahr and Madsen, 1995). The small difference between the size of the zones formed by composites of

'medium' and 'high' drug loading may be attributed to the time-limited nature of the experiments which may have prevented all of the available CIP from diffusing into the agar. As deionised water was used to disperse the composites it is possible that the zones of inhibition observed in these experiments are due to a burst-release of CIP from the composites and that further CIP could have been dispersed from the clay mineral surface if cations had been present for exchange (Jung et al., 2008; Parolo et al., 2010).

These experiments prove that the CIP within the clay-CIP composites remains active against these three important wound pathogens, and are therefore interesting and exciting materials worthy of further research. However, the behaviour of these materials in the wound environment and drug release studies will be needed to gain more understanding into the nature of CIP desorption from these materials.

### 3.4. Conclusions

This research shows that CIP is adsorbed more abundantly onto clay minerals when conditions favour the zwitterionic form, which may be explained by the relative position of the charges on the CIP molecule that could favour perpendicular arrangement and tighter packing at the clay mineral surface. Adsorption was rapid onto KN and MMTK10, and immeasurably fast in the case of LRD. Adsorption followed pseudo-second order kinetics. Isotherms for KN and MMTK10 best fitted the Langmuir model whereas LRD isotherms fitted more closely to the Freundlich model; though this may have been due to experimental limitations.

FTIR analyses indicated that both the positively charged amino-group and the negatively charged carboxyl-group could interact with the clay minerals. This suggests that CIP can interact with both the clay mineral surface and edge groups. Multiple mechanisms of adsorption may therefore be possible including cation exchange, direct complexation, van der Waals interactions, and even hydrogen bonding. Unfortunately, the experiments utilised above were unable to quantify these differing interactions. XRD data did prove that CIP can be incorporated into the interlayer space of MMTK10 and LRD but was limited to the external surfaces of KN.

CIP containing composites were shown to be effective against *S. epidermidis*, *P. acnes* and *P. aeruginosa* and unlike composites of TC and DC, which had questionable activity against *P. aeruginosa* (section 2.3.6), clay-CIP composites were proven to have promising activity against this organism. However, similar patterns between drug-

loading and activity were seen between TC, DC and CIP as KN-drug composites more easily relinquished their drug load.

These data prove that findings discussed in chapter 2 are not specific to TC and DC, but can also be applied to other drug molecules. However, CIP, TC and DC are small molecules and investigating the adsorption of larger, more complex, antimicrobials currently used to treat bacterial skin and skin-structure infections (SSSIs) such as clarithromycin, clindamycin, dalbavancin, and vancomycin (Roberts et al., 2015; Seaton, 2009; Stevens, 2009; Unal, 2009) will be needed to fully develop a wider theorem regarding antimicrobial adsorption onto clay minerals.

The results presented above suggest that clay-CIP composites could be promising materials to use in the treatment of SSSIs. However, powders and pastes are not ideal materials for use in wounds and SSSIs so a more clinically and patient acceptable material needs to be developed (Bennett-Marsden, 2010). Chapter 4 will investigate the incorporation of clay-CIP composites into polymeric matrices for the development of materials that are appropriate for use on wounds.

### 3.5. References

- Athamna, A., Athamna, M., Medlej, B., Bast, D.J., Rubinstein, E., 2004. In vitro post-antibiotic effect of fluoroquinolones, macrolides,  $\beta$ -lactams, tetracyclines, vancomycin, clindamycin, linezolid, chloramphenicol, quinupristin/dalfopristin and rifampicin on *Bacillus anthracis*. *J. Antimicrob. Chemother.* 53, 609–615. doi:10.1093/jac/dkh130
- Bennett-Marsden, M., 2010. How to select a wound dressing. *Clin. Pharm.* 2, 363–366.
- Carrasquillo, A.J., Bruland, G.L., Mackay, A.A., Vasudevan, D., 2008. Sorption of ciprofloxacin and oxytetracycline zwitterions to soils and soil minerals: Influence of compound structure. *Environ. Sci. Technol.* 42, 7634–7642. doi:10.1021/es801277y
- Chang, P.-H., Li, Z., Jiang, W.-T., Jean, J.-S., 2009. Adsorption and intercalation of tetracycline by swelling clay minerals. *Appl. Clay Sci.* 46, 27–36. doi:10.1016/j.clay.2009.07.002
- Chang, P.H., Jiang, W.T., Li, Z., Kuo, C.Y., Wu, Q., Jean, J.S., Lv, G., 2016. Interaction of ciprofloxacin and probe compounds with palygorskite PFI-1. *J. Hazard. Mater.* 303, 55–63. doi:10.1016/j.jhazmat.2015.10.012
- Chatterjee, M., Anju, C.P., Biswas, L., Anil Kumar, V., Gopi Mohan, C., Biswas, R., 2016. Antibiotic resistance in *Pseudomonas aeruginosa* and alternative therapeutic options. *Int. J. Med. Microbiol.* 306, 48–58. doi:10.1016/j.ijmm.2015.11.004
- Chen, X., 2015. Modeling of experimental adsorption isotherm data. *Inf.* 6, 14–22. doi:10.3390/info6010014
- Dada, A., Olalekan, A., Olatunya, A., Dada, O., 2012. Langmuir, Freundlich, Temkin and Dubinin – Radushkevich Isotherms Studies of Equilibrium Sorption of Zn<sup>2+</sup> onto Phosphoric Acid Modified Rice Husk. *IOSR J. Appl. Chem.* 3, 38–45. doi:10.9790/5736-0313845
- Dingle, K.E., Didelot, X., Quan, T.P., Eyre, D.W., Stoesser, N., Golubchik, T., Harding, R.M., Wilson, D.J., Griffiths, D., Vaughan, A., Finney, J.M., Wyllie, D.H., Oakley, S.J., Fawley, W.N., Freeman, J., Morris, K., Martin, J., Howard, P., Gorbach, S., Goldstein, E.J.C., Citron, D.M., Hopkins, S., Hope, R., Johnson, A.P., Wilcox, M.H., Peto, T.E.A., Walker, A.S., Crook, D.W., Del Ojo Elias, C., Crichton, C., Kostiou, V., Giess, A., Davies, J., 2017. Effects of control interventions on *Clostridium difficile* infection in England: an observational study. *Lancet Infect. Dis.* 17, 411–421. doi:10.1016/S1473-3099(16)30514-X
- Eboka, C.J., Okeri, H.A., 2005. Aqueous solubility of ciprofloxacin in the presence of metal cations. *Trop. J. Pharm. Res.* 4, 349–354.
- Gu, C., Karthikeyan, K.G., 2005. Sorption of the antimicrobial ciprofloxacin to aluminum and iron hydrous oxides. *Environ. Sci. Technol.* 39, 9166–73.
- Hamilton, A.R., Hutcheon, G.A., Roberts, M., Gaskell, E.E., 2014. Formulation and

- antibacterial profiles of clay – ciprofloxacin composites. *Appl. Clay Sci.* 87, 129–135. doi:10.1016/j.clay.2013.10.020
- Healy, B., Freedman, A., 2006. *Infections*. *BMJ* 332, 838–841.
- Itodo, A.U., Itodo, H.U., 2010. Sorption energies estimation using Dubinin-Radushkevich and temkin adsorption isotherms. *Life Sci. J.* 7, 68–76.
- Jung, H., Kim, H.-M., Choy, Y. Bin, Hwang, S.-J., Choy, J.-H., 2008. Itraconazole–Laponite: Kinetics and mechanism of drug release. *Appl. Clay Sci.* 40, 99–107. doi:10.1016/j.clay.2007.09.002
- Kahr, G., Madsen, F.T., 1995. Determination of the cation exchange capacity and the surface area of bentonite, illite and kaolinite by methylene blue adsorption. *Appl. Clay Sci.* 9, 327–336. doi:10.1016/0169-1317(94)00028-O
- Kaufhold, S., Dohrmann, R., 2009. Stability of bentonites in salt solutions | sodium chloride. *Appl. Clay Sci.* 45, 171–177. doi:10.1016/j.clay.2009.04.011
- Komadel, P., 2003. Chemically modified smectites. *Clay Miner.* 38, 127–138. doi:10.1180/0009855033810083
- Lagaly, G., Ziesmer, S., 2003. Colloid chemistry of clay minerals: the coagulation of montmorillonite dispersions. *Adv. Colloid Interface Sci.* 100–102, 105–128. doi:10.1016/S0001-8686(02)00064-7
- Lee, S.Y., Kim, S.J., 2002. Delamination behavior of silicate layers by adsorption of cationic surfactants. *J. Colloid Interface Sci.* 248, 231–8. doi:10.1006/jcis.2002.8222
- Lister, P.D., Wolter, D.J., Hanson, N.D., 2009. Antibacterial-resistant *Pseudomonas aeruginosa*: Clinical impact and complex regulation of chromosomally encoded resistance mechanisms. *Clin. Microbiol. Rev.* 22, 582–610. doi:10.1128/CMR.00040-09
- Mackenzie, F.M., Gould, I.M., 1993. Review The post-antibiotic effect 519–537.
- Madejova, J., 2003. FTIR techniques in clay mineral studies. *Vib. Spectrosc.* 31, 1–10.
- Miranda-Trevino, J.C., Coles, C.A., 2003. Kaolinite properties, structure and influence of metal retention on pH. *Appl. Clay Sci.* 23, 133–139. doi:10.1016/S0169-1317(03)00095-4
- Mongondry, P., Tassin, J.F., Nicolai, T., 2005. Revised state diagram of Laponite dispersions. *J. Colloid Interface Sci.* 283, 397–405. doi:10.1016/j.jcis.2004.09.043
- Pálková, H., Madejová, J., Zimowska, M., Bielańska, E., Olejniczak, Z., Lityńska-Dobrzyńska, L., Serwicka, E.M., 2010. Laponite-derived porous clay heterostructures: I. Synthesis and physicochemical characterization. *Microporous Mesoporous Mater.* 127, 228–236. doi:10.1016/j.micromeso.2009.07.019
- Parfitt, G.D., Rochester, C.H., 1983. Adsorption of Small Molecules, in: *Adsorption from*

Solution at the Solid/Liquid Interface. pp. 3–48.

- Parolo, M.E., Avena, M.J., Pettinari, G., Zajonkovsky, I., Valles, J.M., Baschini, M.T., 2010. Antimicrobial properties of tetracycline and minocycline-montmorillonites. *Appl. Clay Sci.* 49, 194–199. doi:10.1016/j.clay.2010.05.005
- Parolo, M.E., Savini, M.C., Vallés, J.M., Baschini, M.T., Avena, M.J., 2008. Tetracycline adsorption on montmorillonite: pH and ionic strength effects. *Appl. Clay Sci.* 40, 179–186. doi:10.1016/j.clay.2007.08.003
- Phillips, G., Johnson, B.E., Ferguson, J., 1990. The loss of antibiotic activity of ciprofloxacin by photodegradation. *J. Antimicrob. Chemother.* 26, 783–9.
- Prabhakar, M., Krahn, A.D., 2004. Ciprofloxacin-induced acquired long QT syndrome. *Hear. Rhythm* 1, 624–626.
- Puttamat, S., Pavarajarn, V., 2016. Adsorption study for removal of Mn(II) ion in aqueous solution by hydrated ferric(III) oxides. *Int. J. Chem. Eng. Appl.* 7, 239–243. doi:10.18178/ijcea.2016.7.4.581
- Ramsay, J.D.F., 1986. Colloidal Properties of Synthetic Hectorite Clay Dispersions I. Rheology. *J. Colloid Interface Sci.* 109, 441–447.
- Rivera, A., Valdés, L., Jiménez, J., Pérez, I., Lam, A., Altshuler, E., De Ménorval, L.C., Fossum, J.O., Hansen, E.L., Rozynek, Z., 2016. Smectite as ciprofloxacin delivery system: Intercalation and temperature-controlled release properties. *Appl. Clay Sci.* 124–125, 150–156. doi:10.1016/j.clay.2016.02.006
- Roberts, K.D., Sulaiman, R.M., Rybak, M.J., 2015. Dalbavancin and Oritavancin: An Innovative Approach to the Treatment of Gram-Positive Infections. *Pharmacotherapy* 35, 935–948. doi:10.1002/phar.1641
- Roca Jalil, M.E., Baschini, M., Sapag, K., 2015. Influence of pH and antibiotic solubility on the removal of ciprofloxacin from aqueous media using montmorillonite. *Appl. Clay Sci.* 114, 69–76. doi:10.1016/j.clay.2015.05.010
- Sandwell and West Birmingham Hospitals NHS Trust, 2011. Antimicrobial Prescribing Formulary. Birmingham City Hospital, Birmingham (UK), [Internal Document].
- Seaton, R.A., 2009. Skin and soft tissue infection diagnosis and management. *Clin. Pharm.* 1, 13–22.
- Stevens, D.L., 2009. Treatments for skin and soft-tissue and surgical site infections due to MDR Gram-positive bacteria. *J. Infect.* 59 Suppl 1, S32-9. doi:10.1016/S0163-4453(09)60006-2
- The Royal Liverpool and Broadgreen University Hospitals NHS Trust, 2012. Skin and Soft Tissue Infections Prescribing Guidance. Royal Liverpool University Hospital, Liverpool (UK), [Internal Document].
- Thomas, F., Michot, L.J., Vantelon, D., Montarge, E., Pre, B., Cruchaudet, M., Delon, J.F., 1999. Layer charge and electrophoretic mobility of smectites. *Colloids Surfaces A*

- Physicochem. Eng. Asp. 159, 351–358.
- Thompson, D.W., Butterworth, J.T., 1992. The Nature of Laponite and Its Aqueous Dispersions. *J. Colloid Interface Sci.* 151, 236–243.
- Trivedi, P., Vasudevan, D., 2007. Spectroscopic investigation of ciprofloxacin speciation at the goethite-water interface. *Environ. Sci. Technol.* 41, 3153–8.
- Tyagi, B., Chudasama, C.D., Jasra, R. V, 2006. Determination of structural modification in acid activated montmorillonite clay by FT-IR spectroscopy. *Spectrochim. Acta. A. Mol. Biomol. Spectrosc.* 64, 273–8. doi:10.1016/j.saa.2005.07.018
- Unal, S., 2009. Treatment options for skin and soft tissue infections: “oldies but goldies”. *Int. J. Antimicrob. Agents* 34 Suppl 1, S20-3. doi:10.1016/S0924-8579(09)70545-X
- Vance-Bryan, K., Guay, D.R.P., Rotschafer, J.C., 1990. Clinical Pharmacokinetics of Ciprofloxacin. *Clin. Pharmacokinetics* 19, 434–461.
- Varanda, F., de Melo, M.J.P., Caco, A.I., Dohrn, R., Makrydaki, F.A., Voutas, E., Tassios, D., Marrucho, I.M., 2006. Solubility of Antibiotics in Different Solvents . 1 . Hydrochloride Forms of Tetracycline, Moxifloxacin, and Ciprofloxacin. *Ind. Eng. Chem. Res.* 45, 6368–6374.
- Vasudevan, D., Bruland, G.L., Torrance, B.S., Upchurch, V.G., MacKay, A. a., 2009. pH-dependent ciprofloxacin sorption to soils: Interaction mechanisms and soil factors influencing sorption. *Geoderma* 151, 68–76. doi:10.1016/j.geoderma.2009.03.007
- Wang, C.-J., Li, Z., Jiang, W.-T., 2011. Adsorption of ciprofloxacin on 2:1 dioctahedral clay minerals. *Appl. Clay Sci.* 53, 723–728. doi:10.1016/j.clay.2011.06.014
- Wang, C.-J., Li, Z., Jiang, W.-T., Jean, J.-S., Liu, C.-C., 2010. Cation exchange interaction between antibiotic ciprofloxacin and montmorillonite. *J. Hazard. Mater.* 183, 309–14. doi:10.1016/j.jhazmat.2010.07.025
- Wispelwey, B., 2005. Clinical implications of pharmacokinetics and pharmacodynamics of fluoroquinolones. *Clin. Infect. Dis.* 41 Suppl 2, S127-35. doi:10.1086/428053
- Wu, Q., Li, Z., Hong, H., Yin, K., Tie, L., 2010. Adsorption and intercalation of ciprofloxacin on montmorillonite. *Appl. Clay Sci.* 50, 204–211. doi:10.1016/j.clay.2010.08.001
- Yan, W., Hu, S., Jing, C., 2012. Enrofloxacin sorption on smectite clays: effects of pH, cations, and humic acid. *J. Colloid Interface Sci.* 372, 141–7. doi:10.1016/j.jcis.2012.01.016
- Zhao, H., Zhou, C.H., Wu, L.M., Lou, J.Y., Li, N., Yang, H.M., Tong, D.S., Yu, W.H., 2013. Catalytic dehydration of glycerol to acrolein over sulfuric acid-activated montmorillonite catalysts. *Appl. Clay Sci.* 74, 154–162. doi:10.1016/j.clay.2012.09.011



## Chapter 4

# Development and evaluation of antibacterial wound dressing materials

### 4.1. Introduction

Wound care and the treatment of diseases of the skin are well defined disciplines within the NHS in England and patients are often managed by a multidisciplinary team of medics, nurses, and pharmacists, amongst others (Bennett-Marsden, 2010; National Prescribing Centre, 2012). Regardless of the wound dressing section of the British National Formulary being one of the fastest growing sections, there is a noticeable lack of topical products that are able to directly treat bacterial skin and skin structure infections (Davis and Mclister, 2016; Joint Formulary Committee, 2017; Morgan, 2002). Where antibacterial therapy is indicated this is generally in the form of systemic treatments given orally, for mild to moderate infections, or parenterally, for severe infections (Healy and Freedman, 2006; Siddiqui and Bernstein, 2010).

In this chapter the potential of phyllosilicate containing materials for wound care will be explored. However, in order to design a potential wound-care material it is important to understand the pathophysiology of wounds and skins and skin-structure infections alongside the pharmaceuticals and therapeutics of modern wound care products

#### 4.1.1. An overview of wounds, wound healing, and the role of infection

Wounds can be described as breaks or disruptions in the normal skin structure or function. Acute wounds, such as minor incisions and most abrasions, generally require up to 12-weeks for healing to be complete. However, more severe wounds such as pressure sores, vascular and diabetic foot ulcers, deep incisions and chronically infected wounds can take months, sometimes, years to resolve (Boateng et al., 2008; Leaper, 2006; Siddiqui and Bernstein, 2010). While the diameter of a wound may initially indicate the severity, the depth of the wound is an important factor to consider (Grey et al., 2006). Superficial wounds generally involve the epidermis only whereas partial-thickness wounds are the result of damage to both the epidermis and dermis. Full-thickness wounds are much deeper and involve the epidermis, dermis, and sub-dermal layers such as subcutaneous fat, muscle, and even the bone (Boateng et al., 2008; Cockbill, 2002). The time taken to heal will depend on the width and depth of the wound, but will also depend on patient specific factors such as nutrition status and any comorbidities (Cockbill, 2002; Hanna and Giacobelli, 1997).

The process of wound healing is often described over four or five overlapping stages (Boateng et al., 2008). The initial stage, which occurs within seconds of injury, is *haemostasis*. The primary aim of bleeding is to flush debris and microorganisms from the wound and to deliver important components to the wound such as clotting factors and platelets. Exposed collagen activates platelets which in turn trigger a number of subsequent actions. Activated platelets trigger the clotting cascade, which results in the transformation of fibrinogen in the blood to a fibrin mesh that plugs the wound (commonly known as a scab) stopping any further blood loss and protecting the wound

from external influences such as bacteria. This fibrin-rich clot also supports the subsequent stages of wound healing, described below, by providing a scaffold for fibroblasts, keratinocytes, and collagen. As well as initiating the clotting process, activated platelets also release a number of important cytokines that result in the recruitment of fibroblasts, keratinocytes, and neutrophils to the wound and also initiate the process of angiogenesis (Boateng et al., 2008; Hanna and Giacobelli, 1997; Strodtbeck, 2001; Williamson and Harding, 2004).

The next stage of healing, which often happens simultaneously alongside haemostasis, is the *inflammatory phase*. Recruitment of neutrophils to the environment results in further release of cytokines including histamine and serotonin, which results in vasodilation and allows for additional white cells such as monocytes to migrate to the wound. Neutrophils ingest and destroy bacteria until infection has been eradicated, after which the monocytes differentiate into macrophages that destroy dead neutrophils, remove dead cell matter, and release nitric oxide to promote wound healing. Macrophages remain present within the wound for the duration of the healing process, regulating the different processes within the wound bed through the release of cytokines (Boateng et al., 2008; Hanna and Giacobelli, 1997; Strodtbeck, 2001; Williamson and Harding, 2004).

The third and fourth stages of wound healing are often described together but the process of *migration* is often completed before *proliferation*. During *migration* keratinocytes move across the wound surface using the fibrin and fibronectin network of the clot, the wound bed, and each other as a network. Wound exudate is vital

during this process to enable the keratinocytes to move freely across the wound. Dry wound environments cause the keratinocytes to burrow until they find moisture to support this process, which can lead to scarring in later stages of wound healing. Migration of the keratinocytes continues until they meet in the middle and the wound surface is enclosed underneath the clot. Not only does this act to create another barrier to the proliferating wound-bed but it also generates a hypoxic environment, which is key to promoting angiogenesis to support proliferation and healthy wound healing (Boateng et al., 2008; Hanna and Giacomelli, 1997; Strodbeck, 2001; Williamson and Harding, 2004).

Occurring alongside the *migration* of keratinocytes is a stage known as *proliferation*. During this stage, the fibrin network is gradually replaced by hyaluronan and fibronectin, which act as supports for cellular growth, protein structures, and revascularisation. Fibroblasts utilise the hyaluronan and fibronectin scaffold to lay down collagen, which adds additional strength to the wound bed and allows groups of fibroblasts to differentiate into myofibroblasts. These myofibroblasts are able to contract and pull the edges of the wound inwards, which adds further structural support to the proliferating wound bed, reducing the overall size of the wound so that *migration* can be completed more quickly and biochemical requirements are reduced. During this stage of healing the fibroblasts and macrophages continue to release cytokines that support angiogenesis and proliferation of the lymphatic system (Boateng et al., 2008; Cockbill, 2002; Hanna and Giacomelli, 1997; Strodbeck, 2001).

The role of exudate is not limited to easing the migration of keratinocytes but plays an important role in the whole of the wound healing process as it prevents desiccation of new cells; promotes autolysis and debridement of dead tissue; provides compounds necessary for wound healing such as electrolytes, minerals, proteins and saccharides. Wound exudate is also vital for the recruitment of leucocytes into the environment, which play an important role in removing bacteria and other microorganisms from the wound-bed. Excessive exudate, however, can lead to maceration of the surrounding healthy tissue, can disrupt and slow down healing, and also promote growth of microorganisms (Boateng et al., 2008; Strodtbeck, 2001)

The final stage of wound healing is *maturation*, which can begin in different locations of the wound-bed whilst other areas are still undergoing *proliferation*. During the *maturation* phase hyaluronan and fibronectin is gradually replaced with different types of collagen creating the final structural network which are then cross-linked to add more strength to the newly forming tissue. As the necessary dermal and subdermal tissues are laid down and mature the number of macrophages, keratinocytes, fibroblasts and myofibroblasts diminishes through controlled apoptosis. Overall, *maturation* (also known as remodelling) of a wound can take many months or years to finish, depending on the size and depth of the wound (Boateng et al., 2008; Cockbill, 2002; Hanna and Giacobelli, 1997; Strodtbeck, 2001; Williamson and Harding, 2004).

Wound contamination is ubiquitous but does not necessarily lead to an infection (Grey et al., 2006; Healy and Freedman, 2006). A contaminated wound is described as one where microorganisms are present but are not replicating at a significant rate and are

easily eradicated by the immune cells within the wound. Whereas a colonised wound is defined by the presence of microorganisms on a wound surface that are growing and replicating. However, such growth in a colonised wound does not cause damage to the host cells and is therefore not considered to be an infection. Depending on the wound environment, host factors, and the species of microorganism present this colonisation may continue until a stage called critical colonisation is reached, which can lead to infection (Healy and Freedman, 2006; Siddiqui and Bernstein, 2010). This stage is termed critical colonisation because the presence of the microorganisms is such that wound healing is interrupted, exudate production increases and the wound bed and granulating tissue becomes weaker, which can result in tenderness and pain. Further progression of this process and increased microbial bioburden leads to infection, which causes proliferation of the wound-bed to cease and new tissues are damaged, exudate is overproduced and may become purulent, accompanied by increased warmth and swelling of the wound and surrounding tissues (Grey et al., 2006; Healy and Freedman, 2006; Siddiqui and Bernstein, 2010). Research has also shown that bacteria are able to form biofilms within the wound environment, which makes them significantly more difficult for the body to eradicate and also makes the bacteria more inherently resistant to antimicrobial compounds (Kucera et al., 2014; Lister et al., 2009; Malik et al., 2013). This local infection, depending on host and microorganism factors, can progress to systemic bacteraemia, which can result in sepsis and even death (Healy and Freedman, 2006; Siddiqui and Bernstein, 2010).

Contamination and colonisation are common because bacteria and other organisms are translocated from other parts of the body or the environment. Therefore, bacteria

implicated in wound colonisation such as *Staphylococcus aureus*, coagulase negative *Staphylococcus* species (such as *Staphylococcus epidermidis*), *Streptococcus* species, and *Pseudomonas aeruginosa* are commonly found within the natural flora of adjacent tissues. Other bacteria that form part of the human microbiota that can colonise a wound are *Propionibacterium acnes*, *Enterococcus* species, *Enterobacteriaceae* species (such as *Escherichia coli*), and *Acinetobacter* species (Dryden, 2009; Siddiqui and Bernstein, 2010; Török and Conlon, 2005).

Other atypical organisms such as fungi (e.g. *Candida* species), protozoa (e.g. *Leishmania* species), and arthropods (e.g. *Cordylobia anthropophaga*) may cause chronic wound infections, but their incidence is low (Dryden, 2009; Siddiqui and Bernstein, 2010). Bacteria are by far the most commonly implicated organisms within infected wounds and cause an increase in morbidity, reduced quality of life, and contribute to the increasing pressures being placed on the health service (Grey et al., 2006). These issues are all being made worse by the increasing problem of antibacterial resistance, which was introduced in section 1.4.

#### 4.1.2. An overview of wound care products

Modern wound care products have been designed to support healing and also protect the wound-bed from external influences. Moisture control is a key property of dressings, with the aim of ensuring a moist environment for healing is maintained whilst preventing maceration or dehydration. To this end, the materials are able to maintain a barrier to moisture evaporation but also absorb excessive exudate, which contains waste products and autolytic enzymes. Allowing gaseous exchange is

important for managing the moisture of the wound but also allowing oxygenation of the new tissue. However, it is also important for these dressings to be impervious to particles and microorganisms (Davis and Mclister, 2016; Jones et al., 2006; Morgan, 2002; Williams, 1996).

As well as maintaining an optimal environment for the wound, modern dressings provide a number of additional benefits including cushioning or protection from further injury, insulating the wound to protect it from external extremes of temperature whilst also maintaining a warm wound environment complimentary to biological functions. These dressings are designed to have little or no adherence so that they do not cause damage to the delicate wound-bed or the surrounding tissue when removed and changed. In addition to this, the overall design of the dressing should allow for as much time as possible between dressing changes to reduce damage to the wound bed, reduce the chance of contamination, reduce costs, and reduce impact on the patient's quality of life (Jones et al., 2006; Morgan, 2002).

Hydrocolloid dressings are available as gel sheets and films formed from carboxymethylcellulose, gelatine, or pectin. These dressings are adherent in nature and are useful in the management of dry wounds where they are able to adhere to and hydrate the eschar or fibrin clot to promote autolysis and debridement. Hydrocolloids are not useful in heavily exuding wounds as they do not have a large absorptive capacity but they are occasionally used on light to moderately exuding wounds whereby they absorb fluid, which in turn allows for increased gaseous exchange through the dressing. These dressings are sometimes combined with other materials



such as foams or alginates to increase their absorptive capacity (Boateng et al., 2008; Hanna and Giacobelli, 1997; Jones et al., 2006; Morgan, 2002).

Alginate dressings are generally formed from the sodium and calcium salts of alginic acid, which is a natural polymer made from guluronic and mannuronic acid. Alginates are able to absorb large quantities of water and readily form hydrogels when in contact with suppurating wounds. Calcium within the wound and the dressings is able to cross-link the polymer chains, notably between guluronic acid rich regions (G-G blocks), which stabilises the polymer matrix and generates pores within which exudate can be held, leading to the generation of a hydrogel (Gacesa, 1988). Dressings rich in mannuronic acid will form soft gels whereas those richer in guluronic acid will form firmer gels, which are much better at supporting cavitation wounds. This ability to absorb large amounts of exudate means alginates should not be used on dry wounds, but are more useful in low, moderate and highly exuding wounds. The alginic acid polymers are also thought to bring additional benefits to the wound environment and have been found to benefit wound inflammation, encourage fibroblast proliferation, and even activate macrophages (Boateng et al., 2008; Hanna and Giacobelli, 1997; Jones et al., 2006; Morgan, 2002).

Dressings that are readily available with high water content are the hydrogels, which are amorphous gels typically formed from a cross-linked polymer matrix of poly(methacrylate) or poly(vinylpyrrolidone). As with the alginates the matrices of hydrogel dressings trap large amounts of fluid so that approximately 70-90% of their mass is water. These hydrogel dressings are useful for dry wounds as they promote

hydration, autolysis and debridement. However, due to their ability to donate moisture to the wound these dressings are not suitable for suppurating wounds and should not be placed on infected wounds, where they can promote growth (Boateng et al., 2008; Hanna and Giacomelli, 1997; Jones et al., 2006; Morgan, 2002).

Semi-permeable films are useful for shallow wounds and when dressings are required in anatomical flexures such as elbows. Often formulated from nylon or polyurethane these semi-permeable films are able to control gaseous exchange into the wound with some being utilised for their ability to occlude the wound, create a hypoxic environment, and thus stimulate angiogenesis. However, their chemistry and formulation means they are poor at absorbing exudate so are not suitable for moderately or highly exuding wounds as they cause fluid accumulation that can cause tissue maceration and promote infection. As such, semi permeable films are often used in combination with other materials such as hydrocolloids or foam-dressings (Boateng et al., 2008; Jones et al., 2006; Morgan, 2002).

The final major classification of modern wound dressings is the foams; typically formulated from polyurethane. The thickness and porosity of these foams controls the amount of exudate they are able to draw up and hold onto, and also dictates their ability to protect the wounds and regulate gaseous transfer. Modifying the internal structure of these materials allows polyurethane foams to be used on a wide range of wounds including dry and heavily exuding. However, the foams can be adherent so often have an additional film layer that is in contact with the wound to reduce

adherence. Some foams are also co-formulated with a film backing to reduce fluid loss (Boateng et al., 2008; Jones et al., 2006; Morgan, 2002).

#### *4.1.3. Polymer-phyllsilicate composites as potential materials for wound care*

Wound healing is a complex process and commercially available dressings are designed to support that process but no single dressing is able to cover all eventualities (Jones et al., 2006). A review by Gaskell and Hamilton (2014) discusses research regarding the development and evaluation of phyllosilicate-polymer composites for wound care applications, which is an emerging field and somewhat understudied compared to phyllosilicate-polymer research for other industries.

The combination of phyllosilicates and polymers into composites has been found to create materials with beneficial characteristics from both the constituents and as such the resultant properties are reliant on the chemistry of the individual phyllosilicate and polymer as well as their interaction mechanism, any polymeric cross linking, and the overall method of composite formation (solution, melt extrusion, or electrospinning for example) (Gao, 2004; Ray and Okamoto, 2003). By use of techniques such as X-ray diffraction (XRD), Fourier-transform infrared spectroscopy (FTIR), and transmission electron microscopy (TEM) it is possible to characterise the internal structure of these composite materials to determine whether they are nanocomposites or microcomposites (Alboofetileh et al., 2013; Wang and Rhim, 2015). Microcomposites form when the phyllosilicate layers do not separate and the polymer arranges itself around the clay-mineral particles, which effectively act as filler within the polymer matrix (figure 4.1 A) (Theng, 2012). Nanocomposites form when the phyllosilicate

layers separate and the polymer can infiltrate the laminar space. In intercalated nanocomposites the clay mineral layers remain associated to each other with polymeric chains within the interlayer space (figure 4.1 B). In exfoliated nanocomposites the clay mineral layers disassociate from each other and become uniformly dispersed throughout the polymeric matrix either in an ordered (figure 4.1 C) or disordered fashion (figure 4.1 D) (Theng, 2012).

A number of different phyllosilicate-polymer combinations have been studied for wound care applications. Montmorillonite and Laponite<sup>®</sup> have been widely studied for their ability to disperse in water and expose a high specific surface with which it can interact with polymers (Bandeira et al., 2012; Gaharwar et al., 2011b, 2010; Joshi et al., 2010; Paul and Robeson, 2008; Sandri et al., 2016; Viseras et al., 2008). Palygorskite, a 2:1 fibrous phyllosilicate, has been utilised for its ability to entangle with itself and polymer chains to form cross-linked matrices (Ruiz-Hitzky et al., 2013).

Laponites<sup>®</sup> have been shown to produce nanocomposite materials with improved strength, increased elasticity, and greater swelling potential (Ghadiri et al., 2013; Shikinaka et al., 2012). A number of synthetic polymers such as polyvinyl alcohol (Ip et al., 2011; Kokabi et al., 2007), polyethylene oxide (Gaharwar et al., 2012, 2011a, 2011b; Schexnailder et al., 2010; Su and Shen, 2009), polyacrylamide (Li et al., 2009), polyethylene glycol (Shikinaka et al., 2012), and polyurethanes (LeBaron et al., 1999; Ray and Okamoto, 2003) amongst others have been utilised in research to develop useful composites. However, significant interest has been paid to the naturally occurring polymers such as chitosan for its low toxicity, biocompatibility, and inherent

antimicrobial properties (Aguzzi et al., 2013, 2010; Han et al., 2010; Salcedo et al., 2013); and alginate for its biocompatibility, current use in wound care products, and its high swelling potential (Bandeira et al., 2012; Darder et al., 2016; Ghadiri et al., 2013; Gonçalves et al., 2013a; Kaygusuz and Erim, 2013).

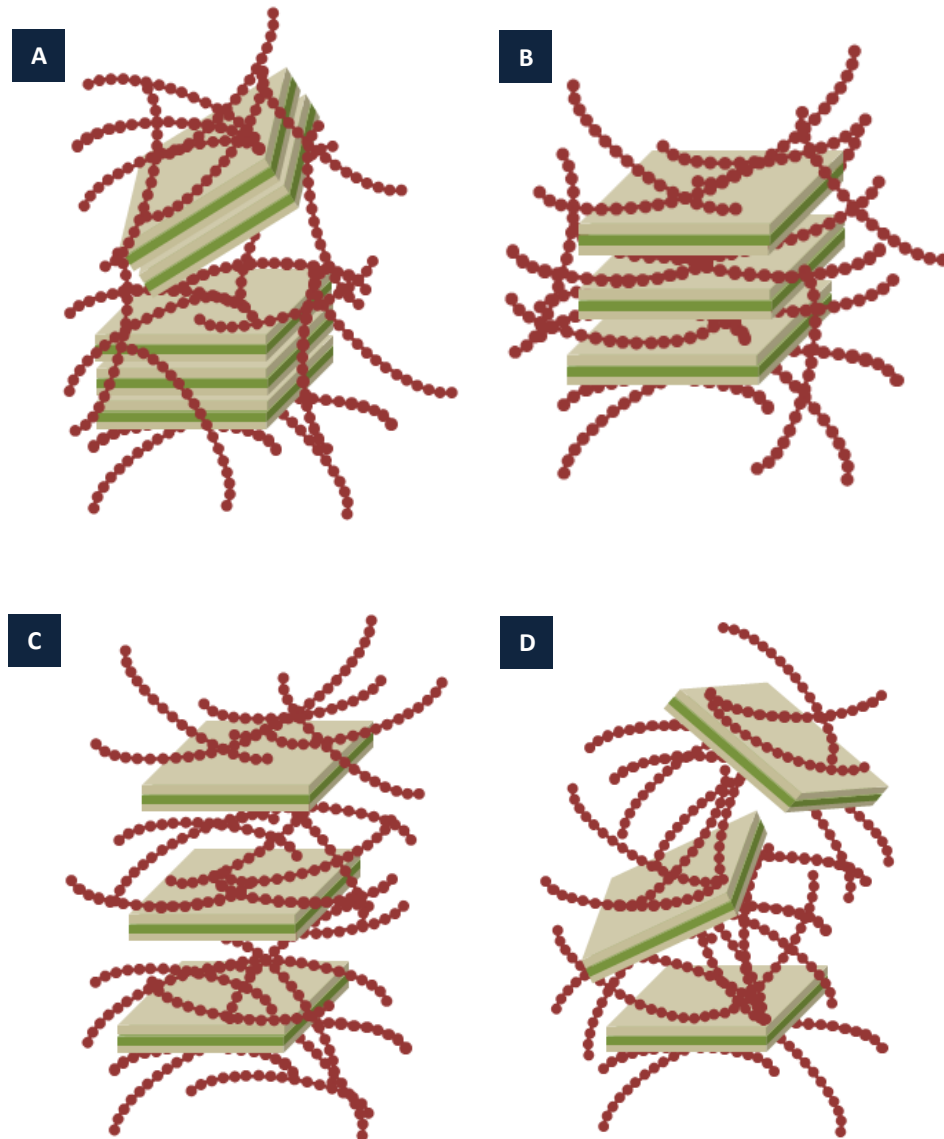


**Figure 4.1.** Artistic representation of 2:1 phyllosilicates (brown and green plates) interacting with polymers (red chains where individual circles indicate monomers) to form microcomposites (a), intercalated nanocomposites (b), ordered exfoliated nanocomposites (c), and disordered exfoliated nanocomposites (d).

#### *4.1.4. Development and evaluation of novel polymer-phyllsilicate composites for wound care applications*

There is a notable lack of products available commercially that directly manage wound infections. However, increasing interest is being paid to the utilisation of polymer-phyllsilicate composites as materials for delivering compounds that will actively manage infected wounds such as the inclusion of antimicrobial drug molecules including tetracycline (Qi et al., 2013), ofloxacin (Hua et al., 2010), and chlorhexidine (Ambrogi et al., 2016). A number of teams have also investigated the inclusion of silver (Aguzzi et al., 2013) and copper (Das et al., 2014) ions as antimicrobial agents within these composites. The overarching aim of this research project is to produce a wound-care product that can support wound healing and also treat infections directly at the source – thus reducing the need for systemic antimicrobial therapy (see section 1.4).

The research presented here takes the knowledge developed in chapter 2 and applied in chapter 3 to design novel composite films and foams that can be further developed into candidate wound dressing materials. Kaolin (KN), montmorillonite-K10 (MMTK10) and Laponite® XL21 (LXL21) were selected based on their differing physicochemical properties. Laponite® XL21 was chosen over Laponite® RD because the latter has a tendency to buffer towards pH 9, which would not be acceptable for a wound environment. Alginate was utilised as the polymeric compound within the composites due to its ability to interact with clay minerals to form composite materials with improved properties (Alboofetileh et al., 2013; Pongjanyakul and Suksri, 2010) that could be beneficial for wound healing. The drug molecule of choice was ciprofloxacin as it has significant activity against common wound pathogens and is also able to

successfully absorb and desorb from the clay-mineral surface (as described in chapter 3).

These composite films and foams were characterised through qualitative and quantitative methods to determine certain mechanical and aesthetic properties, such as flexibility and transparency. Their ability to support healing of an infected wound was evaluated by determining water vapour transmission rate, behaviour in a wound environment, drug release, antimicrobial properties, and keratinocyte viability. Alongside this FTIR, XRD and thermogravimetric analysis (TGA) were used to determine the structure of the composite films and foams, and identify any interactions taking place between the individual components.

## 4.2. Materials and methods

### 4.2.1. Materials

Kaolin (KN) was obtained from Fischer (UK) Montmorillonite K-10 (MMTK10) was obtained from Acros (UK) and Laponite<sup>®</sup> XL21 (LXL21) was obtained from BYK Additives (UK). Sodium alginate powder was obtained (Sigma Aldrich, UK) as a low viscosity alginate (LVAIg, 4-12 cp 1% in water), a moderately viscous alginate (MVAIg, 15-25 cp 1% in water), and a high viscosity alginate (HVAIg, >2000 cp 2% in water). The commercially available wound dressing products Kaltostat<sup>®</sup> (ConvaTec Ltd, UK), Lyofoam<sup>®</sup> (Molnlycke Health Care Ltd, UK) and Opsite<sup>®</sup> (Smith and Nephew Healthcare Ltd, UK) were donated by Royal Liverpool and Broadgreen University Hospitals Trust.

### 4.2.2. Formulation of candidate composites

#### 4.2.2.1. Pre-formulation studies

In order to screen a wide range of excipient combinations a process of pre-formulation was devised. Throughout the pre-formulation studies 1 g of clay mineral was used, whilst the proportion and type of alginate was modified. The proportions of alginate tested against set amounts of clay mineral were 0.25 g, 0.5 g, 1 g, 2 g, and 4 g of LVAIg or MVAIg; or 0.1 g, 0.25 g, 0.5 g, 1 g, and 2 g of HVAIg. The general methodology for obtaining the composite formulations was as follows.

One gram of clay mineral was dispersed in 100 mL deionised water for two hours allowing swelling to complete. Alongside this, varying concentrations of alginate (indicated above) were swollen in 50 mL deionised water for two hours then placed in a sonic bath for 15 minutes to disperse larger air bubbles. The clay mineral dispersion



was then stirred at 7000 rpm and the alginate solution slowly added to this in a steady, fine, stream. Once all the alginate was added the stirring was reduced to 2000 rpm allowing the mixture to become homogenous over a period of 30 minutes.

After this time period 40 mL of mixture was poured into 80 mm diameter plastic casting dishes (petri dishes). Films were formed by placing the casting dish, uncovered, into a fan-oven set to 40 °C for 24 hours. Foam materials were formed by freezing the covered casting dish at -20 °C for 12 hours then drying by lyophilisation (Heto FD 2.5 at -50 °C for 72 hours). Each composite formulation was repeated in triplicate and assessed as per section 4.2.3.

#### *4.2.2.2. Development of candidate films*

The effect of the drying method was investigated by comparing drying in a fan assisted oven at 40 °C for 24 hours to drying in a vacuum oven at 40 °C for 24 hours and drying on bench-top at room temperature. Glycerol (225 mg (approximately 0.2 mL) to 2250 mg (approximately 2 mL)) or polyvinyl alcohol (PVA) (150 mg to 1500 mg) were utilised as additives. These were added at the same time as the alginate solutions. The composite films were repeated in triplicate and assessed as per section 4.2.3.

#### *4.2.2.3. Formulation of ciprofloxacin-containing composite films*

One gram of LXL21 was dispersed in 80 mL of deionised water at 2000 rpm using a magnetic stirrer. After 2 hours the LXL21 dispersion was adjusted to pH 7.4 with dilute HCl and a 20 mL solution containing 20 mg, 130 mg or 160 mg CIP (representing loading below, at, and above monolayer formation as described in section 3.3) was

added and the pH re-adjusted to 7.4 if necessary. This dispersion was protected from light and mixed for a further 1 hour to allow CIP adsorption onto LXL21.

Two grams of MVA<sub>lg</sub> was dispersed in 50 mL deionised water and allowed to swell over three hours after which time bubbles were removed by a sonic bath over 15 minutes. Stirring of the LXL21-CIP dispersion, via magnetic stirrer, was increased to 7000 rpm and the alginate solution added slowly as a fine stream along with 2.25 g glycerol. Once a homogenous mixture was achieved stirring was reduced to 2000 rpm for 30 minutes.

Forty millilitres of the formulation mixture was poured into a plastic casting dish (80 mm diameter) and dried uncovered at 40 °C in a fan oven for 24 hours. This was undertaken in triplicate to determine reproducibility. To prevent moisture being adsorbed by the foams they were stored in a sealed desiccator containing silica gel impregnated with a blue indicator (CoCl<sub>2</sub>). These composite films were repeated in triplicate and assessed as per section 4.2.3.

#### *4.2.2.4. Development of candidate foams*

Once promising composite foams had been identified, glycerol (225 to 2250 mg), CaCl (1 mL 0.1 M to 1 mL 1.0 M), NaCl (1 mL 0.1 M to 1 mL 1.0 M), PVA (150 to 1500mg), and absolute ethanol (0.2 to 2 mL) were each tested as additives. These additives were added to the clay mineral dispersion at the same time as the alginate solution.

The effect of the freezing process on the final material obtained was also investigated to hasten ice formation, and reduce crystal size. Freezing of the formulations at  $-20^{\circ}\text{C}$  over 12-hours was compared to freezing at  $-80^{\circ}\text{C}$  over 12-hours and flash freezing in liquid nitrogen. For the liquid nitrogen method, sealed casting dishes wrapped in film were completely submerged for 5 to 20 minutes (to determine minimum time required), then placed into a  $-20^{\circ}\text{C}$  freezer for 12 hours. All the frozen samples were dried in the freeze drier as described above (section 4.2.2.1) over a period of 72 hours. The composite foams were repeated in triplicate and assessed as per section 4.2.3.

#### *4.2.2.5. Formulation of ciprofloxacin-containing composite foams*

One gram of LXL21 was dispersed in 80 mL of deionised water at 2000 rpm using a magnetic stirrer. After 2 hours the LXL21 dispersion was adjusted to pH 7.4 with dilute HCl and a 20 mL solution containing 20mg, 130mg and 160mg CIP (representing loading below, at, and above monolayer formation) added then pH re-adjusted to 7.4 if necessary. This dispersion was protected from light and mixed for a further 1 hour to allow CIP adsorption onto LXL21.

Four grams of LVAI<sub>g</sub> was dispersed in 50 mL deionised water and allowed to swell over three hours after which bubbles were removed by a sonic bath over 15 minutes. Stirring of the LXL21-CIP dispersion, via magnetic stirrer, was increased to 7000 rpm and the alginate solution added slowly as a fine stream along with 560 mg glycerol. Once a homogenous mixture was obtained stirring was reduced to 2000 rpm for 30 minutes.

Forty millilitres of formulation mixture was poured into each casting dish (80 mm diameter), the lid placed on and dish wrapped tightly in cling film before submersion into a liquid nitrogen bath for 15 minutes. The lids were removed from the frozen samples and covered with laboratory film (Parafilm®). After being stored in a -20 °C freezer overnight the film covers were pierced and the mixtures dried in a freeze dryer for 72 hours. To prevent moisture being adsorbed by the foams they were stored in a sealed desiccator containing silica gel impregnated with a blue indicator (CoCl<sub>2</sub>). The composite foams were repeated in triplicate and assessed as per section 4.2.3.

#### *4.2.3. Qualitative analysis of composite materials*

Visually, the samples were described in terms of colour and structural integrity. Manually, the materials were described in terms of flexibility, robustness, and texture. This was done by one researcher (Ryan Hamilton) to allow for consistent qualitative assessment of the visual and malleable properties.

Each composite material that showed promise was reviewed by a tissue viability nurse (Royal Liverpool and Broadgreen University Hospitals NHS Trust, Liverpool, UK) to qualitatively assess and confirm the desired physical properties (strength, flexibility, and texture for example) through manual manipulation and to grade the visual appeal (described in terms of colour, transparency, and defects for example). The opinions and insights of the tissue viability nurses were pivotal in determining the final formulation for the CIP-containing composites.

#### 4.2.4. *Optical properties of film formulations*

The opacity of the film formulations was assessed with UV-visible spectrophotometry (Perkin Elmer Lambda 25 UV-Vis Spectrometer). Each film was cut into rectangles of appropriate size to fit into the sample compartment, which was adapted with a smaller sample cell-holder that held each film vertically. An empty compartment acted as the reference while samples were scanned in triplicate between 200 and 800 nm at a rate of 240 nm/min. The absorbance at 600 nm and the thickness (measured by digital callipers, WorkZone, UK) of the sample was used to determine the opacity of each film using equation 4.1, as described by Tunç and Duman (2010).

Equation 4.1

$$Opacity = \frac{Abs_{600}}{X}$$

Where  $Abs_{600}$  is the absorbance measured at 600 nm and  $X$  is the thickness of the film (mm).

Foam formulations were not studied as they were opaque and could not be held within the spectrophotometer.

#### 4.2.5. *Semi-quantitative analysis of the mechanical strength of foam materials*

To differentiate between the physical strength of foam nanocomposites a tablet friabilator (Pharma Test model PTFR-A) was utilised as per European Pharmacopoeia standard method 2.9.7 (British Pharmacopoeia Commission, 2016). Ten samples of

each composite foam, approximately 10 x 10 mm in size, were placed into a Perspex drum which was rotated 100 times at a rate of 25 revolutions per minute. The total and average mass for each sample were obtained before and after testing, allowing the percentage mass loss to be calculated. The threshold for tablets failing the friability test is 1% mass loss. This could not be applied here so the percentage mass loss of Lyofoam® and Kaltostat® were used as reference values to which the nanocomposite foams were compared.

#### *4.2.6. FTIR analysis of films and foam formulations*

Fourier-Transform Infrared (FT-IR) analysis was undertaken on a Perkin Elmer Spectrum BX FT-IR spectrometer with a Pike MIRacle ATR attachment. Thirty-two scans were undertaken between 4000-500  $\text{cm}^{-1}$  with an interval of 1.0  $\text{cm}^{-1}$  and a resolution of 2.0.

#### *4.2.7. XRD analysis of films and foam formulations*

Samples were scanned between 3 and 20 deg  $2\theta$  using a Rigaku miniflex with a  $\text{CuK}\alpha 1$  radiation source. Each sample was scanned five times and the individual scans combined to reduce baseline noise and clarify diffractions. Samples were clipped into place, utilising the baseplate clips, to prevent movement during sample tilting. Foam samples required gentle compression before being clipped into place. The interlayer spacing of each sample was calculated from the  $d_{001}$  peak using the internal Rigaku miniflex analysis software.

#### *4.2.8. Thermal analysis of films and foam formulations*

Thermogravimetric analysis (TGA) was undertaken on a TA Instruments TGA Q50. Approximate 10 mg of sample (films, foams, and controls) was weighed into the open platinum crucible and analysis conducted under a flowing nitrogen atmosphere (60 mL/min). Temperatures were increased from room temperature to 800 °C at a rate of 20 °C/min. Analyses were run in triplicate and percentage weight loss determined.

#### *4.2.9. Water vapour permeability of film and foam formulations*

The water vapour transmission rate (WVTR) was measured by adapting the European Pharmacopoeia method described by Kokabi et al. (2007). Thirty-millilitre glass sample bottles (Supelco) were filled with 25 mL deionised water (100% relative humidity) and each film and foam sample was cut to fit over the mouth of each sample bottle. Screw-top caps with 14 mm diameter aperture were affixed onto the top of each bottle to secure the sample, create an air tight seal, and standardise the area (153.94 mm<sup>2</sup>) for vapour exchange.

Sample bottles complete with cap and sample were weighed before being sealed into a desiccator containing a solution of concentrated magnesium chloride, creating a relative humidity of 32% (Wadso et al., 2009). Desiccator chambers were held at a steady temperature of 37 °C in fan assisted ovens. The sample bottles complete with cap and sample were weighed after 24 hours of gaseous exchange. Each sample was repeated in triplicate and the WVTR for each sample was calculated using equation 4.2.

Equation 4.2

$$WVTR (g/m^2/h) = \frac{W_i - W_f}{24 \times A} \times 10^6$$

Where  $W_i$  is the weight of the unit (bottle, water, sample and cap) before placing in the desiccator,  $W_f$  is the weight of the unit after 24 hours, and  $A$  is the area for vapour exchange ( $mm^2$ ).

#### *4.2.10. Behaviour of film and foam formulations in a synthetic wound environment*

The behaviour of film and foam nanocomposites was determined through a synthetic wound model. Bacteriological Agar (Agar N<sup>o</sup> 3, Oxoid, Thermo Scientific) was prepared to a concentration of 0.5% w/v in a solution 0.02 M  $CaCl_2 \cdot 2H_2O$ , 0.4 M NaCl, 0.08 M Trizma base as a synthetic wound fluid (SWF)(Lindsay et al., 2010; Momoh et al., 2015). Bovine serum albumin (BSA) was omitted from the wound model as it denatured during the autoclaving process. The utilisation of bacteriological agar rather than gelatine (Matthews et al., 2005; Ng and Jumaat, 2014) also allowed for the synthetic wound environment to be autoclaved and remain sterile for the 96 hour experiment period.

After autoclaving, 200 mL of the molten agar-SWF was poured into square 245 x 245 mm bioassay dishes (Sigma Aldrich, UK) and allowed to cool and set. This was undertaken within an isolator unit so the bioassay dishes could be left partially open to



allow water vapour to escape, thus reducing condensation within the bioassay dish and also avoiding contamination during the pouring and cooling process.

The resulting gel was soft and moist so as to represent a suppurating wound for testing the fluid absorptive capacity of each nanocomposite (section 4.2.10.1). The gel was also of sufficient strength to allow the bioassay dishes to stand vertically for adhesion studies (section 4.2.10.2).

#### *4.2.10.1. Swelling behaviour of formulations on the synthetic wound surface*

Swelling studies were undertaken on horizontal bioassay dishes so that the effects of gravity did not interfere with the movement of fluid on the synthetic wound surface. Samples were cut to 10 x 10 mm squares; measured accurately with digital callipers. Each sample was weighed before being placed on the synthetic wound surface and pressed down gently to ensure optimal contact. Each sample was repeated in triplicate.

Swelling was allowed to take place over a 96 hour period after which each sample was measured in four positions with digital callipers and the percentage change in length and width calculated. Swollen samples were removed from the surface of the synthetic wound environment, blotted with filter paper to remove excess surface water then weighed to determine the change in mass. Hydration degree (Gaharwar et al., 2010), also termed swelling ratio (Ghadiri et al., 2013), was calculated using equation 4.3.

Equation 4.3

$$\text{Hydration Degree} = \frac{M_{\text{wet}} - M_{\text{init}}}{M_{\text{init}}} \times 100$$

Where  $M_{\text{wet}}$  is the weight (mg) of the wet formulation (after 96 hrs of swelling) and  $M_{\text{init}}$  is the initial weight (mg) of the formulation before placing on the wound surface.

#### 4.2.10.2. Adherence of formulations to the wound surface

A horizontal line was drawn onto the external surface of the base of the bioassay dish at a distance of 45 mm from the top. Samples of foams and films (repeated in triplicate) were cut to 10 x 10 mm in size and placed along the top of the horizontal line in triplicate. Each sample was manually gently pressed onto the synthetic wound surface to ensure optimal contact before the bioassay dish was positioned vertically to test the adherence of each sample. After 24 and 96 hours the distance travelled by each sample was accurately measured using digital callipers and a ruler.

#### 4.2.11. Ciprofloxacin-release profiles from film and foam formulations

Synthetic wound fluid (SWF), as described by Lindsay et al. (2010), was prepared using 0.02 M  $\text{CaCl}_2 \cdot 2\text{H}_2\text{O}$ , 0.4 M NaCl, 0.08 M Trizma base [tris (hydroxymethyl) aminomethane], and 2% w/v bovine serum albumin (BSA) in deionised water. One hundred millilitres of this SWF was added to a two-necked round bottom flask and stirred at 200 rpm to ensure minimal damage to the materials added to the system, but also to allow adequate agitation and mixing of the SWF. A temperature of 37 °C was used to mimic that experienced at the wound surface.

Once the temperature was stable, 100 mg of each film and foam sample was added to the SWF. The release of CIP from these composite materials was compared against desorption and release of CIP from a high-load (627.11 mg/g) LXL21-CIP composite, generated as per chapter 3, to clearly distinguish between the different phases of drug elution from clay-mineral drug composites (Iliescu et al., 2013; Jung et al., 2008; Viseras et al., 2010).

At defined time points, 1 mL of release medium was removed and passed through a 0.2 µm filter to remove any particulate matter. To maintain sink conditions 1 mL of fresh SWF was returned to the release studies. Sampling continued for 24-hours as this is the minimum amount of time a wound dressing would remain in place clinically.

Alongside the samples, standards containing increasing concentrations of CIP in SWF were used to allow semi-quantitative analysis of the CIP content in the actual samples. CIP concentrations were measured on an Agilent® 1200 HPLC system fitted with a UV-Vis diode array detector set at 278 (±8) nm and 227 (±8) nm. The mobile phase was 2% acetic acid (AAC) and 100% acetonitrile (ACN) with a flow rate of 1 mL/min. The sample injection size was 10 µL into a gradient that commenced at 90:10 and finished at 10:90 AAC:ACN over ten minutes, with a 5 minute post-run programme returning to the starting point. A 10 mm guard column (Crawford Scientific ODS-L 5 micron optimal, 20 x 4.6 mm, 5 µm) was fitted prior to the 150 x 4.6 mm internal diameter C13 OD-OES 5 µm column (Crawford Scientific). The guard column was flushed overnight with a reverse flow of switching gradients of 100% H<sub>2</sub>O and 0% ACN to 0% H<sub>2</sub>O and 100% ACN.

Peak areas (mAU) were determined using the built-in integration software (OpenLAB CDS Chemstation Edition) allowing the amount of CIP in the samples to be determined. The release studies were undertaken in triplicate.

#### *4.2.12. Antimicrobial properties of film and foam formulations*

Preparation of growth media and bacterial cultures was similar to those outlined in chapters 2 and 3. As previously, *S. epidermidis*, *P. acnes*, and *P. aeruginosa* were utilised as common pathogens in skin and skin-structure infections (SSSI) and infected wounds. The preparation of inoculated agar for pour plates and also spread plates for CFU counts were undertaken in the same way as previously described in section 2.2.4.

Discs (5 mm diameter) of each candidate wound dressing material were formed using a cork-borer and placed onto the surface of the inoculated agar using aseptic technique. Each sample was tested in triplicate. The plates were incubated in their respective environments for 24 – 48 hours at 37 °C. After adequate growth, the zones of inhibition were measured in five positions using digital callipers and the CFU/mL was determined by colony counting the spread plates.

#### *4.2.13. Cytotoxicity (keratinocyte cell viability) studies of film and foam formulations*

Cell viability in the presence of composite materials was measured using an adapted colorimetric MTT (3-(4,5-dimethylthiazol-2-yl)-2,5-diphenyl tetrazolium bromide) assay (Mosmann, 1983). A keratinocyte cell line (HaCaT) was obtained at fiftieth passage (P50) and cultured (37 °C in 95% humidity and 5% CO<sub>2</sub>) in 75 cm<sup>2</sup> flasks in Dulbecco's

Modified Eagle Medium (DMEM) enriched with 10% foetal calf serum (FCS). Once confluent growth was confirmed through light stage microscopy the cultures were passaged using the method below until P53 was obtained.

A single flask of cells was washed with 15 mL phosphate buffered saline (PBS) then treated with 1.5 mL ethylene-diamine-tetraacetic acid (EDTA) 0.1 mM for 10 minutes at 37 °C. Then 1.5 mL 1% trypsin was added and incubated for a further 3 minutes so that the cells could be dispersed in 13 mL complete DMEM. One millilitre of this cell dispersion was transferred into cell culturing flasks (75 cm<sup>2</sup> for passage, 25 cm<sup>2</sup> for experimentation) and incubated (37 °C in 95% humidity and 5% CO<sub>2</sub>) until the desired confluence was reached. These flasks were incubated until the cells had adhered to the flask surface and a confluence of approximately 40% was achieved.

Samples of film and foam formulations (mass approximately 2 mg) were placed in the flasks with 1 mL of PBS. Standards consisted of the constituents of the film and foam dressings and were weighed out to be the same mass as would be expected in 2 mg of film or foam. Many of these standards were powders or viscous liquids so the 1 mL PBS was used to disperse the standards before being pipetted into the cell culture flasks. Control flasks were set up, to which 1 mL PBS was added without any further treatment. All flasks were incubated at 37 °C for 24 hours and the entire process repeated in triplicate.

Once the treatment period was completed the culture medium and treatments were removed via vacuum and the flasks gently washed with PBS to remove any residual

treatment material. The cells were then treated with DMEM solution containing 0.5 mg/mL MTT and incubated for 2 hours at 37 °C, after which the MTT solution was removed by vacuum and the HaCaT cells lysed with 500 µL isopropanol. Cell debris was removed from the solution by centrifugation at 13,000 rpm.

Three 100 µL aliquots of each of test solution was placed into the wells of a 96-well ELISA plate (each sample was repeated in triplicate). Standards of 100 µL isopropanol were used as the background absorbance. The plates were read on a UV-Vis plate reader (CLARIO Star Microplate reader, BMG Labtech, UK) between 540 and 590 nm, with  $\lambda_{\text{max}}$  observed at 570 nm. Absorbance readings for the control flasks were assumed to represent 100% viability, with the relative viability of cells in the test flasks calculated by comparing the absorbance of the test solutions to that of the control flasks.

#### *4.2.14. Statistical Analysis*

All data was inputted into Microsoft® Excel® for analysis and generation of graphs.

Mean averages and standard deviations were calculated using the standard functionality within Excel®. Statistical significance was calculated by paired t-tests (no difference assumed) using the Excel® data analysis extensions available from Microsoft®.

### **4.3. Results and discussion**

#### *4.3.1. Evaluation and selection of an ideal film formulation*

##### *4.3.1.1. Qualitative analysis of pre-formulation film materials*

Qualitative analysis of the film materials was undertaken to determine their suitability as wound dressings in terms of texture, strength, and flexibility. It is important that film dressings are smooth and flexible, to prevent damage to the wound bed and support the migratory phase of healing, and also conform to the movement of the body, especially in anatomical flexures (Boateng et al., 2008; Morgan, 2002). It is also ideal that film dressings are transparent to allow the wound to be observed without the need to remove the dressing (Jones et al., 2006; Powers et al., 2016). The qualitative analyses below describe the appearance, texture, strength and flexibility of the different formulations. Collaboration with tissue viability nurses at the Liverpool and Broadgreen University Hospitals NHS Trust allowed these interpretations to be validated and also enabled relevant health professionals to inform the future direction of this research.

When using the clay minerals alone no films were produced, only aggregates of dried solid clay mineral that adhered to the surface of the casting dish. Conversely, films obtained when casting the alginates with no clay minerals present were thin, transparent and smooth. However, they were not flexible enough as they cracked and fractured when bent beyond 90° angles (see figure 4.2 A).

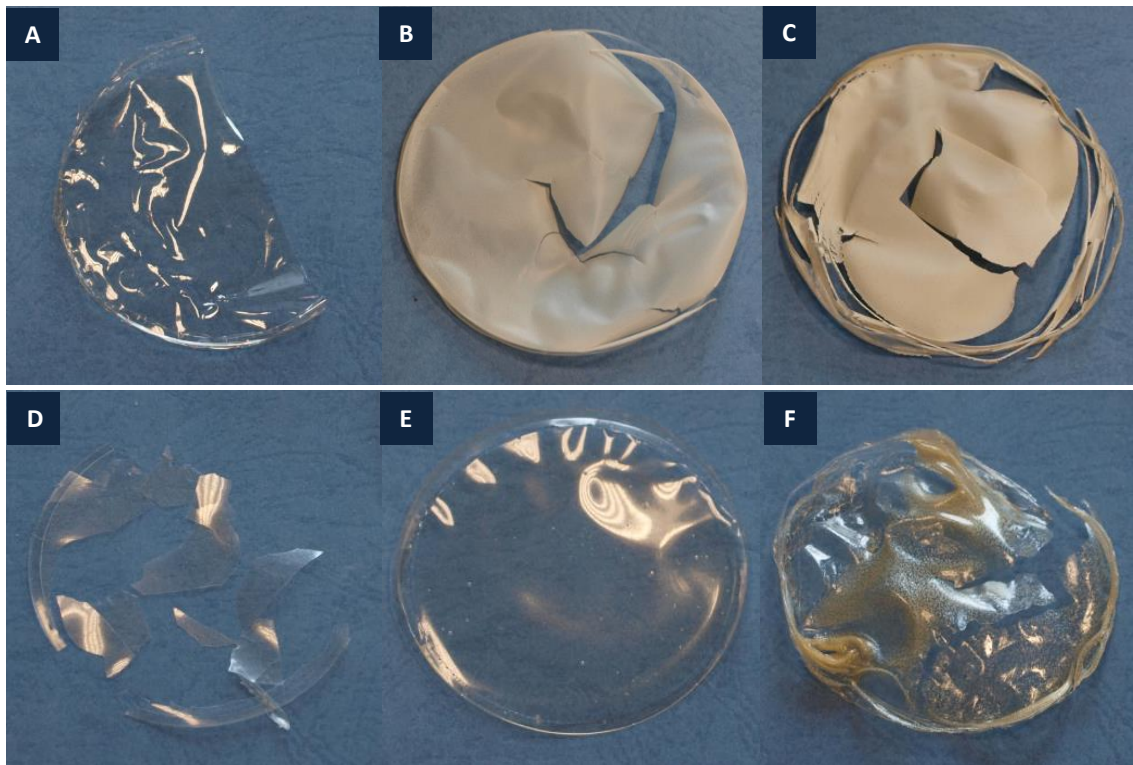


**Figure 4.2.** Films formed from (A) 1 g HVAIg, (B) 1 g KN and 1 g HVAIg, (C) 1 g MMTK10 and 1 g HVAIg, (D) 1 g LXL21 and 0.1 g HVAIg, (E) 1 g LXL21 and 1 g HVAIg, and (F) 1 g LXL21 and 2 g HVAIg.

The appearance and properties of the clay-alginate composite films was affected by both the type of clay-mineral used and the amount and type of alginate utilised. Visual appearance of the films correlated well with the appearance of the clay mineral dispersions, in that KN containing films were off-white and opaque (figure 4.2 B), MMTK10 were light-brown and opaque (figure 4.2 C), whilst films containing LXL21 were transparent (figure 4.2 E).

Composites containing KN did not produce acceptable films. Separation of the components was apparent by a smooth, shiny upper surface and a matte, rough underside. This indicated that KN was unable to form interactions with the alginate polymer, allowing natural sedimentation of KN to the bottom of the casting dish during



the drying process. This resulted in films that flaked or were brittle, and broke easily under gentle manual manipulation (figure 4.2 B).

Films made with MMTK10 and alginates were brittle and broke easily, and phase separation was common with the low and medium viscosity alginate containing formulations. This is likely due to a lack of interaction between the MMTK10 layers and the alginate polymer, which may be attributable to the acid activation process (Section 1.3.1). Cracking and splitting of the main film, and fraying of the edges, were common with these formulations (see figure 4.2 C) and could be caused by the acidic nature of MMTK10. Highly acidic environments are known to cause alginate to convert to insoluble alginic acid (Qin, 2008) and this may have prevented it from forming complete films.

Films formed with LXL21 were clear and transparent and did not contain as many inherent defects as the KN and MMTK10 containing films (see figure 4.2 E). Both sides of the film had the same texture and no powdery residue was present on the underside of the films indicating incorporation of LXL21 into the polymer matrix. This proves that the ability of LXL21 to swell and exfoliate in water facilitated its interaction with the alginate polymers (Bandeira et al., 2012). Formulations containing 1 g of LXL21 and 0.5 to 1 g of HVAIlg were found to be promising as they were flexible and strong in comparison to the other clay minerals tested. Formulations made from 1 g KN or 1 g MMTK10 with 1 g HVAIlg contained many imperfections (cracks and holes) and tended to be brittle. Like the KN and MMTK10 containing formulations, the films

containing LXL21 could not withstand extremes of flexing and bending (greater than 90°) without breaking.

Across all these initial screening studies involving KN, MMTK10, and LXL21 it became clear that the grade and amount of alginate used was important in creating a successful film (table 4.1). Having a sufficient amount of polymer in the 40 mL mixture was necessary to ensure a complete film was formed in the casting dish upon drying. However, it was also shown that having too much alginate in the 40 mL mixture resulted in thick films that were warped, hard, and inflexible.

Composite films made with 0.25 to 2.0 g of LVAIg were very thin and contained large holes so that a complete film was not formed, whilst those made with 4.0 g of LVAIg were thick and warped, making them extremely stiff and brittle. Similar results were obtained for materials containing MVAIg, where 0.25 to 1.0 g MVAIg formed films containing cracks and frayed edges and 2.0 and 4.0g of MVAIg formed thick, warped and brittle films. HVAIg was shown to be the most suitable grade of alginate to use in the formation of clay mineral containing films. Using 0.1 to 0.25 g of HVAIg formed very thin films with many cracks in the structure (figure 4.2 D) whilst a mass of 0.5 to 1 g of HVAIg formed continuous films with a fair degree of flexibility and strength (figure 4.2 E). Increasing the amount of HVAIg to 2.0 g created films that were thick and warped with very little flexibility (figure 4.2 F).

**Table 4.1.** Overview of the films made with 1 g of clay mineral and differing concentrations of varying grades of alginate. Red fields denote formulations that were not carried forward (N) for further study, and orange fields denote formulations that showed potential (✓) and were studied further.

	LVALg (g)					MVALg (g)					HVALg (g)				
	0.25	0.5	1	2	4	0.25	0.5	1	2	4	0.1	0.25	0.5	1	2
KN	N	N	N	N	N	N	N	N	N	N	N	N	N	N	N
MMTK10	N	N	N	N	N	N	N	N	N	N	N	N	N	N	N
LXL21	N	N	N	N	N	N	N	N	✓	N	N	N	N	✓	N

The low drug loading of KN coupled with its inability to form useful films meant it was eliminated from further investigation. Whilst MMTK10 was shown to carry moderate amounts of drug its inability to form complete, flexible films alongside the observed phase separation was problematic. Therefore, MMTK10 was also not considered for further investigation. LXL21 was able to carry large amounts of drug on its surface and was not observed to undergo phase separation in the casting process. Therefore, value was seen in continuing to develop a formulation utilising LXL21 and alginate but with the incorporation of an additive to overcome problems with flexibility. It was also evident that using LVALg was not a viable option for the creation of clay mineral containing films. For the formulation parameters investigated, 1 g of HVALg appeared to be the best polymer grade and amount to use in further studies. However, it was possible that the use of additives to improve flexibility of the films could also allow for greater quantities of other grades of alginate to be used. An overview of the formulations prepared and the decision on whether they were carried forward for further study can be seen in table 4.1.

Altering the drying method had very little effect on the formulation of LXL21-containing films. Those dried at room temperature created very similar films to those

obtained from the 40 °C fan oven however they took over 72-hours to form. Films that were dried at 40 °C under vacuum did not dry as fast as those in the fan assisted 40 °C oven and formed films that were mottled and non-uniform in appearance, and cracked. This was likely caused by the vacuum removing water in an uneven fashion, compared to the fan-oven. The hastened drying time in the fan-assisted oven was attributed to the circulation of air, removing water from the surface and allowing further evaporation to take place at a faster rate than the vacuum oven.

Glycerol and PVA were investigated for their ability to act as plasticisers and softeners in film-materials for healthcare applications (Jarray et al., 2016; Momoh et al., 2015; Singh et al., 2013; Vieira et al., 2011). Glycerol was found to have beneficial effects on the properties of the films produced. Addition of 225 mg to 562.5 mg glycerol had little effect on the appearance and flexibility of the films, whilst 1.125 g showed signs of improved flexibility. When 1.6875 g or 2.25 g of glycerol was added to the formulation containing 1 g HVAIlg the films produced were uniform in thickness, clear and transparent, soft to touch, and could withstand extremes of bending and even folding (figure 4.3). Equally promising results were also seen for films created from 1 g LXL21, 2 g MVAIlg with either 1.6875 g or 2.25 mg glycerol. These films were slightly thicker as a result of increased polymer content, but just as flexible as the HVAIlg films.

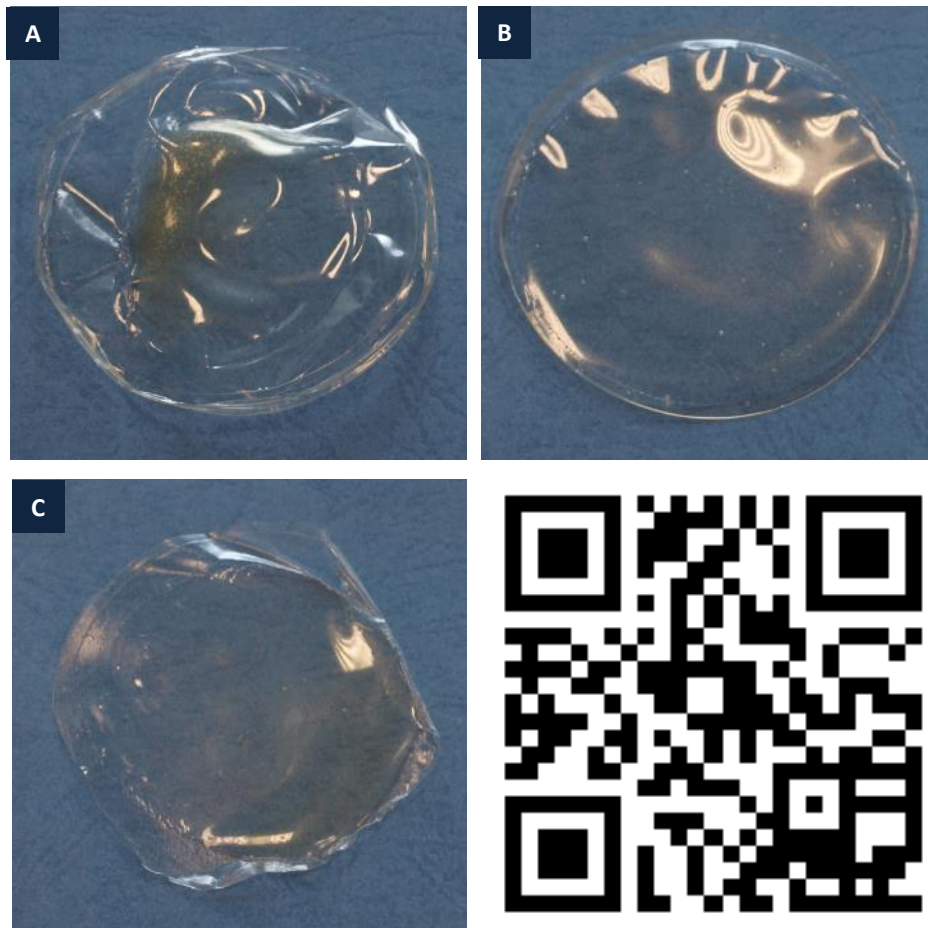


**Figure 4.3.** Images demonstrating the progression of the film formulations produced containing (A) 1 g LXL21 and 2 g HVAIlg; (B) 1 g LXL21 and 1 g HVAIlg; and (C) 1 g LXL21, 1 g HVAIlg, and 2.25 g glycerol. The QR code can be scanned with mobile and tablet devices and will open a YouTube video demonstrating the properties of these materials [url: <http://youtu.be/p0coEiBqaQ>].

Tissue viability nurses from The Royal Liverpool and Broadgreen University Hospitals NHS Trust independently assessed and critiqued the film dressings prepared. They confirmed that formulations without glycerol were not appropriate for wound care as their brittle nature would not allow use in body-flexures as any cracking or breaking *in situ* could cause pain and further damage to the wound bed. Of the two possible formulations containing glycerol it was decided that the film containing 1 g LXL21 and

2 g MVAIlg should be used for the final drug-containing formulations due to its increased thickness, which could enhance its exudate adsorbing potential.

#### *4.3.1.2. Qualitative evaluation of ciprofloxacin-containing films*

When 20 mg CIP (0.38% w/w) was included the composite looked identical to the films that contained no drug at all. As the concentration of the drug increased, minor changes were observed in the appearance of the film materials obtained. At 130 mg (2.42% w/w) CIP a complete film with no obvious faults and transparency was obtained. At this concentration it can be assumed that a monolayer of CIP will have formed at the LXL21 surface (as determined in section 3.3.3). The transparency of the formulation indicates that the LXL21 layers had not undergone significant flocculation and the equally good material properties suggest that no changes in interaction between the clay-drug composites and the alginate chains occurred.

As the drug concentration was further increased beyond the monolayer point a number of changes in the materials created was observed. At 160 mg (2.96% w/w) CIP the film was complete, soft, and flexible like previous films but a slight opaque appearance was observed. This opacity may have been caused by an increase in drug concentration but may equally have been as a result of flocculation of the LXL21 layers. This opacity was markedly increased and a yellow hue observed as the CIP content was increased to 200 mg (3.67% w/w). At this high concentration a number of defects in the film structure were also observed in the form of cracks and small holes. This may be a result of flocculation of LXL21 before addition of alginate or competition between CIP and alginate for interaction sites on the LXL21 layers. These defects may also have

been caused by an excess of CIP within the mixture interfering with film formation during drying. At this level of CIP content, composite films containing 2 g MVAIlg were observed to have fewer and smaller defects in their structure when compared to those containing 1 g HVAIlg. These films were also slightly thicker and softer than the HVAIlg containing films, which could possibly increase their water adsorption capacity and also integrity at the wound surface. Independent evaluation by the tissue viability nursing team also confirmed these determinations.

Controls without LXL21 demonstrated that the clay mineral was a vital component. When 20 mg CIP was added to the alginate only formulations the film was transparent but had taken on a slight yellow hue. However, when the CIP content was increased to 120 mg and 160 mg the film was no longer clear but white and opaque, with the opacity forming rings across the film surface. This was likely caused by the CIP precipitating out of solution during the drying process, as the concentration of CIP in solution increased beyond its solubility point. No such opacity or precipitation of CIP was observed when LXL21 was present in the formulation, indicating that adsorption onto the clay mineral surface allows for much greater drug loading within the film.

Thus, the final film formulation selected was 1 g LXL21, 2 g MVAIlg, and 2.25 g glycerol. It should be noted that glycerol, at the amount used, cannot be considered an additive as it makes up a significant proportion of the final formulation. The composite films containing 20 mg, 120 mg, and 160 mg CIP were also considered for further analysis.

**Table 4.2.** Composition of the composite films that were taken forward for quantitative analysis.

Film composition						Sample Code
KN	MMTK10	LXL21	MVAIg	GLY	CIP	
-	-	-	2 g	-	-	MVAIg
-	-	-	2 g	2.25 g	-	MVAIg-GLY
1 g	-	-	2 g	-	-	MVAIg-KN
-	1 g	-	2 g	-	-	MVAIg-MMTK10
-	-	1 g	2 g	-	-	MVAIg-LXL21
-	-	1 g	2 g	2.25 g	-	LXL21-MVAIg-LXL21-GLY
-	-	-	2 g	2.25 g	20 mg	MVAIg-GLY-20CIP
-	-	-	2 g	2.25 g	130 mg	MVAIg-GLY-130CIP
-	-	-	2 g	2.25 g	160 mg	MVAIg-GLY-160CIP
-	-	1 g	2 g	2.25 g	20 mg	MVAIg-LXL21-GLY-20CIP
-	-	1 g	2 g	2.25 g	130 mg	MVAIg-LXL21-GLY-130CIP
-	-	1 g	2 g	2.25 g	160 mg	MVAIg-LXL21-GLY-160CIP

Table 4.2 gives an overview of the composite films that were taken forward for further analysis along with a sample code that will be referred to in the analytical sections below.

#### 4.3.1.3. Optical properties of film formulations

Transparency is a desirable property for film dressings as it facilitates accurate application on the wound site and allows for the wound environment to be monitored whilst the dressing is in place (Boateng et al., 2008; Smith et al., 2016), reducing the need to remove the dressing thus reducing the risk of damaging the wound bed. Measuring the absorbance and transmittance (figure 4.4) of light through films is a recognised way of quantifying film opacity and transparency (Abdollahi et al., 2013; Alboofetileh et al., 2013; Shankar et al., 2016).

As shown in figure 4.4 measuring the proportion of visible light transmitted through the sample is a useful way to represent the transparency of the film, with higher



percentage transmittance indicating greater transparency. By measuring the absorbance at 600 nm and accounting for film thickness (see equation 4.1) it is possible to obtain a value for film opacity (see table 4.3).

Films containing MMTK10 were shown to be the most opaque as they transmitted no light (0%) and had an opacity value of 22.819; the highest obtained for the samples tested. Films containing KN were also shown to be transmitters of light and had a relatively high opacity of 12.237. For this reason films containing MMTK10 and KN would not be considered optimal clay-minerals for use within these alginate based dressings.

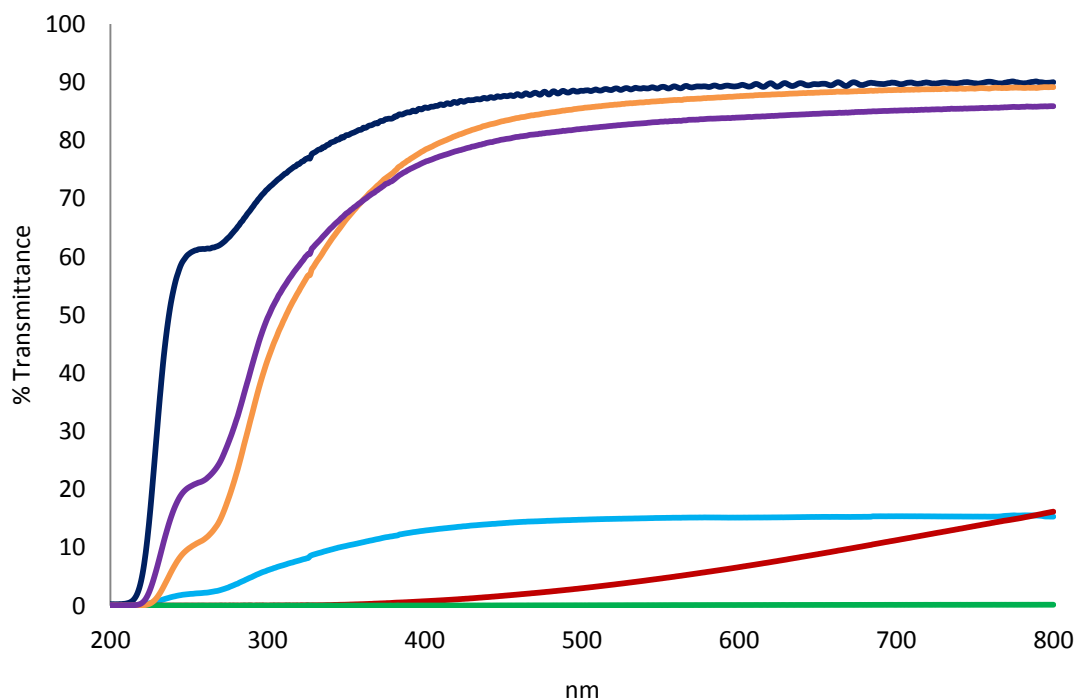


**Figure 4.4.** Percentage of light transmitted through films composed of MVA-Alg (dark blue), MVA-Alg-KN (red), MVA-Alg-MMTK10 (green), MVA-Alg-LXL21 (light blue), MVA-Alg-GLY (purple), and MVA-Alg-LXL21-GLY (orange).

Interestingly, LXL21-MVAIlg films only transmitted approximately 15% of visible light (at 600 nm) but this was better than the MMKT10 and KN containing films. LXL21 particles are much smaller in size compared to MMTK10 and KN, and are also able to exfoliate to a greater extent in water (Mongondry et al., 2005), which may explain why the transmittance of these films is higher and the opacity value is lower.

When glycerol is present within the samples the percentage transmittance of LXL21-MVAIlg films is greatly increased and the opacity value is greatly decreased indicating this nanocomposite film to be the most transparent of those tested. While the percentage of light transmitted by MVAIlg-GLY films was perceived to decrease slightly compared to the simple MVAIlg film, the opacity value of the MVAIlg-GLY films indicates improved transparency.

The presence of CIP within the films was also shown to affect the optical properties of the films; effectively reducing the amount of light transmitted through the sample and increasing the opacity of the film as the concentration of CIP increased.

Sample	Abs <sub>600</sub>	Opacity (±SD)
MVAIlg	0.0467	2.491 (±1.279)
MVAIlg-GLY	0.0795	0.713 (±0.055)
MVAIlg-KN	1.1238	12.237 (±0.558)
MVAIlg-MMTK10	2.8558	22.819 (±2.130)
MVAIlg-LXL21	0.7070	5.165 (±2.407)
MVAIlg-LXL21- GLY	0.0531	0.202 (±0.057)
MVAIlg-GLY-20CIP	0.0866	0.777 (±0.060)
MVAIlg-GLY-130CIP	0.8446	7.576 (±0.582)
MVAIlg-GLY-160CIP	1.4973	13.430 (±1.032)
MVAIlg-LXL21- GLY-20CIP	0.0621	0.236 (±0.066)
MVAIlg-LXL21- GLY-130CIP	0.2880	1.093 (±0.307)
MVAIlg-LXL21- GLY-160CIP	0.3253	1.235 (±0.347)

This could also be seen visually by the increased intensity of yellow tones within the formulations containing more CIP (as described in section 4.3.1.2). However, these optical evaluations demonstrate the effect was significantly ( $p < 0.001$ ) less pronounced in films containing LXL21 (figure 4.5 and table 4.3).

Chapter 3 indicated that when CIP was adsorbed onto clay mineral surfaces it acquired an amorphous arrangement and the FTIR and XRD data for these composite materials (sections 4.3.3 and 4.3.4, respectively) also suggest that CIP was adsorbed into the interlayer space of the LXL21 within the film nanocomposites. Amorphous arrangements can affect optical properties of solids, which may account for the increased transparency in LXL21 containing films, even at high CIP content.

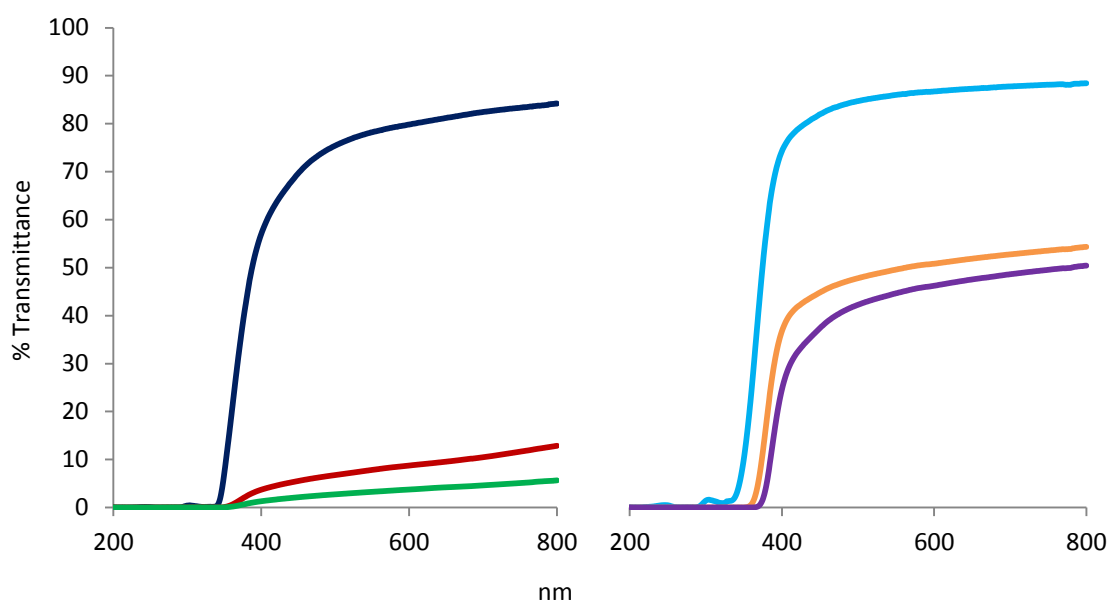


**Figure 4.5.** Percentage of light transmitted through films composing of MVAIg-GLY-20CIP (dark blue), MVAIg-GLY-130CIP (red), MVAIg-GLY-160CIP (green), MVAIg-LXL21-GLY-20CIP (light blue), MVAIg-LXL21-130CIP (orange), and MVAIg-LXL21-160CIP (purple).

Conversely, an absence of LXL21 within the films could have resulted in the precipitation of CIP during the drying process thus resulting in the presence of CIP particles throughout the formulation causing greater opacity.

A serendipitous finding of this experiment was the reduced transmission of ultraviolet light (below 400 nm). This reduction in transmission indicates that these nanocomposite films may also be able to protect the fragile wound bed from ultraviolet radiation, which is known to be harmful to the skin and wound-healing (Williams, 1996). Clay minerals are known to absorb UV radiation (Hoang-Minh et al., 2010), so the reduced transmission in non-clay-mineral containing samples suggests that alginate also has a role to play in UV absorption. There was practically no transmission of radiation at wavelengths shorter than 325 nm in the CIP containing composite (figure 4.5), compared to the non-CIP containing composites that allowed much more radiation to be transmitted at wavelengths shorter than 325 nm (figure 4.4). This shows that CIP was also able to absorb UV light but it is not known whether this resulted in degradation of the drug (Phillips et al., 1990), which should be investigated in future work to determine whether further UV-protection is required.

Overall, these data prove that LXL21 is a useful additive for alginate films as it is able to preserve the transparent properties that are desirable in film dressings. These results also support the decision to exclude KN and MMTK10 from ongoing formulation studies and that efforts should be made to optimise the properties of the LXL21-Alginate composite films. Future research is required to determine whether these films

can protect the wound environment from UV radiation, and whether this process negatively or positively impacts on the stability of CIP.

#### *4.3.2. Evaluation and selection of an ideal foam formulation*

##### *4.3.2.1. Qualitative analysis of pre-formulation foam materials*

Qualitative analysis of the foam-like materials was undertaken to describe their texture, strength, flexibility, and plasticity (ability to rebound once compressed). These are important properties for foam dressings as they need to be able to cushion and protect the wound from further damage, and be flexible enough to be used on the curvature and flexures of the human anatomy (Boateng et al., 2008; Powers et al., 2016). The narrative below describes the appearance, texture, strength and cushioning-properties of the different formulations developed. Collaboration with tissue viability nurses at the Liverpool and Broadgreen University Hospitals NHS Trust allowed these interpretations to be confirmed, and allowed these specialist health professionals to inform the future direction of this research.

Unlike the film formulations, the colour of the foams was not significantly affected by the clay mineral content. Foams containing KN and LXL21 were off-white in colour, whilst those formed with MMTK10 were equally as opaque but were more cream in colour.

Separation and flocculation of KN and MMTK10 from the alginate dispersion was observed during the formulation of foam materials. This phase separation appeared to be more profound in the foam formulations as a large amount of clay mineral powder

remained in the casting dish when the foam was lifted out. Using higher amounts of high viscosity alginate (4 g MVAIlg and 2 g HVAIlg) only partially overcame this problem and differences in the appearance of the upper and lower surfaces were evident. This confirmed that KN and MMTK10 were unable to form physicochemical interactions with the alginate polymer chains and were therefore considered inappropriate for further study as ingredients in the foam materials. LXL21 performed best out of the clay minerals tested. No phase separation was observed and for this reason, and for its ability to carry high amounts of CIP, LXL21 was chosen for further study.

Formulations containing low concentrations of all grades of alginate did not result in viable foams and instead flaky, fibrous, and particulate materials were obtained. This is likely a result of there not being enough polymeric material in the final frozen volume to form stable, interlinked, foams. In contrast, high concentrations of more viscous alginates (4 g MVAIlg and 2 g HVAIlg for example) formed foams that were too rigid, giving very little of the needed cushioning and flexibility – likely a result of a denser internal structure and more interactions between polymeric units. Large amounts of LVAIlg (4 g) and moderate amounts of MVAIlg (2 g) were found to create the most promising foam-like materials, especially when formulated with LXL21. These materials did not tear easily and had some degree of flexibility and compressibility. For this reason composites containing 4 g LVAIlg and 2 g MVAIlg were carried forward for further study. An overview of the foam component combinations studied and their potential for further study are outlined in table 4.4.

**Table 4.4.** Overview of the potential of foams made with 1 g of clay mineral and differing concentrations of varying grades of alginate. Red fields denote formulations that were not (N) carried forward for further study, and orange fields denote formulations that showed potential (✓) and were studied further.

	LVAIg (g)					MVAIg (g)					HVAIg (g)				
	0.25	0.5	1	2	4	0.25	0.5	1	2	4	0.1	0.25	0.5	1	2
KN	N	N	N	N	N	N	N	N	N	N	N	N	N	N	N
MMTK10	N	N	N	N	N	N	N	N	N	N	N	N	N	N	N
LXL21	N	N	N	N	✓	N	N	N	✓	N	N	N	N	N	N

A number of problems still remained within the promising formulations. It is vital that foam wound-dressings are soft and flexible and the two composite foams identified above would not provide the necessary cushioning or flexibility required by patients and were therefore not fit for purpose. Glycerol was also employed as a plasticiser here as it was found to give extremely good properties to the film formulations. Much less glycerol, however, was needed to achieve the desired softness for the foams compared to the films (562.5 mg vs 2.25 g). This is likely due to the relative density of the materials formed as the foam-like materials had much less alginate mass and polymer chain interactions per unit volume in comparison to the films. Therefore, less glycerol was required to modify the interactions between the polymer chains to reduce the rigidity of the material. Using too much glycerol (1.6875 g to 2.25 g) resulted in excess glycerol separating from the foam-like materials, resulting in a greasy material that would not rebound once compressed. In contrast, materials formed using 562.5 mg glycerol would rebound after moderate compression and thus had promising cushioning properties (see video in figure 4.6).

Even though the softness of the foam-like materials had been enhanced, the tissue viability nursing team from The Royal Liverpool and Broadgreen University hospital still

found the materials to be clinically inappropriate. Whilst the materials had cushioning properties the integrity of the overall foam was considered unacceptable. This was caused by striations of foam and voids throughout the material that resulted in structural weaknesses that broke easily on bending. It was likely that these striations were caused by arrangements of ice crystals forming during the freezing process and it was therefore vital to eliminate ice crystal formation.

A number of compounds known to inhibit the formation of ice crystals (Fink, 2015; Giuliani et al., 2012; Inada and Modak, 2006; Soykeabkaew et al., 2015) were studied but none of these provided the necessary effects at the concentrations tested. Salts of sodium and calcium are employed industrially to prevent the formation of ice crystals, or promote melting. However, neither was seen to have significant effects on the formation of striations within the composite foams and both were found to increase the hardness of the materials obtained. This effect of calcium is well known to increase gel strength and structure in alginates as it forms strong bridges between the G-G units on the alginate chains (Qin, 2008). Ethanol performed better than the salts, resulting in smaller ice crystals that were concentrated at the edges and bottom surface of the foam-like materials obtained. However, the striations formed in the materials containing ethanol were not reduced enough to provide any remarkable improvement in physical strength.

The results above suggest that ice crystals were being formed during the freezing process and this was likely to be due to the casting dish, the clay minerals, and alginate providing nucleation points for ice-crystal formation. Therefore, hastening of the



freezing process was investigated. Speeding up the freezing process using a  $-80\text{ }^{\circ}\text{C}$  freezer did not have much effect on reducing striation (figure 4.6 A). The vast majority of striation still occurred at the edges and underside of the foams, proving that the casting dish was acting as a nucleation site for ice crystals.

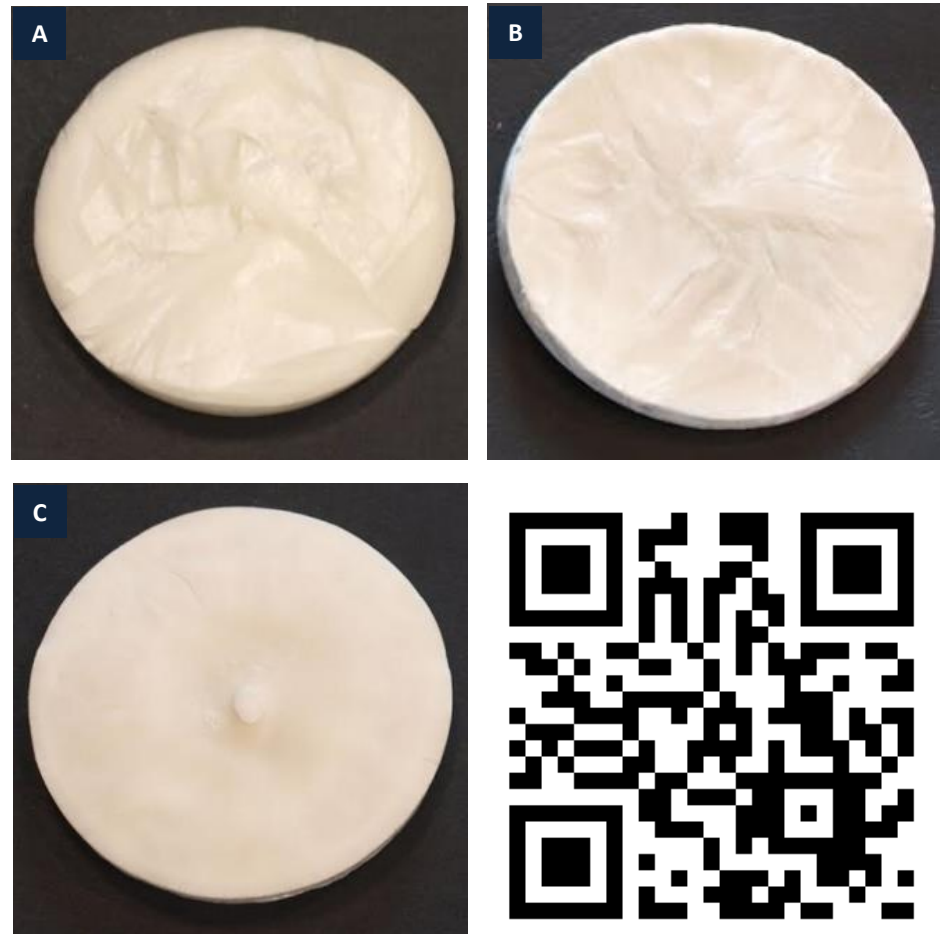


**Figure 4.6.** Images demonstrating the progression of foam formulations consisting of (A) 1 g LXL21 and 4g LVALg, frozen at  $-80\text{ }^{\circ}\text{C}$ ; (B) 1g LXL21 and 4g LVALg, frozen in liquid nitrogen; and (C) 1g LXL21 and 4g LVALg with 562.5 mg glycerol, frozen in liquid nitrogen. The QR code can be scanned with mobile and tablet devices and will open a YouTube video demonstrating the properties of these materials [url: [https://youtu.be/nW\\_61H5ipbw](https://youtu.be/nW_61H5ipbw)].

Flash-freezing by submersion in liquid nitrogen allowed the generation of an improved foam structure. Submersion into liquid nitrogen caused freezing of the formulation mixture from the edges inwards. Short freezing times (5 minutes) resulted in incomplete freezing of the sample so that the formulation mixture in the centre of sample was still a liquid, which only froze overnight at  $-20^{\circ}\text{C}$  and led to striations and weakness at the centre of the foams. Ensuring adequate submersion times (greater than 15 minutes) allowed the entire formulation mixture, in the casting dish, to be sufficiently frozen. The majority of striation was removed by this freezing process (figure 4.6 B) and a more uniform product was obtained that had improved flexibility and rebound when glycerol was present (figure 4.6 C).

The formulation selected for further investigation of foam-like materials contained 1 g LXL21, 4 g LVAIlg and 562.5 mg glycerol prepared by submersing the casting dish in liquid nitrogen for 15 minutes, following storage at  $-20^{\circ}\text{C}$  before freeze-drying. As shown in figure 4.6 C the foam that was produced was uniform in nature with no striation due to water crystal formation. The physical properties were also much improved compared to the other pre-formulation samples (see video in figure 4.6), having improved flexibility and rebound behaviour. However, the behaviour and properties of these materials may change in the wound environment and this was further investigated in sections 4.3.7 and 4.3.8.

#### *4.3.2.2. Qualitative evaluation of ciprofloxacin-containing foam materials*

Foams formulated with LXL21 and 20 mg (0.36% w/w) CIP were identical in appearance to those without CIP. As the concentration of CIP within the formulation

increased to 160 mg (2.80% w/w) the foam took on a yellow hue but no obvious structural defects were observed. The incorporation of 200 mg (3.47% w/w) CIP into the composite resulted in major defects and a material that was a strong yellow colour made of loosely connected flakes and lumps. As for the film formulation, it is likely that this high CIP loading caused the LXL21 to flocculate leading to poor interactions between the clay mineral layers and the alginate chains. Independent feedback from the nursing team confirmed that these foam materials were promising but still needed further development. Whilst the foams were soft and responsive to compression they could not withstand aggressive folding and bending without breaking or forming particulates.

Before further refinement of the foam formulations was considered the potential of the composites highlighted above (1 g LXL21, 4 g LVAIg, and 562.5 mg glycerol) were investigated as potential carriers for CIP.

Final foam-like formulations were repeated without the inclusion of LXL21 to act as comparators. CIP did not precipitate in the formulations containing LXL21 but this is not a reliable indication of whether the CIP remained in solution or not. The formulation mixtures for clay-free composites were distinctly whiter than those containing LXL21, suggesting that CIP precipitated out before or during the casting stage. This explains the ring-like patterns observed in the foam, as these patterns would have been induced by the drying process. Therefore, it is likely that the CIP did not remain solubilised in the foams and was simply dispersed throughout the dressing, held in place by the rapid freezing process.

**Table 4.5.** Composition of the composite foams that were taken forward for quantitative analysis. Where LN represented the liquid nitrogen freezing technique.

Sample composition					Sample Code
Clay mineral (1g)	Alginate	Glycerol	CIP	Freezing method	
-	4 g LVAIlg	-	-	LN	LVAIlg
-	4 g LVAIlg	562.5 mg	-	LN	LVAIlg-GLY
KN	4 g LVAIlg	-	-	LN	LVAIlg-KN
MMTK10	4 g LVAIlg	-	-	LN	LVAIlg-MMTK10
LXL21	4 g LVAIlg	-	-	LN	LVAIlg-LXL21
LXL21	2 g MVAIlg	-	-	LN	MVAIlg-LXL21
LXL21	1 g HVAIlg	-	-	LN	HVAIlg-LXL21
LXL21	4 g LVAIlg	562.5 mg	-	- 20 °C	LVAIlg-LXL21- GLY-m20
LXL21	4 g LVAIlg	562.5 mg	-	- 80 °C	LVAIlg-LXL21- GLY-m80
LXL21	4 g LVAIlg	562.5 mg	-	LN	LVAIlg-LXL21- GLY-LiqN
-	4 g LVAIlg	562.5 mg	20 mg	LN	LVAIlg-GLY-20CIP
-	4 g LVAIlg	562.5 mg	130 mg	LN	LVAIlg-GLY-130CIP
-	4 g LVAIlg	562.5 mg	160 mg	LN	LVAIlg-GLY-160CIP
LXL21	4 g LVAIlg	562.5 mg	20 mg	LN	LVAIlg-LXL21- GLY-20CIP
LXL21	4 g LVAIlg	562.5 mg	130 mg	LN	LVAIlg-LXL21- GLY-130CIP
LXL21	4 g LVAIlg	562.5 mg	160 mg	LN	LVAIlg-LXL21- GLY-160CIP

Table 4.5 gives an overview of the composite files that were taken forward for further analysis along with a sample code that will be referred to in the analytical sections below.

#### 4.3.2.3. Semi-quantitative analysis of the mechanical strength of foam materials

Friability testing was utilised to estimate the overall mechanical strength and robustness of the foam materials obtained. The results shown in figure 4.7 display the percentage weight loss of the foams after tumbling and indicate the effect of each ingredient on the structural integrity of the composite material. The commercially available dressings Kaltostat® and Lyofoam® did not lose any mass during tumbling, which was set as the target weight loss for the composite materials.

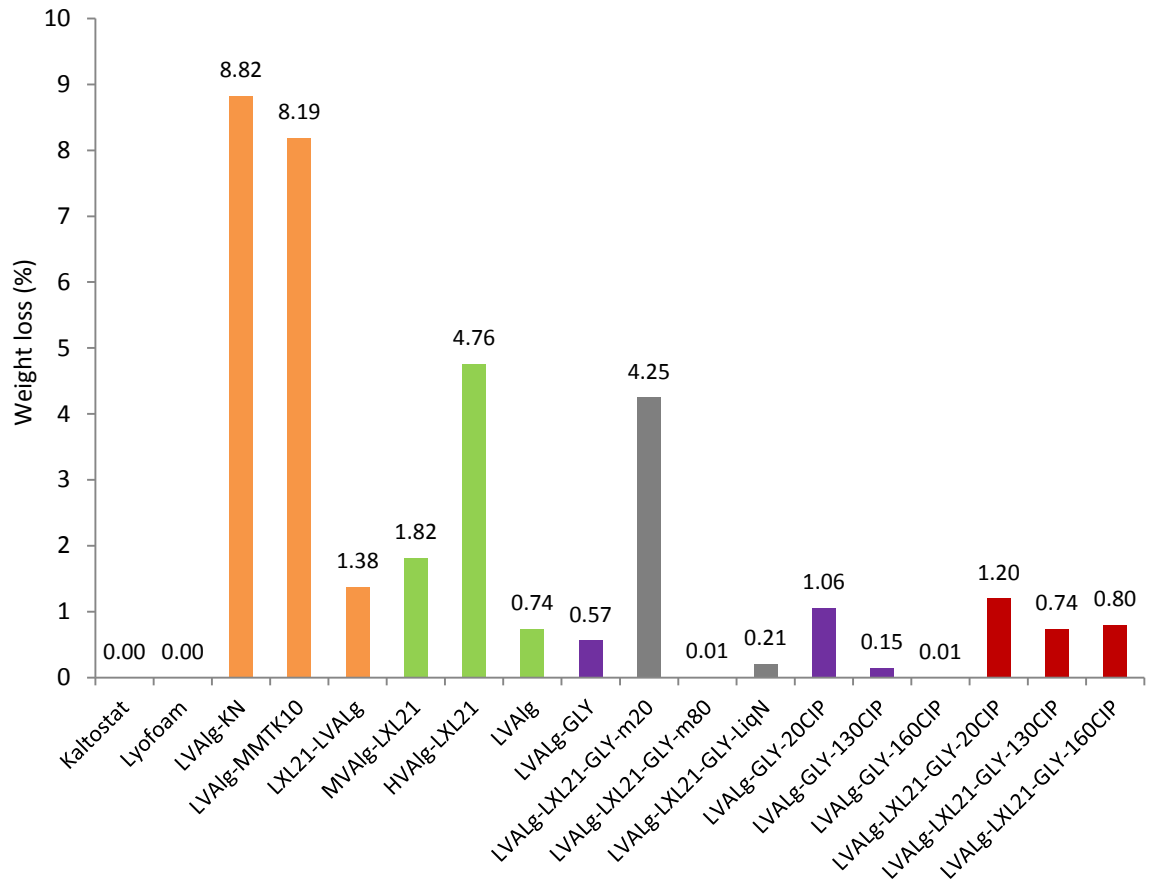


**Figure 4.7.** Percentage weight loss (average, based on 10 samples) of selected foam-like materials after friability testing, demonstrating the effects of differing clay minerals (orange), alginate grades (green), freezing parameters (grey) drug loading (red), and absence of LXL21 from the final formulation (purple). Calculated percentage losses are explicitly given for each material.

The type of clay mineral used was shown to have the greatest impact on the friability of the foam like materials obtained. KN and MMTK10 were both shown to perform extremely poorly and would therefore not be acceptable for the clinical care of wounds. As described above it is likely that KN and MMK10 were not able to form interactions with the alginate polymer chains, resulting in a fragile structure based on alginate-alginate chain interactions only.

The grade and mass of alginate used was also shown to be important in the overall robustness of the foam materials obtained. Foams of LVAIlg, containing no other components, were shown to lose only 0.742 % of their mass during testing. In the presence of LXL21 the composite foam containing 4 g LVAIlg was shown to lose less of its overall mass (1.381 %) compared to 2 g MVAIlg (1.817 %) and 1 g HVAIlg (4.758 %). This is likely caused by a higher mass of alginate allowing for increased inter-polymer interactions and also increased abundance of interactions with the LXL21 present. It is also plausible that using lower concentrations of longer chain polymers (such as 1 g HVAIlg) allows for the matrix to be more flexible, less dense, and therefore easier to break apart during friability testing.

Altering the freezing process of the foams was shown to have a positive effect on the strength of the foams. Those frozen at  $-20\text{ }^{\circ}\text{C}$  lost large amounts of mass (4.25%) during testing compared to those frozen at  $-80\text{ }^{\circ}\text{C}$  (0.01% mass loss). Those frozen in liquid nitrogen lost 0.207 % of their mass during testing. These data show that the reduced ice-crystal formation and greater visual homogeneity in these rapidly frozen samples also awarded the composites more structural integrity compared to those frozen in the  $-20\text{ }^{\circ}\text{C}$  freezer.

The results of the friability testing suggest that addition of non-swelling clay minerals (KN and MMTK10) to the alginate polymers creates a less structurally sound composite foam when compared to the swelling clay LXL21. This is supported by scientific literature showing that the presence of a 2:1 clay mineral within polymeric matrices can increase the structural robustness of foam composites (Ray and Okamoto, 2003).

These data therefore support the decision to retire KN and MMTK10 from further study and to focus on the role of LXL21 within these composite foam materials. However, it may be possible that the methodology used here is not sensitive enough to fully characterise material strength. Therefore, future work needs to include analysis of tensile properties, flexure properties, and compression-rebound properties (Boateng et al., 2008; Ray and Okamoto, 2003; Thu et al., 2012).

#### *4.3.3. FTIR analysis of films and foam formulations*

FTIR is extensively used in the evaluation of clay-polymer composites to determine the location and nature of clay-polymer interactions (Bandeira et al., 2012). The FTIR spectrum for LXL21 is discussed in section 2.3.5 and is provided again in figure 4.8 below.

As with the spectra for other organic molecules, such as CIP (discussed in section 3.3.5 and provided again in figure 4.8), the fingerprint for MVALg and LVALg can be seen between  $550 - 1800 \text{ cm}^{-1}$ . Characteristic absorbance bands appear in the same positions for LVALg and MVALg at  $3265 \text{ cm}^{-1}$  for the hydroxyl groups,  $1596 \text{ cm}^{-1}$  for  $-\text{COOH}$  symmetric stretching,  $1406 \text{ cm}^{-1}$  for  $-\text{COOH}$  asymmetric stretching, and  $1025 \text{ cm}^{-1}$  for C-O-C stretching (Benli et al., 2011; Ghadiri et al., 2013; Pongjanyakul, 2009).

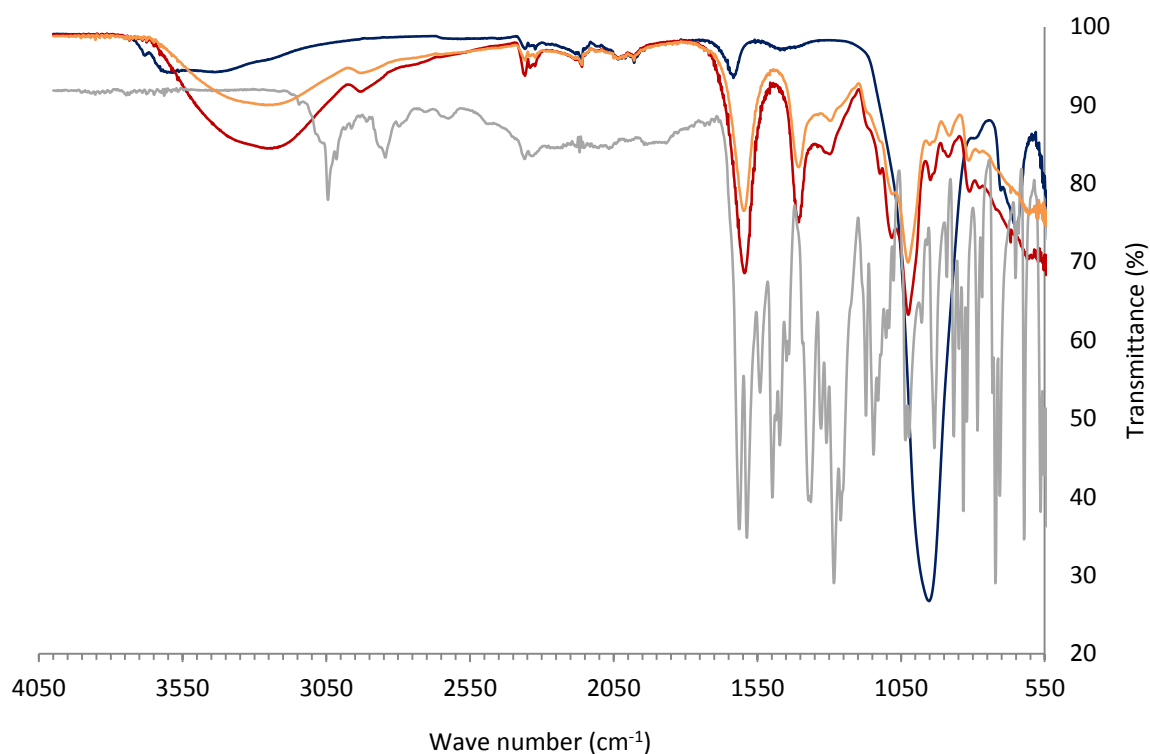


**Figure 4.8.** Full FTIR spectra for LXL21 (dark blue), CIP (light grey), LVAIlg (orange) and MVAIlg (red).

No change in the position of the absorbance peaks were observed when LXL21 was physically mixed with the alginates indicating that no chemical or physical interaction took place during this process. When formulated into a film without LXL21 or glycerol the positions of the absorbance bands for MVAIlg remained unchanged when compared to the original powder (figure 4.9). This suggests that no change in the chemical or physical structure of MVAIlg took place during the dispersion, casting, and drying processes. When LXL21 was present within the film formulation, the symmetric  $\text{-COOH}$  absorbance shifted to  $1602\text{ cm}^{-1}$  and the asymmetric  $\text{-COOH}$  absorbance shifted to  $1410\text{ cm}^{-1}$ . This shift to a higher wavenumber is suggestive of hydrogen bonds being formed between the  $\text{-COOH}$  groups on the alginate polymer chain and the LXL21 particles (Bandeira et al., 2012; Benli et al., 2011). In this sample the Si-O-Si stretch absorbance, characteristic to LXL21, was shifted to  $975\text{ cm}^{-1}$  and the Si-O



bending absorbance was shifted to  $625\text{ cm}^{-1}$ , which is suggestive of an interaction occurring at the exposed silanols at the clay-mineral edge sites (Bandeira et al., 2012; Ghadiri et al., 2013). The presence of glycerol within the film formulations could be detected by the double absorbance at  $2935$  and  $2883\text{ cm}^{-1}$ , assigned to the  $-\text{OH}$  vibrations (Calvino-Casilda et al., 2011), and the bands at  $1078$  and  $1028\text{ cm}^{-1}$ , which are attributed to the  $\text{CH}_2\text{OH}$  vibration (Tan et al., 2016).

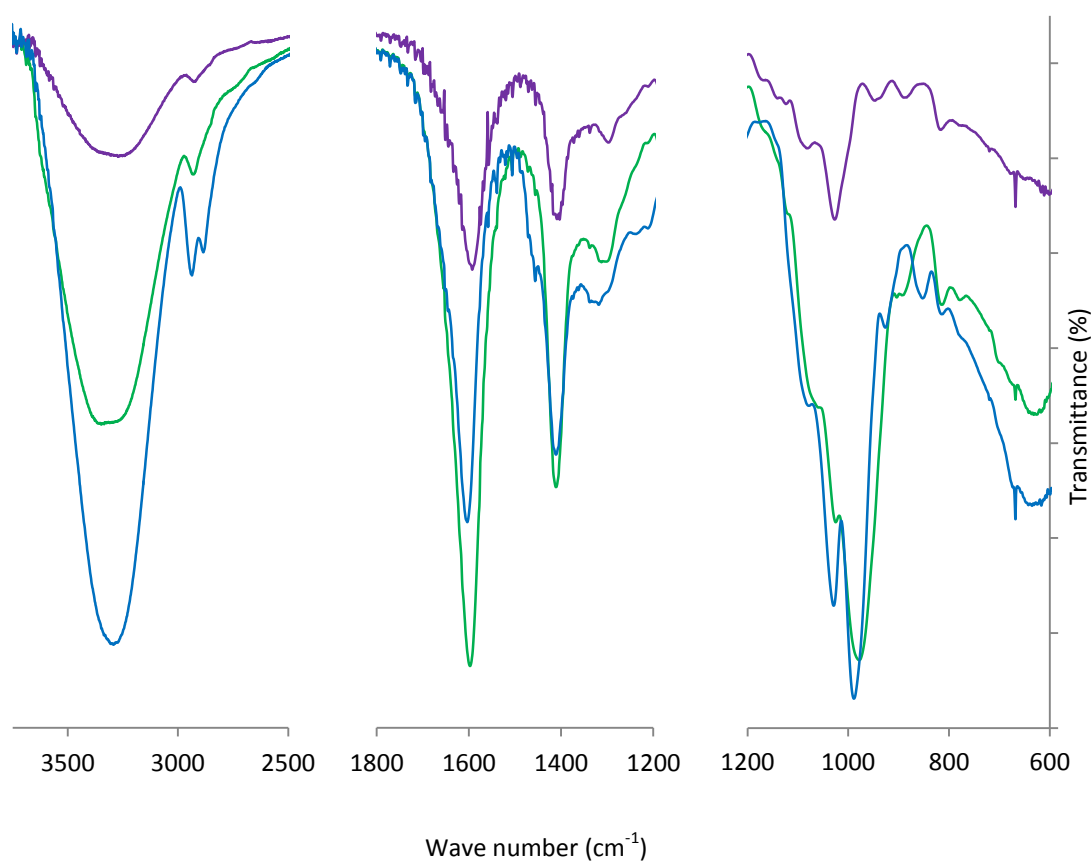


**Figure 4.9.** Enlarged sections of the FTIR spectra for MVAIlg film (purple), MVAIlg-LXL21 film (green), and MVAIlg-LXL21-GLY film (light blue).

When assessing the spectra for films containing MVAIlg-GLY-160CIP and LXL21-MVAIlg-GLY-160CIP a number of key observations can be made. The absorbance peaks for glycerol appear at the same wavenumber as in the LXL21-MVAIlg-GLY film (figure 4.9). The characteristic absorbance bands for MVAIlg also remained at the same position as previously observed above. As discussed by Singh et al. (2013) in their work on antibiotic hydrogel wound dressings, glycerol is often used to reduce the intermolecular forces between polymer chains but no details are given as to any physicochemical interaction that takes place. The academic literature also provides little evidence of an interaction between glycerol and alginate chains. Therefore, the lack of interaction picked up by FTIR in this research may be truly representative of the weak interaction between glycerol and MVAIlg. However, a slight shift in the Si-O-Si absorbance of LXL21 is observed in the sample of the final formulation. The appearance of this peak at  $987\text{ cm}^{-1}$  (appears at  $950\text{ cm}^{-1}$  in unmodified LXL21, and  $975\text{ cm}^{-1}$  in the LXL21-MVAIlg film) in the LXL21-MVAIlg-GLY film and the LXL21-MVAIlg-GLY-160CIP film suggests there is an interaction between LXL21 and glycerol. Even though the interaction between glycerol and clay mineral surfaces, specifically the interlayer space, has been recognised for a number of years it is not well characterised (Lagaly et al., 2013; Madsen, 1977; Tan et al., 2017). It may be possible that the ability of glycerol to act as a plasticiser is not detectable through FTIR, hence why no absorbance shifts are observed here. Given the reported interaction between 2:1 clay minerals and glycerol in the literature it may be possible that the shift in the Si-O-Si absorbance is suggestive of an interaction between glycerol and LXL21.

In section 3.3.5, key absorbance peaks for CIP were shown to shift, indicating an interaction between the zwitterionic CIP molecule and the edges and interlayer surfaces of the clay mineral particles. However, the absorbance assigned to the positively charged amino group appeared in its original position at  $1373\text{ cm}^{-1}$ . Other characteristic CIP peaks that were previously observed at  $1588$  and  $1617\text{ cm}^{-1}$  could not be detected in these samples as they were masked by the  $\text{COO}^-$  asymmetric stretch of MVALg (figure 4.10).

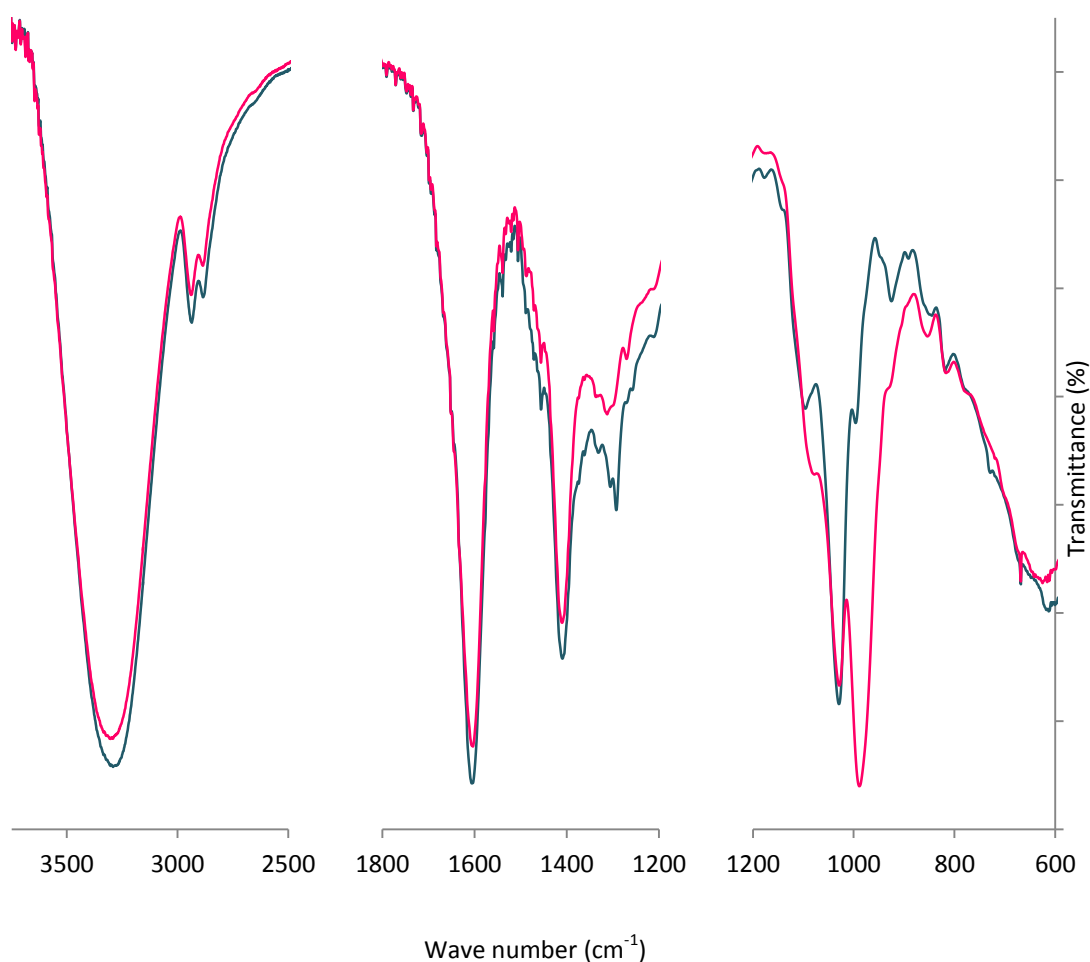


**Figure 4.10.** Enlarged sections of the FTIR spectra for the film containing MVALg-GLY-160CIP (teal) and MVALg-LXL21-GLY-160CIP (pink).

Therefore, it is not possible to determine whether CIP has remained within the LXL21 laminar space when formulated with MVAIlg. It is possible that the appearance of the  $\text{NH}_2^+$  absorbance in its original position means that CIP is not interacting with the LXL21 surface (Chang et al., 2016; Wang et al., 2010) and may have been displaced by glycerol (figure 4.10).

Similar analyses and cross comparisons were undertaken for the foam formulations (figure 4.11). In the samples containing LXL21 the  $\text{-COOH}$  symmetric and asymmetric stretching absorbance peaks were shifted to higher wavenumbers at 1600 and 1410  $\text{cm}^{-1}$ , respectively. The Si-O-Si stretching absorbance was shown to shift significantly to 985  $\text{cm}^{-1}$  and a smaller shift in the Si-O bending absorbance to 625  $\text{cm}^{-1}$  was also observed. The shift in these characteristic bands is indicative of an electrostatic interaction between the carboxyl groups of the alginate polymer and the positively charged exposed silanols at the LXL21 particle edge sites (Bandeira et al., 2012; Darder et al., 2016). Characteristic absorbance bands can be observed when glycerol is present within the composites, but the bands are not as well resolved as in the film formulations described above. The proportion of glycerol within the foam composites was significantly smaller than the film composites, accounting for these low intensity bands.

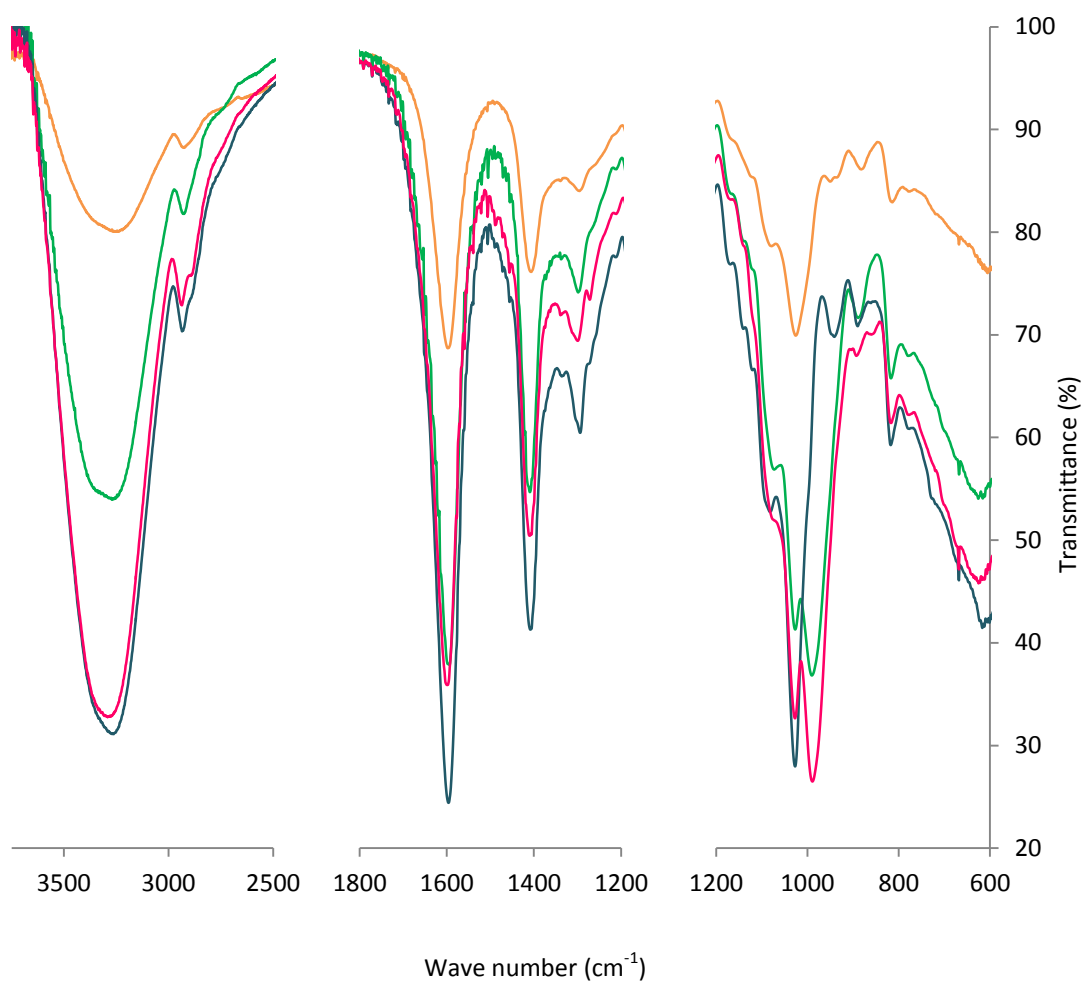


**Figure 4.11.** Enlarged sections of the FTIR spectra for LVAIg powder (orange) and foams containing LVAIg-LXL21 (green), LVAIg-GLY-160CIP (teal), and LVAIg-LXL21-GLY-160CIP (pink).

None of the characteristic CIP absorbance peaks could be identified in the FTIR spectra of the foam composites as the large absorbance bands of LVAIg at  $1600$  and  $1410\text{ cm}^{-1}$  were masking the smaller CIP absorbance. Unfortunately this means no accurate conclusions can be drawn about the interaction of CIP with LXL21 and LVAIg in these foam composites. It may be reasonable, however, to assume that the interactions between LXL21, LVAIg, glycerol, and CIP in the foam composites are similar to those observed in the film composites. Therefore, CIP is likely adsorbed onto the internal surfaces with LVAIg chains interacting with the LXL21 particle edge sites. In the film

composites it was proposed that glycerol could compete with, and displace, CIP from the LXL21 surface. While it may be possible for the same process to occur in the production of the foam composites the degree of CIP displacement may well be lower due to the smaller amount of glycerol used within the formulation process. While the release-studies and antimicrobial testing discussed below prove that CIP was still present in these foam composites pXRD analyses were necessary to determine the location of both CIP and glycerol within these composite materials.

#### *4.3.4. XRD analysis of film and foam composites*

X-ray diffraction is a useful technique to determine whether microcomposites, intercalated nanocomposites, or exfoliated nanocomposites are formed through clay-mineral polymer interactions (Alboofetileh et al., 2013; Zhang et al., 2009). The diffraction pattern for LXL21 is characteristic of Laponite® as seen in chapters 2 and 3 with a broad, low intensity, reflection at 6.81 degrees  $2\theta$  representing a  $d_{001}$  spacing of 13.61 Å. The diffractogram for MVAAlg powder revealed this product was amorphous in nature with a broad diffraction at 6.56 degrees  $2\theta$  and a rise in baseline at 18.25 degrees  $2\theta$  onwards, which is characteristically reported in the literature (Alboofetileh et al., 2013; Ghadiri et al., 2013; Yang et al., 2012). The physical mixture of these two compounds does not cause any alteration of the interlayer space of LXL21 but a muting of its diffraction peaks due to the proportion of MVAAlg present (figure 4.12 A).

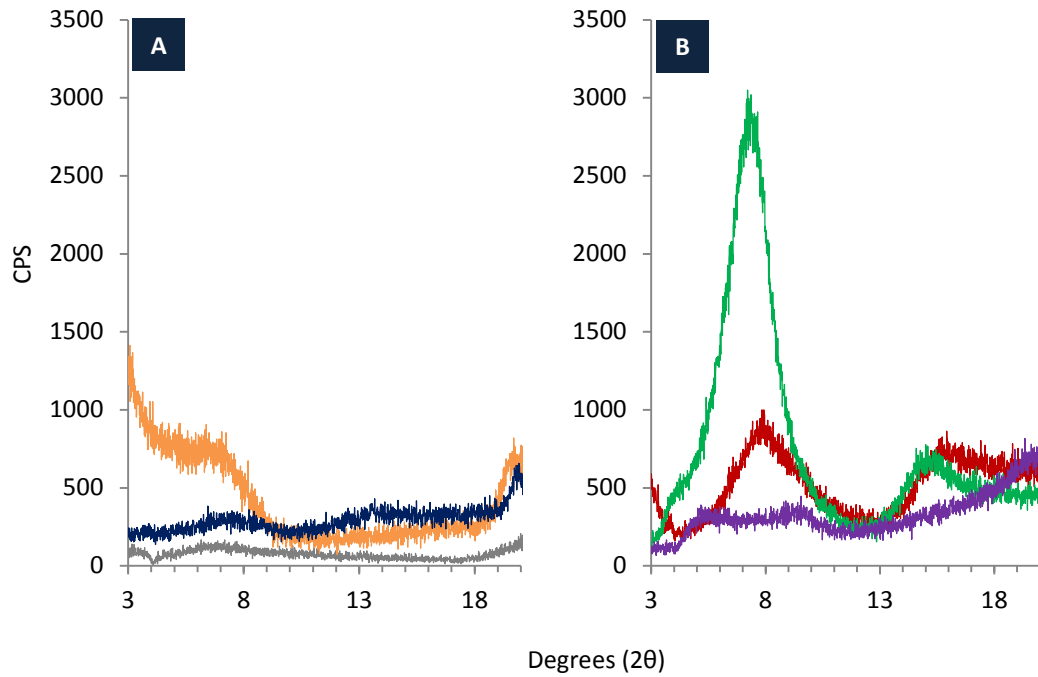


**Figure 4.12.** XRD diffractograms for (A) LXL21 powder (orange), MVAAlg powder (grey), and a physical mix of LXL21 and MVAAlg (dark blue), and (B) MVAAlg film (red), MVAAlg-LXL21 film (green), and MVAAlg-LXL21-GLY film (purple).

When formulated as a film the MVAAlg polymers formed a more ordered structure as indicated by the higher intensity peak at 7.95 degrees  $2\theta$ . The addition of LXL21 to the formulation produced a diffractogram indicative of a structure more ordered than the LXL21 powder and MVAAlg films (figure 4.12 B).

The initial diffraction at 7.33 degrees  $2\theta$  suggests that the  $d_{001}$  spacing of LXL21 was reduced to 12.01 Å. While alginate is believed to interact with the interlayer surfaces of other swelling minerals such as MMT, the data presented here suggest that does not happen with LXL21 as the interlayer space did not increase. A similar conclusion was drawn by Ghadiri et al. (2013) who observed an intensification of diffractions but no shift in position, indicating increased order within the matrices but no change in

Laponite® XLG interlayer spacing. Therefore, it is likely that the negatively charged carboxyl groups, and the high density negative charge of the G-G regions, of MVAIlg were interacting with the positively charged exposed hydroxyl groups at the edge of the LXL21 platelets.

The addition of glycerol into MVAIlg-LXL21 film system caused significant changes in the diffractogram with broad low intensity diffractions appearing at 5.32, 9.58 and 19.69 degrees  $2\theta$ . It is probable that the diffraction at 5.32 degrees  $2\theta$  is due to the LXL21 with an increased  $d_{001}$  spacing of 16.6 Å due to glycerol adsorption into the interlayer space of LXL21. This reduction of order within the diffractogram is suggestive of reduced crystallinity (Chang et al., 2009) and order within the films containing glycerol, which supports the qualitative analysis that declared glycerol a good softener and plasticiser for these films.

The diffraction pattern for LVAIlg (figure 4.13) was very similar to that for MVAIlg, which showed an amorphous structure. The diffractogram for the physical mixture of LXL21 and LVAIlg generated diffractions at 6.81 and 19.67 degrees  $2\theta$  indicating that there was no separation of the clay mineral layers through the process of creating a physical mixture. Although the baseline appears to have shifted upwards on the intensity scale a new low-intensity, broad, diffraction can be observed at 13.69 degrees  $2\theta$ , which is also observed at 13.51 degrees  $2\theta$  in the physical mix of LXL21 and MVAIlg above. As demonstrated by Chang et al., (2009) not all clay-mineral diffractions are detected but it is possible to apply Bragg's Law (equation 2.9) to predict at what angles these diffractions should appear. Therefore, it is probable that these new diffractions



represent the  $d_{002}$  reflection with the diffractions at 6.81 and 19.67 degrees  $2\theta$  representing the  $d_{001}$  and  $d_{003}$  reflections, respectively.

Unlike the diffraction pattern for the MVAIlg film, which showed increased order compared to the powder, the diffraction pattern for the MVAIlg foam indicated this material was amorphous with no order induced by the casting or freeze-drying processes. The addition of LXL21 to the LVAIlg foam resulted in increased order within the material, as indicated by the reflection at 7.87 degrees  $2\theta$ . This shift in  $d_{001}$  reflection suggests that the interlayer space of LXL21 has decreased to around 11.22 Å.

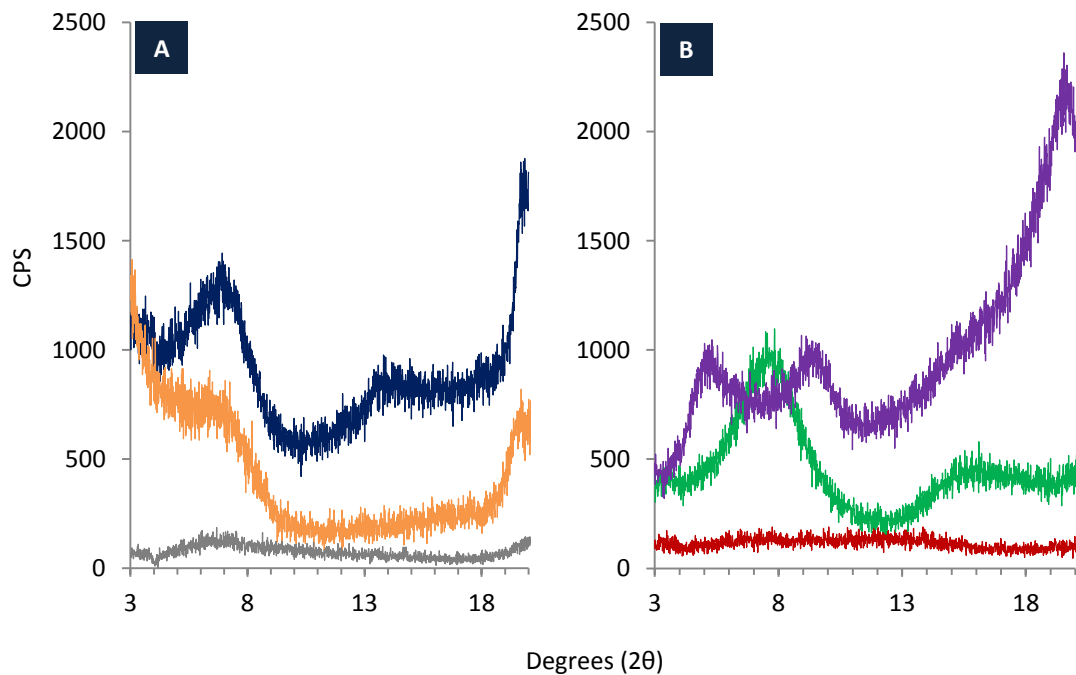


**Figure 4.13.** XRD diffractograms for (A) LXL21 powder (orange), LVAIlg powder (grey), and a physical mix of LXL21 and LVAIlg (dark blue), and (B) LVAIlg foam (red), LVAIlg-LXL21 foam (green), and LVAIlg-LXL21-GLY foam (purple).

Finally, addition of glycerol to the foam formulation did not reduce the order within the material as much as was observed in the film formulations, which may have been due to the reduced amount of glycerol used within the foam formulations. However, the reflections at 5.32, 9.42 and 19.63 degrees  $2\theta$  observed in this sample were in similar locations to those observed in the LVAIlg-LXL21-GLY film. The reflection at 5.32 degrees  $2\theta$  is likely caused by the LXL21 with an increased  $d_{001}$  space of 16.6 Å. As proposed above, it is probable that the glycerol was absorbed into the interlayer space of LXL21.

#### *4.3.5. Thermal analysis of film and foam formulations*

By examining the thermal behaviour of the individual components, in isolation and together, of the final formulations it was also possible to determine the role of each component within the film (figure 4.14) and foam nanocomposites (figure 4.15) on the thermal stability and cross-linking of the materials formed (Ghadiri et al., 2013; Ray and Okamoto, 2003; Shikinaka et al., 2012)

The first loss of mass observed on all the TGA experiments started at approximately 30°C temperature and was due to the loss of water within the sample. The size of this mass loss can be related to the amount of water held within each sample (Matthews et al., 2005; Pongjanyakul and Puttipipatkachorn, 2008). The powder of MVAIlg alone showed moisture loss between 30 °C and around 105 °C, which was followed by a significant loss of mass between 210– 270 °C and a smaller mass loss between 360 – 410 °C (figure 4.14). These mass changes were due to the depolymerisation and decomposition of the alginate polymer. Subsequent combustion of the alginate

polymer residues can be observed between 550 – 710 °C (Ghadiri et al., 2013; Iliescu et al., 2013; Pongjanyakul and Puttipatkhachorn, 2008). When MVAIlg was formed into a simple film the loss of mass due to unbound, surface, water was approximately 4% greater than for the powder form, indicating that even in the dry state the film was able to retain a certain degree of water. No change in the initial decomposition of the alginate polymer was observed, however the third mass loss was recorded between 390 – 490 °C. This shift to a higher temperature may be caused by reduced heat conduction (Chen et al., 2012) and possible increased thermal stability in the alginate film in comparison to the powder form (Bandeira et al., 2012; Tezcan et al., 2012). This shift in thermal stability can also be observed through the final residue combustion commencing at 635 °C in the film sample.

The addition of glycerol resulted in marked changes in the thermal properties of the MVAIlg film. The second mass loss at 140 °C is an indication of glycerol mass loss rather than early decomposition of the alginate polymer (Momoh et al., 2015), which was seen to follow similar decomposition behaviour to the MVAIlg film. The second and third mass losses at 390 – 490 °C and 660 °C, respectively, indicate that the enhanced thermal stability of the MVAIlg film is maintained in the presence of glycerol.

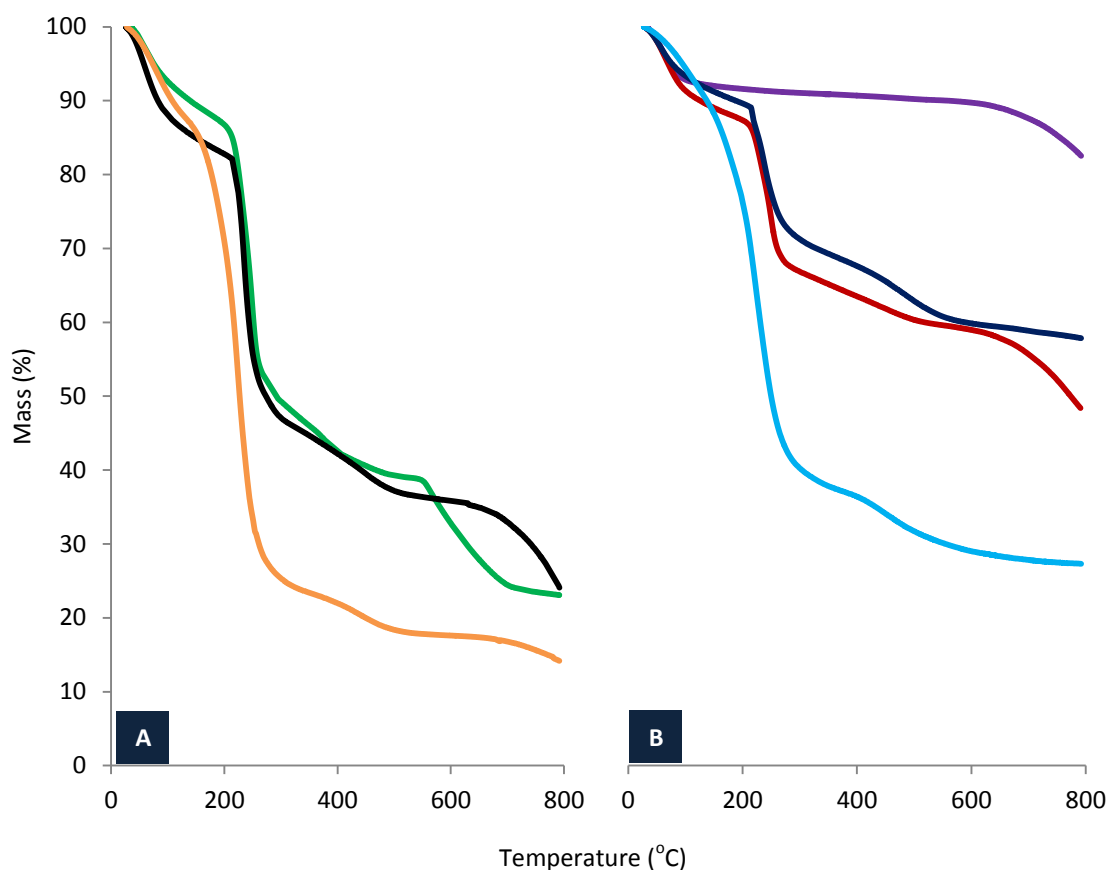


**Figure 4.14.** Mass change (%) of (A) MVAIg powder (green), MVAIg film (black), and MVAIg-GLY film (orange), and (B) LXL21 powder (purple), physical mix of LXL21 and MVAIg (red), MVAIg-LXL21 film (dark blue), and a MVAIg-LXL21-GLY film (light blue) when heated from room temperature to 800 °C.

The thermal behaviour of LXL21 is unique in these set of experiments as its inorganic chemistry does not provide for multiple combustible compounds in the same way as organic molecules. The two main events in the LXL21 TGA curves (figure 4.14) can be explained by evaporation of water from the surface and interlayer spaces of the clay-mineral between 35 – 90 °C then dehydroxylation of the clay-mineral structure above 660 °C (Bandeira et al., 2012; Iliescu et al., 2013; Pongjanyakul and Puttipipatkachorn, 2008). The physical mixture of LXL21 and MVAIg powders did not demonstrate any changes in degradation of alginate at 210 °C, indicating there was no interaction taking

place between the LXL21 and MVAIlg. However, the latter half of the analyses more closely resembled that of LXL21 decomposition with no features of alginate residue combustion. Chen et al. (2012) reported that silicates can retard the diffusion of organic decomposition products and elevate the char yield as the organic compounds experience elongated time at these elevated temperatures. While LXL21 was not forming cross links with MVAIlg it may have been possible for LXL21 to reduce the mobility of MVAIlg decomposition products, which could explain the lack of mass loss expected at 550 °C. The final mass loss of the physical mixture, commencing at 660 °C, was larger than LXL21 alone, which could indicate the release of MVAIlg decomposition product as the clay-mineral structure was destroyed.

When LXL21 and MVAIlg were formulated into a film the thermal behaviour changed significantly (figure 4.14). Whilst the evaporation of water and initiation of MVAIlg decomposition remained unchanged (commencing at 215 °C) the second mass loss from alginate destruction occurred at higher temperature of 425 – 550 °C and the final decomposition, expected at 660 °C, was not observed. The above explanation regarding immobilisation of alginate combustion products does not fit the data presented here and may be explained by an interaction between the LXL21 particles and the MVAIlg polymer chains. The addition of a clay-mineral to alginate has been shown to improve thermal stability by other research teams (Bandeira et al., 2012; Benli et al., 2011; Ray and Okamoto, 2003; Tezcan et al., 2012; Yang et al., 2009) and is the likely explanation here also.

The thermal behaviour of LVAIg powder was almost identical compared to the LVAIg foam with no LXL21 or additives (figure 4.15). This is in contrast to what was observed when alginate was formulated into a film. The foam formulations are less dense and more aerated than the films, which may result in improved heat transfer and combustion during the TGA experimental process. When glycerol was added to the LVAIg foam formulation a number of changes in its thermal behaviour were observed. The initial evaporation of water was more rapid than in the simple LVAIg foam, suggesting that water was less tightly bound within the glycerol-containing foam. The percentage weight loss at this stage was also slightly larger in the glycerol-containing foam, indicating there was around 5.1% more water present (mass loss from water 13.3% vs 8.2%). The mass losses observed at 190 – 280 °C and 390 – 530 °C are due to the depolymerisation and decomposition of the alginate polymer, with the final mass loss commencing at 610 °C representing combustion of the alginate residues (Ghadiri et al., 2013; Iliescu et al., 2013; Pongjanyakul and Puttipipatkachorn, 2008).

The thermal behaviour of a physical mix of LVAIg and LXL21 (figure 4.15) produced similar results to those obtained for the physical mixture of MVAIg and LXL21 (figure 4.14). The initial mass loss due to alginate decomposition was observed at the same temperatures as the control experiment. However, the second decomposition mass loss that appeared at 390 – 530 °C in the control samples was not observed here. As in the MVAIg experiments this may have been due to the LXL21 inhibiting the mobilisation of alginate combustion products (Chen et al., 2012). This is supported by the third mass loss commencing at a cooler temperature of 540 °C which likely

represented the combustion and increased mobility of the alginate residues as the LXL21 is dehydroxylated and decomposed (Ghadiri et al., 2013).

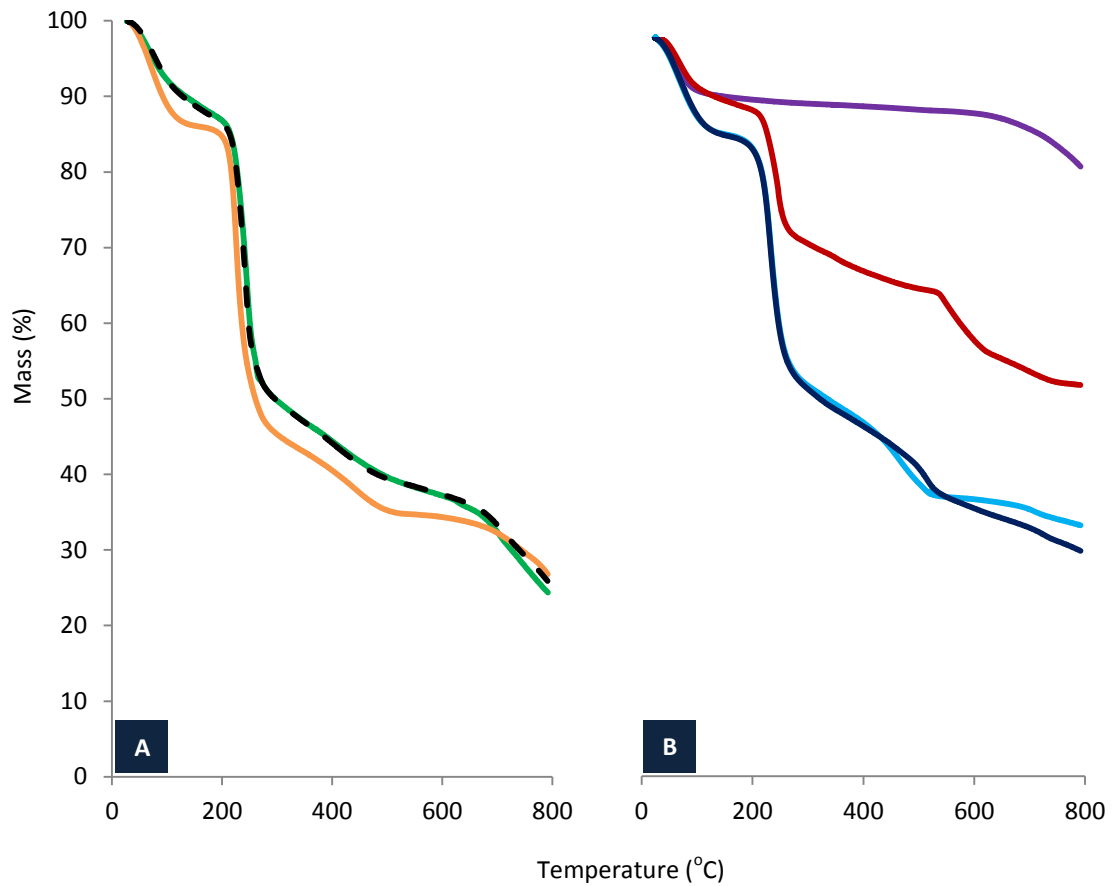


**Figure 4.15.** Mass change (%) of (A) LVALg powder (green), LVALg foam (black dashed), and LVALg-GLY foam (orange), and (B) LXL21 powder (purple), physical mix of LXL21 and LVALg (red), LVALg-LXL21 foam (dark blue), and a LVALg-LXL21-GLY foam (light blue) when heated from room temperature to 800 °C.

The addition of LXL21 into the LVAIlg foam formulation resulted in a number of changes in the TGA results. The initial loss of water was much greater in this formulation, indicating that the LXL21 was able to recruit a significant amount of water to the formulation. The loss of water, and therefore the proportion of water within the foam, was 6% greater compared to the physical mixture of the components. The first stage of alginate decomposition was much larger in the foam sample, compared to the powders, suggesting that the porous nature of the foam allowed for better heat transference through the sample and greater mobilisation of the combustion products. Unlike the film formulations, where the addition of LXL21 was shown to improve thermal stability, this effect was not observed in the foam formulations containing LXL21. The final combustion of alginate residues was seen to commence at 510 °C (30 °C cooler than the physical mixture) which may be a result of the diffuse distribution of LXL21 throughout the formulation being unable to inhibit the decomposition of alginate in the same way it does in a closely-packed film. The addition of glycerol into the LVAIlg-LXL21 foam formulation did not appear to make any significant impact on the thermal behaviour of the resultant formulation. The mass loss recorded between 410 – 530 °C is unlikely to be a result of earlier combustion of LVAIlg but is likely to be a mixture of glycerol volatilisation and LVAIlg decomposition and combustion (Momoh et al., 2015; Shankar et al., 2016). Throughout the TGA of the foam formulations glycerol was shown to have less of an effect on the thermal behaviour than in the film formulations. This is likely due to the proportions of glycerol in each formulation, which are four times greater in the film formulations.



The TGA of CIP shows the powder contains less than 0.8 % water and that, after melting, almost complete decomposition and combustion occurs between 260 – 500 °C (Berhane et al., 2016). The decomposition of CIP is difficult to identify in the TGA for the films and foams (figure 4.16) due to the small amounts of drug present in the formulations in comparison to the amounts of LXL21, alginate, and glycerol. An interesting observation was the amount of sample remaining at 800 °C was higher in both films and foams that contained more CIP.

Logic dictates that samples containing more CIP would combust to a greater extent due to their organic nature, thus leaving less residual mass (Bugatti et al., 2011; Chen et al., 2012). However, this was not observed in these experiments.

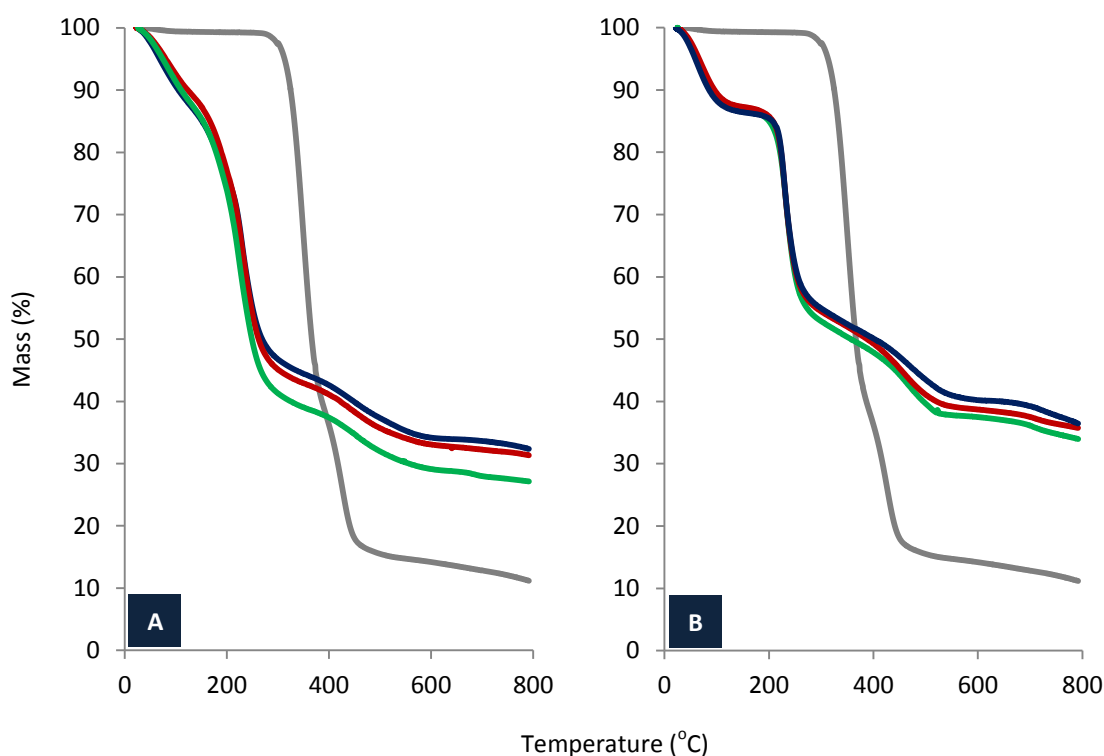


**Figure 4.16.** Mass change (%) of CIP (grey line) containing films (A) and foams (B) made with 20 mg CIP (green line), 130 mg CIP (red line), and 160 mg CIP (dark blue line).

Whilst it is unlikely that the formulation protects the drug at such extremes of temperature it is possible that mobility of these combustion products was reduced, thus increasing the char yield (Chen et al., 2012; Ray and Okamoto, 2003). Therefore, more CIP in the sample could result in a higher char yield and thus a higher mass remaining at the end of the experiments.

#### *4.3.6. Water vapour permeability of film and foam formulations*

Water vapour permeability, expressed as water vapour transfer rate (WVTR,  $\text{g/m}^2/\text{h}$ ), is a vital property of wound care products as it determines a dressing's ability to maintain a moist wound environment and can dictate whether a product can be used on low, moderate or highly exudative wounds (Matthews et al., 2005; Thu et al., 2012). Maintaining a moist wound environment is important for the healing process as it promotes epithelialisation, angiogenesis, debridement, and wound closure as well as reducing pain (Jones et al., 2006; Kokabi et al., 2007; Palfreyman et al., 2010; Singh et al., 2013). A dressing with WVTR of less than  $35 \text{ g/m}^2/\text{h}$  is considered an occlusive dressing in medical practice literature (Bolton et al., 1992) and a WVTR of  $36 - 56 \text{ g/m}^2/\text{h}$  is considered, in the scientific literature, to also maintain a moist wound environment (Kokabi et al., 2007). However, Thu et al. (2012) describe dressings with a WVTR of  $79.2 - 241.7 \text{ g/m}^2/\text{h}$  being suitable for low exuding wounds only and higher WVTR being required for more suppurating wounds. For this reason a control with no dressing was used to represent an open, uncovered, wound and set the baseline WVTR. Commercially available dressings were also examined as comparators.

The control system exhibited a WVTR of 48.42 g/m<sup>2</sup>/h and Opsite® was proven to be an occlusive film dressing with a WVTR of 4.91 g/m<sup>2</sup>/h. KN was shown to significantly reduce WVTR (figure 4.17) whereas no significant change was observed when MMTK10, LXL21 or glycerol were added to the MVAI<sub>g</sub> film. KN has poor swelling and hydration properties when compared to MMTK10 and LXL21. Therefore the 2:1 clays are more likely to adsorb water and hinder the movement of moisture through the films compared to KN. However, when LXL21 and glycerol were present together within the CIP containing films a significant decrease in the WVTR was observed compared to the other samples (except Opsite®) and the control. Depending on the system within which it is present glycerol can either increase or decrease the WVTR of biocomposite films (Vieira et al., 2011). In this research glycerol was only able to induce a reduction in WVTR when CIP was present within the system. As suggested in the FTIR and XRD studies (sections 4.3.3 and 4.3.4, respectively), CIP and glycerol may be able to compete for the LXL21 surface. Therefore, this could increase the proportion of glycerol available not adsorbed onto the LXL21 to affect the nanocomposite film structure thus inhibiting water vapour loss through the film (Singh et al., 2013), improving its ability to maintain a moist wound environment.

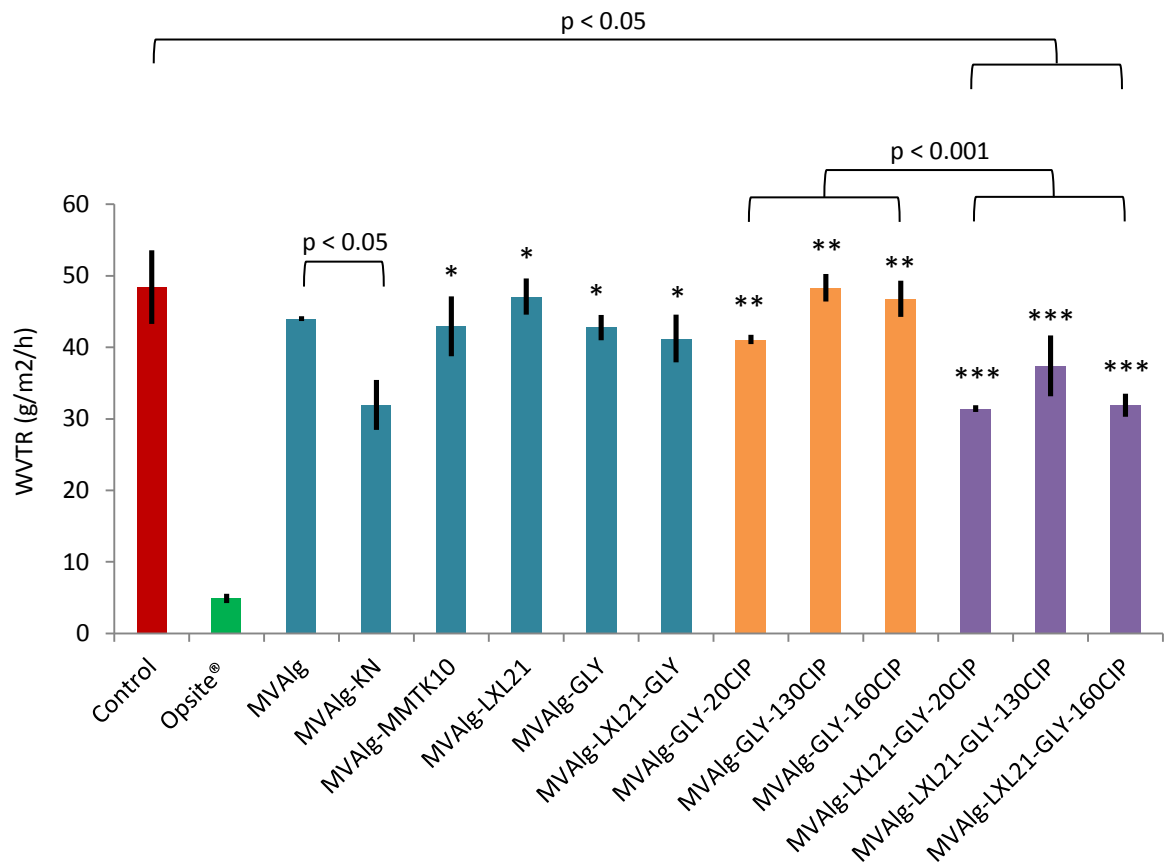


**Figure 4.17.** Water vapour transmission rates (WVTR) for film formulations (mean  $\pm$ SD, n=3). \* Indicates no significant difference in WVTR between the preformulation samples. \*\* Indicates no significant difference in WVTR between CIP containing samples that do not contain LXL21. \*\*\* Indicates no significant difference between the WVTR of the candidate film formulation samples.

All the foam composites tested in this study caused a reduction in the WVTR when compared to the control (figure 4.18), suggesting they can promote moisture retention at the wound surface. The nanocomposite foams were shown to have similar WVTR to Kaltostat®, which is a fibrous non-woven pad made from sodium and calcium alginates (Voncina et al., 2015). These data therefore suggest that the nanocomposite foams handled water vapour and gaseous exchange in a similar way to the branded

equivalent. Lyofoam Max<sup>®</sup> was able to demonstrably ( $p < 0.001$ ) reduce WVTR when compared to Kaltostat<sup>®</sup> and the nanocomposite foams because of its denser, hydrophobic, polyurethane structure (Powers et al., 2016).

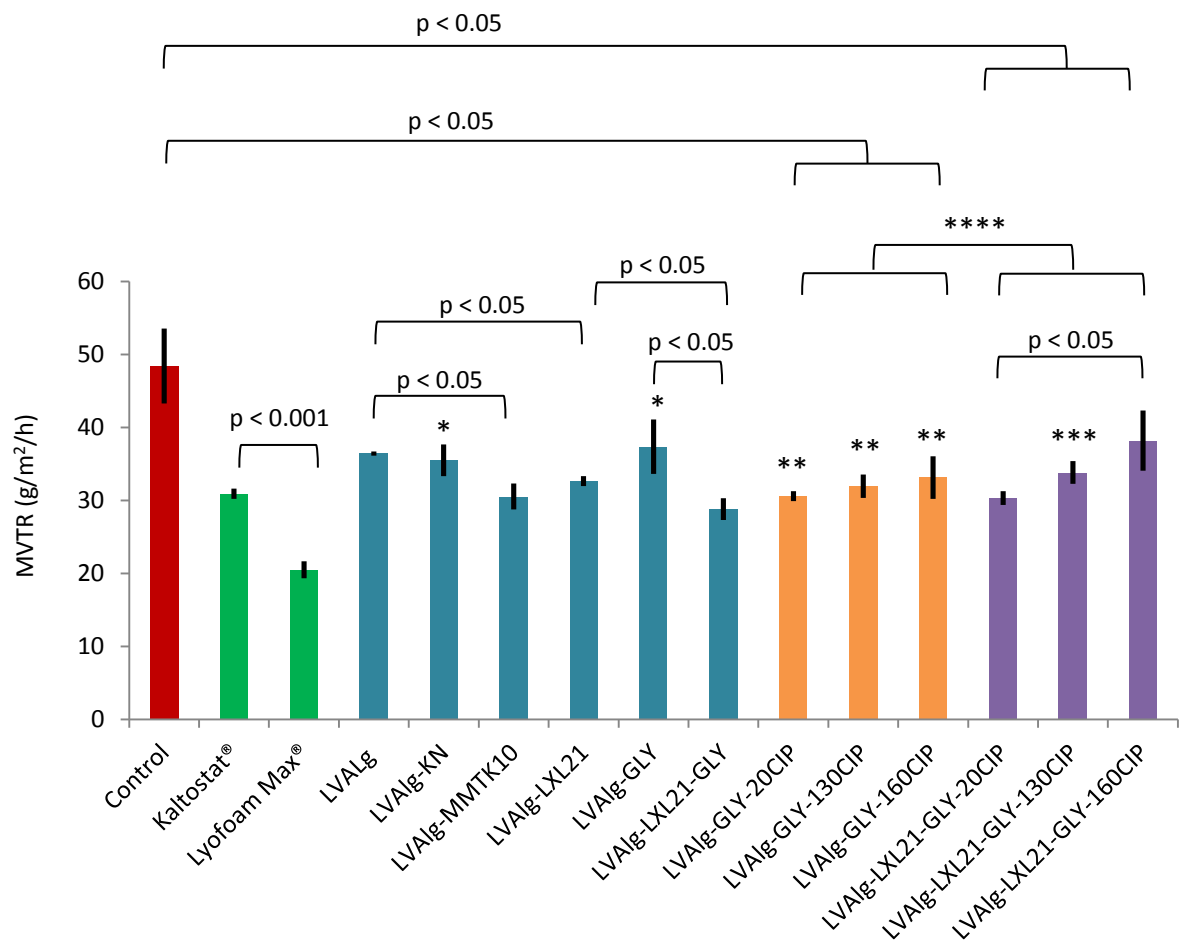


**Figure 4.18.** Water vapour transmission rates (WVTR) for foam formulations. \* Indicates no significant difference in WVTR between LVAAlg, LVAAlg-GLY and LVAAlg-KN samples. \*\* Indicates no significant difference in WVTR between CIP containing samples that do not contain LXL21. \*\*\* Indicates no significant difference between the WVTR of the LXL21-LVAAlg-GLY-130CIP film and the other CIP containing samples. \*\*\*\* Indicates no significant difference in WVTR between the two groups of CIP containing composites.

The increased thickness of these foam composites, compared to the film composites above, may result in an increase in water vapour diffusion time through the composite (Thu et al., 2012), which can explain the difference in WVTR observed. Another contrast between the foam and the film composites was that the LVAIlg-MMKT10 and LVAIlg-LXL21 foams reduced the WVTR significantly ( $p < 0.05$ ) more than the LVAIlg-KN composite. In the preformulation studies it was noted that KN precipitated out during the casting stage and remained in the casting dish after drying. Therefore, it is unlikely that there was sufficient KN available to affect WVTR.

The LVAIlg-LXL21-GLY foam demonstrated a significantly lower WVTR compared to the LVAIlg and LVAIlg-GLY foams. Vieira et al (2011) discussed how glycerol can both increase and decrease the WVTR of a biocomposite film and the data presented here suggest glycerol can have varying effects on alginate films and foams depending on the physical structure of the composite, the amount of glycerol, and presence of clay minerals or drugs. No significant change in the WVTR of the CIP containing biocomposites was observed when compared to the non-drug containing composites. A small degree of intragroup variability was observed, with the LVAIlg-LXL21-GLY nanocomposite containing 160 mg CIP having a greater WVTR than the 20 mg containing composite.

As described above, the competition between CIP and glycerol for the LXL21 surface may increase the amount of glycerol available to alter the nanocomposite structure and thus the WVTR (Singh et al., 2013). It should also be noted that high drug loads can also affect the structure of LXL21. This effect in surface environment and platelet

organisation may result in reduced interactions with water molecules, thus increasing the chance and rate of water vapour transmission through the composite.

Both the film and foam nanocomposites containing LXL21 provided a marked reduction in WVTR compared to the controls, which suggests they are able to retain moisture within the wound and thus promote healing. The wound environment (sections 4.3.7 and 4.3.8) and cytotoxicity experiments (section 4.3.11) described below will be equally important in determining whether these candidate materials show promise for clinical application.

#### *4.3.7. Swelling behaviour of formulations on the wound surface*

Maintaining a moist environment is an important feature of wound dressings, as described above, but the ability of a wound care product to absorb excess moisture and exudate from a wound is equally important. Whilst a moist environment can promote wound healing, too much moisture can promote bacterial growth and also maceration of the surrounding healthy tissue. The data presented here demonstrate differences between the film and foam formulations that may indicate applications for different types of wounds. Both the film and foam dressings were shown to absorb a large amount of SWF during the 96 hour testing period. However, the hydration degree, and therefore amount of SWF absorbed, by the foam nanocomposites was demonstrably greater ( $p < 0.001$ ) than for the film composites (table 4.6). This may well have been the result of increased porosity within the foam composites, caused by the lyophilisation process, allowing for faster and greater SWF uptake.

**Table 4.6.** Hydration degree of film and foam formulations on the synthetic wound surface.

Film sample	Hydration degree	Foam sample	Hydration degree
Opsite®	0.70 ( $\pm 0.90$ )	Kaltostat®	404.78 ( $\pm 159.51$ )
MVAlg	356.22 ( $\pm 34.13$ )	Lyof foam®	949.87 ( $\pm 23.62$ )
MVAlg-KN	365.29 ( $\pm 138.39$ )	LVAIg	907.26 ( $\pm 111.14$ )
MVAlg-MMTK10	285.74 ( $\pm 29.29$ )	LVAIg-KN	764.21 ( $\pm 48.52$ )
MVAlg-LXL21	414.69 ( $\pm 40.14$ )	LVAIg-MMTK10	765.18 ( $\pm 38.93$ )
MVAlg-GLY	522.56 ( $\pm 33.78$ )	LVAIg-LXL2	719.71 ( $\pm 34.95$ )
MVAlg-LXL21-GLY	391.80 ( $\pm 10.99$ )	LVAIg-GLY	1212.57 ( $\pm 114.50$ )
MVAlg-GLY-20CIP	562.13 ( $\pm 17.32$ )	LVAIg-LXL21- GLY	980.38 ( $\pm 70.35$ )
MVAlg-GLY-130CIP	495.71 ( $\pm 21.22$ )	LVAIg-GLY-20CIP	1174.51 ( $\pm 38.64$ )
MVAlg-GLY-160CIP	489.65 ( $\pm 35.30$ )	LVAIg-GLY-130CIP	1103.87 ( $\pm 41.83$ )
MVAlg-LXL21-GLY-20CIP	357.07 ( $\pm 20.11$ )	LVAIg-GLY-160CIP	1196.38 ( $\pm 51.99$ )
MVAlg-LXL21-GLY-130CIP	327.32 ( $\pm 64.87$ )	LVAIg-LXL21- GLY-20CIP	1022.94 ( $\pm 118.33$ )
MVAlg-LXL21-GLY-160CIP	313.73 ( $\pm 11.98$ )	LVAIg-LXL21- GLY-130CIP	923.22 ( $\pm 27.95$ )
		LVAIg-LXL21- GLY-160CIP	700.80 ( $\pm 47.26$ )

Over the 96 hour duration, the film samples changed from being transparent to an opaque white colour. Whilst the foam samples were opaque at the start of the test, the end product was a hydrogel with similar opaque-white tones as the films. This change in light transmission is likely the result of calcium ions within the absorbed SWF creating cross-links between the G-G blocks of the alginate chains (Davidovich-Pinhas and Bianco-Peled, 2010). This effect is also the reason why the alginate film and foam samples did not lose structural integrity during the tests, as has been described in other examinations of alginate as a wound-dressing material.

The change in size of MVAlg films containing clay-minerals was significantly less ( $p < 0.05$ ) compared to the MVAlg with no other additives (figure 4.19). It is well known that clay-minerals can act as cross-linkers within a wide range of polymeric materials, which is why they have been examined as an additive to these materials (Alboofetileh et al., 2013; Ghadiri et al., 2013; Shikinaka et al., 2012; Zhang et al., 2009).



As demonstrated by the FTIR analyses (section 4.3.3), LXL21 was able to form hydrogen bonds with the MVAIlg chains and is therefore likely to be acting as a cross-linker between MVAIlg chains. This will result in more rigidity within the nanocomposite materials and therefore restrict polymer mobility on hydration and result in less change in size on SWF absorption. However, the addition of LXL21, KN, and MMTK10 did not result in a significant change in the hydration degree of these film materials (table 4.6), suggesting that the overall ability to absorb fluid from a wound is not impeded. Moreover, the absorption of fluid may be supported by the presence of LXL21, compared to the other clay-minerals, as its high surface area allows for greater interaction with water.

The addition of glycerol to the MVAIlg films also resulted in a reduced size change compared to the MVAIlg film containing no additives. As a plasticiser glycerol reduces the interactions between polymeric chains so this effect is unlikely a direct result of alginate-glycerol interactions. Glycerol is a hygroscopic compound and has been used as an osmolyte, to enhance water absorption (Björklund et al., 2013). Therefore, it is reasonable to suspect that glycerol was able to enhance the absorption of SWF into the alginate film so that calcium bridges were formed faster, thus limiting the change in size. This enhanced fluid absorption is also demonstrated in table 4.6, which demonstrates the significant ( $p < 0.05$ ) increase in hydration degree of the MVAIlg-GLY film compared to the MVAIlg film.

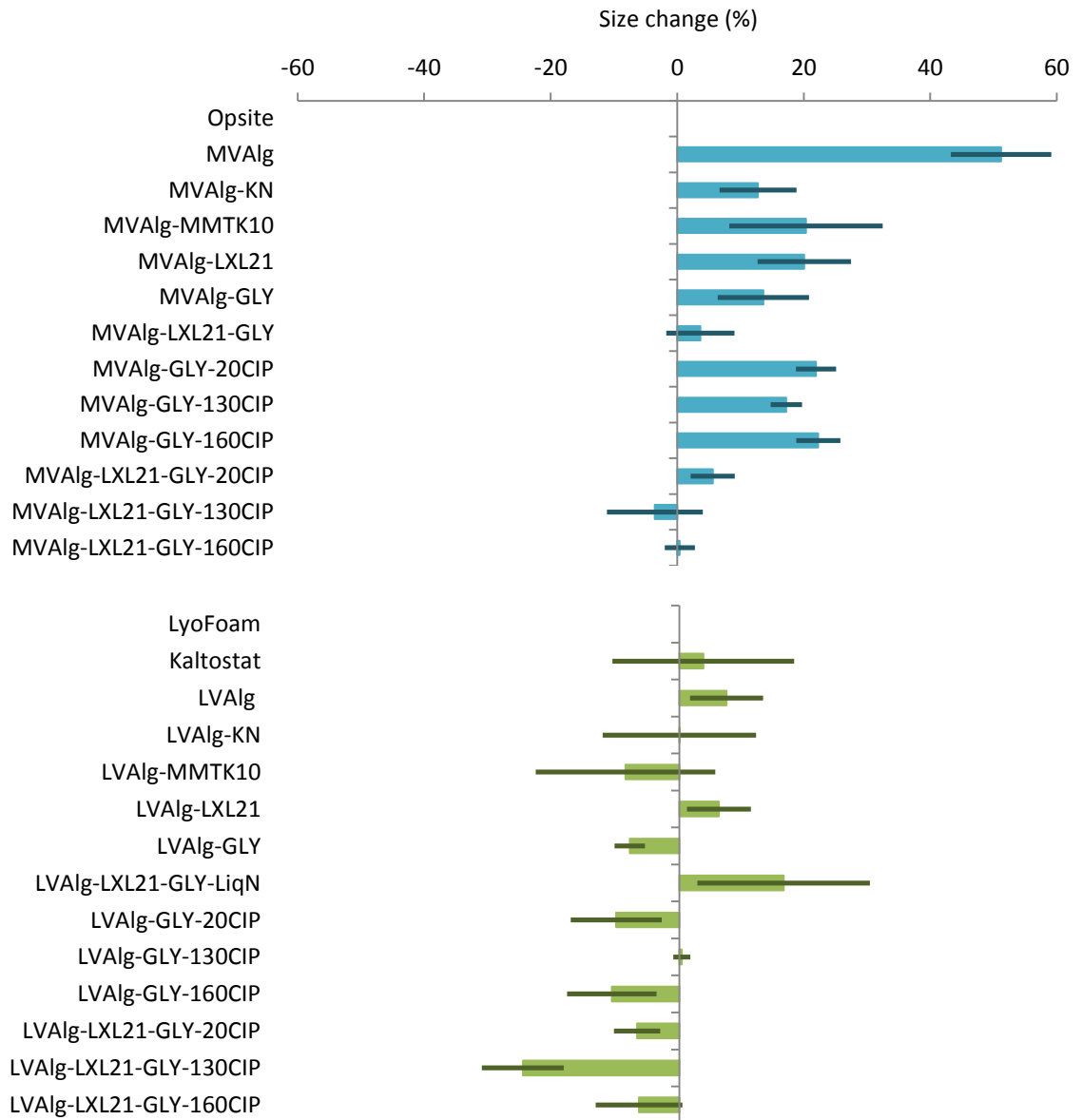


**Figure 4.19.** Average (mean  $\pm$ SD, n=3) percentage change in size of nanocomposite films (blue bars) and foams (green bars) when on the synthetic wound environment.

This effect of glycerol is not seen in the presence of LXL21 as the percentage change in size of films containing MVAIg-LXL21-GLY was significantly ( $p < 0.05$ ) smaller compared to those films that did not contain both of these additives. The hydration degree of the MVAIg-LXL21-GLY films was also significantly ( $p < 0.001$ ) lower compared to the

other composite films examined. These results point towards a complex interaction between the MVAIlg, LXL21, and glycerol and not just a simple restriction in the mobility of alginate chains. As described in the FTIR and XRD analyses, glycerol may be able to interact with and adsorb onto LXL21. This may have the dual-effect of reducing the hygroscopic properties of glycerol, but also reducing the water and electrolyte adsorptive capacity of LXL21, resulting in an overall limitation on swelling size change and hydration degree.

As shown in figure 4.19 the nanocomposite foams behaved very differently compared to the films. The foams had a propensity to shrink or remain a relatively static size and expressed a higher degree of inter-sample variation. The shrinkage of these materials on absorption of SWF is a result of calcium ions forming bridges between alginate strands, especially in the G-G blocks, resulting in a much tighter, contracted, network of alginate chains. The effects of glycerol within these composite foams were similar to those observed in the composite film materials in that the LVAIlg-GLY foam shrank, whereas the LVAIlg foam with no additives was shown to increase in size. This supports the theory that glycerol was able to promote the rapid absorption of SWF into the composites, resulting in enhanced calcium-bridge formation. The hygroscopic effects of glycerol are also demonstrated through the significant ( $p < 0.001$ ) increase in hydration degree of the LVAIlg-GLY foam compared to the LVAIlg foam with no additives.

In a similar vein to the films, the addition of glycerol to the LVAIlg-LXL21-CIP foam composites also lead to a significant drop in hydration degree ( $p < 0.05$ , when compared as groups) although this effect was much less pronounced in the foam

composites; likely due to the reduced amount of glycerol used in formulating the foams. The influence of LXL21's ability to absorb fluid within these nanocomposites is demonstrated in the series of foams containing LXL21 and CIP. As the amount of CIP absorbed onto the LXL21 was increased the hydration degree decreased due to a reduced uptake of fluid, supporting the theory that substrates absorbed onto the LXL21 surface will lead to a reduction in SWF uptake.

These results show that both film and foam nanocomposites are able to absorb large amounts of wound fluid making them promising candidate materials for use on suppurating wounds. These data also prove these materials remain structurally intact over a 96 hour period, thus requiring less frequent changing, and the calcium bridges formed within the alginate matrix could also prevent particulate matter being generated during dressing changes. In particular, the ability of LXL21 to restrict size change during fluid absorption, and also contribute to the absorption process, is an important finding of this work. It was also proven that glycerol makes multiple important contributions to these composite materials.

As well as giving a useful estimation into the swelling behaviour of these composite materials, this study has also developed and utilised a novel synthetic wound environment not yet reported in the scientific literature. The research presented here makes several advances on previously published work that have used over-ripe melon (Matthews et al., 2005), simple gelatine gels (Ng and Jumaat, 2014; Thu et al., 2012), electrolyte solutions (Momoh et al., 2015; Rezvanain et al., 2017), or water (Kokabi et

al., 2007) to predict the behaviour of polymeric composites, both with and without phyllosilicates, in a wound environment.

#### *4.3.8. Adherence of formulations to the wound surface*

Ideally, wound dressings should have low or no adherence to the wound surface so that the migratory phase and re-epithelialisation occurs unopposed and that damage is not inflicted upon the wound-bed when the dressing is removed or changed (Hutchinson, 1990; Morgan, 2002). Non-adherent dressings are of benefit in dry wounds, whereas low adherent dressings may be of particular benefit in suppurating wounds (Hanna and Giacomelli, 1997; Palfreyman et al., 2010; Scottish Intercollegiate Guidelines Network, 2010). As the methodology utilised in this study is essentially a semi-quantitative method, adapted from Matthews et al (2005), particular attention needs to be paid to how the composite films and foams behave in comparison to the readily available commercial products Opsite<sup>®</sup>, Kaltostat<sup>®</sup>, and Lyofoam<sup>®</sup>.

Of the films, Opsite<sup>®</sup> was shown to be the most adherent as it did not migrate throughout the duration of the experiments (Figure 4.20 A). This observation, coupled with its negligible hydration degree and low WVTR, fits well to the clinical indication for this dressing as it is only intended for lightly exuding wounds (Joint Formulary Committee, 2017). These observations may also be extrapolated to suggest that the methodologies used in these studies are able to predict the behaviour of the composite materials in a wound environment. Therefore, it is reasonable to suggest that all the other composite films tested were less adherent to the wound surface and therefore may be beneficial in wounds generating a greater amount of exudate.

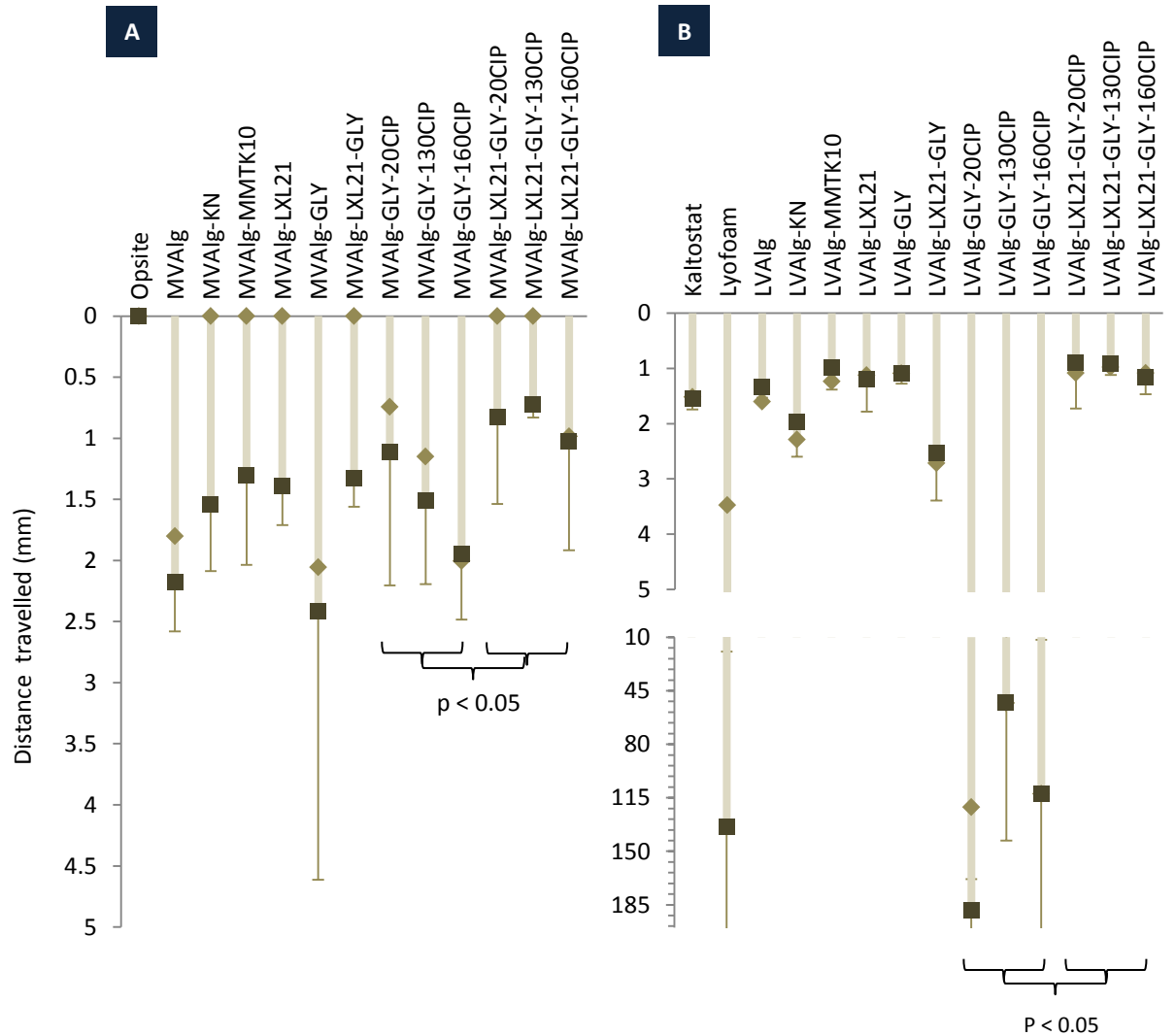


**Figure 4.20.** Movement of film (A) and foam (B) dressings down the synthetic wound surface over 24 hours (light brown diamonds) and 96 hours (dark brown squares). Thick lines represent the average (mean, n=3) movement of formulations down the wound surface. Standard deviations are given by the thin lines (error bars)

Composite films containing clay minerals were shown to reside for at least 24 hours before migrating, unlike the films of MVAIlg, MVAIlg-GLY, and MVAIlg-GLY-CIP that all showed migration within 24 hours. By 96 hours all of the composite films had migrated down the synthetic wound surface due to the increasing mass of the composites over time as they took on more fluid.

When analysed as groups, the MVAIlg-LXL21-GLY-CIP films were significantly ( $p < 0.05$ ) more adherent than the MVAIlg-GLY-CIP films, which further proves that LXL21 is able to increase adherence to the synthetic wound surface. This phenomenon has also been reported in other studies where clay-minerals are proposed to increase adherence to the wound surface through i) interactions between the clay-mineral surface and important proteins such as fibronectin, and ii) through clay-mineral particles acting as a focus for cellular adherence (Gaharwar et al., 2012; Ghadiri et al., 2013).

Although not statistically significant, the increasing proportion of CIP within the non LXL21 containing films appeared to reduce the surface adherence. The adherence properties of alginates are known to be derived from the large number of carboxyl and hydroxyl groups which are able to form hydrogen bonds with other materials, such as agar (Wang and Rhim, 2015), and the protein and polysaccharide rich wound-bed (Pongjanyakul and Suksri, 2010). While not detected by FTIR due to masking of characteristic absorbance bands, the observations made in this study hint at an interaction between CIP and the MVAIlg polymer resulting in reduced ability to form hydrogen bonds with the synthetic wound surface.

Of the commercially available foams Kaltostat® was shown to be significantly ( $p < 0.05$ ) more adherent than Lyofoam®. Broadly speaking, the composite foams expressed similar adhesive strength to the composite films and were comparable to the adhesiveness of Kaltostat®, except the LVAIg-GLY-CIP composite foams that demonstrated greatly reduced surface adhesion that was more comparable to Lyofoam® (figure 4.20 B). Therefore, it would be fair to assume that these composite foams could be suitable for use on moderately exuding wounds in the same way as Kaltostat® and Lyofoam® (Bennett-Marsden, 2010; Joint Formulary Committee, 2017). The absence of LXL21 in the CIP containing foams resulted in a significant decrease in the surface adherence. This may be explained, as above, by a potential interaction between CIP and alginate resulting in a reduced opportunity for the alginate to form hydrogen bonds with the synthetic wound surface (Pongjanyakul and Suksri, 2010). The absence of LXL21 in these samples also means the ability of a clay-mineral to also form interactions with the wound surface is not present, resulting in lower adhesion (Ghadiri et al., 2013).

These results are limited by their design and future research into the optimisation and clinical application of these materials will need to employ more sensitive methods to fully quantify wound-bed (Pongjanyakul and Suksri, 2010; Singh et al., 2013) and cellular adhesion (Ghadiri et al., 2013; Qi et al., 2013). However, it is promising that the migrations observed were comparable to readily available products suggesting that they should not adhere to the wound-bed in a harmful way.



#### 4.3.9. Drug-release profiles

Achieving modified and prolonged release of drugs is often desirable to achieve therapeutic benefit, reduce toxicity, and to encourage patient adherence (Rodrigues et al., 2013; Viseras et al., 2008). Whereas many modified-release oral preparations aim to reduce dosing to once or twice a day, dependant on pharmacokinetics (Qiu and Lee, 2017), the ideal release profile for a wound dressing should be in the order of days (Sandstrom, 2011). This would ensure that sufficient drug is eluted into the tissue continuously between dressing changes, which should be as infrequent as possible to support wound healing.

Figures 4.21 and 4.22 demonstrate the difference in the release profile of the LXL21-CIP composite compared to the MVAIlg-LXL21-GLY-CIP nanocomposite films and foams. Release of CIP from the LXL21-CIP composite showed rapid drug release within the first 15 minutes, followed by a slower release profile that reduced in rate as time progressed – notably between 4 to 6 hours of release. This initial burst release is likely related to the presence of CIP on the external surface of the LXL21 particles (Iliescu et al., 2013), and would have been plentiful given the large CIP load of this composite. The reducing rate of release between 15 minutes and 6 hours is a result of CIP being released from the interlayer space of LXL21, initially through swelling of the layers and diffusion of the drug, then subsequent release of the CIP adsorbed onto the clay mineral surface (Hua et al., 2010; Iliescu et al., 2013). In chapters 2 and 3 it was proposed that drug adsorption onto these clay minerals was likely down to cation exchange, alongside other interactions. In total, 87.7% of the CIP within the LXL21-CIP composite was released over the 24 hour period measured.

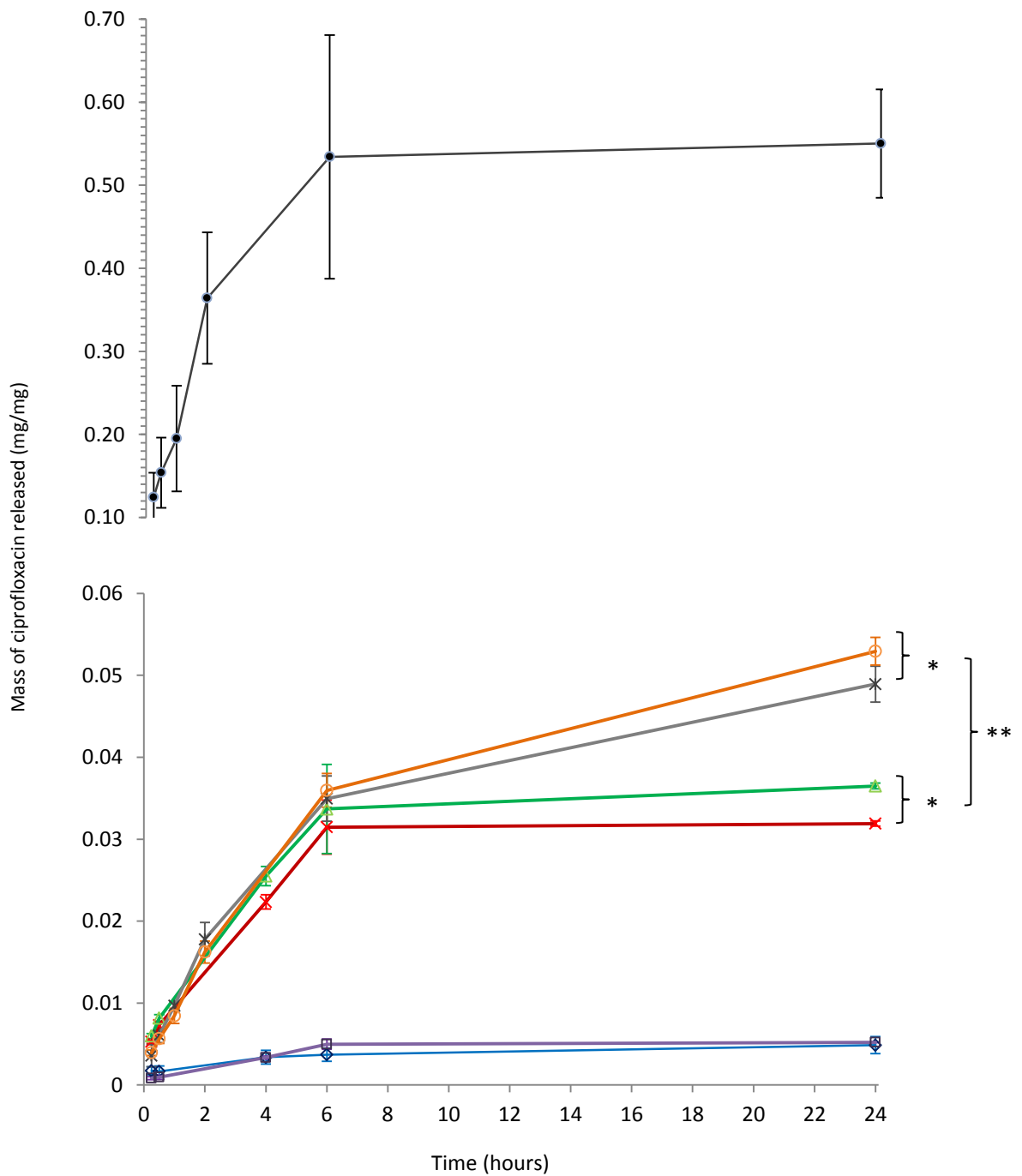


**Figure 4.21.** Profiles of ciprofloxacin released (mean average mass of CIP per mg of sample,  $\pm$ SD,  $n=3$ ) from film formulations containing MVALg-LXL21-GLY-20CIP (blue diamonds), MVALg-LXL21-GLY-130CIP (red crosses), and MVALg-LXL21-GLY-160CIP (green triangles), alongside foams containing LVALg-LXL21-GLY-20CIP (purple squares), LVALg-LXL21-GLY-130CIP (grey crosses), LVALg-LXL21-GLY-160CIP (orange rings), and LXL21-CIP (black circles). \* and \*\* indicate significant difference at  $p < 0.05$  and  $p < 0.001$ , respectively, between highlighted values.

The remaining 12.3% (77.12 mg) was less than the calculated monolayer coverage, which is suggestive of cation exchange taking place between the CIP and the cations ( $\text{Ca}^{2+}$  and  $\text{Na}^+$ ) within the SWF (Iliescu et al., 2013; Joshi et al., 2009; Pongjanyakul and Suksri, 2010) but may also suggest that the remaining CIP was interacting with the LXL21 via different mechanisms (Hua et al., 2010; Joshi et al., 2010). Jung et al (2008) describe a 'zipping effect' that can take place as cations from the release medium exchange with the drug molecules on a Laponite<sup>®</sup> surface. As the inorganic cations are much smaller than the organic drug molecules a reduction in interlayer space occurs at the edge of clay mineral platelets, essentially zipping the structure together and inhibiting drug release from the inner-most regions of the interlayer space. This phenomenon may have been taking place in the LXL-CIP composite, resulting in retention of CIP after 6 hours.

The release of CIP from the nanocomposite films and foams increased as the amount of drug within the composites increased. As could be expected, significantly ( $p < 0.05$ ) more CIP was released from the composites containing 160 mg CIP compared to those containing 130 mg CIP. Laws of diffusion are thought to play a significant role in the release of drugs from phyllosilicate-polymer composites, with concentration gradient being of notable importance (Dziadkowiec et al., 2016; Pongjanyakul and Suksri, 2010). The concentration gradients within the nanocomposites containing 160 mg would have been higher than for the 130 mg containing composites, and been maintained for a longer period, therefore increasing the amount of CIP released.

After 4-hours significantly ( $p < 0.001$ ) greater amounts of CIP were released from the nanocomposite foams containing 130 mg and 160 mg CIP compared to their film counterparts (figure 4.21). By examining the relative percentage CIP released over time (figure 4.22) it can also be seen that the nanocomposite foams containing 130 mg and 160 mg CIP had less of a profound burst release and demonstrated a release profile that was more appropriate to a modified release preparation. These differences in release profiles may be directly related to the internal structure of the film and foam matrices. For example, the nanocomposite films were much thinner and had a denser structure when compared to the foams, which would have resulted in a greater concentration of CIP per unit volume of composite, therefore creating a greater concentration gradient that resulted in more rapid CIP release.

While the zipping effect of the SWF cations on LXL21 is likely to be similar between the different formulation types, the effect of calcium ions on the alginate matrix may have differing effects on the release of CIP from these formulations. When Gonçalves et al. (2013) investigated the release of doxorubicin from Laponite-alginate matrices they noted the effect of calcium bridging on rate of drug release; concluding that alginate matrix shrinkage made the release of drug more arduous. This effect may also explain some of the differences observed in the release of CIP whereby the formation of calcium-alginate bridges within the films resulted in a denser matrix structure (Davidovich-Pinhas and Bianco-Peled, 2010) and thus greater inhibition in CIP release compared to in the foams. This is supported by the ongoing, yet, slowed release of CIP from the nanocomposite foams after 6 hours in SWF.

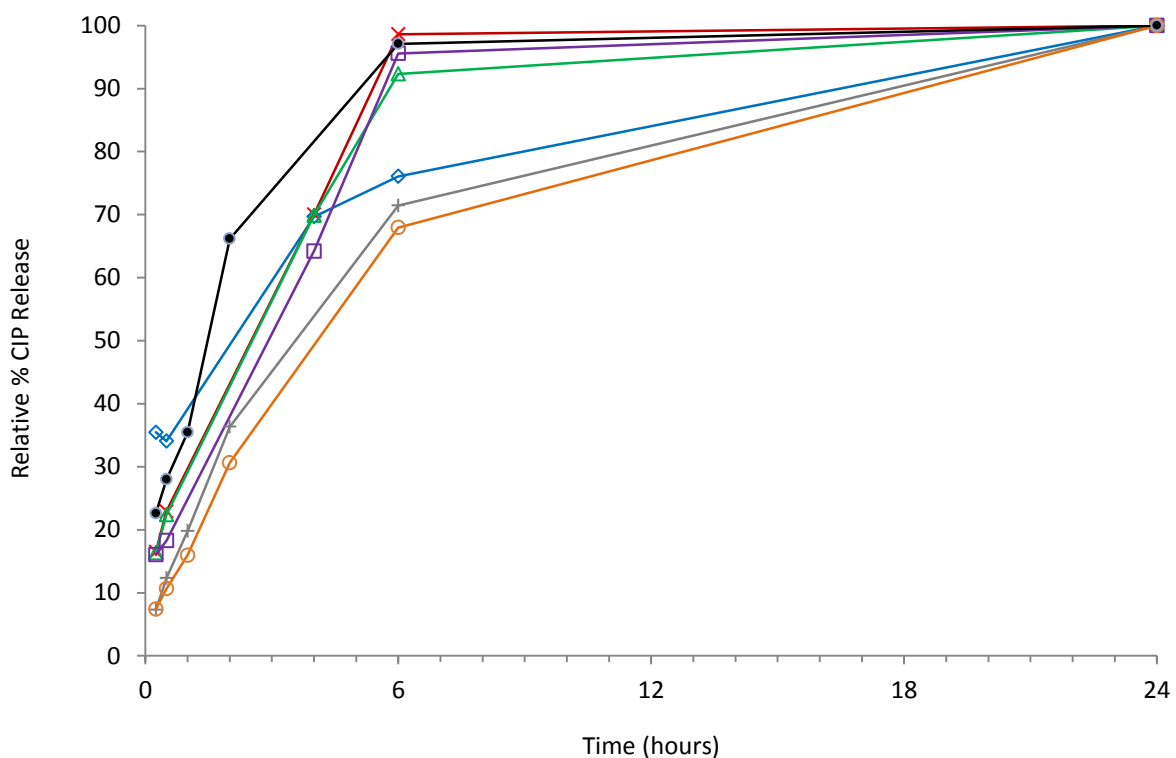


**Figure 4.22.** Profiles of ciprofloxacin released (% relative to 100% released by each sample, mean average,  $n=3$ ) from film formulations containing MVAIlg-LXL21-GLY-20CIP (blue diamonds), MVAIlg-LXL21-GLY-130CIP (red crosses), and MVAIlg-LXL21-GLY-160CIP (green triangles), alongside foams containing LVAIlg-LXL21-GLY-20CIP (purple squares), LVAIlg-LXL21-GLY-130CIP (grey crosses), LVAIlg-LXL21-GLY-160CIP (orange rings), and LXL21-CIP (black circles).

While this study is limited to a 24-hour window it can be seen that the incorporation of LXL21-CIP composites into an alginate matrix modifies and prolongs drug release. These data suggest that the nanocomposite foams containing 130 mg CIP or greater may be able to continue beyond the 24-hour period, which is a promising property for these candidate wound dressing materials. Further studies will be required to determine the release profiles of these materials over a 96-hour period and will also

need to consider alternative methodologies such as the utilisation of Franz-cells (Ito et al., 2001; Perkins and Heard, 1999; Thu et al., 2012) and animal models (Vijayan et al., 2013) to fully determine dermis, subcutaneous and wound-bed penetration and systemic absorption.

#### *4.3.10. Antimicrobial properties*

These microbiological studies adapted the methods described in section 2.2.4, which impregnated the molten agar with bacterial cultures so that confluent growth occurs throughout the medium. Other research in this field applied the bacterial culture to the surface of the ready-set agar (Ambrogi et al., 2016; Das et al., 2014), which can result in uneven growth across the plate (Matuschek et al., 2014) but is also not representative of an infected wound environment where bacteria can grow within the deeper tissues (Siddiqui and Bernstein, 2010). Therefore, the methods used in this study are more representative of activity in an infected wound environment.

The nanocomposite films and foams that did not contain CIP were not shown to generate clearance zones and it can therefore be assumed that these materials have no inherent activity on the bacterial species tested against (figures 4.23 and 4.24). This finding also supports the conclusion that any zones of inhibition observed was a result of CIP being released from the composites in an active form.

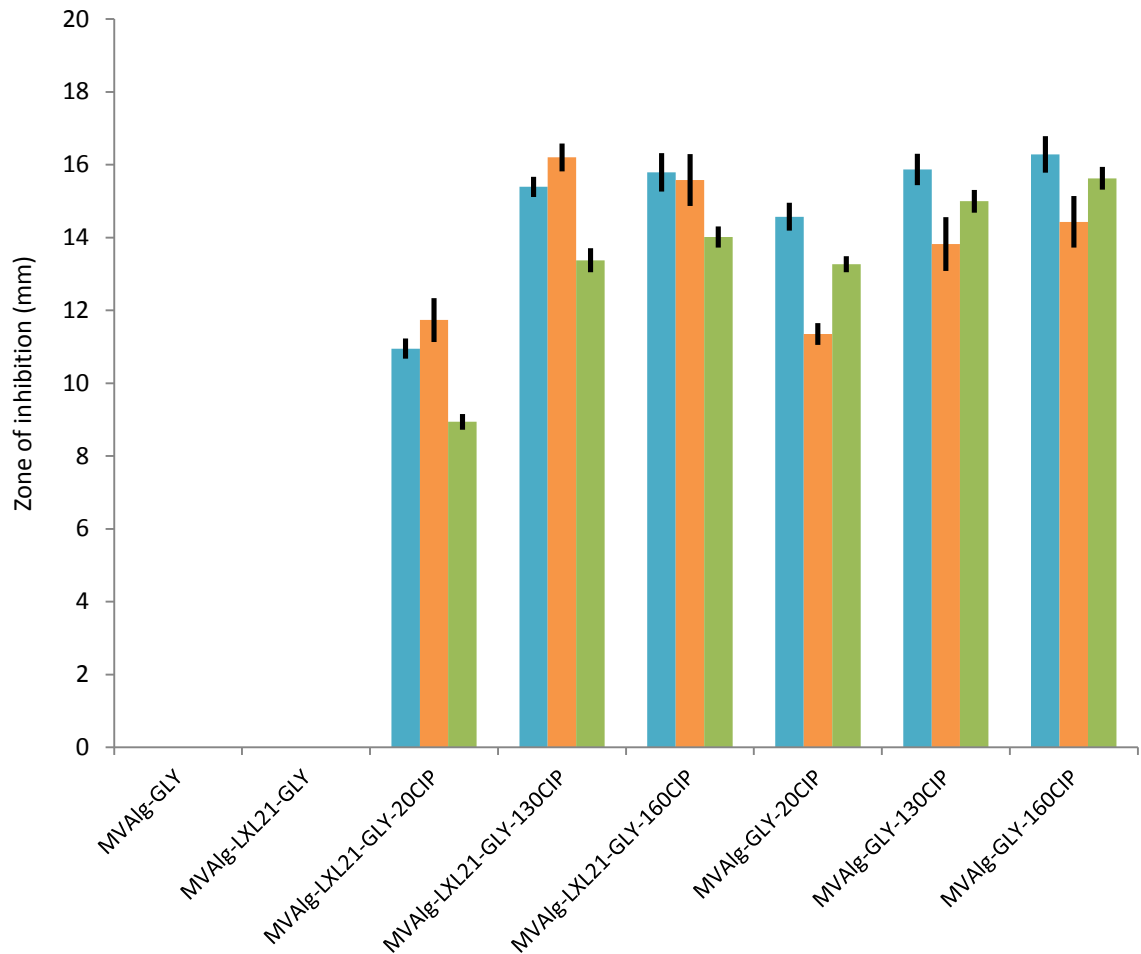


**Figure 4.23.** Zones of inhibition (mean  $\pm$ SD, n=3) generated by CIP containing nanocomposite films against *P. aeruginosa* (blue), *S. epidermidis* (orange), and *P. acnes* (green).

Through its unique mode of action of affecting bacterial DNA functionality, CIP was able to inhibit the growth of *S. epidermidis*, *P. aeruginosa* and *P. acnes* (Vance-Bryan et al., 1990; Wispelwey, 2005). The zones of inhibition extended beyond the dimensions of the composite samples placed onto the agar, demonstrating that CIP was able to diffuse away from the nanocomposite matrix and through the growth medium. These zones of inhibition, as demonstrated in chapters 2 and 3, grew in diameter as the concentration of CIP within the composite increased. A significant ( $p < 0.05$ ) increase in

efficacy was observed between the composites containing the lowest concentration of CIP compared to those containing higher concentrations. However, while the efficacy was shown to increase as the concentration of CIP was increased from 2.42% to 2.96% w/w in nanocomposite films and 2.28% to 2.80% w/w in nanocomposite foams the difference was not statistically significant ( $p$  0.078 – 0.465).

It is worth noting that the zones of inhibition only demonstrate efficacy over a period less than 24 hours, due to the design of the test and the rapid proliferation of these bacterial strains (Matuschek et al., 2014). It should also be noted that CIP exhibits concentration-dependant killing; requiring high concentrations to be bactericidal (Silva et al., 2011). Therefore, when CIP induces bacteriostasis it halts cellular activities and proliferation to such an extent that the host's immune system can destroy the bacteria. Given the prolonged release profiles observed in section 4.3.9, especially for the nanocomposite foams, it is likely that the data presented in figure 4.24 is an underestimation of the true efficacy of these materials. Coupled with ongoing drug release and wound-bed neutrophils, macrophages and leucocytes (Boateng et al., 2008) the true clearance of bacteria from the wound is likely to be greater. However, animal and human modelling will be needed to fully characterise this effect and also determine the role of absorption and clearance through the capillary bed.



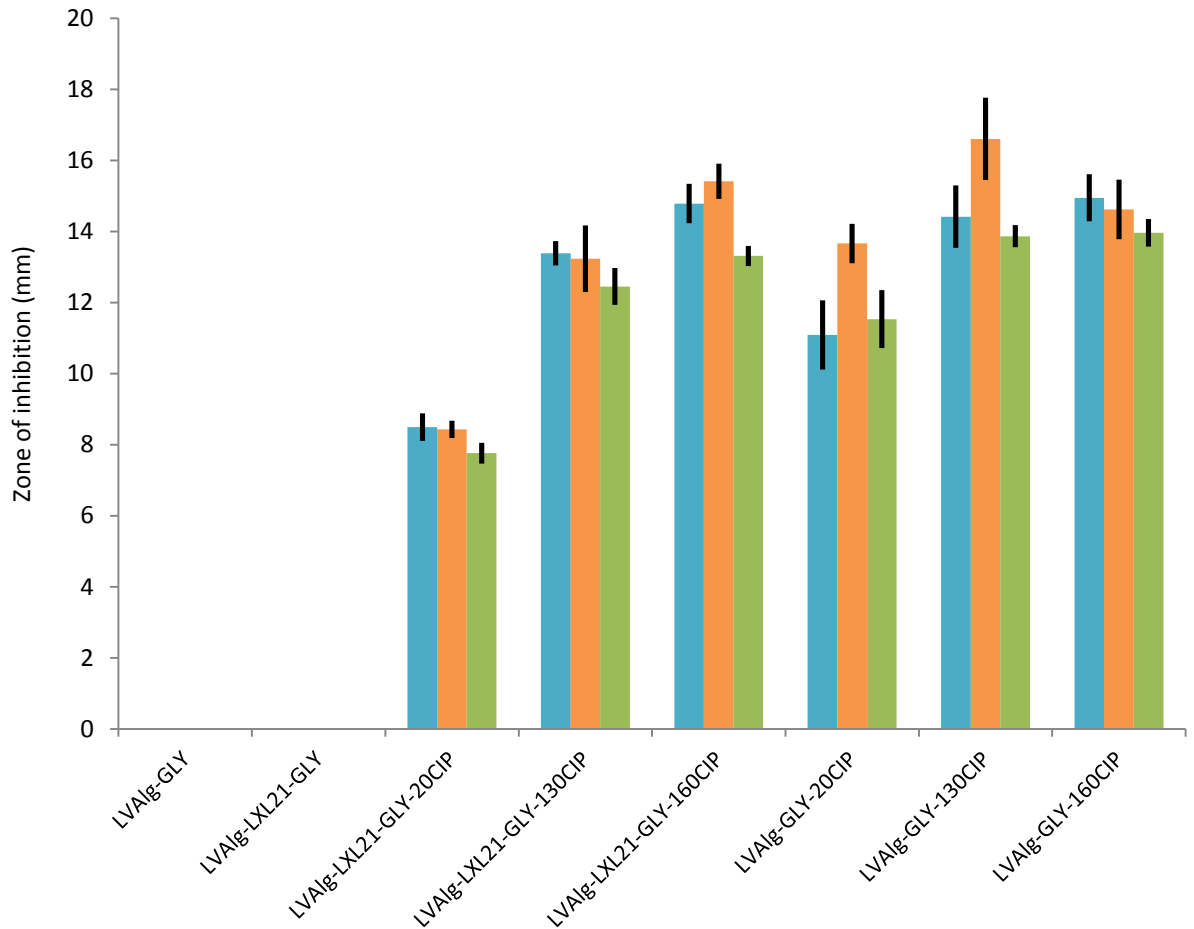


**Figure 4.24.** Zones of inhibition (mean  $\pm$ SD, n=3) generated by CIP containing nanocomposite foams against *P. aeruginosa* (blue), *S. epidermidis* (orange), and *P. acnes* (green).

The results presented here prove that these nanocomposite materials are able to affect a broad spectrum of common wound pathogens, making them promising materials for wound care. The extended zones of inhibition are also a promising property of these materials as it may be possible to design targeted therapies for more localised infections, or design hybridised-dressings where the CIP-containing materials are in distinct domains that deliver adequate CIP to the wound but allow other beneficial wound care materials to be present concurrently.

#### 4.3.11. Keratinocyte cell viability

Determining the effect of new materials on cell viability is an important step before moving onto animal then human models (Rezvanain et al., 2017). By measuring the impact of a material on cell viability it is possible to determine whether the material is i) biocompatible and ii) able to support cell growth. Research into the effects of polymer-phyllsilicate composites on cell function is in its infancy (Dawson and Oreffo, 2013) and as such there is currently scant evidence regarding the effects of these types of materials on keratinocytes. Ambrogi et al (2017) reported reduced cytotoxicity of keratinocyte and fibroblast cell lines when chlorhexidine was loaded into a montmorillonite-chitosan nanocomposite, compared to chlorhexidine alone.

All the materials tested allowed for greater than 70% viability (figure 4.25) of the keratinocyte (HaCaT) cell-line and therefore acceptable biocompatibility as described in ISO 10993-5 (British Standards Institute, 2009; Rezvanain et al., 2017). LVAIlg, MVAIlg, and LXL21 powders were all shown to significantly reduce HaCaT viability over the time period tested, as did the nanocomposite film of LVAIlg-LXL21-GLY and all of the nanocomposite foams. Glycerol and ciprofloxacin did not result in a reduction in cell viability, thus affirming the safety in this human cell line. While the safety of systemic CIP has been known for years, through its regular use in modern medicine (Wispelwey, 2005), the data presented here may represent evidence of the safety of CIP when applied topically to the wound environment; vital information for this research.

The CIP containing nanocomposite films did not cause a significant reduction in HaCaT cell viability ( $p = 0.077, 0.074, 0.375$ ) and were found to support cell growth

significantly ( $p < 0.05$ ) better than the nanocomposite foams. This is not necessarily a reflection of different toxicity/safety levels as no significant difference ( $p > 0.05$ ) in cell viability between LVAIg and MVAIg was observed. This difference may be explained by the differences in formulating each type of composite (Ghadiri et al., 2013).

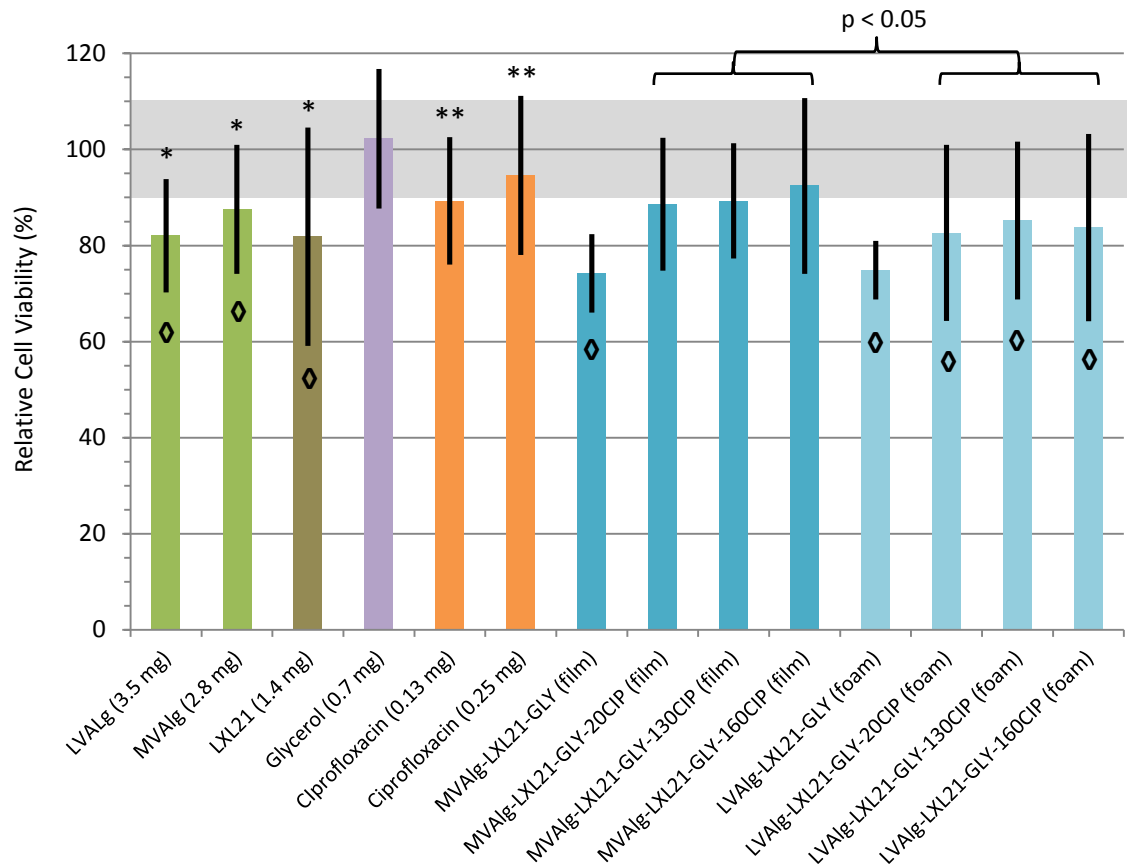


**Figure 4.25.** HaCaT cell viability after 24 hours treatment with test materials (mean  $\pm$ SD,  $n=3$ ), relative to the cell viability of untreated HaCaT cells (grey zone;  $100 \pm 9.9\%$ ). \* Indicates no significant difference between these components. \*\* Indicates no significant difference between these CIP samples. ◊ Indicates these samples have significantly ( $p < 0.05$ ) reduced cell viability compared to the control.

Research investigating the effect of phyllosilicate-polymer composites has given particular attention to the role of phyllosilicates within these materials. A number of teams have shown that clay-mineral particles can increase cell adhesion by directly interacting with surface proteins, such as fibronectin, and even acting as a point of attachment for cells (Ghadiri et al., 2013; Schexnailder et al., 2010; Zheng et al., 2007). With regards to this latter point, microscopy undertaken by Ghadiri et al. (2013) and Gaharwar et al. (2011) showed how Laponite® within a formulation can promote cell adherence and increasing quantities can support cells to stretch across the surface of the nanocomposite films, assumedly attaching to Laponite® particles, which may be beneficial for the migratory phase of wound-healing. Similar work has also been undertaken on gelatine-montmorillonite-chitosan composites that encouraged stromal cell attachment via filopodia, which supported onward proliferation of the cells (Zheng et al., 2007).

In the work presented here the nanocomposite films have a higher proportion of LXL21 within their structure (18.48 to 18.97%) when compared to the foams (17.48 to 17.91%). The internal structure of these materials may also play an important role in the availability of LXL21, which is likely to be reduced in the foams as their porous nature and thicker dimensions may result in a large proportion of the bound LXL21 not coming into contact with the cells. These derivations support the increased HaCaT cell viability observed for the CIP containing nanocomposite films.

The results presented here prove good biocompatibility of the nanocomposite films and foams, and relative cytocompatibility of the individual components. It is also

promising that the nanocomposite films did not significantly reduce cell proliferation as promotion of keratinocyte migration and proliferation is vital in the *migratory* phase early in the wound healing process. Further work should investigate the behaviour of cell adherence and movement across these composites and move onto animal models (Emami-Razavi et al., 2006) to determine their behaviour in true wound environments.

#### 4.4. Conclusions

Through a series of pre-formulation and refinement studies a set of novel and unique materials have been created containing Laponite® XL21, alginate, glycerol and ciprofloxacin. Of these materials the nanocomposite films were shown to be most promising and were supported by the tissue viability nursing team at Liverpool and Broadgreen University Hospitals NHS Trust for their malleability, softness, and transparency that was confirmed spectrophotometrically. While the nanocomposite foam materials were deemed to require further work to increase their physical strength and integrity, they still bore some promising characteristics such as increased fluid absorption and prolonged drug release.

Nanocomposite films and foams were able to reduce water vapour transmission rate in such a way that they would still allow gaseous exchange but could also prevent desiccation of the wound environment. Both types of material were also shown to have impressive fluid absorption capacities without losing their overall shape or integrity. The research described here is the first within clay-mineral studies to include commercially available products as comparisons. The nanocomposite films were shown to have greater wound-fluid adsorption potential and less surface adherence compared to Opsite®, whereas the nanocomposite foams were also shown to be more absorbent than Kaltostat®, equally as absorbent as Lyofoam®, and have similar surface adherence properties to Kaltostat®. This ability to absorb more fluid will be important for their application to infected wounds, which generally produce more exudate that can become purulent (Healy and Freedman, 2006; Stevens et al., 2014).

The incorporation of LXL21-CIP composites into alginate allowed for slower and controlled release of drug into the SWF, which was more pronounced in the nanocomposite foam samples. This ability to release CIP was also demonstrated against bacteria commonly found in infected wounds. When applied to a culture of keratinocytes these film and foam nanocomposites, and their individual components, were proven to have good biocompatibility with the film nanocomposites causing no adverse effect on cell proliferation.

Overall, these nanocomposite materials warrant further investigation beyond the remit of this project to fully realise their potential. For the nanocomposite foams, a number of polymers of differing molecular weights such as chitosan, polyvinyl alcohol, and polyurethanes should be investigated to determine which provides the best mechanical and biological properties. To further characterise the structure of the nanocomposite films and foams, scanning electron microscopy (SEM) and transmission electron microscopy (TEM) can be used. A number of additional, pharmaceutically relevant, techniques should also be utilised, such as texture analysis, tensile strength, deformation testing, and drug and formulation stability over time. Moreover, future work should use the knowledge developed within this thesis and move its application forward to animal and clinical studies.

#### 4.5. References

- Abdollahi, M., Alboofetileh, M., Rezaei, M., Behrooz, R., 2013. Comparing physico-mechanical and thermal properties of alginate nanocomposite films reinforced with organic and/or inorganic nanofillers. *Food Hydrocoll.* 32, 416–424. doi:10.1016/j.foodhyd.2013.02.006
- Aguzzi, C., Capra, P., Bonferoni, C., Cerezo, P., Salcedo, I., Sánchez, R., Caramella, C., Viseras, C., 2010. Chitosan–silicate biocomposites to be used in modified drug release of 5-aminosalicylic acid (5-ASA). *Appl. Clay Sci.* 50, 106–111. doi:10.1016/j.clay.2010.07.011
- Aguzzi, C., Sandri, G., Bonferoni, C., Cerezo, P., Rossi, S., Ferrari, F., Caramella, C., Viseras, C., 2013. Solid state characterisation of silver sulfadiazine loaded on montmorillonite/chitosan nanocomposite for wound healing. *Colloids Surf. B. Biointerfaces* 113C, 152–157. doi:10.1016/j.colsurfb.2013.08.043
- Alboofetileh, M., Rezaei, M., Hosseini, H., Abdollahi, M., 2013. Effect of montmorillonite clay and biopolymer concentration on the physical and mechanical properties of alginate nanocomposite films. *J. Food Eng.* 117, 26–33. doi:10.1016/j.jfoodeng.2013.01.042
- Alboofetileh, M., Rezaei, M., Hosseini, H., Abdollahi, M., 2013. Effect of Nanoclay and Cross-Linking Degree on the Properties of Alginate-Based Nanocomposite Film. *J. Food Process. Preserv.* 1, n/a-n/a. doi:10.1111/jfpp.12124
- Ambrogi, V., Pietrella, D., Nocchetti, M., Casagrande, S., Moretti, V., De Marco, S., Ricci, M., 2016. Montmorillonite–chitosan–chlorhexidine composite films with antibiofilm activity and improved cytotoxicity for wound dressing. *J. Colloid Interface Sci.* 491, 265–272. doi:10.1016/j.jcis.2016.12.058
- Bandeira, L.C., Calefi, P.S., Ciuffi, K.J., de Faria, E.H., Nassar, E.J., Vicente, M. a, Trujillano, R., 2012. Preparation of composites of laponite with alginate and alginic acid polysaccharides. *Polym. Int.* 61, 1170–1176. doi:10.1002/pi.4196
- Benli, B., Boylu, F., Can, M.F., Karakas, F., 2011. Characterization of Alginate – Bentonite Biocomposites 16, 19–28. doi:10.1002/app
- Benli, B., Boylu, F., Can, M.F., Karakaş, F., Çinku, K., Ersever, G., 2011. Rheological, electrokinetic, and morphological characterization of alginate-bentonite biocomposites. *J. Appl. Polym. Sci.* 122, 19–28. doi:10.1002/app.33627
- Bennett-Marsden, M., 2010. How to select a wound dressing. *Clin. Pharm.* 2, 363–366.
- Berhane, T.M., Levy, J., Krekeler, M.P.S., Danielson, N.D., 2016. Adsorption of bisphenol A and ciprofloxacin by palygorskite-montmorillonite: Effect of granule size, solution chemistry and temperature. *Appl. Clay Sci.* 132–133, 518–527. doi:10.1016/j.clay.2016.07.023
- Björklund, S., Engblom, J., Thuresson, K., Sparr, E., 2013. Glycerol and urea can be used to increase skin permeability in reduced hydration conditions. *Eur. J. Pharm. Sci.*



50, 638–645. doi:10.1016/j.ejps.2013.04.022

Boateng, J.S., Matthews, K.H., Stevens, H.N.E., Eccleston, G.M., 2008. Wound healing dressings and drug delivery systems: A review. *J. Pharm. Sci.* 97, 2892–2923. doi:10.1002/jps.21210

Bolton, L.L., Johnson, C.L., Van Rijswijk, L., 1992. Occlusive dressings: therapeutic agents and effects on drug delivery. *Clin. Dermatol.* 9, 573–583.

British Pharmacopoeia Commission, 2016. Friability, in: *British Pharmacopoeia* (Appendix XVII).

British Standards Institute, 2009. BS EN ISO 10993-5: Biological evaluation of medical devices. Tests for in vitro cytotoxicity. British Standards Institute, London.

Bugatti, V., Gorrasi, G., Montanari, F., Nocchetti, M., Tammaro, L., Vittoria, V., 2011. Modified layered double hydroxides in polycaprolactone as a tunable delivery system: in vitro release of antimicrobial benzoate derivatives. *Appl. Clay Sci.* 52, 34–40. doi:10.1016/j.clay.2011.01.025

Calvino-Casilda, V., Mul, G., Fernández, J.F., Rubio-Marcos, F., Bañares, M.A., 2011. Monitoring the catalytic synthesis of glycerol carbonate by real-time attenuated total reflection FTIR spectroscopy. *Appl. Catal. A Gen.* 409–410, 106–112. doi:10.1016/j.apcata.2011.09.036

Chang, P.-H., Li, Z., Jiang, W.-T., Jean, J.-S., 2009. Adsorption and intercalation of tetracycline by swelling clay minerals. *Appl. Clay Sci.* 46, 27–36. doi:10.1016/j.clay.2009.07.002

Chang, P.H., Jiang, W.T., Li, Z., Kuo, C.Y., Wu, Q., Jean, J.S., Lv, G., 2016. Interaction of ciprofloxacin and probe compounds with palygorskite PFI-1. *J. Hazard. Mater.* 303, 55–63. doi:10.1016/j.jhazmat.2015.10.012

Chen, H.-B., Wang, Y.-Z., Sánchez-Soto, M., Schiraldi, D. a., 2012. Low flammability, foam-like materials based on ammonium alginate and sodium montmorillonite clay. *Polymer (Guildf)*. 53, 5825–5831. doi:10.1016/j.polymer.2012.10.029

Cockbill, S., 2002. Wounds - The healing process. *Hosp. Pharm.* 9, 255–260.

Darder, M., Matos, C.R.S., Aranda, P., Gouveia, R.F., Ruiz-Hitzky, E., 2016. Bionanocomposite foams based on the assembly of starch and alginate with sepiolite fibrous clay. *Carbohydr. Polym.* 157, 1933–1939. doi:10.1016/j.carbpol.2016.11.079

Das, G., Kalita, R.D., Gogoi, P., Buragohain, A.K., Karak, N., 2014. Antibacterial activities of copper nanoparticle-decorated organically modified montmorillonite/epoxy nanocomposites. *Appl. Clay Sci.* 90, 18–26. doi:10.1016/j.clay.2014.01.002

Davidovich-Pinhas, M., Bianco-Peled, H., 2010. A quantitative analysis of alginate swelling. *Carbohydr. Polym.* 79, 1020–1027. doi:10.1016/j.carbpol.2009.10.036

Davis, J., Mclister, A., 2016. *History and Evolution of Bandages, Dressings, and Plasters*,

- Smart Bandage Technologies: Design and Application. Elsevier Inc.  
doi:10.1016/B978-0-12-803762-1.00003-5
- Dawson, J.I., Oreffo, R.O.C., 2013. Clay: new opportunities for tissue regeneration and biomaterial design. *Adv. Mater.* 25, 4069–86. doi:10.1002/adma.201301034
- Dryden, M.S., 2009. Skin and soft tissue infection: microbiology and epidemiology. *Int. J. Antimicrob. Agents* 34 Suppl 1, S2-7. doi:10.1016/S0924-8579(09)70541-2
- Dziadkowiec, J., Mansa, R., Quintela, A., Rocha, F., Detellier, C., 2016. Preparation, characterization and application in controlled release of Ibuprofen-loaded Guar Gum/Montmorillonite Bionanocomposites. *Appl. Clay Sci.*  
doi:10.1016/j.clay.2016.09.003
- Emami-Razavi, S.H., Esmaili, N., Forouzannia, S.K., Amanpour, S., Rabbani, S., Alizadeh, A.M., Mohagheghi, M.A., 2006. EFFECT OF BENTONITE ON SKIN WOUND HEALING : EXPERIMENTAL STUDY IN THE RAT MODEL. *Acta Med. Iran.* 44, 235–240.
- Fink, J., 2015. Additives for General Uses, in: *Water-Based Chemicals and Technology for Drilling, Completion, and Workover Fluids.* pp. 209–250. doi:10.1016/B978-0-12-802505-5.00005-6
- Gacesa, P., 1988. Alginates. *Carbohydr. Polym.* 8, 161–182. doi:10.1016/0144-8617(88)90001-X
- Gaharwar, A.K., Kishore, V., Rivera, C., Bullock, W., Wu, C.-J., Akkus, O., Schmidt, G., 2012. Physically crosslinked nanocomposites from silicate-crosslinked PEO: mechanical properties and osteogenic differentiation of human mesenchymal stem cells. *Macromol. Biosci.* 12, 779–93. doi:10.1002/mabi.201100508
- Gaharwar, A.K., Rivera, C.P., Wu, C.-J., Schmidt, G., 2011a. Transparent, elastomeric and tough hydrogels from poly(ethylene glycol) and silicate nanoparticles. *Acta Biomater.* 7, 4139–48. doi:10.1016/j.actbio.2011.07.023
- Gaharwar, A.K., Schexnailder, P.J., Jin, Q., Wu, C.-J., Schmidt, G., 2010. Addition of chitosan to silicate cross-linked PEO for tuning osteoblast cell adhesion and mineralization. *ACS Appl. Mater. Interfaces* 2, 3119–27. doi:10.1021/am100609t
- Gaharwar, A.K., Schexnailder, P.J., Kline, B.P., Schmidt, G., 2011b. Assessment of using laponite cross-linked poly(ethylene oxide) for controlled cell adhesion and mineralization. *Acta Biomater.* 7, 568–77. doi:10.1016/j.actbio.2010.09.015
- Gao, F., 2004. Clay / polymer composites: the story. *Mater. Today* 7, 50–55.
- Gaskell, E.E., Hamilton, A.R., 2014. Antimicrobial clay-based materials for wound care. *Future Med. Chem.* 6, 641.
- Ghadiri, M., Chrzanowski, W., Lee, W.H., Fathi, A., Dehghani, F., Rohanizadeh, R., 2013. Physico-chemical, mechanical and cytotoxicity characterizations of Laponite®/alginate nanocomposite. *Appl. Clay Sci.* 85, 64–73.

doi:10.1016/j.clay.2013.08.049

- Giuliani, F., Merusi, F., Polacco, G., Filippi, S., Paci, M., 2012. Effectiveness of sodium chloride-based anti-icing filler in asphalt mixtures. *Constr. Build. Mater.* 30, 174–179. doi:10.1016/j.conbuildmat.2011.12.036
- Gonçalves, M., Figueira, P., Maciel, D., Rodrigues, J., Qu, X., Liu, C., Tomás, H., Li, Y., 2013a. pH-sensitive Laponite/doxorubicin/alginate nanohybrids with improved anticancer efficacy. *Acta Biomater.* doi:10.1016/j.actbio.2013.09.013
- Gonçalves, M., Figueira, P., Maciel, D., Rodrigues, J., Shi, X., Tomás, H., Li, Y., 2013b. Antitumor Efficacy of Doxorubicin-Loaded Laponite/Alginate Hybrid Hydrogels. *Macromol. Biosci.* 1–11. doi:10.1002/mabi.201300241
- Grey, J.E., Enoch, S., Harding, K.G., 2006. Wound assessment. *BMJ* 332, 285–8. doi:10.1136/bmj.332.7536.285
- Han, Y.-S., Lee, S.-H., Choi, K.H., Park, I., 2010. Preparation and characterization of chitosan–clay nanocomposites with antimicrobial activity. *J. Phys. Chem. Solids* 71, 464–467. doi:10.1016/j.jpcs.2009.12.012
- Hanna, J.R., Giacomelli, J. a., 1997. A review of wound healing and wound dressing products. *J. Foot Ankle Surg.* 36, 2–14. doi:10.1016/S1067-2516(97)80003-8
- Healy, B., Freedman, A., 2006. Infections. *BMJ* 332, 838–841.
- Hoang-Minh, T., Le, T.L., Kasbohm, J., Gieré, R., 2010. UV-protection characteristics of some clays. *Appl. Clay Sci.* 48, 349–357. doi:10.1016/j.clay.2010.01.005
- Hua, S., Yang, H., Wang, W., Wang, A., 2010. Controlled release of ofloxacin from chitosan–montmorillonite hydrogel. *Appl. Clay Sci.* 50, 112–117. doi:10.1016/j.clay.2010.07.012
- Hutchinson, J.J., 1990. Occlusive dressings: A microbiologic and clinical review. *Am. J. Infect. Control* 18, 257–268.
- Iliescu, R.I., Andronescu, E., Ghitulica, C.D., Voicu, G., Ficai, A., Hoteteu, M., 2013. Montmorillonite-alginate nanocomposite as a drug delivery system - incorporation and in vitro release of irinotecan. *Int. J. Pharm.* doi:10.1016/j.ijpharm.2013.08.043
- Inada, T., Modak, P.R., 2006. Growth control of ice crystals by poly(vinyl alcohol) and antifreeze protein in ice slurries. *Chem. Eng. Sci.* 61, 3149–3158. doi:10.1016/j.ces.2005.12.005
- Ip, K.H., Stuart, B.H., Thomas, P.S., Ray, A., 2011. Characterisation of poly(vinyl alcohol)–montmorillonite composites with higher clay contents. *Polym. Test.* 30, 732–736. doi:10.1016/j.polymertesting.2011.06.004
- Ito, T., Sugafuji, T., Maruyama, M., 2001. Skin Penetration by Indomethacin is Enhanced by Use of an Indomethacin / Smectite Complex. *J. Supramol. Chem.* 1 217–219.

- Jarray, A., Gerbaud, V., Hemati, M., 2016. Polymer-plasticizer compatibility during coating formulation: A multi-scale investigation. *Prog. Org. Coatings* 101, 195–206. doi:10.1016/j.porgcoat.2016.08.008
- Joint Formulary Committee, 2017. Appendix 4 - Wound management products and elasticated garments, in: Khanderia, S. (Ed.), *British National Formulary (Online Edition)*. Pharmaceutical Press and BMJ Group, London, p. 1368.
- Jones, V., Grey, J.E., Harding, K.G., 2006. Wound dressings. *BMJ* 332, 777–780.
- Joshi, G. V., Patel, H. a., Kevadiya, B.D., Bajaj, H.C., 2009. Montmorillonite intercalated with vitamin B1 as drug carrier. *Appl. Clay Sci.* 45, 248–253. doi:10.1016/j.clay.2009.06.001
- Joshi, G. V, Kevadiya, B.D., Bajaj, H.C., 2010. Controlled release formulation of ranitidine-containing montmorillonite and Eudragit E-100. *Drug Dev. Ind. Pharm.* 36, 1046–53. doi:10.3109/03639041003642073
- Jung, H., Kim, H.-M., Choy, Y. Bin, Hwang, S.-J., Choy, J.-H., 2008. Itraconazole–Laponite: Kinetics and mechanism of drug release. *Appl. Clay Sci.* 40, 99–107. doi:10.1016/j.clay.2007.09.002
- Kaygusuz, H., Erim, F.B., 2013. Alginate/BSA/montmorillonite composites with enhanced protein entrapment and controlled release efficiency. *React. Funct. Polym.* 73, 1420–1425. doi:10.1016/j.reactfunctpolym.2013.07.014
- Kokabi, M., Sirousazar, M., Hassan, Z.M., 2007. PVA–clay nanocomposite hydrogels for wound dressing. *Eur. Polym. J.* 43, 773–781. doi:10.1016/j.eurpolymj.2006.11.030
- Kucera, J., Sojka, M., Pavlik, V., Szuszkiewicz, K., Velebny, V., Klein, P., 2014. Multispecies biofilm in an artificial wound bed-A novel model for in vitro assessment of solid antimicrobial dressings. *J. Microbiol. Methods* 103, 18–24. doi:10.1016/j.mimet.2014.05.008
- Lagaly, G., Ogawa, M., Dekany, I., 2013. Clay Mineral-Organic Interactions, in: *Handbook of Clay Science Part A: Fundamentals*. pp. 435–487.
- Leaper, D.J., 2006. Traumatic and surgical wounds. *BMJ* 332, 532–535. doi:10.1136/bmj.332.7540.532
- LeBaron, P.C., Wang, Z., Pinnavaia, T.J., 1999. Polymer-layered silicate nanocomposites : an overview. *Appl. Clay Sci.* 15, 11–29.
- Li, P., Siddaramaiah, Kim, N.H., Yoo, G.-H., Lee, J.-H., 2009. Poly(Acrylamide/Laponite) Nanocomposite Hydrogels: Swelling and Cationic Dye Adsorption Properties. *J. Appl. Polym. Sci.* 111, 1786–1798. doi:10.1002/app
- Lindsay, S., Delbono, M., Stevenson, R., Stephens, S., Cullen, B., 2010. The silver release profile of antimicrobial wound dressings : standardizing in vitro evaluations. Gargrave, UK.
- Lister, P.D., Wolter, D.J., Hanson, N.D., 2009. Antibacterial-resistant *Pseudomonas*

aeruginosa: Clinical impact and complex regulation of chromosomally encoded resistance mechanisms. *Clin. Microbiol. Rev.* 22, 582–610.  
doi:10.1128/CMR.00040-09

Madsen, F.T., 1977. SURFACE AREA MEASUREMENTS OF CLAY MINERALS BY GLYCEROL SORPTION ON A THERMOBALANCE. *Thermochim. Acta* 21, 89–93.

Malik, A., Mohammad, Z., Ahmad, J., 2013. The diabetic foot infections: biofilms and antimicrobial resistance. *Diabetes Metab. Syndr.* 7, 101–7.  
doi:10.1016/j.dsx.2013.02.006

Matthews, K.H., Stevens, H.N.E., Auffret, a D., Humphrey, M.J., Eccleston, G.M., 2005. Lyophilised wafers as a drug delivery system for wound healing containing methylcellulose as a viscosity modifier. *Int. J. Pharm.* 289, 51–62.  
doi:10.1016/j.ijpharm.2004.10.022

Matuschek, E., Brown, D.F.J., Kahlmeter, G., 2014. Development of the EUCAST disk diffusion antimicrobial susceptibility testing method and its implementation in routine microbiology laboratories. *Clin. Microbiol. Infect.* 20, O255–O266.  
doi:10.1111/1469-0691.12373

Momoh, F.U., Boateng, J.S., Richardson, S.C.W., Chowdhry, B.Z., Mitchell, J.C., 2015. Development and functional characterization of alginate dressing as potential protein delivery system for wound healing. *Int. J. Biol. Macromol.* 81, 137–150.  
doi:10.1016/j.ijbiomac.2015.07.037

Mongondry, P., Tassin, J.F., Nicolai, T., 2005. Revised state diagram of Laponite dispersions. *J. Colloid Interface Sci.* 283, 397–405. doi:10.1016/j.jcis.2004.09.043

Morgan, D., 2002. Wounds - what should a dressings formulary include? *Hosp. Pharm.* 9, 261–266.

Mosmann, T., 1983. Rapid colorimetric assay for cellular growth and survival: application to proliferation and cytotoxicity assays. *J. Immunol. Methods* 65, 55–63.

National Prescribing Centre, 2012. Prescribing of dressings: Guiding principles for improving the systems and processes for the supply and prescribing of wound dressings.

Ng, S.-F., Jumaat, N., 2014. Carboxymethyl cellulose wafers containing antimicrobials: a modern drug delivery system for wound infections. *Eur. J. Pharm. Sci.* 51, 173–9.  
doi:10.1016/j.ejps.2013.09.015

Palfreyman, S., Nelson, E., Lochiel, R., Michaels, J., 2010. Dressings for healing venous leg ulcers ( Review ). *Cochrane Libr.*

Paul, D.R., Robeson, L.M., 2008. Polymer nanotechnology: Nanocomposites. *Polymer (Guildf)*. 49, 3187–3204. doi:10.1016/j.polymer.2008.04.017

Perkins, N.C., Heard, C.M., 1999. In vitro dermal and transdermal delivery of

- doxycycline from ethanol/miglyol 840 vehicles. *Int. J. Pharm.* 190, 155–64.
- Phillips, G., Johnson, B.E., Ferguson, J., 1990. The loss of antibiotic activity of ciprofloxacin by photodegradation. *J. Antimicrob. Chemother.* 26, 783–9.
- Pongjanyakul, T., 2009. Alginate-magnesium aluminum silicate films: importance of alginate block structures. *Int. J. Pharm.* 365, 100–8. doi:10.1016/j.ijpharm.2008.08.025
- Pongjanyakul, T., Puttipipatkachorn, S., 2008. Alginate-magnesium aluminum silicate composite films: effect of film thickness on physical characteristics and permeability. *Int. J. Pharm.* 346, 1–9. doi:10.1016/j.ijpharm.2007.05.058
- Pongjanyakul, T., Suksri, H., 2010. Nicotine-loaded sodium alginate–magnesium aluminum silicate (SA–MAS) films: Importance of SA–MAS ratio. *Carbohydr. Polym.* 80, 1018–1027. doi:10.1016/j.carbpol.2010.01.019
- Powers, J.G., Higham, C., Broussard, K., Phillips, T.J., 2016. Wound healing and treating wounds Chronic wound care and management. *J. Am. Acad. Dermatol.* 74, 607–625. doi:10.1016/j.jaad.2015.08.070
- Qi, R., Guo, R., Zheng, F., Liu, H., Yu, J., Shi, X., 2013. Controlled release and antibacterial activity of antibiotic-loaded electrospun halloysite/poly(lactic-co-glycolic acid) composite nanofibers. *Colloids Surf. B. Biointerfaces* 110, 148–55. doi:10.1016/j.colsurfb.2013.04.036
- Qin, Y., 2008. Alginate fibres : an overview of the production processes and applications. *Polym. Int.* 57, 171–180. doi:10.1002/pi
- Qiu, Y., Lee, P.I., 2017. Chapter 19 – Rational Design of Oral Modified-Release Drug Delivery Systems, in: *Developing Solid Oral Dosage Forms*. pp. 519–554. doi:10.1016/B978-0-12-802447-8.00019-4
- Ray, S.S., Okamoto, M., 2003. Polymer/layered silicate nanocomposites: a review from preparation to processing. *Prog. Polym. Sci.* 28, 1539–1641. doi:10.1016/j.progpolymsci.2003.08.002
- Rezvanain, M., Ahmad, N., Cairul, M., Mohd, I., Ng, S., 2017. Optimization, characterization, and in vitro assessment of alginate-pectin ionic cross-linked hydrogel film for wound dressing applications. *Int. J. Biol. Macromol.* 97, 131–140. doi:10.1016/j.ijbiomac.2016.12.079
- Rodrigues, L.A.D.S., Figueiras, A., Veiga, F., de Freitas, R.M., Nunes, L.C.C., da Silva Filho, E.C., da Silva Leite, C.M., 2013. The systems containing clays and clay minerals from modified drug release: a review. *Colloids Surf. B. Biointerfaces* 103, 642–51. doi:10.1016/j.colsurfb.2012.10.068
- Ruiz-Hitzky, E., Darder, M., Fernandes, F.M., Wicklein, B., Alcântara, A.C.S., Aranda, P., 2013. Fibrous clays based bionanocomposites. *Prog. Polym. Sci.* 38, 1392–1414. doi:10.1016/j.progpolymsci.2013.05.004

- Salcedo, I., Sandri, G., Aguzzi, C., Bonferoni, C., Cerezo, P., Sánchez-Espejo, R., Viseras, C., 2013. Intestinal permeability of oxytetracycline from chitosan-montmorillonite nanocomposites. *Colloids Surf. B. Biointerfaces*. doi:10.1016/j.colsurfb.2013.11.009
- Sandri, G., Bonferoni, M.C., Rossi, S., Ferrari, F., Aguzzi, C., Viseras, C., Caramella, C., 2016. Clay minerals for tissue regeneration, repair, and engineering, *Wound Healing Biomaterials*. Elsevier Ltd. doi:10.1016/B978-1-78242-456-7.00019-2
- Sandstrom, S., 2011. The antibacterial effect of silver with different release kinetics. Chalmers University of Technology.
- Schexnailder, P.J., Gaharwar, A.K., Bartlett, R.L., Seal, B.L., Schmidt, G., 2010. Tuning cell adhesion by incorporation of charged silicate nanoparticles as cross-linkers to polyethylene oxide. *Macromol. Biosci.* 10, 1416–23. doi:10.1002/mabi.201000053
- Scottish Intercollegiate Guidelines Network, 2010. Management of chronic venous leg ulcers. (SIGN Guideline No 120).
- Shankar, S., Wang, L.F., Rhim, J.W., 2016. Preparations and characterization of alginate/silver composite films: Effect of types of silver particles. *Carbohydr. Polym.* 146, 208–216. doi:10.1016/j.carbpol.2016.03.026
- Shikinaka, K., Aizawa, K., Murakami, Y., Osada, Y., Tokita, M., Watanabe, J., Shigehara, K., 2012. Structural and mechanical properties of Laponite-PEG hybrid films. *J. Colloid Interface Sci.* 369, 470–6. doi:10.1016/j.jcis.2011.11.079
- Siddiqui, A.R., Bernstein, J.M., 2010. Chronic wound infection: facts and controversies. *Clin. Dermatol.* 28, 519–26. doi:10.1016/j.clindermatol.2010.03.009
- Silva, F., Lourenço, O., Queiroz, J. a, Domingues, F.C., 2011. Bacteriostatic versus bactericidal activity of ciprofloxacin in *Escherichia coli* assessed by flow cytometry using a novel far-red dye. *J. Antibiot. (Tokyo)*. 64, 321–325. doi:10.1038/ja.2011.5
- Singh, B., Sharma, S., Dhiman, A., 2013. Design of antibiotic containing hydrogel wound dressings: Biomedical properties and histological study of wound healing. *Int. J. Pharm.* 457, 82–91. doi:10.1016/j.ijpharm.2013.09.028
- Sinha Ray, S., Okamoto, M., 2003. Polymer/layered silicate nanocomposites: a review from preparation to processing. *Prog. Polym. Sci.* 28, 1539–1641. doi:10.1016/j.progpolymsci.2003.08.002
- Smith, A.M., Moxon, S., Morris, G.A., 2016. Biopolymers as wound healing materials, *Wound Healing Biomaterials*. Elsevier Ltd. doi:10.1016/B978-1-78242-456-7.00013-1
- Soykeabkaew, N., Thanomsilp, C., Suwantong, O., 2015. A review: Starch-based composite foams. *Compos. Part A Appl. Sci. Manuf.* 78, 246–263. doi:10.1016/j.compositesa.2015.08.014
- Stevens, D.L., Bisno, A.L., Chambers, H.F., Dellinger, E.P., Goldstein, E.J.C., Gorbach, S.L.,

- Hirschmann, J. V, Kaplan, S.L., Montoya, J.G., Wade, J.C., 2014. Practice Guidelines for the Diagnosis and Management of Skin and Soft Tissue Infections: 2014 Update by the Infectious Diseases Society of America. *Clin. Infect. Dis.* 59, e10-52. doi:10.1093/cid/ciu296
- Strodtbeck, F., 2001. Physiology of wound healing. *Newborn Infant Nurs. Rev.* 1, 43–52. doi:10.1053/nbin.2001.23176
- Su, C.-C., Shen, Y.-H., 2009. Adsorption of poly(ethylene oxide) on smectite: Effect of layer charge. *J. Colloid Interface Sci.* 332, 11–5. doi:10.1016/j.jcis.2008.12.024
- Tan, D.T., Cai, C., Zhang, Y., Wang, N., Pang, S.F., Zhang, Y.H., 2016. Crystallization kinetics from mixture Na<sub>2</sub>SO<sub>4</sub>/glycerol droplets of Na<sub>2</sub>SO<sub>4</sub> by FTIR-ATR. *Chem. Phys.* 475, 131–135. doi:10.1016/j.chemphys.2016.07.007
- Tan, X., Liu, F., Hu, L., Reed, A.H., Furukawa, Y., Zhang, G., 2017. Evaluation of the particle sizes of four clay minerals. *Appl. Clay Sci.* 135, 313–324. doi:10.1016/j.clay.2016.10.012
- Tezcan, F., Günister, E., Ozen, G., Erim, F.B., 2012. Biocomposite films based on alginate and organically modified clay. *Int. J. Biol. Macromol.* 50, 1165–8. doi:10.1016/j.ijbiomac.2012.01.006
- Theng, B.K.G., 2012. Polymer-clay nanocomposites, in: *Formation and Properties of Clay-Polymer Complexes (Developments in Clay Science)*. Elsevier, Oxford, UK, pp. 201–241.
- Thu, H.-E., Zulfakar, M.H., Ng, S.-F., 2012. Alginate based bilayer hydrocolloid films as potential slow-release modern wound dressing. *Int. J. Pharm.* 434, 375–83. doi:10.1016/j.ijpharm.2012.05.044
- Török, E., Conlon, C.P., 2005. Skin and soft tissue infections. *Medicine (Baltimore)*. 33, 84–88. doi:10.1383/medc.33.4.84.64357
- Tunç, S., Duman, O., 2010. Preparation and characterization of biodegradable methyl cellulose/montmorillonite nanocomposite films. *Appl. Clay Sci.* 48, 414–424. doi:10.1016/j.clay.2010.01.016
- Vance-Bryan, K., Guay, D.R.P., Rotschafer, J.C., 1990. Clinical Pharmacokinetics of Ciprofloxacin. *Clin. Pharmacokinetics* 19, 434–461.
- Vieira, M.G.A., da Silva, M.A., dos Santos, L.O., Beppu, M.M., 2011. Natural-based plasticizers and biopolymer films: A review. *Eur. Polym. J.* 47, 254–263. doi:10.1016/j.eurpolymj.2010.12.011
- Vijayan, V., Reddy, K.R., Sakthivel, S., Swetha, C., 2013. Optimization and Characterization of Repaglinide Biodegradable Polymeric Nanoparticle Loaded Transdermal Patches: In-Vitro & In-Vivo Studies. *Colloids Surfaces B Biointerfaces* 111, 150–155. doi:10.1016/j.colsurfb.2013.05.020
- Viseras, C., Aguzzi, C., Cerezo, P., Bedmar, M.C., 2008. Biopolymer–clay



- nanocomposites for controlled drug delivery. *Mater. Sci. Technol.* 24, 1020–1026. doi:10.1179/174328408X341708
- Viseras, C., Cerezo, P., Sanchez, R., Salcedo, I., Aguzzi, C., 2010. Current challenges in clay minerals for drug delivery. *Appl. Clay Sci.* 48, 291–295. doi:10.1016/j.clay.2010.01.007
- Voncina, B., Frascino, L.Z., Ristic, T., 2015. Active Textile Dressings for Wound Healing. *Adv. Smart Med. Text. Treat. Heal. Monit.* 73–92. doi:10.1016/B978-1-78242-379-9.00004-9
- Wadso, L., Anderberg, A., Aslund, I., Soderman, O., 2009. An improved method to validate the relative humidity generation in sorption balances. *Eur. J. Pharm. Biopharm.* 72, 99–104. doi:10.1016/j.ejpb.2008.10.013
- Wang, C.-J., Li, Z., Jiang, W.-T., Jean, J.-S., Liu, C.-C., 2010. Cation exchange interaction between antibiotic ciprofloxacin and montmorillonite. *J. Hazard. Mater.* 183, 309–314. doi:10.1016/j.jhazmat.2010.07.025
- Wang, L.F., Rhim, J.W., 2015. Preparation and application of agar/alginate/collagen ternary blend functional food packaging films. *Int. J. Biol. Macromol.* 80, 460–468. doi:10.1016/j.ijbiomac.2015.07.007
- Williams, D.R., 1996. Wounds : decontamination and healing. *Coord. Chem. Rev.* 151, 161–174.
- Williamson, D., Harding, K., 2004. Wound healing. *Medicine (Baltimore)*. 32, 4–7. doi:10.1383/medc.32.12.4.55399
- Wispelwey, B., 2005. Clinical implications of pharmacokinetics and pharmacodynamics of fluoroquinolones. *Clin. Infect. Dis.* 41 Suppl 2, S127-35. doi:10.1086/428053
- Yang, L., Liang, G., Zhang, Z., He, S., Wang, J., 2009. Sodium alginate/Na<sup>+</sup>-rectorite composite films: Preparation, characterization, and properties. *J. Appl. Polym. Sci.* 114, 1235–1240. doi:10.1002/app.30521
- Yang, L., Ma, X., Guo, N., 2012. Sodium alginate/Na<sup>+</sup>-rectorite composite microspheres: preparation, characterization, and dye adsorption. *Carbohydr. Polym.* 90, 853–8. doi:10.1016/j.carbpol.2012.06.011
- Zhang, Q., Li, X., Zhao, Y., Chen, L., 2009. Preparation and performance of nanocomposite hydrogels based on different clay. *Appl. Clay Sci.* 46, 346–350. doi:10.1016/j.clay.2009.09.003
- Zheng, J.P., Wang, C.Z., Wang, X.X., Wang, H.Y., Zhuang, H., Yao, K. De, 2007. Preparation of biomimetic three-dimensional gelatin/montmorillonite–chitosan scaffold for tissue engineering. *React. Funct. Polym.* 67, 780–788. doi:10.1016/j.reactfunctpolym.2006.12.002

## Chapter 5

### Concluding remarks & future directions

The management of infected wounds is often complex and can result in prolonged and repeated courses of antimicrobial agents alongside supportive therapies to promote wound healing. The current lack of appropriate wound-care materials that can sufficiently kill bacteria or inhibit bacterial growth results in patients receiving antimicrobial therapy systemically, which puts them at risk of adverse drug reactions (Tamma et al., 2017) and the development of secondary infections from organisms such as *Clostridium difficile* (Aldeyab et al., 2009). Repeated and prolonged antimicrobial therapy can also result in the development of antimicrobial resistance within the human microbiota (Jernberg et al., 2010; Price et al., 2009), which can ultimately result in infections that are more difficult to treat and may only respond to the most toxic and expensive agents available (Chatterjee et al., 2016; Grice and Segre, 2011).

Antimicrobial resistance has been identified as a world-wide-issue and impending crisis for human and animal health. Although there are many ways to prevent the development of antimicrobial resistance the World Health Organisation, the UK Department of Health, and the Royal Pharmaceutical Society have stressed the importance of developing new ways to utilise the available antimicrobial arsenal (Davies, 2013; Royal Pharmaceutical Society, 2014; World Health Organization, 2012).

The work presented in this thesis highlights the ability of clay-minerals to act as carriers for antimicrobial agents and potentially benefit the wound-healing process.

By treating the infection at the source it may be possible to reduce selection pressures, for antimicrobial resistance, on the rest of the microbiota and also allow for smaller doses to be used; reducing the risk of adverse drug reactions. In turn these nanocomposite materials may reduce the burden on the patient and the healthcare system as patients may not require systemic antimicrobial therapy within the inpatient or outpatient setting.

Tetracycline, doxycycline (chapter 2) and ciprofloxacin (chapter 3) were successfully adsorbed onto the surfaces of clay mineral layers. The chemistry and physical-structure of the clay minerals examined was key to determining the amount of drug that could be adsorbed onto the mineral surfaces. Non-swelling 1:1 minerals with small surface areas and poor cation exchange capacities (i.e. kaolin) were shown to adsorb the least amount of drug onto their outer particle surfaces, whereas swelling 2:1 minerals, which generally have much larger surface areas and significantly greater cation exchange capacities, were able to adsorb much more drug into the laminar space between mineral layers and onto positively charged edge-groups. The chemistry of the adsorbate also influenced the quantity of drug adsorbed onto the different clay mineral surfaces. A dispersion which favoured the zwitterionic state of each drug molecule was clearly shown to favour greater drug adsorption, possibly through tighter arrangement of drug molecules at the clay mineral surface.

These antibacterial agents were shown to be able to desorb from these the clay-drug composites in a series of microbiological experiments that were specially designed to better represent a chronically infected wound. Through these experiments the desorbed drugs were shown to inhibit the growth of *Staphylococcus epidermidis*, *Propionibacterium acnes*, and *Pseudomonas aeruginosa*; important skin, skin-structure, and wound pathogens.

Through a series of pre-formulation and formulation studies (chapter 4), ciprofloxacin clay-mineral composites were successfully incorporated into alginate polymer matrices to create films and foams. The alginate was shown to interact with the edge-sites of the clay mineral layers to form a nanocomposite that afforded increased thermal stability to the composite. Glycerol was shown to be a useful softener and plasticiser in these composite materials, whereas freezing parameters were an important factor in improving foam structure.

Novel methods were developed, utilising synthetic wound fluid, to predict the behaviour of these nanocomposite materials on a suppurating wound, which not only demonstrated promising physical characteristics but also proved the release of ciprofloxacin from these materials was modified. Ciprofloxacin released from these nanocomposite materials was also shown to be effective at inhibiting the growth of a range of clinically important bacteria. Finally, these nanocomposite materials were shown to be biocompatible with keratinocytes and the findings within this work suggest the films may even be able to promote the wound-healing process.

While the nanocomposite materials developed in this research show a great deal of promise for a future role in healthcare, more work is needed to fully characterise their properties and understand their role within the management of infected wounds. The nanocomposite film formulations developed in this research showed the most promise for future use in clinical practice and were deemed to be acceptable materials by the tissue viability nurse. These nanocomposite films were sufficiently flexible, transparent, allowed for gaseous exchange, adsorbed significant quantities of wound exudate, and had low adherence to the wound surface.

Although the nanocomposite foams were also able to adsorb large amounts of wound exudate and allow for gaseous exchange, significantly more research is required to obtain a formulation that is appropriate for clinical applications. In order to develop composite foams that are optimised for the management of infected wounds it will be necessary to investigate different polymers with differing properties. Polymers such as chitosan, polyvinyl alcohol, polyethylene glycol, and polyurethanes could be investigated initially as they have already been used in the development of clay-polymer composites and are known to be biocompatible (Aguzzi et al., 2010; Da Silva et al., 2013; Kokabi et al., 2007; Sandri et al., 2016; Viseras et al., 2008; Zhu et al., 2013). The possibility of using combinations of these polymers should not be ruled out if it could result in beneficial properties being utilised from each polymer. As well as investigating different polymers it will also be useful to examine the role of different additives to improve structure and mechanical properties, and it will also be necessary to examine different formulation techniques that can produce porous-foam materials

such as temperature-controlled and cycled lyophilisation, particulate leaching, phase separation, and gas foaming (Salerno and Nettis, 2014).

It should be noted, however, that the pharmaceutical analysis of these nanocomposite films and foams was limited by the techniques available during the project. Future research into these materials will need to focus on quantitative analyses to fully characterise and quantify their behaviour. Texture analysis should be utilised to measure tensile strength, elongation properties, Young's modulus and adhesion onto the wound surface (Matthews et al., 2005; Momoh et al., 2015; Zare et al., 2017). Additional thermal analysis with differential scanning calorimetry (DSC) and TGA-evolved gas analysis (TGA-EGA) alongside more precise imaging techniques such as high-resolution transmission electron microscopy (HRTEM) or micro-computed tomography analysis ( $\mu$ -CT) should allow the internal structure of these nanocomposites to be fully characterised (Aguzzi et al., 2013; Ghadiri et al., 2013; Mofokeng et al., 2016; Shikinaka et al., 2012). Utilisation of techniques such as magic angle scanning NMR (MAS-NMR), solid-state NMR, near infrared spectroscopy (NIR), and zeta-potential could also unveil new information about the specific interactions between drugs, clay minerals, and polymer molecules (Gil et al., 2011; Gonçalves et al., 2013; Madejova, 2003; Ray and Okamoto, 2003; Shikinaka et al., 2012).

Regardless of the development of this fundamental knowledge it will be vitally important to test these materials in line with international standards for healthcare products. The suitability of these nanocomposite materials for wound care will need to be tested in line with the ISO 10993 standards to characterise their interaction with

blood, determine their degradation products, and also predict their potential to cause local and systemic sensitivities and adverse effects. Such an approach will allow the work to be taken forward to animal and eventually human models.

It should also be highlighted that whilst the tetracycline and quinolone classes remain useful options for the management of wound, skin, and skin-structure infections (Stevens et al., 2014), their widespread use for other infective indications, alongside poor antimicrobial stewardship, is resulting in increasing rates of wound and skin and skin structure infections that resist treatment with these drugs (Fraise, 2006; Stevens, 2009). Flucloxacillin is still widely recommended for the management of skin and skin-structure infections (National Institute of Health and Care Excellence, 2015) and could prove to be an interesting candidate for inclusion into the composite materials developed in this work.

It would be particularly interesting for the knowledge developed in this thesis to be taken forward to examine the potential for clay-minerals to carry other, much larger and chemically complex, antimicrobials that are useful in the management of drug-resistant skin, skin-structure, and wound infections such as daptomycin, dalbavancin, rifampicin and vancomycin (Enoch et al., 2007; Roberts et al., 2015; Unal, 2009). In addition to this, testing these composites against other clinically relevant bacterial species such as *Streptococcus pyogenes*, methicillin sensitive and methicillin resistant *Staphylococcus aureus*, and various Enterobacteriaceae will be important (Dryden, 2009; Grice and Segre, 2011; Malik et al., 2013). It will also be important to consider utilising international standards for microbiological testing, such as the European

Society of Clinical Microbiology and Infectious Diseases (2017) antibacterial susceptibility testing methods.

To fully realise the potential of these nanocomposite materials, future research projects will require significant investment in terms of time and resources, and will also require a multidisciplinary approach with collaborations between pharmaceutical scientists, biomedical scientists, specialist pharmacists, tissue viability nurses, and medics specialised in microbiology, infectious diseases, and dermatology. A multidisciplinary approach will also ensure the work remains clinically relevant and addresses the changing needs of modern healthcare and the ever evolving patterns to antimicrobial resistance.



## 5.1. References

- Aguzzi, C., Capra, P., Bonferoni, C., Cerezo, P., Salcedo, I., Sánchez, R., Caramella, C., Viseras, C., 2010. Chitosan–silicate biocomposites to be used in modified drug release of 5-aminosalicylic acid (5-ASA). *Appl. Clay Sci.* 50, 106–111. doi:10.1016/j.clay.2010.07.011
- Aguzzi, C., Sandri, G., Bonferoni, C., Cerezo, P., Rossi, S., Ferrari, F., Caramella, C., Viseras, C., 2013. Solid state characterisation of silver sulfadiazine loaded on montmorillonite/chitosan nanocomposite for wound healing. *Colloids Surf. B. Biointerfaces* 113C, 152–157. doi:10.1016/j.colsurfb.2013.08.043
- Aldeyab, M.A., Harbarth, S., Vernaz, N., Kearney, M.P., Scott, M.G., Funston, C., Savage, K., Kelly, D., Aldiab, M.A., McElnay, J.C., 2009. Quasiexperimental study of the effects of antibiotic use, gastric acid-suppressive agents, and infection control practices on the incidence of *Clostridium difficile*-associated diarrhea in hospitalized patients. *Antimicrob. Agents Chemother.* 53, 2082–2088. doi:10.1128/AAC.01214-08
- Chatterjee, M., Anju, C.P., Biswas, L., Anil Kumar, V., Gopi Mohan, C., Biswas, R., 2016. Antibiotic resistance in *Pseudomonas aeruginosa* and alternative therapeutic options. *Int. J. Med. Microbiol.* 306, 48–58. doi:10.1016/j.ijmm.2015.11.004
- Da Silva, G.R., Da Silva-Cunha, A., Vieira, L.C., Silva, L.M., Ayres, E., Oréfice, R.L., Fialho, S.L., Saliba, J.B., Behar-Cohen, F., 2013. Montmorillonite clay based polyurethane nanocomposite as substrate for retinal pigment epithelial cell growth. *J. Mater. Sci. Mater. Med.* 24, 13091317.
- Davies, S.C., 2013. Annual Report of the Chief Medical Officer, Volume Two, 2011, Infections and the rise of antimicrobial resistance. Department of Health, London.
- Dryden, M.S., 2009. Skin and soft tissue infection: microbiology and epidemiology. *Int. J. Antimicrob. Agents* 34 Suppl 1, S2-7. doi:10.1016/S0924-8579(09)70541-2
- Enoch, D. a, Bygott, J.M., Daly, M.-L., Karas, J.A., 2007. Daptomycin. *J. Infect.* 55, 205–13. doi:10.1016/j.jinf.2007.05.180
- European Society of Clinical Microbiology and Infectious Diseases, 2017. Antimicrobial susceptibility testing EUCAST disk diffusion method - Version 6.0.
- Fraise, A.P., 2006. Tigecycline: the answer to beta-lactam and fluoroquinolone resistance? *J. Infect.* 53, 293–300. doi:10.1016/j.jinf.2006.05.014
- Ghadiri, M., Chrzanowski, W., Lee, W.H., Fathi, A., Dehghani, F., Rohanizadeh, R., 2013. Physico-chemical, mechanical and cytotoxicity characterizations of Laponite®/alginate nanocomposite. *Appl. Clay Sci.* 85, 64–73. doi:10.1016/j.clay.2013.08.049
- Gil, A., Korili, S. a., Trujillano, R., Vicente, M.A., 2011. A review on characterization of pillared clays by specific techniques. *Appl. Clay Sci.* 53, 97–105. doi:10.1016/j.clay.2010.09.018

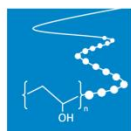
- Gonçalves, M., Figueira, P., Maciel, D., Rodrigues, J., Qu, X., Liu, C., Tomás, H., Li, Y., 2013. pH-sensitive Laponite/doxorubicin/alginate nanohybrids with improved anticancer efficacy. *Acta Biomater.* doi:10.1016/j.actbio.2013.09.013
- Grice, E.A., Segre, J.A., 2011. The skin microbiome. *Nat Rev Microbiol* 9, 244–253. doi:10.1038/nrmicro2537.The
- Jernberg, C., Löfmark, S., Edlund, C., Jansson, J.K., 2010. Long-term impacts of antibiotic exposure on the human intestinal microbiota. *Microbiology* 156, 3216–3223. doi:10.1099/mic.0.040618-0
- Kokabi, M., Sirousazar, M., Hassan, Z.M., 2007. PVA–clay nanocomposite hydrogels for wound dressing. *Eur. Polym. J.* 43, 773–781. doi:10.1016/j.eurpolymj.2006.11.030
- Madejova, J., 2003. FTIR techniques in clay mineral studies. *Vib. Spectrosc.* 31, 1–10.
- Malik, A., Mohammad, Z., Ahmad, J., 2013. The diabetic foot infections: biofilms and antimicrobial resistance. *Diabetes Metab. Syndr.* 7, 101–7. doi:10.1016/j.dsx.2013.02.006
- Matthews, K.H., Stevens, H.N.E., Auffret, a D., Humphrey, M.J., Eccleston, G.M., 2005. Lyophilised wafers as a drug delivery system for wound healing containing methylcellulose as a viscosity modifier. *Int. J. Pharm.* 289, 51–62. doi:10.1016/j.ijpharm.2004.10.022
- Mofokeng, J.P., Kelnar, I., Luyt, A.S., 2016. Effect of layered silicates on the thermal stability of PCL/PLA microfibrillar composites. *Polym. Test.* 50, 9–14. doi:10.1016/j.polymertesting.2015.12.004
- Momoh, F.U., Boateng, J.S., Richardson, S.C.W., Chowdhry, B.Z., Mitchell, J.C., 2015. Development and functional characterization of alginate dressing as potential protein delivery system for wound healing. *Int. J. Biol. Macromol.* 81, 137–150. doi:10.1016/j.ijbiomac.2015.07.037
- National Institute of Health and Care Excellence, 2015. Clinical Knowledge Summaries: Cellulitis - acute [WWW Document]. URL <https://cks.nice.org.uk/cellulitis-acute> (accessed 11.1.16).
- Price, L.B., Liu, C.M., Melendez, J.H., Frankel, Y.M., Engelthaler, D., Aziz, M., Bowers, J., Rattray, R., Ravel, J., Kingsley, C., Keim, P.S., Lazarus, G.S., Zenilman, J.M., 2009. Community analysis of chronic wound bacteria using 16S rRNA gene-based pyrosequencing: Impact of diabetes and antibiotics on chronic wound microbiota. *PLoS One* 4. doi:10.1371/journal.pone.0006462
- Ray, S.S., Okamoto, M., 2003. Polymer/layered silicate nanocomposites: a review from preparation to processing. *Prog. Polym. Sci.* 28, 1539–1641. doi:10.1016/j.progpolymsci.2003.08.002
- Roberts, K.D., Sulaiman, R.M., Rybak, M.J., 2015. Dalbavancin and Oritavancin: An Innovative Approach to the Treatment of Gram-Positive Infections. *Pharmacotherapy* 35, 935–948. doi:10.1002/phar.1641

- Royal Pharmaceutical Society, 2014. *New Medicines, Better Medicines, Better use of Medicines - A Guide to the Science Underpinning Pharmaceutical Practice*. London.
- Salerno, A., Nettis, P.A., 2014. Optimal design and manufacture of biomedical foam pore structure for tissue engineering applications BT - *Biomedical Foams for Tissue Engineering Applications*, in: *Biomedical Foams for Tissue Engineering Applications*. pp. 71–100. doi:<http://dx.doi.org/10.1533/9780857097033.1.71>
- Sandri, G., Bonferoni, M.C., Rossi, S., Ferrari, F., Aguzzi, C., Viseras, C., Caramella, C., 2016. Clay minerals for tissue regeneration, repair, and engineering, *Wound Healing Biomaterials*. Elsevier Ltd. doi:10.1016/B978-1-78242-456-7.00019-2
- Shikinaka, K., Aizawa, K., Murakami, Y., Osada, Y., Tokita, M., Watanabe, J., Shigehara, K., 2012. Structural and mechanical properties of Laponite-PEG hybrid films. *J. Colloid Interface Sci.* 369, 470–6. doi:10.1016/j.jcis.2011.11.079
- Stevens, D.L., 2009. Treatments for skin and soft-tissue and surgical site infections due to MDR Gram-positive bacteria. *J. Infect.* 59 Suppl 1, S32-9. doi:10.1016/S0163-4453(09)60006-2
- Stevens, D.L., Bisno, A.L., Chambers, H.F., Dellinger, E.P., Goldstein, E.J.C., Gorbach, S.L., Hirschmann, J. V, Kaplan, S.L., Montoya, J.G., Wade, J.C., 2014. Practice Guidelines for the Diagnosis and Management of Skin and Soft Tissue Infections: 2014 Update by the Infectious Diseases Society of America. *Clin. Infect. Dis.* 59, e10-52. doi:10.1093/cid/ciu296
- Tamma, P., Avdic, E., Li, D., 2017. Association of Adverse Events With Antibiotic Use in Hospitalized Patients. *JAMA Intern Med* 177, 1308–1315.
- Unal, S., 2009. Treatment options for skin and soft tissue infections: “oldies but goldies”. *Int. J. Antimicrob. Agents* 34 Suppl 1, S20-3. doi:10.1016/S0924-8579(09)70545-X
- Viseras, C., Aguzzi, C., Cerezo, P., Bedmar, M.C., 2008. Biopolymer–clay nanocomposites for controlled drug delivery. *Mater. Sci. Technol.* 24, 1020–1026. doi:10.1179/174328408X341708
- World Health Organization, 2012. *The evolving threat of antimicrobial resistance: Options for action*. World Health Organization, Switzerland.
- Zare, Y., Fasihi, M., Rhee, K.Y., 2017. Efficiency of stress transfer between polymer matrix and nanoplatelets in clay/polymer nanocomposites. *Appl. Clay Sci.* 143, 265–272. doi:10.1016/j.clay.2017.03.043
- Zhu, S., Chen, J., Li, H., Cao, Y., 2013. Structure and conformation of poly(ethylene glycol) in confined space of montmorillonite. *Appl. Surf. Sci.* 264, 500–506. doi:10.1016/j.apsusc.2012.10.052

## Appendix I - Posters presented at conferences

### The development of novel antimicrobial polymer-clay composite systems for the treatment of infected wounds

Presented at the 51<sup>st</sup> Annual Meeting of the Clay Minerals Society, Texas, USA, May 2014



Formulation & Drug Delivery Research

### The Development and Evaluation of Antibacterial Polymer-Phyllosilicate Composite Systems for the Treatment of Infected Wounds

Hamilton, A.R., Roberts, M., Hutcheon, G.A., & Gaskell, E.E.

School of Pharmacy and Biomolecular Sciences, Liverpool John Moores University, L3 3AF, UK

#### Introduction

Clays have been used for health purposes throughout ancient and modern history in many forms and applications [1]. Of note, and possibly the oldest application, is their use in the treatment of skin conditions and wounds.

The Chief Medical Officer published a hard-hitting report into antimicrobial prescribing and resistance, and set out a number of suggestions and challenges for the future [2].

This work acts as a pathfinder project that shows the potential application of antibacterial polymer-phyllosilicate composite systems within wound care.

#### Methods

Ciprofloxacin, tetracycline and doxycycline were adsorbed onto kaolin, refined montmorillonite, montmorillonite K-10, Laponite® RD, and Laponite® XL21 as described by Hamilton *et al.* (2014) [3]. Adsorption kinetics and isotherms were obtained through UV-Vis, with the mechanism of interaction determined through XRD and FTIR. The antimicrobial effects were determined through zone-of-inhibition of *Propionibacterium acnes*, *Pseudomonas aeruginosa* and *Staphylococcus epidermidis*.

Sodium alginate or varying viscosity was added to the phyllosilicate-drug composite dispersions. The materials were dried at 35°C to obtain films, or lyophilised to obtain foams. Once ideal proportions of polymer-phyllosilicate were identified glycerol was used as a plasticiser and ciprofloxacin was incorporated.

### Results and Discussion

#### Adsorption

Kaolin adsorbed least drug and at the slowest rate. Both Laponites® adsorbed large amounts of drug very rapidly. A dispersion pH that allows the drug to be in zwitterionic state is the most favourable for adsorption onto the clay mineral surface.

FTIR indicated the interaction of positively charged groups on the drug molecules with the phyllosilicate surface. XRD showed that the drugs adsorbed into the interlayer space of montmorillonites and Laponites® but only the external surface of kaolin.

These phenomena can be explained through the complex and differing chemistry of the phyllosilicates studied [3].

#### Antimicrobial properties

Tetracycline and doxycycline were effective against *P. acnes* and *S. epidermidis*, but only marginally effective against *P. aeruginosa*. Ciprofloxacin was effective against all three strains.

Composites of kaolin performed better than expected, releasing more drug than the montmorillonites and Laponites®. The differing surface charge of the clays (Laponite® > Kaolin) is likely to have effected the subsequent release.

#### Formulation

Laponites® outperformed the other phyllosilicates during qualitative analysis. Higher viscosity alginates were able to achieve suitable films, whilst high amounts of low viscosity alginates were needed to create foams (fig 1). Glycerol proved to be a valuable softer and plasticiser in both formulations. Up to 160 mg ciprofloxacin was able to be contained within each of the formulations.

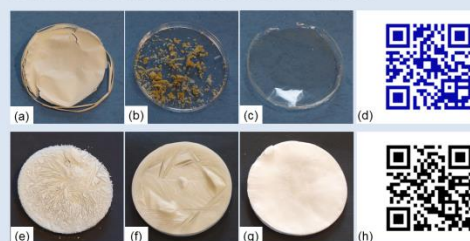


Figure 1. Composite films formed from oven drying (a) Montmorillonite K-10 and high-viscosity alginate; (b) refined montmorillonite and high-viscosity alginate, containing an excess of ciprofloxacin; and (c) Laponite® XL21 with high-viscosity alginate and glycerol. Foams were formed by lyophilising (e) kaolin and low-viscosity alginate; (f) refined montmorillonite and high-viscosity alginate; and (g) Laponite XL21 with low-viscosity alginate frozen in liquid nitrogen.

The QR codes link to videos demonstrating the flexibility of optimal and sub-optimal formulations of Laponite XL21 and alginate films (d) and foams (h).

### Conclusions

A number of antibacterial agents were successfully adsorbed onto a range of phyllosilicate materials. Clay chemistry was shown to play an important role in adsorption, as was dispersion pH and drug-charge. Antibacterial properties were maintained against three important bacterial strains. Finally, promising formulations have been produced that may be considered as candidate materials for clinical use.

#### References

- Gaskell, E.E., & Hamilton, A.R. (2014) Antibacterial clay-based materials for wound care. *Future Medicinal Chemistry*, 6(6):841-855
- Davies, S.C. (2013) Annual Report of the Chief Medical Officer, Vol. 2, Infections and the rise of antimicrobial resistance. Department of Health, London, UK.
- Hamilton, A.R., Hutcheon, G.A., Roberts, M., & Gaskell, E.E. (2014) Formulation and antibacterial profiles of clay-ciprofloxacin composites. *Applied Clay Science*, 87:129-135



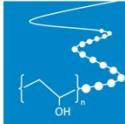

#### Acknowledgements

The authors would like to thank BYK Additives Ltd for their continued support of the research and for kindly supplying the phyllosilicate materials used throughout this project. The authors also thank the tissue viability team at the Royal Liverpool and Broadgreen University Hospitals NHS Foundation Trust for their invaluable clinical insight.



## The antimicrobial properties of clay composites containing tetracycline and ciprofloxacin,

- Presented at the 6th Mid-European Clay Conference, Průhonice, Czech Republic, 4th-9th September 2012. [This work won first prize in the poster awards]
- Presented at PharmSci 2012, Nottingham, UK, 13th September 2012.

**Formulation & Drug  
Delivery Research**

### The antimicrobial properties of clay composites containing tetracycline and ciprofloxacin

A. R. Hamilton, O. Bonenfant, M. Roberts, G. A. Hutcheon, E. E. Gaskell  
School of Pharmacy and Biomolecular Sciences, Liverpool John Moores University, UK

#### Introduction

Humans have used clays since prehistoric times and may have been mimicking animals that use clays to heal wounds. Clays have negatively charged surfaces allowing the adsorption of cations including drug molecules. Other research teams have adsorbed drugs onto clays though few have investigated drug release or applied this to clinical problems<sup>1,2</sup>. This study aims to adsorb the antibiotics ciprofloxacin (CIP) and tetracycline (TC) onto the clays kaolin (KN), montmorillonite K-10 (MMTK10), and Laponite® RD (LRD). Subsequent release of the drugs and antimicrobial activity against skin pathogens will also be examined.

#### Methods

1% w/v KN, MMTK10, and LRD dispersions were swollen for 2 hours in deionised water then CIP and TC solutions were added and pH adjusted with dilute HCl and NaOH. The pH that favoured the zwitterionic state was 7.4 and 5.0 for CIP and TC<sup>3,4</sup>, respectively. Reactions were stirred for 24 hours and the composites freeze-dried for analysis. Release of drug was investigated by dispersion of 10mg clay-drug composite in 100ml Phosphate Buffer Saline (PBS) at 37°C for up to 96 hours. UV-Visible spectrophotometry (Genesis 6 spectrophotometer) determined the amounts of drug bound and released to the clays. Powder X-ray diffraction (pXRD) was undertaken on a Rigaku miniflex between 3-12 deg2θ on an aluminium backplate. Infrared spectra were obtained on a Perkin Elmer FTIR Spectrum BX and GladiATR attachment between 400-4000cm<sup>-1</sup> with 16 scans at a resolution of 2cm<sup>-1</sup>. Cultures of *Propionibacterium acnes* (NCTC 737) and *Staphylococcus epidermidis* (NCTC 11047) equivalent to McFarland 0.5 were cultured at 37°C in brain-heart agar and nutrient agar, respectively. *P. acnes* cultures were grown in an anaerobic chamber. 2mg samples of clay-drug composite and varying drug concentrations were tested against both strains. Digital callipers were used to measure zones of inhibition (ZOI).

#### Impact

176 in every 100,000 hospital admissions in the UK are due to skin or soft-tissue infections<sup>5</sup>. Systemic antibiotics are indicated as drug-resistance occurs when currently available topical antimicrobials are used. This work may lead to the development of clinically appropriate, cost-effective, topical antimicrobials for such infections.

#### Results and Discussion

##### Drug Adsorption

Adsorption isotherms were plotted and Langmuir monolayer adsorption equations were applied to estimate the amount of CIP or TC required for monolayer coverage (eSm) under the conditions studied. As expected KN adsorbed the least amount of drug, taking up to 51.06mg/g (eSm=25.06mg/g) TC and 81.55mg/g (eSm=39.84mg/g) CIP. MMTK10 adsorbed up to 156.78mg/g (eSm=123.47mg/g) TC and 193.79mg/g (eSm=122.54mg/g) CIP (figure 1), whilst LRD adsorbed up to 199.75mg/g TC and 128.09mg/g CIP. Adsorption isotherms indicate that LRD can facilitate larger drug adsorptions but flocculation became problematic at higher drug concentrations resulting in unreliable reaction mixing. Increased  $d_{001}$  spacing of MMTK10 and LRD was observed as the amount of drug in these composites increased. After the monolayer had been formed gradual de-lamination of the clay was observed through loss of definition of the  $d_{001}$  peak (figure 2). This shows the drug molecules were adsorbed into the interlayer spaces of the clay, pushing them apart at higher concentrations. KN did not exhibit an expansion in interlayer spacing. FTIR analysis of the pure drugs and clay-drug composites showed the positive group of the zwitterionic form was interacting with the negatively charged clay surface.

##### Drug Release

Drug was detected in the PBS release media for all the clay-drug composites tested. The amount of drug released from KN composites showed little variation over the time period examined, which can be explained by the lower amounts of drug adsorbed and lack of interlayer space adsorption. The release of drug from MMTK10 and LRD composites was observed to be retarded and therefore more favourable for future clinical applications. Release of TC and CIP from LRD composites appeared to follow a bimodal pattern.

##### Antibacterial Activity

All clay-drug composites tested showed antibacterial activity against both strains of bacteria whereas the un-modified clays showed no antibacterial activity. Examples are shown in figure 3. KN composites produced large ZOI compared to the amount of drug adsorbed indicating dose-dumping, which mirrors the observations of the release studies. MMTK10 composites produced smaller ZOI suggesting greater retention of antibiotic whilst LRD composites released more drug in-line with their increased adsorption.

#### Conclusions

CIP and TC were successfully adsorbed onto KN, MMTK10, and LRD. Both drugs were shown to have adsorbed into the interlayer space of MMTK10 and LRD, leading to de-lamination of the clay structure at higher drug-loading. Utilising the zwitterionic form of TC and CIP resulted in large proportions of drug within the composites and allowed the positive portion of the drug to interact with the negative clay surface. Release of drug from the composites was retarded when compared to the pure drug but this did not dampen any antibacterial affect. Future work will aim to determine the continued effect of the clay-drug composites against liquid cultures of bacteria. Moreover, this work has shown the composites formed are of sufficient antibacterial character and are promising candidates for further work in the area of infection management.

#### References

- M.E. Paroto, *et al.*, (2010), *Appl. Clay Sci.*, **49**, 194-199
- R.A. Seaton, (2009) *Clinical Pharmacist*, **1**, 13-22
- C.-J. Wang, Z. Li, and W.-T. Jiang, (2011), *Appl. Clay Sci.*, **53**, 723-728
- P.-H. Chang, *et al.*, (2009), *Colloid. Surface A.*, **399**, 94-99


#### Acknowledgements

The authors would like to thank Rockwood Additives Ltd. (Widnes, UK) for the generous supply of Laponite® RD.


**Figure 1.** MMTK10 TC and CIP adsorption isotherms.

**Figure 2.** pXRD traces of MMTK10-TC composites containing varying amounts of TC per gram of MMTK10.

**Figure 3.** *S. epidermidis* in the presence of (a) pure MMTK10, (b-d) MMTK10-CIP composites and (e-g) MMTK10-TC composites. The composites contain increasing amounts of drug.



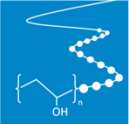



The Royal Liverpool and  
Broadgreen University Hospitals



## An investigation of ciprofloxacin adsorption onto clays for optimal drug release

- Presented at the LJMU Faculty of Science Research Seminar, Liverpool John Moores University, UK, 9th May 2012. [This work won second prize in the poster awards]
- Presented at the Salford Postgraduate Annual Research Conference, Salford University, UK, 30th-31st May 2012.

Formulation & Drug Delivery Research

### An investigation of ciprofloxacin adsorption onto clays for optimal drug release

A R Hamilton, M Roberts, G A Hutcheon, E E Gaskell  
School of Pharmacy and Biomolecular Sciences, Liverpool John Moores University, UK

#### Introduction

176 in every 100,000 hospital admissions in the UK are due to skin and soft-tissue infections<sup>[1]</sup>. Systemic antibiotics are indicated for infected wounds as drug-resistance can occur when currently available topical antimicrobials are deployed.

Humans have been using clays since prehistoric times as therapeutic agents to heal wounds. Clays have a negative surface

charge allowing the adsorption of water, bacteria, toxins and drugs. A number of research teams have adsorbed antimicrobials onto clays but few have investigated the subsequent release or applied this to clinical problems<sup>[2]</sup>.

This work sets out to define which parameters effect ciprofloxacin adsorption onto clays and how these also affect release.

#### Methods

One gram montmorillonite K-10 (MMTK10) was dispersed in deionised water and swollen for 2 hours, after which ciprofloxacin (CIP) in 20ml 0.1M HCl was added. The effects of time, pH and initial CIP concentration were investigated.

Amount of CIP adsorbed and released was determined using UV-Visible spectrophotometry. The mechanism of adsorption was determined through Fourier Transform Infrared Spectroscopy (FT-IR) and powder X-Ray Diffraction (XRD). Optimised methodology was applied to Laponites® RD (LRD) and WXFP (LWXFP).

#### Results and Discussion

##### Method optimisation

Longer adsorption periods yielded only small increases in CIP adsorption. Higher concentrations resulted in greater adsorption but a plateau was observed to commence between 5mg/ml and 10mg/ml.

Maximum CIP adsorption occurred at pH 8 when in its zwitterionic state<sup>[3]</sup>. No adsorption was observed at pH 12 when the MMTK10 changes composition and CIP was in its anionic form<sup>[3]</sup>.

##### Application to Laponite®

The optimised method used 500mg CIP at pH 8 for two hours. MMTK10 adsorbed slightly more CIP than either LRD and LWXFP.

##### Mechanism of adsorption

FT-IR showed the positively charged amino group of CIP interacted with the clays<sup>[4]</sup>, indicating cation exchange as the adsorption mechanism.

Increased  $d_{001}$  values, determined through XRD spectra, indicated increased interlayer spacing. This showed CIP was adsorbed in between clay layers.

##### Release studies

Release profiles for all three composites were similar until about 80 hours. The LRD composite released the least CIP in the time examined. The slow release observed indicates that the release of CIP is modified when adsorbed onto clays.

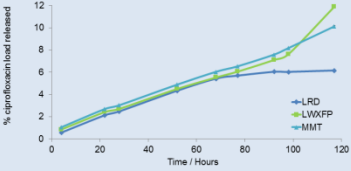


Figure 1. Release profiles for the three clay-ciprofloxacin composites formed under optimal conditions.

#### Conclusions


Ciprofloxacin was adsorbed into the interlayer spaces of montmorillonite K-10, Laponite® RD and Laponite® WXFP. Ciprofloxacin release was sustained, with Laponite® RD observed to release the least. These clay-ciprofloxacin composites could be useful in the treatment of infected wounds through their ability to control ciprofloxacin release and also absorb excess fluid from wounds.

##### References

- Seaton, R.A. (2009) Skin and soft tissue infection diagnosis and management. *Clinical/Pharmacist* 1, 13-22.
- Piarolo, M.E., et al. (2010) Antimicrobial properties of tetracycline and minocycline-montmorillonites. *Appl. Clay Sci.*, 49, 194-199.
- Wang, C.-J., et al. (2011) Adsorption of ciprofloxacin on 2:1 dioctahedral clay minerals. *Appl. Clay Sci.*, 53, 723-728.
- Socrates, G. (1994) Infrared and Raman characteristic group frequencies: tables and charts (2<sup>nd</sup> Edition). Wiley, Chichester, UK

##### Acknowledgements

The authors would like to thank Rockwood Additives Ltd. (Widnes, UK) for the generous supply of Laponite® RD and Laponite® WXFP.



The Royal Liverpool and Broadgreen University Hospitals  
NHS Trust

## Utilising montmorillonite K-10 and Laponite® for delivery of ciprofloxacin.

Presented at the UK & Ireland Controlled Release Society, Aston University, UK, 2nd May 2012.



## Utilising montmorillonite K-10 and Laponite® for the delivery of ciprofloxacin

A R Hamilton, M Roberts, G A Hutcheon, E E Gaskell  
School of Pharmacy and Biomolecular Sciences, Liverpool John Moores University, UK

### Introduction

Clays have been used since prehistoric times to heal wounds and more recently as pharmaceutical excipients [1]. Clays have negatively charged surfaces which allows the adsorption of cations including drug molecules. Other research teams have adsorbed drugs onto clays though few have investigated the subsequent release and applied this to therapeutic problems [2].

This study investigates new ways of using clays to deliver antibiotics. Adsorption of the antibiotic ciprofloxacin was optimised on montmorillonite K-10 then applied to two grades of Laponite®.

Release of adsorbed ciprofloxacin was measured to determine if modified release was achieved.

### Methods

One gram montmorillonite K-10 (MMTK10) was dispersed in 80ml deionised water and swollen for 2 hours, after which ciprofloxacin (CIP) in 20ml 0.1M HCl was added. The effects of time (1 to 24 hours), pH (0.05 to 12.0) and initial CIP concentration (0.625mg/ml to 10.00mg/ml) were investigated. All dispersions were protected from light and mixed at 700rpm.

Amount of CIP adsorbed was determined using UV-Visible spectrophotometry scanning between 190-500nm. The mechanism of adsorption was determined through Fourier Transform Infrared Spectroscopy (FT-IR) and powder X-Ray Diffraction (XRD). Optimised methodology was applied to Laponites® RD (LRD) and WXFP (LWXFP). Release of CIP was measured using UV-Visible spectrophotometry.

### Results and Discussion

#### MMTK10 method optimisation

Longer adsorption periods yielded only small increases in CIP adsorption.

Maximum CIP adsorption occurred at pH 8 when in its zwitterionic state [3]. No adsorption was observed at pH 12 when the MMTK10 changed composition and CIP was in its anionic form [3].

Higher concentrations resulted in greater adsorption but a plateau was observed to commence between 5mg/ml and 10mg/ml.

#### Adsorption onto Laponite®

The optimised method used 5mg/ml CIP at pH 8 for two hours. LRD and LWXFP did not adsorb as much CIP as MMTK10 (figure 1). This may be due to the effect low pH has on the Laponite® structure.

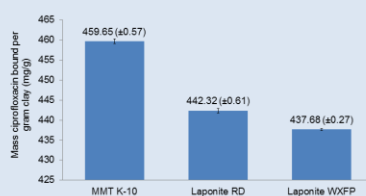


Figure 1. Mass of ciprofloxacin adsorbed per gram of clay for all three clays investigated under the optimised conditions.

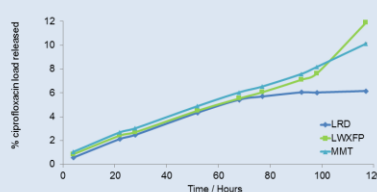


Figure 2. Release profiles for the three clay-ciprofloxacin composites formed under optimal conditions.

#### Mechanism of adsorption

FT-IR showed the positively charged amino group (2700-2250 cm<sup>-1</sup>) of CIP interacted with the clays [4], indicating cation exchange as the adsorption mechanism.

Increased d<sub>001</sub> values, determined through XRD analysis, indicated increased interlayer spacing. This showed CIP was adsorbed in between clay layers.

#### Release studies

Release profiles for all three composites were similar until about 80 hours. LRD was shown to have finished releasing its load at around 100 hours.

The slow release observed indicates that the release of CIP is modified when adsorbed onto clays.

### Conclusions

Ciprofloxacin was adsorbed into the interlayer spaces of montmorillonite K-10, Laponite® RD and Laponite® WXFP. Ciprofloxacin release was modified, with Laponite WXFP® releasing most during the examined time. However, less than 12% of the available ciprofloxacin was released showing strong adsorption onto the clay surface. These clays could therefore be exploited for drug delivery purposes.

#### References

1. Carrelaro, M. I. (2002) Clay minerals and their beneficial effects upon human health. *Appl. Clay Sci.* 21, 155-163.
2. Parolo, M.E., et al. (2010) Antimicrobial properties of tetracycline and minocycline-montmorillonites. *Appl. Clay Sci.* 49, 194-199.
3. Wang, C.-J., et al. (2011) Adsorption of ciprofloxacin on 2:1 dioctahedral clay minerals. *Appl. Clay Sci.* 53, 723-728.
4. Socrates, G. (1994) Infrared and Raman characteristic group frequencies: tables and charts (2<sup>nd</sup> Edition). Wiley, Chichester, UK.

#### Acknowledgements

The authors would like to thank Rockwood Additives Ltd. (Widnes, UK) for the generous supply of Laponite® RD and Laponite® WXFP.

**ROCKWOOD**  
Additives Limited

The Royal Liverpool and **NHS**  
Broadgreen University Hospitals  
NHS Trust